DEPARTMENT OF CHEMICAL ENGINEERING
FACULTY OF SCIENCE AND ENGINEERING

PhD THESIS

A STUDY OF THE DESIGN AND OPERATION OF CENTRIFUGAL COMPRESSORS FOR SUPERCRITICAL CO_2 PIPELINE TRANSPORTATION

CHIMAOGE .N. OKEZUE

Supervisor: Dr. Dmitriy Kuvshinov

August 2019

This thesis is submitted in fulfilment of the requirements for a Doctor of Philosophy (PhD) Degree in Engineering

ABSTRACT

Carbon Capture and Storage (CCS) is one of the technological options recommended by the United Nations Inter-Governmental Panel on Climate Change (IPCC) for achieving a net reduction in CO_2 emissions to the atmosphere. CCS process is made up of three aspects, namely: carbon capture, transport and storage. Historically, researchers tended to focus heavily on the capture and storage aspects of the CCS process chain with the CO_2 transport aspect receiving less attention. However, in recent years, the level of research in CO_2 transport has increased sharply. Research shows that pipelines are the most viable means of transporting large volumes of anthropogenic carbon dioxide from offshore and onshore sources of emission to the place of permanent storage. In pipelines, CO_2 can be transported in gaseous, liquid or supercritical state. Supercritical CO_2 occurs when its pressure and temperature are both above the critical point (73.76 bar; 30.97°C). Carbon dioxide in supercritical state has high density close to that of a liquid and low viscosity comparable to that of a gas. This means that a larger amount of CO_2 per unit time can be transported in supercritical state than in gaseous or liquid state with low pipeline frictional pressure drop per unit mass and less energy costs. Therefore, for long distance pipeline transportation, it is economically sound to convey CO_2 in supercritical state rather than in gaseous or liquid states.

Pipeline infrastructure required in the CCS context is on a scale that vastly outsizes similar infrastructure commonly used for transportation of air, natural gas, petroleum, etc. CCS pipeline networks operate on an industrial scale, transporting several metric megatons of anthropogenic CO_2 per annum captured from multiple power stations and other process plants to designated places of storage. A large amount of energy is consumed by compressors and booster pumps in building up and maintaining the high pressure required to ensure anthropogenic CO_2 mixtures are in a supercritical state within the pipeline. Furthermore, pure and impure supercritical CO_2 exhibit erratic internal flow behaviour, a consequence of large, abrupt and barely controllable changes to its fluid properties provoked by minor shifts in pressure and temperature. All these make design and operation of supercritical CO_2 pipeline networks more challenging and costlier than conventional natural gas pipelines where compression pressures and volumetric delivery rates are relatively lower and

neither phase change nor radical variations in thermophysical properties are expected.

A review of published literature on supercritical CO_2 pipeline transportation shows a lot of effort has been made by other researchers to address design issues such as pipeline sizing, corrosion and fracture propagation and operational issues such as start-up, shut-down, rapid depressurization, valve blockage, etc. All these studies have reduced several of the technical challenges in the design and operation of the pipeline. Yet there is still a wide scope for further improvements and new developments. Compressors and booster pumps are responsible for most of the high amount of energy consumed in the operation of the pipeline. Therefore, the long-term economic feasibility of running a supercritical CO_2 pipeline networks is achievable only if energy consumption and associated operating costs of both machines can be kept as low as possible. One way of reducing energy consumption is by sizing compressors and booster pumps optimally to ensure that power losses in both machines are minimized.

In this PhD thesis, a new mathematical model was developed from first principles. This new mathematical model uniquely combines the geometry and working processes of a centrifugal machine with anomalous and erratic non-linear real fluid flow behavior peculiar to supercritical CO_2 and its mixtures. Successfully validated with available experimental data, the model was used to carry out a detailed investigation of the performance of centrifugal compressor handling supercritical carbon dioxide of varying purity under different operating conditions. Results of the investigation showed that parameters that characterize compressor performance such as power requirement, isentropic efficiency and pressure ratio are strongly dependent on impeller size, shaft speed, mass flow rate and the chemical composition of the supercritical CO_2 and its mixtures.

More importantly, the work carried out in this thesis also demonstrated that the quasi-dimensional model can be used as a robust tool for optimal sizing of centrifugal compressors and booster pumps installed on a supercritical carbon dioxide transport pipeline.

DEDICATION

I will like to dedicate the success of this PhD project to my parents, my siblings and my friends Eni Oko and Osman Yansaneh for their moral support throughout the duration of the project. I will also like to include Dr. Dmitriy Kuvshinov and Dr. Sharif Zein in this dedication for providing guidance and support which was crucial to the successful completion this project work.

RESEARCH PUBLICATIONS AND TECHNICAL REPORTS

Over the course of this PhD research project, several conference and journal papers were published in which I was in the position of lead-author or co-author. One technical report was also produced in the course of the project. A list of them have been provided below:

Research Papers:

Okezue, C. and. Kuvshinov, D., 2018. "A comprehensive study of the effect of chemical impurities on selection and sizing of centrifugal machines for supercritical carbon dioxide transport pipelines". Applied Energy, Vol. 230, pp.816-835.

Okezue, C. and Kuvshinov, D., 2017. "Effect of chemical impurities on centrifugal machine performance: implications for compressor sizing in a CO_2 transport pipeline". Energy Procedia, Vol. 142, pp. 3675–3682.

Okezue, C. and Wang, M., 2016. "Performance evaluation of a pump used for CO_2 Transport". 11th European Conference on Coal Research and Its Applications, Sheffield, United Kingdom.

Okezue, C. and Wang, M., 2014. "A study of the effect of chemical impurities on the performance of a supercritical CO_2 pump for CCS transport pipelines". 10th European Conference on Coal Research and Its Applications, Hull City, United Kingdom.

Luo, X., Mistry, K., Okezue, C., Wang, M., Cooper, R., Oko, E. and Field, J., 2014a. "Process simulation and analysis for CO_2 transport pipeline design and operation–case study for the Humber region in the UK". Computer Aided Chemical Engineering, Vol. 33, pp. 1633-1638

Luo, X., Wang, M., Oko, E. and Okezue, C., 2014b. "Simulation-based techno-economic evaluation for optimal design of CO_2 transport pipeline network". Applied Energy, Vol. 132, pp.610-620.

Technical Report:

Okezue, C., 2017. "Comparing the effect of rotor sizing versus rotor speed adjustment on centrifugal compressor energy requirements for CO_2 pipeline transportation". Technical Report Prepared in School of Engineering and Computer Science, University of Hull. Available at: https://hydra.hull.ac.uk/assets/hull:15468/content

CONTENTS

LIST OF FIGURES

LIST OF DATA TABLES

Nomenclature

A	Area [m^2]
b	Impeller Width [m]
d, D	Diameter [m]
dF	Change In Force [N]
f	Fanning's Friction Factor [–]
Gap	Width of Clearance Between Impeller and Compressor Housing [m]
h	Specific Enthalpy at Static Conditions [J/kg]
H	Height [m]
K	Loss Coefficient [–]
L	Characteristic Length [m]
$\dot{m}$	Mass Flow Rate [kg/s]
n_B	Number Of Impeller Blades [–]
N	Rotor Shaft Speed [rpm]
N_{RUN}	Total Number Of Data Points In A Dataset [-]
P	Static Pressure [bar]
r	Radius [m]
Re	Reynolds Number [–]
s	Specific Entropy [J/kg.k]
S_F	Slip Factor [–]
T	Static Temperature [K]
û	Specific Internal Energy At Static Conditions [J/kg]
U	Impeller Blade Tip Speed [m/s]
V	Velocity [m/s]
W	Specific Work [J/kg]
Z	Compressibility Factor [-]

Greek Symbols

β	Impeller Blade Angle
Δ	Finite Difference [–]
δ	Relative Change [%]
μ	Viscosity [mPa.s]
ρ	Fluid Density [kg/m^3]
θ	Wrap Angle [deg]
ϕ	Convergence Angle [deg]
η	Efficiency [–]
π	Pi Constant [–]
ω	Angular Speed [rad/s]
τ	Shear Stress [Pa]

Subscripts

1	Compressor inlet (Suction); leading edge of impeller
2	Compressor outlet (Discharge); trailing edge of impeller
a	Actual value

ave	Average value
con	Converging duct
crit	Critical value
curv	Curved surface
disk	Disk friction
euler	Ideal value
gap	Impeller tip leakage channel
HYD	Hydraulic value
i	Root of impeller eye (Impeller hub)
IMP	Impeller
INPUT	Actual input value
ISEN	Isentropic value
leak	Leakage
losses	Losses
m	Meridional direction
o	Tip of impeller eye
rad	Radial coordinate
rel	Relative value
RUN	Index number of a data point
sum	Sum of values
t	Tangential coordinate

Abbreviations

APE	Average Percentage Relative Error
AAPE	Average Absolute Percentage Relative Error
BWR	Benedict-Webb-Rubin EoS Correlation
BWRS	Benedict-Webb-Rubin-Starling EoS Correlation
CAPEX	Capital Expenditure or Capital Cost
CCS	Carbon Capture and Storage
GERG	Groupe Européen de Recherches Gazières
EOR	Enhanced Oil Recovery
EoS	Equation of State
EoS-CG	Equation of State for Combustion Gases & Combustion Gas-like Mixtures
LK	Lee-Kessler
LKP	Lee-Kessler-Plocker
OPEX	Operating Expenditure or Operating Cost
PR	Peng-Robinson
SAFT	Statistical Associating Fluid Theory EoS Correlation
SRK	Soave-Redlich-Kwong
SW	Span and Wagner
STANDEV	Standard Deviation about the Average Percentage Relative Error
VLE	Vapour-Liquid Phase Equilibrium

CHAPTER 1

INTRODUCTION

1.1 MOTIVATION FOR RESEARCH WORK

Compressors and booster pumps are two individual components that jointly constitute the “heart” of a pipeline network because they consume most of the required energy input. In other words, most of the operating expenditure (OPEX) for the CO_2 transport pipeline is spent on the running of compressors and pumps. Yet, there are only a few studies evaluating their performance under various operating conditions.

A review of published literature on supercritical CO_2 pipeline transportation reveals many studies on design issues such as pipeline sizing, recompression distance, energy requirement, corrosion and fracture propagation and operational issues such as start-up, shutdown, rapid depressurization, valve blockage and variation of fluid flow rate. In these studies, compressors and pumps are not analyzed in great depth because the focus is usually on a globalized evaluation of the entire transport pipeline network rather than a localized analysis of individual key components in the network.

A few studies have been published comparing centrifugal compressors of various multistage configurations, combined gas compressor–cryogenic liquid pump units and shockwave compressors to determine which of the fluid compression strategies will yield the least energy requirement given a particular chemical composition of the anthropogenic CO_2 mixture to be transported in the pipeline under supercritical or dense phase conditions. While these studies provide useful information on where significant savings can be made in operating costs of the supercritical CO_2 pipeline, they are still lacking in practical details.

For the practical implementation of any of the compression or pumping strategies in open literature, the actual centrifugal machines involved must be sized appropriately, considering the thermophysical properties of the impure CO_2 stream and the operating conditions of the transport pipeline network. This is necessary for the optimal performance of these machines and the reduction in the overall energy costs of the transport pipeline.

Unfortunately, despite the large amount of published research on supercritical CO_2 pipeline transportation, there has been no work on a systematic method for selection and sizing of centrifugal compressors and pumps to ensure minimal power losses in both machines. A large number of hydraulic models of pipeline networks have been published in literature. In most of them, fluid compression is simulated with adiabatic or polytropic process equations, which neglect the geometry and complex internal fluid flow processes within the centrifugal machines. While this globalized approach to modelling fluid compression is generally sufficient for estimating energy requirement of compressors in a supercritical CO_2 pipeline under different operating conditions, it is unsuitable for optimal design of bespoke centrifugal machines or appropriate sizing and selection of existing ready-to-use centrifugal machines.

Moreover, in adiabatic and polytropic equations, a single constant isentropic efficiency value is assumed and used to calculate the compressor power requirement regardless of the working fluid's chemical composition. In reality, isentropic efficiency is not constant, but varies with change in the purity of CO_2 stream and operating conditions of the compressor. Variation in efficiency can be quite significant if the concentration of certain impurities (e.g. hydrogen) in the supercritical CO_2 stream is high. Given the radical effect that certain chemical impurities—even in trace amounts— have on the normal thermophysical properties of CO_2 stream at the vicinity of its critical point, the variation in efficiency can be quite considerable. In fact, Okezue and Wang (2016) demonstrated that isentropic efficiency of a compressor varies significantly if the concentration of certain impurities (e.g. hydrogen) in the supercritical CO_2 stream is high.

In conclusion, the long-term economic feasibility of running a transport pipeline network is strongly dependent on curbing high operating costs associated with compression and maintenance of pure or impure CO_2 above its critical point. Significant savings in energy costs can be made by rightsizing compressors and booster pumps in order to minimize power losses. Compressor performance maps, traditionally been used for this purpose, are unsuitable in the CCS context, as none account for anomalous (and sometimes erratic) flow behaviour exhibited by CO_2 mixtures at supercritical or dense phase conditions.

The absence of a systematic method of selecting and sizing compressors for supercritical CO_2 pipeline networks in published literature represents a significant gap in knowledge. A prerequisite for appropriate selection and sizing compressors/pump is an investigation of the poorly understood and under-researched behaviour of anthropogenic CO_2 stream within the internal flow channels of both machines at supercritical conditions. This is important because anthropogenic CO_2 stream, which the pipeline network is expected to transport, tend to contain chemical impurities such as hydrogen, nitrogen, methane, carbon monoxide and oxygen. Under supercritical conditions, these impurities will induce radical changes in the thermodynamic behaviour of CO_2 with great implications for the overall energy requirement of compressors and pumps.

1.2 AIM OF PHD PROJECT

The aim of this PhD project is to investigate the geometry, internal fluid flow and working processes of centrifugal machines and develop an algorithmic tool for optimizing the performance of compressors and booster pumps installed in a supercritical CO_2 pipeline network in order to reduce energy penalty and operating costs. To achieve the declared research aim, the objectives are set:

- The evaluation of various existing equations of state (EoS) correlations to find which ones give the most accurate prediction of thermodynamic properties of CO_2 either in its pure form or in mixture with various chemical impurities for conditions within the operating envelope of a supercritical CO_2 compressor.
- Development and validation of a mathematical model combining the detailed geometry, internal fluid flow and working processes of a centrifugal machine handling supercritical CO_2 of varying chemical purity.
- Application of the model in a detailed investigation of identified compressor performance parameters in order to evaluate their effects on isentropic efficiency and energy requirement of the centrifugal machines installed in a CO_2 pipeline network. Knowledge gained from the parametric investigation is then used to develop a procedure for optimal sizing and selection of ready-to-use compressors to ensure that machines with the best attainable efficiency per power utilized are installed in the pipeline network

1.3 RESEARCH METHODOLOGY

In other to achieve the aim and objectives set above, the research project was split into “work packages” namely:

- Problem definition
- Developing modelling strategies
- Model validation and iteration process

These “work packages” were further split into a series of tasks and sub-tasks, each mapped to a specific timeline in a Gantt chart that was reviewed and updated periodically for effective micro-management of the PhD project.

1.3.1 Work breakdown structure (WBS)

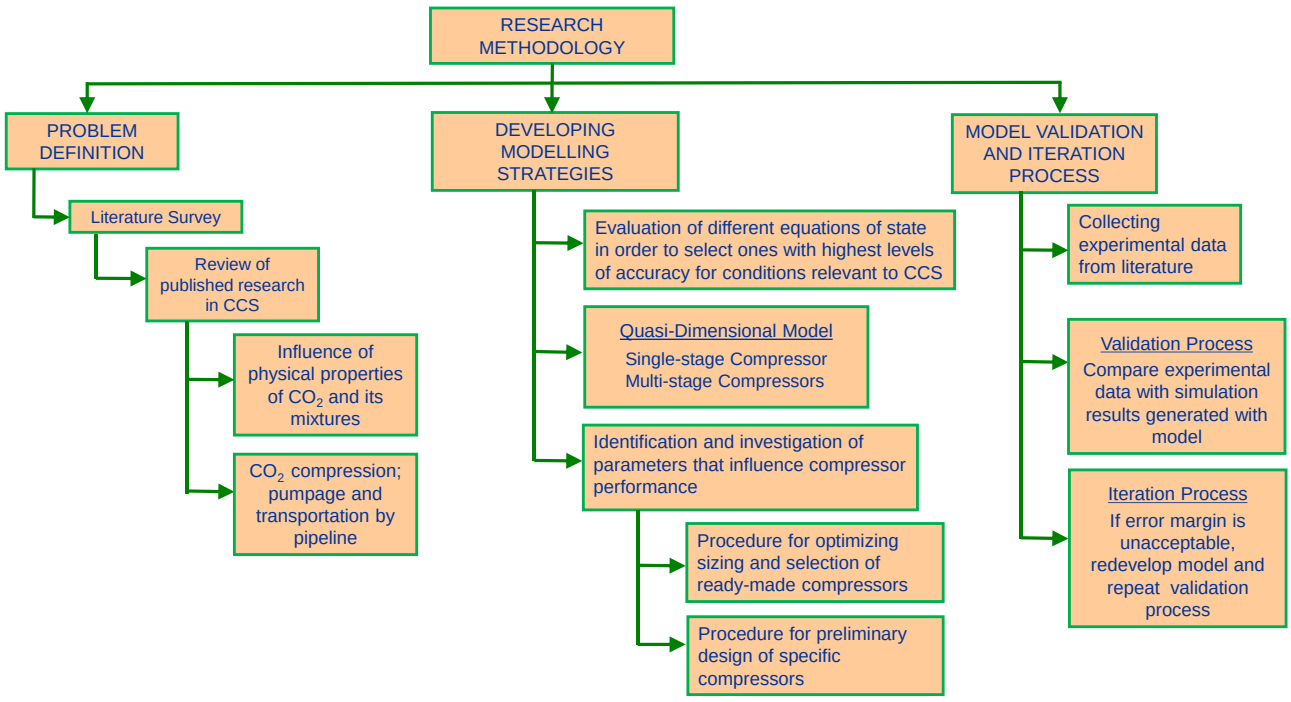

Fig. 1.1 Work breakdown structure (WBS) showing a methodology of achieving research aims

Research stages of the PhD programme and major tasks under them were graphically represented with aid of a project tree-diagram called a work breakdown structure (WBS) as shown in Fig. 1.1. Sub-tasks used in the Gantt chart for this PhD project were produced from information in the WBS.

1.3.2 Type of model and software tools used in this study

A mathematical model describing the geometry, internal fluid flow and working processes of a centrifugal compressor was developed. The model consist of steady-state mass and energy conservation equations applied to a control volume, which is defined as encompassing the interior working space of the centrifugal machine. The use of steady-state forms of the conservation equations is justified by the fact that the working fluid flows rapidly in and out of the control volume and barely has time to accumulate within the body of the machine due to the action of impeller blades rotating at high speed.

The mathematical model used in this study can be classified as being "quasi-dimensional model" since it consists of non-differential steady-state conservation equations applied to a coordinate-free control volume. This is in contrast to conventional 1-D, 2-D and 3-D models, which consists of differential conservative equations acting along one, two and three coordinate directions of a discretised volume, respectively.

Within the quasi-dimensional model, the thermodynamic properties of the pure or impure supercritical CO_2 working fluid compressed in the centrifugal machine is calculated with two equations of state (EoS) correlations, namely Span and Wagner (SW) and GERG-2008. The pair were chosen from a list of several EoS correlations after a comparative study indicated that they gave the most accurate predictions of CO_2 properties under the supercritical and dense phase conditions prescribed for pipeline transportation in CCS.

The algorithm for the quasi-dimensional model for single-stage centrifugal compressor was created in MATLAB®.

1.4 ORIGINAL CONTRIBUTIONS TO KNOWLEDGE

Significant gaps in knowledge in the area of anthropogenic CO_2 transportation research have been closed because of the work reported in this PhD thesis. In the context of CCS research, prior to this work, no other researcher has ever investigated the relationship among the following variables—composition of impure supercritical CO_2 mixtures, compressor size, compressor speed, pressure and compressor power requirement.

Given the effect of these variables, particularly size and speed, on compressor power requirements of CO_2 pipeline transportation; it is quite surprising that there has been no research (prior to this work) on compressor sizing and selection. It should be noted that compressors consume most of the energy required to run pipelines transporting anthropogenic CO_2 under supercritical conditions. Therefore, there is a need to have optimally sized compressors installed in the pipeline networks to reduce energy costs.

The following novel contributions were made:

- A highly mechanistic quasi-dimensional model, governed by the laws of conservation, has been developed and validated with available experimental data. This mathematical model differs from other compressor models used in previous CO_2 transport studies because it combines detailed information on centrifugal machine geometry with the peculiar anomalous, abrupt and erratic flow behaviour of supercritical CO_2 and its mixtures.

- The common practice among many researchers of using unreliable empirical coefficients or correlations to account for energy losses within compressor models was jettisoned. An original mechanistic sub-model describing various types of energy losses (i.e. disk friction, leakage and hydraulic losses) was developed separately and then merged into the larger quasi-dimensional model. Apart from accounting for various energy losses, the mechanistic sub-model also captures some of the 3-D internal fluid flow effects neglected in the larger quasi-dimensional model. The sub-model does this through the inclusion of equations describing the overall shape of semi-shrouded impeller, the curved and convergent geometry of impeller blade channels and the clearance between the periphery of the rotating impeller and the stationary interior walls of the compressor housing. Interactions between the supercritical working fluid, the rotating surface of the impeller and the stationary interior walls of the compressor housing are also captured in that sub-model

- The application of the quasi-dimensional model in an in-depth study of centrifugal compressors and booster pumps beyond what is available in previous studies on supercritical CO_2 pipeline transport in the CCS context. For example, applying the quasi-D model in this manner has allowed the following to be done:

    - The identification of impeller size, shaft speed, mass flow rate and chemical composition of the supercritical CO_2 stream as key parameters that characterize compressor performance. The varied effects of these parameters on power losses and the overall power requirement of a centrifugal machine of a given size used for pipeline transportation were thoroughly investigated. The results of the investigation demonstrated that the synergetic relationship among the above mentioned parameters could be potentially harnessed to control and minimize power losses. This knowledge forms the basis for the development of the compressor sizing methodology applied by the quasi-D model presented in this PhD thesis

    - Unlike studies carried out by other CCS researchers, the isentropic efficiency of a compressor is not assumed to be a single constant value that remains fixed regardless of the changing chemical composition of the impure CO_2 stream. This allows for a thorough investigation of the effects of various impurities in the supercritical CO_2 stream on isentropic efficiency over a range of operating conditions

    - A comprehensive investigation of the behaviour of pure and impure CO_2 within the internal flow channels of a compressor of given size operating at conditions above the critical point. This investigation is an attempt to understand the local changes in the thermophysical properties of the supercritical CO_2 stream occurring as it travels through flow channels between the stationary and rotating parts of the centrifugal machine. These changes to fluid properties such as density, specific enthalpy and compressibility occur due to local pressure and temperature variation within the channels and play a key role in better

understanding the internal flow behaviour of supercritical CO_2 stream and its effects on the overall performance of a centrifugal machine. This localized study which has never been done in the context of CCS research is also essential background knowledge for devising a systematic method for optimal selection and sizing of supercritical CO_2 compressors and booster pumps

- The application of the quasi-dimensional model as an effective tool for selection and sizing of centrifugal machines for installation in a pipeline network transporting supercritical CO_2 mixtures of various chemical compositions.

- Although outside the scope of this thesis, the quasi-dimensional model is applicable as a tool in the preliminary design of bespoke centrifugal machines for different working fluids, especially those in supercritical state.

1.5 STRUCTURE OF THE THESIS

Chapter 1 explains the motivation behind this research project. The objectives and the methods of achieving them are also explained in the chapter. An overview of the type of model and software tools used in the PhD study was given.

Chapter 2 gives background information on the effect of greenhouse gases on climate and the role of carbon capture and storage (CCS) as a means of mitigating the emission of the carbon dioxide, a greenhouse gas. Different aspects of the CCS chain are examined and the transport aspect is explained in details, including technical challenges in building and operating transport pipeline networks. The chapter also reports the influence of CO_2 thermo-physical properties on the pipeline transportation process. Comparisons are drawn between the performance of pipeline networks transporting pure CO_2 and those transporting CO_2 in mixtures with various chemical impurities

Chapter 3 contains a detailed comparative study of different equations of state, which was carried out to select those that produce accurate predictions for a given set of thermodynamic conditions and various chemical compositions of CO_2 mixtures. This is a prerequisite for the development of a quasi-dimensional mathematical model

capable of functioning as an algorithmic tool for selection and sizing of centrifugal machines installed on a supercritical CO_2 pipeline network

Chapter 4 describes development of a quasi-dimensional mathematical model of the geometry, internal fluid and working process of a single-stage centrifugal compressor used for supercritical CO_2 pipeline transportation. The validation of the mathematical model with experimental data was also discussed in this chapter.

Chapter 5 presents the application of the quasi-dimensional model in the evaluation of compressor performance under different operating conditions. The effects of different chemical impurities in the CO_2 working fluid on compressor performance was also analysed. This chapter also features a parametric investigation of the impact of changing diameter and speed of the impeller on the actual power requirement of centrifugal compressors for a given supercritical working fluid.

Chapter 6 demonstrates how the quasi-dimensional model is applied as a tool for optimal sizing and selection of commercially available ready-to-use centrifugal compressors suitable for installation in a pipeline network transporting particular CO_2 mixtures.

Chapters 7 and 8 respectively contain conclusions drawn from the PhD research project and recommendations for future research work.

CHAPTER 2

LITERATURE SURVEY

Emission of greenhouse gases is responsible for climate change. According to Inter-governmental Panel on Climate Change (IPCC), anthropogenic CO_2 constitutes 77% of the total greenhouse gas emitted into the atmosphere. This makes CO_2 emission the greatest cause of climate change (Mertz *et al.*, 2005). The rapid growth of formerly under-developed countries such as Brazil, India and China are driven by expansion of energy-intensive industries, namely power plants; refineries; cement plants; steelworks, etc. Most of these industries depend on the burning fossil fuels such coal, natural gas and petroleum, which continues to increase the concentration of carbon dioxide in the atmosphere leading to sustained global warming.

2.1 THE CARBON CAPTURE AND STORAGE (CCS) PROCESS CHAIN

Carbon Capture and Storage (CCS) process is widely acknowledged as best technological option for achieving a net reduction in CO_2 emissions to the atmosphere.

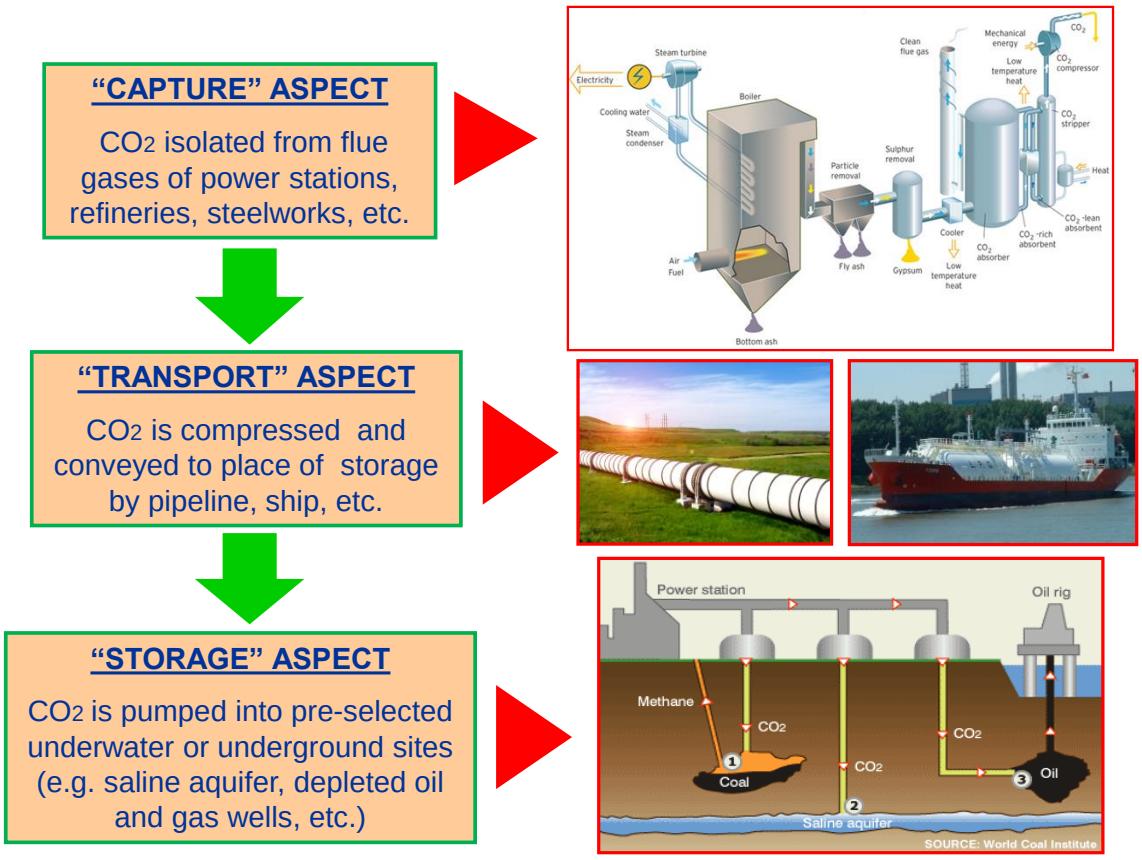

Fig. 2.1 A diagram depicting all three aspects of the CCS process chain

The amount of CO_2 emitted by industrial plants globally in 2011 was has been estimated to be around 31.2 Gt (IEA, 2013). It is expected that by the year 2050, 21%–45% of the CO_2 will be captured, transported and sequestered using CCS technologies (Mertz *et al.*, 2005).

2.1.1 Capture Aspect of the CCS Process Chain

CCS process chain consists of carbon capture, transport and storage as shown in Fig. 2.1. In the “capture” aspect of the CCS chain, the carbon dioxide within the flue gases sourced from industrial plants is isolated and conditioned for transportation and storage. CO_2 can be separated from flue gases through three main methods namely: post-combustion capture, pre-combustion capture and oxy-fuel combustion capture (Mertz *et al.*, 2005; Seevam *et al.*, 2007; Oosterkamp and Ramsen, 2008).

Post-combustion capture involves the separation of CO_2 from a mixture of flue gases generated from the combustion of fuel in the presence of air. In post-combustion capture, CO_2 removal from the flue gases can be achieved through several means including chemical absorption, physical adsorption, cryogenics separation or membrane absorption (Wang *et al*., 2011). In post-combustion capture, chemical absorption is the most widely used means of scrubbing CO_2 from the flue gases because of its low cost (Rao *et al.* 2004; Wang *et al*., 2011)

Pre-combustion capture involves the separation of carbon dioxide from the fuel before it is burned to produce energy. To achieve pre-combustion capture, the fuel is reacted with steam and air (or oxygen) to generate “synthesis gas” or “syngas”. The “syngas” which consists of carbon monoxide and hydrogen is subject to further processing. The carbon monoxide component of the “syngas” is reacted with steam in a catalytic reactor to yield CO_2 and more hydrogen. The CO_2 is then removed by means of absorption, adsorption or membrane separation while the remaining hydrogen component of the “syngas” is burned as fuel to generate energy for industrial plants (Mertz *et al.*, 2005; Porter *et al.* 2015).

In oxy-fuel combustion capture, the fuel is burned in the presence of pure or almost pure oxygen instead air resulting in the production of flue gases consisting mainly of carbon dioxide and water vapour. The water is condensed, leaving behind

concentrated CO_2, which can then be easily captured by absorption, adsorption or any other suitable separation process (Dillon *et al.*, 2004; Mertz *et al.* 2005).

For a particular kind of fuel burned, each of these capture methods will produce CO_2 streams containing different types and concentrations of impurities (Oosterkamp and Ramsen, 2008; Seevam *et al.*, 2007 and 2010; Race *et al.,* 2012; Porter *et al.* 2015).

Of all the mentioned capture methods, post-combustion capture is best suited for commercialization since it is a matured technology that can easily be retrofitted into existing industrial plants (Wang *et al*., 2011; Oko *et al*., 2015). Moreover, post-combustion produces CO_2 with higher level of purity than the other two capture methods. Oxy-fuel combustion capture process requires a large amount of energy to operate and provides the least pure CO_2 compared to the other capture methods (IEA GHG, 2006; Seevam *et al.*, 2008; Cosham, 2012).

2.1.2 Transport Aspect of the CCS Process Chain

The “transport” aspect involves the compression and conveyance of CO_2 to a designated place of sequestration. Road/rail-based tankers, pipelines and ship tankers are methods that can be used to achieve CO_2 transportation. Out of the mentioned options, pipeline and ship transportation are the only viable means of conveying large volumes of CO_2 from offshore and onshore sources of emission to the place of sequestration.

Svensson *et al.* (2004) performed analytical work that showed pipeline transportation is most feasible way of moving large volumes of CO_2 in onshore and offshore applications. The results of their analytical work has been corroborated by other feasibility and viability studies (Mertz *et al.*, 2005; McCoy and Rubin, 2008; Demofonti and Spinelli, 2011; Lazic *et al.*, 2014). Although pipeline transportation is a matured technology having been used for decades to convey natural gas and naturally occurring CO_2, it is quite a challenge when applied at the kind of scale required for CCS. There is little or no experience of transporting anthropogenic CO_2 in pipelines (Mertz *et al.*, 2005). These challenges are discussed in details in section 2.2.2

Ship transportation is more flexible than pipeline transportation in terms of transport routes. However, other factors make it less cost-effective namely, the need for loading

terminals; ship fuel costs and traffic delays in harbours. Moreover, Ship transportation is only economically viable for long distance offshore conveyance where the construction of pipelines would be impractical or in cases where less than a few million tonnes of CO_2 per annum is to be transported (Mertz *et al.*, 2005).

2.1.3 Storage Aspect of the CCS Process

The storage aspect of CCS process chain involves the deposition of the captured CO_2 in a place of sequestration usually onshore and offshore geological formations such as depleted oil and gas wells, saline aquifers and deep unminable coal seams (Mertz *et al.*, 2005).

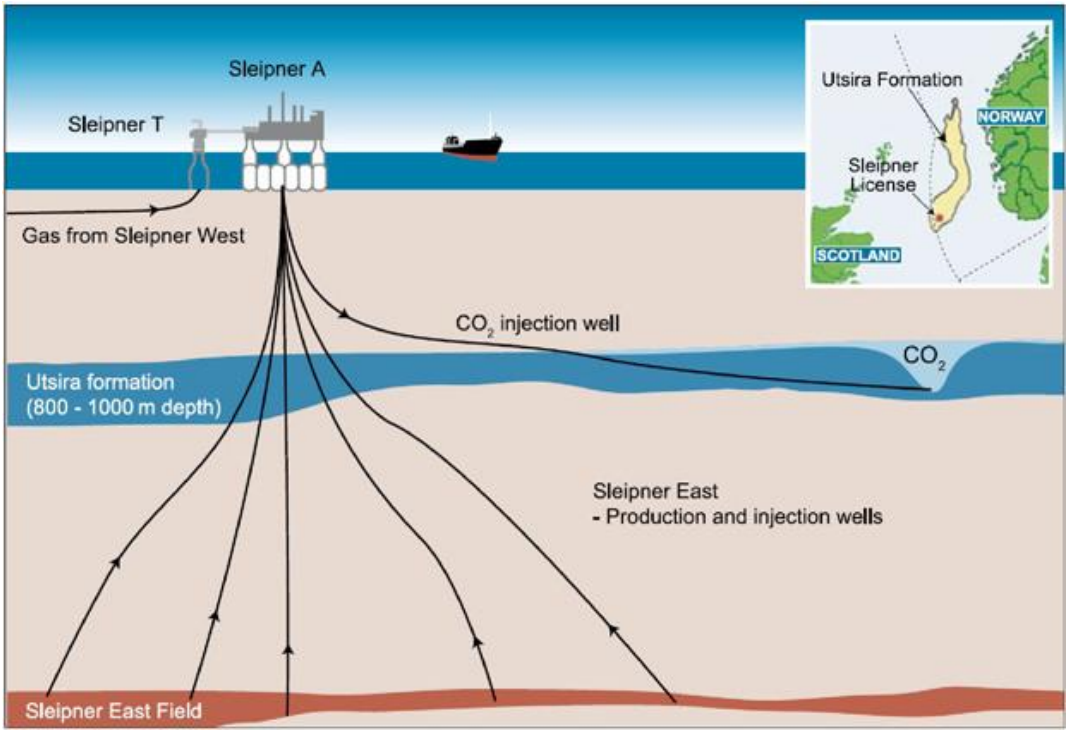

Fig. 2.2 Diagram of Sleipner CCS Project with insert showing location of Utsira Saline Acquifer (Mertz et al., 2005).

There is a wealth of experience in enhanced oil recovery (EOR) — a process in which naturally occurring (and nearly pure) carbon dioxide is injected into depleted oil wells in order to displace and recover any remaining crude oil (McCoy and Rubin, 2008). With appropriate adjustments, EOR technology can be applied in the CCS context of storing anthropogenic CO_2 in marginal oil wells. A good example is the Weyburn-Midale Carbon Dioxide Project in which about 1 million tonnes of carbon dioxide sourced from Boundary Dam Power Station (Saskatchewan, Canada) and Dakota Gasification Company (North Dakota, USA) is transported to the onshore Weyburn

oilfields of Canada for use in enhanced oil recovery (Mertz *et al.*, 2005; IEA GHG, 2005; Oosterkamp and Ramsen, 2008).

Unlike the Weyburn-Midale CO_2 Project, the Sleipner and Snohvit projects involve the injection of CO_2 stripped from natural gas into deep water saline formations (Monaghan and Brennan, 2006; Oosterkamp and Ramsen, 2008; Lindeberg *et al.* 2009). The Sleipner CCS Project shown in Fig. 2.2 is the world's oldest offshore CCS project having been in operation since October 1996 (Mertz *et al.*, 2005; IEA, 2013).

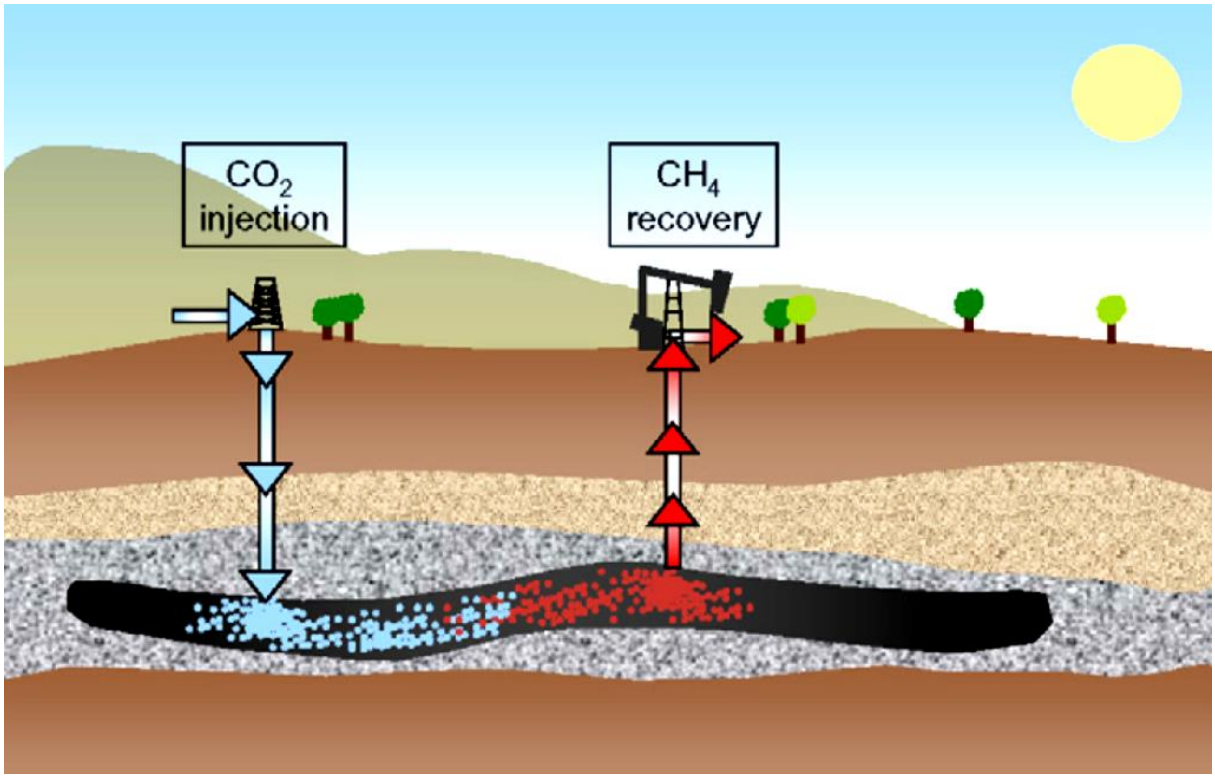

Fig.2.3 Diagram showing the process of Enhanced Coal Bed Methane Recovery (Mazzotti et al., 2009)

Captured carbon dioxide can also be injected and stored in coal seams that are so deep underwater that they cannot be reached for the purposes of mining (Mertz *et al.*, 2005). The surface of coal beds contain pores and fractures, which tend to contain gases including methane. Injecting carbon dioxide into the seam will result in its adsorption by the coal and the displacement the coal bed gases, including methane. The displaced methane recovered can be sold in order to recoup the cost of injecting the carbon dioxide (Mertz *et al.*, 2005; Monaghan and Brennan, 2006; IEA, 2013). As illustrated in Fig. 2.3, the process of recovering methane from unminable coal seams through the preferential adsorption of CO_2 on coal is called "enhanced coal bed methane recovery (ECBM). Provided the coal seam remains unmined, the CO_2

adsorbed by the coal will never be released from the depths of the ocean (Mertz *et al.*, 2005). Although ECBM shows a lot of future promise, it is currently one of the least developed options for carbon storage (Monaghan and Brennan, 2006; Mazzotti *et al.* 2009).

2.2 CHARACTERISTICS OF CO_2 PIPELINE TRANSPORTATION

2.2.1 The Basics of CO_2 Pipeline Transportation

Carbon dioxide can be transported by pipeline in gaseous, dense or supercritical state. Supercritical CO_2 occurs when both temperature and pressure are above critical point (73.76 bar; 30.97°C). Carbon dioxide is in dense phase (also called "dense-liquid phase") when its pressure is above the critical point while its temperature is below the critical point (Svensson *et al*., 2004; Zhang *et al*., 2006; Lazic *et al*., 2014).

CO_2 stream in supercritical state have high density close to that of liquid CO_2 and low viscosity close to that of gaseous CO_2 (Jung and Nicot, 2010). This means that a larger amount of CO_2 per unit time can be transported in supercritical state than in gaseous or liquid state with low pipeline frictional pressure drop per unit mass (since viscosity is quite low). Therefore, for long distance transportation, it is more economically sound to convey CO_2 in dense or supercritical phase than in gaseous phase (Zhang *et al*., 2006; Seevam *et al.*, 2007; Serpa *et al.*, 2011; Luo *et al.*, 2014).

A CO_2 transport pipeline network consists of pipes, valves, compressors, booster pumps and control stations for monitoring fluid flow and pressure (Serpa *et al.*, 2011). Compressors pressurize CO_2 beyond its critical point in order to convert it from gaseous to supercritical phase. Booster pumps are required to ensure that the operating pressure inside the transport pipeline does not drop below the critical pressure of CO_2 (Okezue and Wang, 2016).

2.2.2 Challenges of CO_2 Pipeline Transport in the CCS Context

As explained in section 2.1.2, pipeline transportation is the most viable means of conveying captured carbon dioxide from industrial plants to a place of storage. However, pipeline transportation in the CCS context is not without its challenges considering that there is very little experience conveying anthropogenic CO_2 on a large scale (Mertz *et al.*, 2005). There are health hazards associated with CO_2

pipelines operating in the CCS context since the transportation of since many of them (especially in Europe) will be expected to pass through populated urban centres. Although buried underground, if these pipelines were to leak concentrated carbon dioxide then all life on the ground above will be threatened with mass asphyxiation Furthermore, in some parts of the world, the lack of political will, regulatory bureaucracies and economic considerations constitute a barrier to the construction and operation of CO_2 pipelines. This section of the thesis examines these challenges enumerated above in details.

2.2.2.1 Pipeline Transport: EOR versus CCS

CO_2 has been conveyed in the pipelines for purposes of Enhanced Oil Recovery (EOR) in the USA for the last three decades. However, EOR pipelines tend to carry pure CO_2 (or almost pure CO_2) sourced from naturally occurring CO_2 reservoirs and coal gasification plants (Mertz *et al.*, 2005; Oosterkamp and Ramsen, 2008; Seevam *et al.*, 2010).

In the context of CCS, the pipelines are expected to carry anthropogenic CO_2 generated from power stations and other process industries using fossil fuels. Unlike naturally occurring pure CO_2, anthropogenic CO_2 tend to contain chemical impurities such as N_2, H_2, CH_4, H_2O, H_2S, CO, O_2, SO_X and NO_X (Mertz *et al.*, 2005; Seevam *et al.*, 2007; Demofonti and Spinelli, 2011; Serpa *et al*., 2011). For economic reasons, the impure CO_2 gas will have be to converted to supercritical or dense phase prior to transportation (Mertz *et al.*, 2005)

At supercritical conditions, these impurities, even in trace amounts, can substantially alter the normal thermodynamic properties of CO_2. Examples of such properties include phase behaviour, compressibility, density, enthalpy and viscosity, thereby significantly affecting the design and operation of the pipeline network (Seevam *et al.*, 2008; Li and Yan, 2009a; Jung and Nicot, 2010; Goos *et al.*, 2011; Demetriades *et al.*, 2013; Wetenhall *et al.*, 2014a).

As illustrated in Fig. 2.4, energy requirement for compressors and booster pumps; repressurization distance; pipeline capacity; corrosion rate and fracture propagation rate are examples of design and operational issues influenced by the change in CO_2 properties brought on by the presence of impurities.

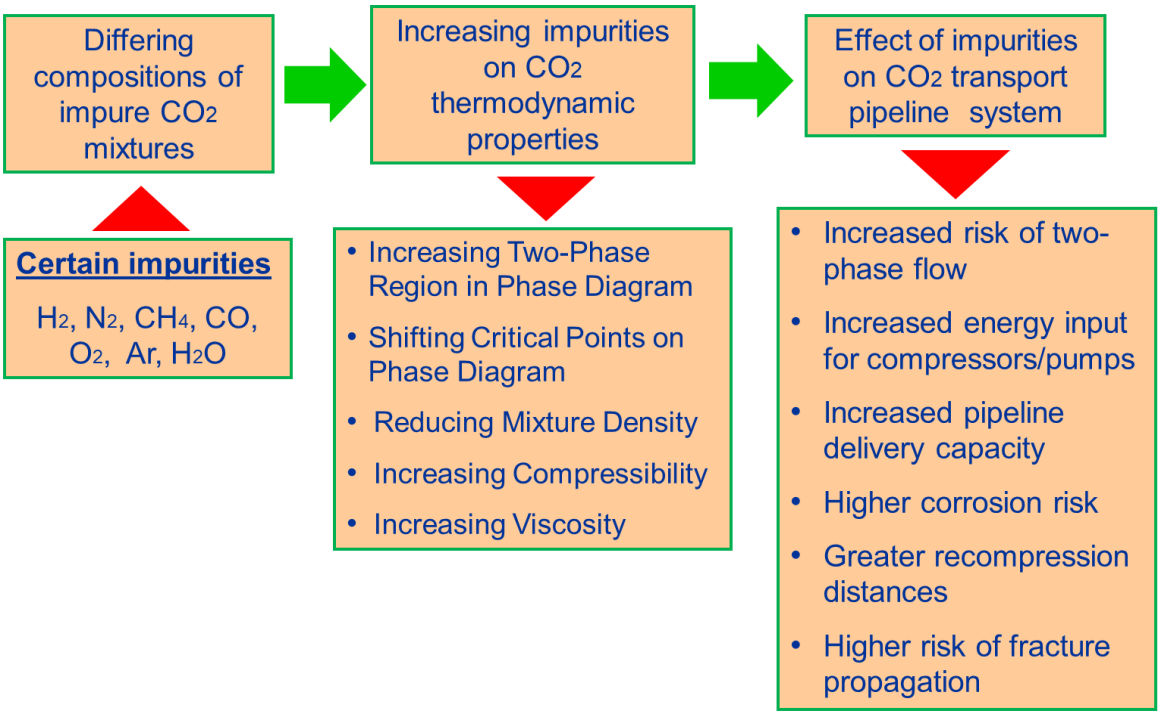

Fig.2.4 An illustration of the effect of impurities on CO_2 properties and operation of a transport pipeline

2.2.2.2 Health Hazards associated with CO_2 Pipeline Transport

Carbon dioxide exists in nature as a colourless, odourless and tasteless gas. It is present in the air that all living organism breathe. The concentration of the CO_2 in nature is quite low and pose little to treat to life. However, carbon dioxide transported in pipelines for the purposes of EOR or CCS is highly concentrated (Mertz *et al.*, 2005). CO_2 in high concentrations is dangerous to humans and animals because it acts as an asphyxiating agent by limiting the ability of the haemoglobin in blood to circulate oxygen to organs in the body.

One of the great differences between carbon dioxide transport in the EOR context and in the CCS context is in the route taken by the pipeline. CO_2 pipelines used for EOR tend to be located near oil fields in remote areas far from populated urban areas (Seevam *et al.* 2007; Oosterkamp and Ramsen, 2008; Demofonti and Spinelli, 2011; Cooper, 2012). Therefore, the consequences of a leak from a ruptured pipeline is small because the escaping concentrated CO_2 is likely to dissipate in air before reaching the local population (Seevam *et al.* 2007).

In contrast, many of the CO_2 transport pipelines meant for CCS mitigation (especially in Europe) are expected to pass underground through populated urban centres where

most power stations are located. In other words, the risk of mass asphyxiation of the local populace due to the leakage of concentrated CO_2 is higher in the CCS context (Seevam *et al.* 2007; Cooper, 2012; Aursand *et al.* 2013; Wen *et al.*, 2013,).

It also does not help that unlike the pure CO_2 conveyed in EOR pipelines, CCS pipelines carry anthropogenic CO_2 including impurities such as H_2O, H_2S, O_2, SO_X and NO_X, that increase the rate of pipe corrosion (Demofonti and Spinelli, 2011). The presence of certain impurities such as H_2, CO, Ar, N_2, CH_4 and O_2 in anthropogenic CO_2 increase the pipeline's susceptibility to a running ductile fracture (Demofonti and Spinelli, 2011; Cosham, 2012; Race *et al.,* 2012). Corrosion and fracture both lead to pipe rupture and leakage of concentrated CO_2 and therefore must be tackled before any pipeline is allowed to traverse populated areas. Furthermore, in CCS context, safety regulations consider not just the toxicity of concentrated CO_2, but also the toxicity of impurities themselves (Oosterkamp and Ramsen, 2008; Race *et al.,* 2012).

2.2.2.3 Political, Societal and Regulatory Barriers to CO_2 Pipeline Transport

Given the health hazard associated with the leakage of concentrated CO_2, it is no surprise that there are stringent safety regulations that would need to be fulfilled before the deployment of transport pipelines are permitted in populated urban centres. Safety regulatory procedures—which are time-consuming— have the effect of delaying the construction, deployment and operation of the transport pipelines and adds to the capital costs (Demofonti and Spinelli, 2011; Serpa *et al.*, 2011).

Societal resistance to the location of CO_2 pipelines in their areas cannot be separated from political objections to them. In some countries, political parties are often divided on whether to support or oppose CCS projects including transport pipelines. Parties in favour of CCS will often speak of how important they are and those who are opposed will point to potential health hazards of allowing CO_2 pipelines to pass through urban centres and will keep harping on that point even when all stringent measures are taken to guarantee the safety of the pipeline (Kuijper, 2011). The public who are mostly not versed in scientific principles, sometimes, along with the political opposition to such projects. A case in point being the popular resistance in Barendrecht Town (Netherlands) to the location of a CCS transport pipeline and storage project that would have sequestered carbon dioxide sourced from a

petroleum refinery into depleted natural gas fields (Brunsting et al., 2011; Kuijper, 2011). Despite an environmental impact assessment (EIA) declaring the project plan safe, the Netherlands government was unable to convince the people of Barendrecht that the project was hazard-free. Local politicians in the town played a leading role in inciting local resistance, claiming without foundation that the project was risky. Due to the overwhelming local opposition, the project was cancelled (Brunsting et al., 2011; Kuijper, 2011).

2.2.2.4 Economics of CO_2 Pipeline Transport

Pipeline System Design

When designing a pipeline, the key parameters to determine are namely, pipe diameter, pipe length, pipe wall thickness, inlet pressure, temperature, pressure drop and the flow rate of the working fluid to be conveyed in it. (Seevam *et al.*, 2008; Serpa *et al.*, 2011; Race *et al.*, 2012). In developing a pipeline design that meets standard regulatory requirements for pipe material integrity, operation and health and safety, appropriate values for the aforementioned parameters will have to be selected.

However, as illustrated in Fig.2.4, certain impurities change the normal thermodynamic properties of CO_2 and therefore have a strong impact on the design and operation of the pipeline network. For instance, impurities such as nitrogen, hydrogen and carbon monoxide decrease the overall density of the impure CO_2 stream resulting in greater temperature and pressure drops across the length of the pipeline than would be the case if the working fluid had been a pure CO_2 stream (Seevam *et al.*, 2007). To ensure that pipeline pressure does not drop below the critical point, resulting in the formation of the undesirable two-phase flow, the following alternative steps can be taken:

- Diameter of the pipeline should be increased
- Do not increase pipe diameter; shorten the pipeline repressurization distance by increasing the number of compressors or booster pumps along the pipe's length to compensate for the pressure losses
- Do not shorten repressurization distance nor increase pipe diameter, but exponentially raise the initial pressure at the pipeline's point of entry in order

to ensure that the expected losses will not cause operating pressure to drop below the critical point

Each of these alternatives will increase capital (CAPEX) and operating (OPEX) expenditure of the pipeline network (Mertz *et al.*, 2005; Race *et al.*, 2012). A pipeline of large diameter will need far more material than a pipeline of smaller diameter. Therefore, capital cost will increase linearly in proportion to any increase in pipeline diameter (Mertz *et al.*, 2005; Serpa *et al.*, 2011). Moreover, increasing the diameter of the pipeline has the unintended effect of increasing mechanical stress on the pipe material, which may result in its rupture. To avert this, the pipe walls will have to be much thicker. More material is required to manufacture thick-walled pipelines. Therefore, the capital costs increase as the pipe wall gets thicker (Cosham, 2012; Cooper, 2012, Lazic *et al.*, 2014; Luo *et al.*, 2014). Alternatively, the pipeline can made out of an expensive, but much stronger material (Race *et al.*, 2012).

Tackling the risk of two-phase fluid formation by shortening the repressurization distance will result in higher operating expenditure (OPEX) since total energy required for operating compressors or booster pumps will increases as their unit numbers along the length of the pipeline increases (Seevam *et al.*, 2007 and 2008). Procurement costs (i.e. CAPEX) per unit machine will rise in as the number of compressors/pumps increases.

Adoption of the third option—retaining original pipe diameter while increasing initial pressure at the pipeline's point of entry— will to higher capital expenditure. This is because higher pressures will subject the pipeline to greater levels of mechanical strain, which can lead to its rupture (Oosterkamp and Ramsen, 2008). Increasing the pipe wall thickness is the only way to stop damage. As stated earlier, more material is required to construct thick-walled pipelines. Hence, the higher capital costs (Cosham, 2012; Cooper, 2012, Luo *et al.*, 2014).

As earlier stated in section 2.2.2.2, corrosion and ductile fracture both lead to pipe rupture and the dangerous leakage and dispersal of concentrated carbon dioxide. The presence of impurities in the CO_2 stream increase the risk of corrosion and the pipeline's susceptibility to a running ductile fracture.

Fracture propagation in the pipeline depends on the saturation pressure and decompression wave speed of the working fluid and the toughness of the pipe material (Oosterkamp and Ramsen, 2008). The presence of certain types and concentration of impurities tend to increase saturation pressure of the impure CO_2 stream thereby increasing the propensity of the pipeline to a running ductile fracture (Demofonti and Spinelli, 2011; Cosham, 2012; Mahgerefteh *et al.*, 2012a; Race *et al.,* 2012). When a fracture is initiated on the pipeline (perhaps, by an external force), its ability to propagate will depend on the toughness of the pipe material. If the pipe toughness is high enough, the propagation of the fracture will "arrest" (i.e. stop) within a short distance and prevent pipeline rupture. In other words, fracture propagation is limited by pipeline toughness (Demofonti and Spinelli, 2011; Mahgerefteh *et al.*, 2012a; Martynov *et al.*, 2017). Therefore, increasing pipeline toughness linearly reduces the risk of fracture propagation. Toughness can be increased by using stronger materials (e.g. superior grade of steel) in pipeline construction or the pipe wall can be made thicker (Cosham, 2012; Race *et al.,* 2012). As stated in earlier, capital costs (CAPEX) increases as the pipe wall thickness increases. The alternative solution—the use of expensive, but superior materials in pipe construction— also increases CAPEX (Race *et al.,* 2012).

The presence of water in CO_2 stream is problematic since a reaction between the two substances will result in the formation of carbonic acid, which has a corrosive effect on pipeline material (Oosterkamp and Ramsen, 2008; Cooper, 2012). In addition to water, the presence of impurities such as H_2S, O_2, SO_X and NO_X exacerbates the problem by accelerating the rate of pipe corrosion (Demofonti and Spinelli, 2011; Cooper, 2012; Zargarzadeh *et al.*, 2013). One solution to corrosion problem is to eliminate water from CO_2 stream from prior to entry into the pipeline. However, water removal will incur additional operating costs. Another solution is to adopt pipelines with thicker walls as a method of corrosion mitigation, which will inevitably drive up CAPEX (Cooper, 2012; Race *et al.*, 2012; Eickhoff *et al.*, 2014). Corrosion-resistant materials in pipe construction are also viable, but expensive (Patchigolla and Oakey, 2013; Lazic *et al.*, 2014).

As a rule, a pipeline designed to carry a CO_2 stream containing impurities will incur higher CAPEX than one designed to carry a pure CO_2 stream. This can be attributed

to the fact that pipelines carrying impure CO_2 need to be thicker to combat fracture propagation and corrosion. For the same reason, a pipeline carrying an impure CO_2 stream with a higher concentration of impurities will cost more than a pipeline carrying an impure stream with a lower concentration of impurities (Cooper, 2012).

Compressors and Booster Pumps

Installed compressors and booster pumps consume most of the energy required to operate an entire CO_2 pipeline network. To convert gaseous CO_2 in supercritical or dense phase and maintain it, compressors and booster pumps will need to generate extremely high pressures within the pipeline—far above the critical pressure of the CO_2 stream. This is necessary to reduce the risk of single-phase supercritical fluid transforming into a gas-liquid two-phase fluid if there is a slight pressure drop in the pipeline (Seevam *et al.*, 2008; Demofonti and Spinelli, 2011; Race *et al.*, 2012). Two-phase fluid is undesirable because it can lead to cavitation and slugging, which can damage compressors, pumps and the pipeline itself (Oosterkamp and Ramsen, 2008; Lazic *et al*., 2014; Okezue and Wang, 2016).

In order to generate the high pressure ratios necessary for converting carbon dioxide from gaseous to supercritical phase, the compressors need a high amount of energy. Individual booster pumps operate at much lower pressure ratios and therefore consume less energy than individual compressors (Demofonti and Spinelli, 2011). Compared to a conventional liquid pump, an individual booster pump consumes a greater amount of energy because its working fluid, supercritical or dense-phase CO_2, is compressible (Adams, 2011; Bergamini *et al.*, 2011). In order to compensate for pressure losses and maintain the CO_2 stream in dense or supercritical state, several booster pump units are installed at various positions along the length of the pipeline (Oosterkamp and Ramsen, 2008; Seevam *et al.*, 2008; Race *et al.*, 2012).

The high energy requirement of compressors and pumps makes the operation of a supercritical CO_2 transport pipeline network expensive. A study conducted by Moore *et al.* (2011) indicated that the energy required to compress pure CO_2 in a CCS facility connected to a power station can reduce the overall efficiency of that station by 8-12%. The energy penalty is even greater if the CO_2 stream in the compressor contains certain impurities (Nimtz *et al.*, 2010; Race et al., 2012; Martynov *et al.*, 2016; Okezue and Wang, 2016).

The presence of impurities in the CO_2 stream has a two-fold effect on the running costs of booster pumps installed in the pipeline network. As illustrated in Fig. 2.4, impurities reduces the overall density of the CO_2 stream while increasing its compressibility and critical point. First, the combined impact of increased compressibility and reduced density causes the discharge pressure of each individual booster pump to drop and the energy requirement to increase. To maintain discharge pressure above the critical point of the impure CO_2, the speed or size of the pump's impeller will have to be increased, resulting in further increase in energy requirement and consequently, higher operating costs per unit pump. Secondly, impurities increase pressure losses along the length of the pipeline, which can be compensated by increasing the number of individual booster pump units, resulting in the multiplication of operating costs (Oosterkamp and Ramsen, 2008; Seevam *et al.*, 2008; Demofonti and Spinelli, 2011; Lazic *et al*., 2014).

Therefore, the long-term economic feasibility of running a CO_2 transport pipeline network is strongly dependent on whether savings can be made in operating costs of installed compressors and booster pumps.

2.3 INFLUENCE OF THERMOPHYSICAL PROPERTIES OF CO_2 AND ITS MIXTURES ON THE PROCESS OF PIPELINE TRANSPORTATION

The key thermodynamic properties of carbon dioxide that influence the working process of a supercritical CO_2 transport pipeline were identified in section 2.2.2.1 and the effect of impurities on each of these properties were illustrated in Fig 2.4. An overview of the effects of the impurities on the safety, costs, design and operation of the entire transport pipeline network (including compressors and pumps) was carried out in sections 2.2.2.2 and 2.2.2.4.

This section expands on the overview given in sections 2.2.2.1, 2.2.2.2 and 2.2.2.4 by detailed examination of the impact of pressure and temperature variation on those identified pure CO_2 properties as well as the effect of chemical impurities on each of them.

2.3.1 Thermophysical Properties of Pure CO_2

At the vicinity of the critical point, minor changes in temperature and pressure result in radical and huge changes in pure CO_2 properties. This makes the design and

operation of supercritical CO_2 pipeline more challenging and costlier than conventional natural gas pipelines where no phase change and radical variations in flow properties are expected (Serpa *et al.*, 2011; Seevam *et al.*, 2008; Luo *et al.*, 2014). Therefore, excellent knowledge of the peculiar behaviour of pure CO_2 at the vicinity of its critical point is a prerequisite for the optimal design and operation of facilities for the compression and pipeline transportation of supercritical carbon dioxide (Mertz *et al.,* 2005; Seevam *et al.*, 2008; Lazic *et al*., 2014; Munkejord et al., 2016; Tan *et al.*, 2016). In this section, the following CO_2 properties were studied: phase behaviour, density, compressibility, specific enthalpy and viscosity.

2.3.1.1 Phase Behaviour

A key property for the optimal design and operation of equipment for supercritical CO_2 transport pipeline is the vapour-liquid phase characteristic of carbon dioxide illustrated in the phase diagram below (Fig. 2.5).

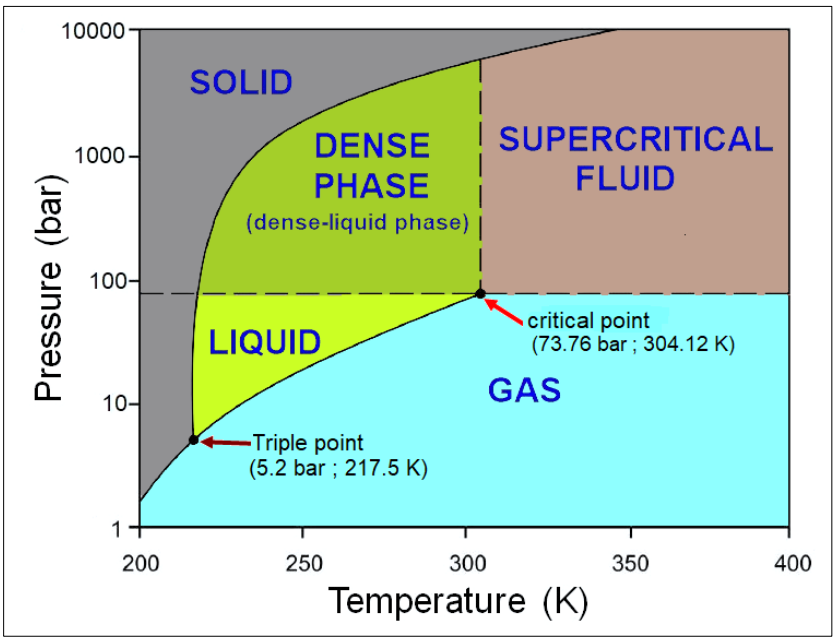

Fig.2.5 Phase diagram for pure carbon dioxide

The phase diagram is a graphic display of the distinct physical states in which carbon dioxide can either occur separately or co-exist together under different pressures and temperatures. As shown in Fig. 2.5, depending on the pressure and temperature, carbon dioxide can exist either as a solid, gas, liquid, “dense-liquid” or supercritical fluid. At certain pressure and temperatures, carbon dioxide can exist simultaneously in multiple phases. At the “triple point” where pressure is 5.2 bar and temperature is

217.5 K (-56 ºC), carbon dioxide exists simultaneously as a solid, gas and a liquid in thermodynamic equilibrium. Between the triple point and the “critical point”, the vapour-liquid equilibrium (VLE) curve marks the boundary between gas and liquid. Along this VLE curve, carbon dioxide exists as a mixture of gas and liquid. In thermodynamic terms, the VLE curve is not merely a line, but an “area” or “region” of the phase diagram that can expand in size under certain conditions (see section 2.3.2.1 for details). Therefore, the VLE curve, along with corresponding pressure and temperature conditions, is referred to as the “two-phase region” of the CO_2 phase envelope in most CCS research literature (Seevam *et al.*, 2008; Serpa *et al.*, 2011; Lazic *et al.*, 2014; Munkerjord *et al.*, 2016).

The “critical point” describes the thermodynamic state at which the properties of gas and liquid phases of a substance converge. In case of pure carbon dioxide, it occurs when the pressure and temperature is 73.76 bar and 304.12 K (30.97 ºC), respectively. Carbon dioxide exists as “dense-liquid” (also known as “dense phase fluid”) when its pressure is above the critical point while its temperature remains below the critical point. When both pressure and temperature are above the critical point, carbon dioxide is neither liquid nor gas, but a supercritical fluid with high density close to that of a liquid CO_2 and low viscosity close to that of gaseous CO_2. Supercritical CO_2 is also able to expand and fill up a confined space as if it were a gas. In other words, it is a highly compressible fluid (Svensson *et al*., 2004; Mertz *et al.,* 2005; Zhang *et al*., 2006; Lazic *et al.*, 2014). Compressors and booster pumps can be used to pressurize a supercritical fluid.

In the CCS context, “dense-liquid” is commonly treated as if it were a distinct phase. In reality, dense-liquid phase is just liquid phase exhibiting anomalous behaviour because of its proximity to the critical point. Normally, liquid is almost incompressible and its viscosity can be quite high. However, at the vicinity of the critical point, liquid becomes compressible and viscosity diminishes to the extent of being comparable to that of a gas. Hence, the term “dense-liquid” phase. Contrary to normal liquid behaviour, the density of a “dense-liquid” increases significantly with minor reductions in temperature (Seevam *et al.*, 2007 and 2008; Serpa *et al.*, 2011; Race *et al.*, 2012). In fact, “dense-liquid” behaviour is closer to that of a supercritical fluid than that of a liquid below the critical point.

As stated in section 2.2.1, for long-distance pipeline transportation, it is cost-effective to convey carbon dioxide in a dense-liquid or supercritical state. Therefore, designers and operators of pipeline transport systems need to have an excellent knowledge of phase behaviour of pure CO_2 with respect to pressure and temperature. This would be essential for:

- Designing pipelines with walls thick enough to withstand high pressures necessary for carbon dioxide to exist in supercritical or dense-liquid state
- Estimating the energy requirement for compressors tasked with converting carbon dioxide from a gas to either “dense” liquid or supercritical fluid
- Calculating the number of booster pumps needed at various repressurization points along the length of the pipeline to prevent pressure and temperature from dropping to levels corresponding to the two-phase region of CO_2 phase envelope.

The transformation of dense phase/supercritical CO_2 to a gas-liquid two-phase fluid is undesirable because it can lead to cavitation and slugging, which can damage compressors, pumps, valves and the pipeline itself (Oosterkamp and Ramsen, 2008; Knoope *et al.*, 2013; Lazic *et al.*, 2014; Okezue and Wang, 2016).

2.3.1.2 Fluid Density

Density is another important thermophysical property that affects the working processes of compressors, pumps and pipelines for CO_2 transportation.
A deep understanding of how this property changes with pressure and temperature is very important, especially at the vicinity of the critical point (Serpa *et al.*, 2011; Lazic *et al*., 2014; Munkerjord *et al.*, 2016; Tan *et al*., 2016).

As shown in Fig. 2.6, the density of pure CO_2 has a non-linear relationship with pressure and temperature. Density increases with increasing pressure and decreasing temperature. At the vicinity of the vapour-liquid equilibrium (VLE) curve, there are sharp discontinuities in density due to phase change from liquid to either mixed gas-liquid two-phase fluid or gaseous CO_2 (Zhang *et al.*, 2006; Seevam *et al.*, 2008; Wetenhall *et al.*, 2014b). As clearly marked in Fig. 2.6, where these sharp discontinuities are encountered, minor changes in pressure and temperature engender

rapid and large changes in fluid density. To avoid the formation of two-phase fluid and disruptive fluctuations in the density of the CO_2, the transport pipeline must be operated at pressure and temperature conditions far from the vicinity of the VLE curve.

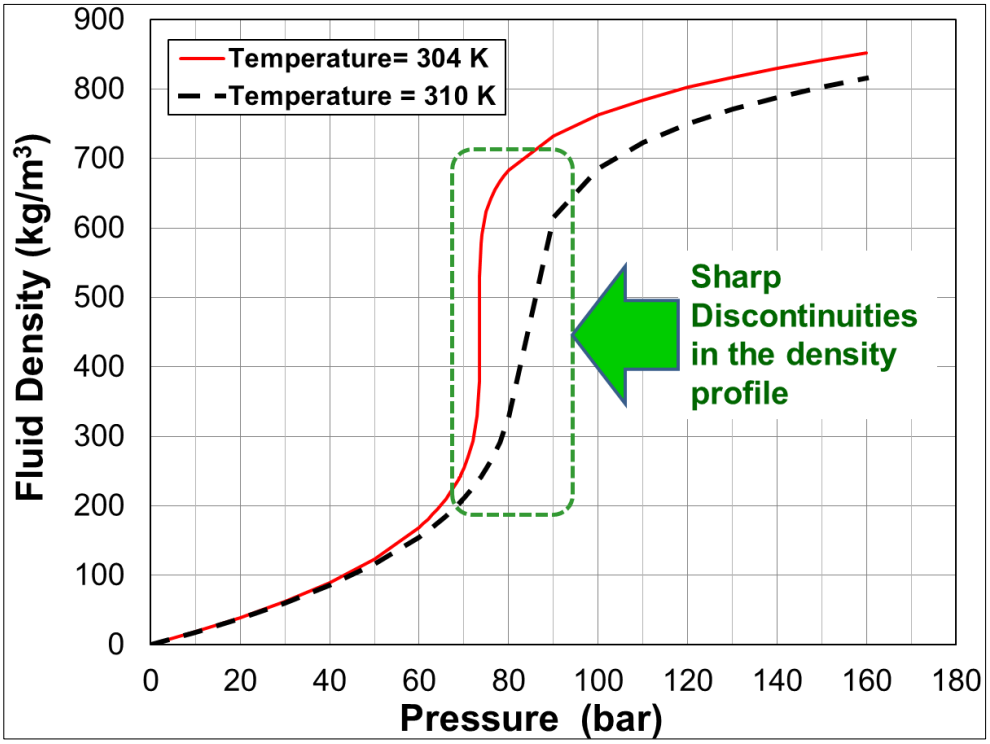

Fig.2.6 Density of pure CO_2 as a function of pressure and temperature

Pressure drop and flow rate are functions of density and flow area. Density decreases with increasing pressure drop and flow rate. Large pressure drops result in undesirable "choking" conditions and ultimately, two-phase flow. These problems can be avoided by inserting booster pumps at various locations along the length of the pipeline to re-pressurize the CO_2 stream periodically. This increases energy consumption and by extension, the operating cost of the pipeline network (Zhang *et al.*, 2006; Eickhoff *et al.*, 2014; Lazic *et al*., 2014, Tan *et al.*, 2016). For a given mass flow rate, density is inversely proportional to flow area. Therefore, subcooled liquid carbon dioxide can be transported in smaller-sized pipelines at a mass flow rate comparable to that of larger-sized pipeline used to transport gaseous carbon dioxide. Small-sized pipelines (i.e. pipes with small diameters) allows for savings in both capital and operating expenditure (Race *et al.*, 2012; Wetenhall *et al.*, 2014b). However, it should be noted that if CO_2 is liquid, the large pressure drop generated within that pipeline due to the liquid's high viscosity and the large energy costs of sub-cooling liquid CO_2 would offset the advantage gained in using small-sized

transport pipelines. Carbon dioxide in “dense-liquid” or supercritical phase is preferable since both have high densities and low viscosities at the same time, which allows transportation in small pipelines with generation of relatively low pressure drop (Jung and Nicot, 2010; Serpa *et al.*, 2011; Lazic *et al*., 2014). Similar to pipelines, the size of booster pumps are dependent on fluid density (Tan *et al.*, 2016; Okezue and Kuvshinov, 2017).

The thermodynamic path followed by a compressor is mainly a consequence of density. Density is directly proportional to the compressor’s discharge pressure and inversely proportional to its discharge temperature and isentropic efficiency (Okezue and Kuvshinov, 2018). Operating costs associated with compressor duty increases as density decreases (Eickhoff *et al.*, 2014; Tan *et al.*, 2016; Okezue and Kuvshinov, 2018).

Given its importance, knowledge of density is essential for the cost-effective design and operation of CO_2 transport pipeline network (Li and Yan, 2009; Li *et al.*, 2011b). Accurate calculation of density is prerequisite for designing bespoke compressors and pumps (Wilhelmsen *et al.*, 2012) or facilitating correct sizing and selection of ready-made compressors and pumps (Wadas, 2010). It is also a prerequisite for accurate fiscal metering of carbon dioxide transport pipelines (Munkerjord *et al.*, 2016; Collie *et al.*, 2017).

2.3.1.3 Specific Enthalpy

Enthalpy is an important parameter in pipeline, compressor and pump design. It describes the process of heat transfer in the pipeline used to transport CO_2 (Tan *et al.*, 2016). Actual work input of compressors and booster pumps are functions of change in enthalpy across the inlet and outlet ports of both machines. Compressor pressure ratio, isentropic efficiency and discharge temperature are affected by enthalpy (Wright *et al.*, 2010; Tan *et al.*, 2016; Okezue and Kuvshinov, 2018).

As stated in section 2.4.1, at the vicinity of the critical point, a slight change in pressure and temperature quickly results in large changes in the magnitude of various CO_2 properties including enthalpy. The steep sections of the curves on Fig. 2.7 demonstrate the dramatic effect of minor changes in pressure and temperature on specific enthalpy.

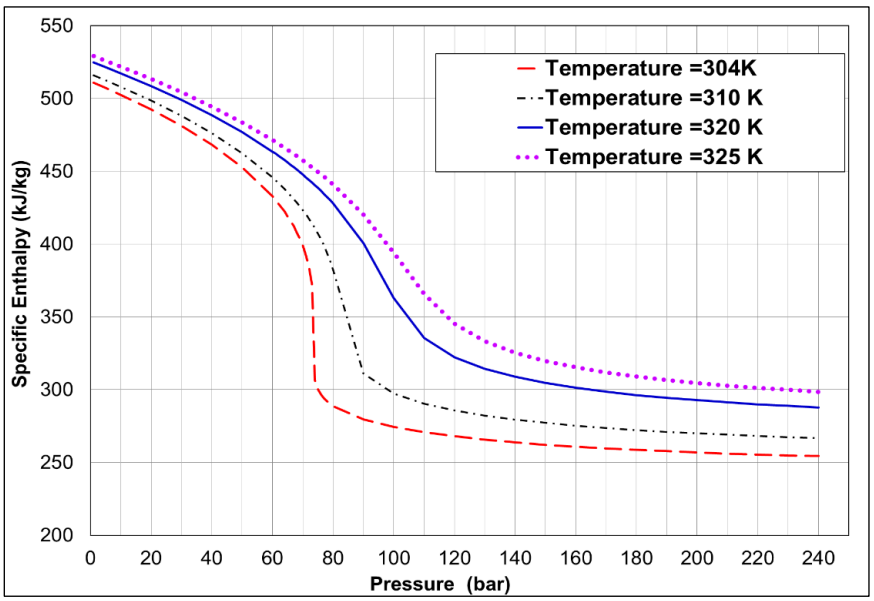

Fig.2.7 Specific enthalpy of pure CO_2 as a function of pressure and temperature

Equations of state (EoS) correlations generally encounter reliability problems when used to predict the behaviour of carbon dioxide under "dense-liquid" or supercritical fluid conditions. This is because these correlations cannot properly simulate the abrupt changes in CO_2 properties that occur in response to minor variations in pressure and temperature near the critical point (Imre *et al.*, 2015). The reliability problems of the EoS is worse when applied in the calculation of properties that vary non-monotonically with pressure and temperature. EoS correlations generate large errors when applied in calculating specific enthalpy (which varies monotonically) because it is derived from isobaric specific heat capacity, which varies non-linearly and non-monotonically near the critical point of CO_2 (Bergamini *et al.*, 2011; Imre and Tiselj, 2012; Okezue and Wang, 2016).

In the analysis of compressors and booster pumps, specific enthalpy is an important parameter (Lee *et al.*, 2016; Okezue and Kuvshinov, 2018). Many commercial software tools used in the design and evaluation of compressors and pumps are based on adiabatic or polytropic process equations using specific enthalpy values calculated with EoS correlations. These tools tend to perform well when applied in the analysis of machines operating under subcritical CO_2 conditions. However, when applied in the analysis of compressors operating at conditions close to the critical point of the pure or impure CO_2 fluid, the constituent adiabatic/polytropic equations of the software tools generate high calculation errors (Wright *et al.*, 2009 and 2010;

Pham *et al.*, 2016). To tackle this problem, an alternative method for calculating change in specific enthalpy (Δh) for an isentropic fluid compression process—which does not involve an equation of state (EoS) — was proposed in Chapter 4 of this PhD thesis. The proposed method also appears in Okezue and Kuvshinov (2017 and 2018).

2.3.1.4 Fluid Compressibility

Understanding the compressible behaviour of supercritical carbon dioxide is vital for the design and operation of equipment for the pipeline transportation of supercritical carbon dioxide. Compressibility factor (Z) is the property that is commonly employed in this regard. Absolute values of Z are merely corrective factors that quantifies the deviation of the specific volume of a real fluid from that of an ideal gas for a given pressure and temperature. By themselves, they cannot be used to describe the compressible behaviour (i.e. actual compressibility) of a working fluid. However, variation of compressibility factor (Z) with respect to pressure or temperature can be used to characterize the actual compressibility of a working fluid (Baltadjiev *et al.*, 2015; Okezue and Kuvshinov, 2018).

Actual compressibility is a quantitative indicator of the sensitivity of a fluid's specific volume to pressure change. In other words, actual compressibility depends on how high the specific volume of a fluid rises in response to pressure increment. Fluids that experience large increments in specific volume in response to pressure rise are considered "highly compressible". In contrast, fluids that experience little rise in specific volume are considered "incompressible".

Compressibility has a strong influence on the overall performance of compressors and booster pumps installed in the supercritical CO_2 pipeline network (Tan *et al.*, 2016; Okezue and Kuvshinov, 2018). This is because compressibility plays a role in shaping the thermodynamic path followed by compressors and booster pumps handling supercritical CO_2. Compressibility is inversely proportional to fluid density and directly proportional to energy losses and the actual energy input. This means that working fluids with higher compressibility and lower densities (e.g. gases) require a greater amount of energy to compress than working fluids with lower compressibility and greater densities (e.g. dense-liquids and supercritical fluids). High fluid compressibility translates to greater energy losses in compressors, which in turn,

result in lower isentropic efficiencies (Utamura *et al.*, 2012; Kim *et al.*, 2014; Wetenhall *et al.*, 2014; Okezue and Kuvshinov, 2018).

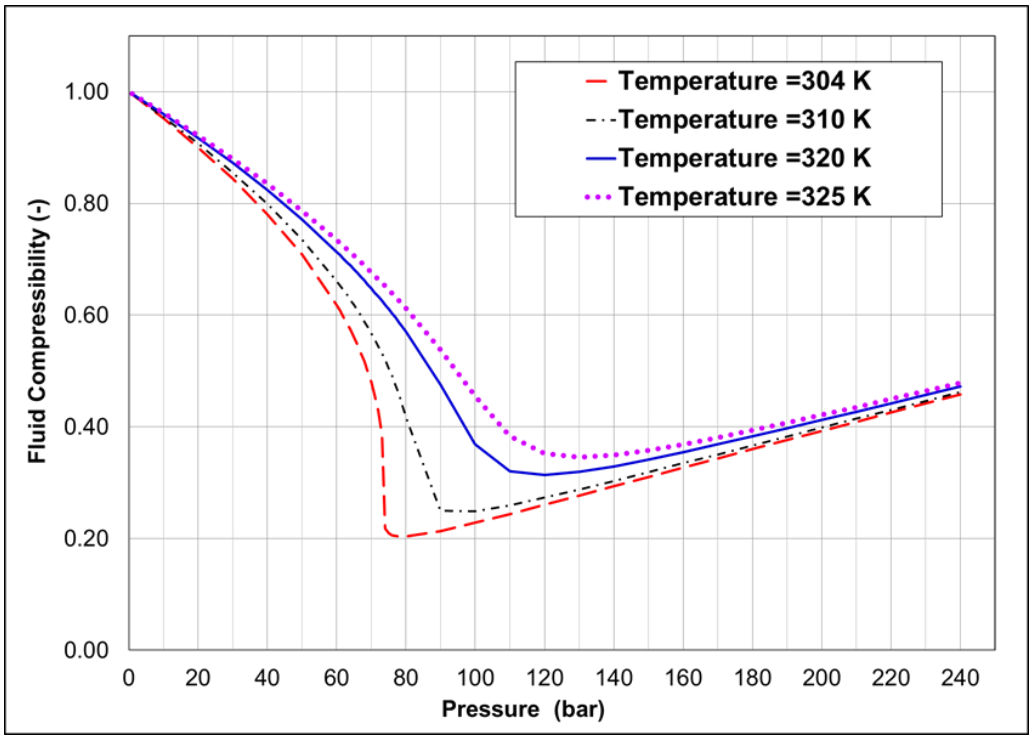

Fig.2.8 For a given temperature, pure CO_2 compressibility varies non-monotonically with pressure

Given its impact on pipeline volumetric delivery flow rate and the efficiency of compressors and booster pumps, knowledge of fluid compressibility is a prerequisite for designing and rightsizing compressors and booster pumps for supercritical CO_2 pipeline transportation (Bergamini *et al.*, 2011; Tan *et al.*, 2016; Okezue and Kuvshinov, 2018). As shown in the steep downward slope of the curves in Fig. 2.8, CO_2 compressibility can change abruptly in response to minor changes in pressure. Operating pipeline transport equipment at conditions where abrupt change in CO_2 compressibility occurs presents problems of fluid flow regulation. Rapid variation in fluid compressibility is accompanied by density fluctuations, which degrade the performance of the pipeline network system, especially components such as compressors and pumps. It is difficult to design a pipeline network to perform optimally under conditions where abrupt compressibility change occurs. Therefore, the common recommendation is to avoid unstable conditions where rapid fluid compressibility variations are likely to occur when operating a pipeline network. McCoy and Rubin (2008) and Witkowski *et al.* (2014) both suggest pipeline pressures above 86 bar in order to eliminate the possibility of abrupt compressibility change

occurring over a wide range of temperatures commonly encountered in the operation of a pipeline network system.

2.3.1.5 Viscosity

Viscosity quantifies the resistance of a fluid to flow. Because of its effect on frictional pressure drop, viscosity is one of the thermophysical properties considered in the optimal sizing of transport pipelines and determination of the energy requirement for compressors and booster pumps (Serpa *et al.*, 2011; Wetenhall *et al.*, 2014b; Tan *et al.*, 2016).

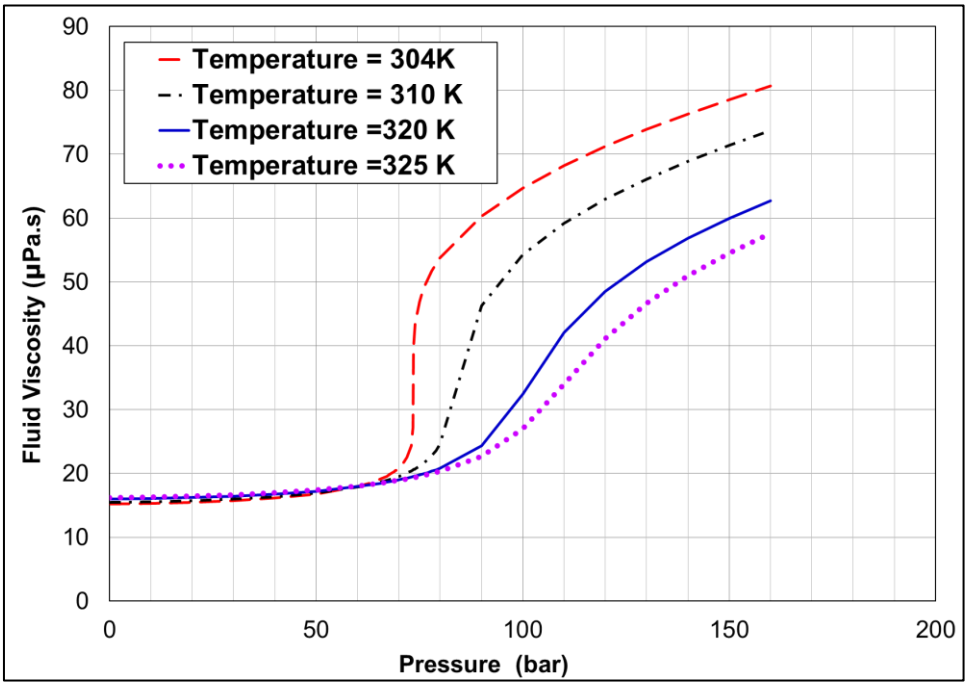

Fig.2.9 Viscosity of pure CO_2 as a function of pressure and temperature

Generally, viscosity of pure CO_2 increases non-linearly with increasing pressure and decreasing temperature as shown in Fig. 2.9. The steep sections of the curves in the graph demonstrate that small changes in pressure and temperature translate to dramatic changes in viscosity at the vicinity of critical point of pure CO_2.

As stated earlier, viscosity is considered in sizing pipe sections used in the construction of the pipeline transport network system and in the determination of energy requirement of compressors and pumps installed in that network system. This can be attributed to the fact that skin friction contact between the working fluid and internal walls of each pipe sections contribute to the overall pressure drop across the pipeline network. Energy requirement of compressors and booster pumps is

dependent on the overall pressure of the pipeline network (Eickhoff *et al.*, 2014). Greater pressure drop is compensated either by raising the discharge pressure of compressors or by increasing the number of booster pumps mounted at points along the pipeline. Either way, energy consumption of compressors/booster pumps increases significantly. Skin friction is directly proportional to fluid viscosity. Therefore, viscosity reduction is one method of reducing overall pressure drop and energy requirement of compressors and pumps (Zhang *et al.*, 2006; Li *et al.*, 2011b; Wetenhall *et al.*, 2014b).

However, it is worth noting that variation of the overall pressure drop in the pipeline is a consequence of the synergetic effects of both viscosity and density of CO_2. An increase in fluid density causes a decrease in the velocity of CO_2 flowing in the pipeline, which in turn, decreases pressure drop. Fluid velocity is greater contributor to the generation of pressure drop than skin friction. In other words, pressure drop is more sensitive to variation in fluid density than it is to an equivalent variation in fluid viscosity (Oosterkamp and Ramsen, 2008; Tan *et al.*, 2016).

In order to keep capital costs (CAPEX) low as possible, viscosity and density should be considered together when sizing pipelines for CO_2 transportation. Operating costs (OPEX) can be minimized by transporting CO_2 in supercritical or “dense-liquid” phase. As explained in section 2.2.1, “dense-liquids” and supercritical fluids have the double advantage of having high density and very low viscosity. These properties translate to lower pipeline pressure drop and consequently, lower energy requirement for both compressors and pumps (Seevam *et al.*, 2007; Serpa *et al.*, 2011; Eickhoff *et al.*, 2014).

2.3.2 Impact of Chemical Impurities on CO_2 Thermophysical Properties

In section 2.2.2.1, energy requirement for compressors and booster pumps; repressurization/recompression distance; pipeline delivery capacity; corrosion rate and fracture propagation rate are mentioned as examples of design and operational parameters of transport pipeline network systems that increase with higher concentration of certain chemical impurities within anthropogenic CO_2. As explained in 2.2.2.2 and 2.2.2.4, an increase in any of the above-mentioned parameters under supercritical conditions have serious negative implications for the economics of designing, constructing and operating a supercritical CO_2 pipeline network system.

Design parameters such as fracture propagation and corrosion rates heighten risks to the health and safety of people living in areas through which the pipeline is routed.

Impurities are able to increase the above-mentioned design and operational parameters of the transport pipelines by intensifying the radical variations in the normal thermophysical properties of CO_2 that occur when minor changes in temperature and pressure are made at the vicinity of the critical point.

Sections 2.3.2.1 to 2.3.2.5 demonstrates the effect of these impurities on phase behaviour, density, enthalpy, compressibility and viscosity in graphic details.

2.3.2.1 Effect of Impurities on the Phase Behaviour of CO_2

The design and operation of pipeline network systems for the purpose of transporting anthropogenic CO_2 in the form of a dense-liquid or supercritical fluid requires a good understanding of the effect of various impurities on phase behaviour (Seevam *et al.*, 2008; Goos *et al.*, 2011; Lazic *et al.*, 2014; Tan *et al.*, 2016).

The impact of various impurities on phase behaviour of CO_2 can be observed in the shifting of the critical point and the changing size of the gas-liquid two-phase region within the phase diagram (See Fig. 2.10). The degree of change in phase behaviour is dictated by the type, concentration and combination of impurities present since these impurities interact both with CO_2 and each other (Jung and Nicot, 2010; Race *et al.*, 2012; Munkejord *et al.*, 2016).

The position of the critical point and size of the two-phase region is not the only thing affected by the presence of impurities within CO_2. The size of the “dense-liquid” and supercritical phase regions of the CO_2 phase diagram is also affected as well. Impurities that cause an upward shift in the critical point (i.e. an increase both the critical pressure and critical temperature) increases the size of the two-phase region while simultaneously decreases the size of the supercritical region within the CO_2 phase diagram, thereby narrowing the optimal operating envelope of the transport pipeline network. The reverse is true for the kind of impurities that result in the downward shift of the critical point—i.e. decrease in critical pressure and critical temperature (Seevam *et al.*, 2007; Wetenhall *et al.*, 2014b).

All chemical impurities that can be expected to be found in anthropogenic CO_2 increases the size of the two-phase region of the phase envelope. However, the thermophysical properties of the chemical impurities play a role in this.

As shown in Fig. 2.10, the presence of impurities such as hydrogen, nitrogen, methane and carbon monoxide cause the enlargement of the two-phase region and its relocation above that of pure CO_2. Consequently, the critical point of CO_2 mixtures is higher than that of pure CO_2.

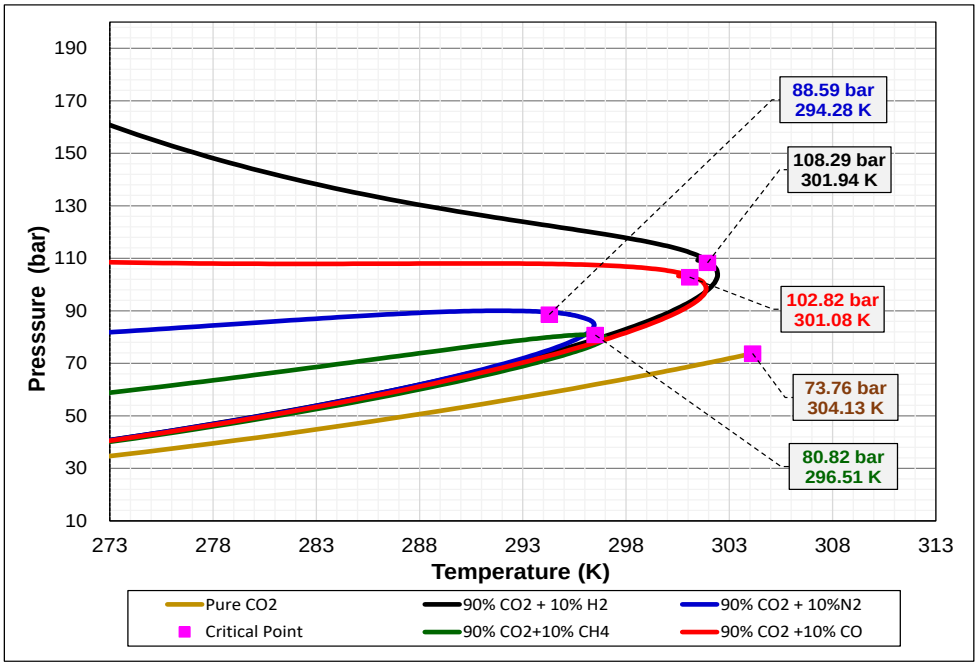

Fig.2.10 Effect of impurities on the phase envelope of CO_2 (Okezue and Kuvshinov, 2018)

All these effects can be attributed to fact that each of the above-mentioned impurities have lower molar masses than that of pure CO_2. The greater the difference between the molar masses of the impurity and pure CO_2, the larger the size of the two-phase region of the mixture and accordingly, the higher the critical point. As shown in Fig. 2.10, a binary mixture of CO_2 (44.01g/mol.) and hydrogen (2.016 g/mol.) will have a larger two-phase region and higher critical point than those of a binary mixture of CO_2 (44.01 g/mol.) and methane (16.04 g/mol.). As stated earlier, impurities that enlarge the two-phase region simultaneously cause the shrinkage of the supercritical region (Seevam *et al.*, 2007; Lazic *et al.*, 2014). Therefore, the size of the supercritical region for binary CO_2/H_2 mixture is smaller than that of the CO_2/CH_4 mixture.

The effects of impurities on CO_2 phase behaviour described above have serious consequences for design and operation of the transport pipeline system. Any increase in the size of the two-phase region of the CO_2 phase envelope increases the risk of single-phase supercritical fluid transforming into a gas-liquid two-phase fluid if there is a slight pressure drop in the pipeline (Wetenhall *et al*., 2014b; Martynov *et al.*, 2016; Lemontzoglou *et al.*, 2017; Okezue and Wang, 2017). As explained in section 2.2.2.4, the only way to avert the risk of two-phase formation is to ensure that the impure CO_2 mixture remains in supercritical phase. This can be achieved by maintaining a very high pipeline operating pressure, far above the critical pressure of the CO_2 mixture.

The critical pressures of the CO_2 mixtures are greater than that of pure CO_2. Therefore, a pipeline network transporting CO_2 mixtures must be maintained at much higher operating pressures than would be the case if the pipeline were carrying pure CO_2. This means that pipelines carrying CO_2 mixtures will need thicker pipe walls than those carrying pure CO_2 to arrest any potential fracture propagation and rupture. Capital expenditure (CAPEX) increases as the pipe wall gets thicker. Therefore, a pipeline for CO_2 mixtures will cost more to build than one used for pure CO_2 (Demofonti and Spinelli, 2011; Cosham, 2012; Cooper, 2012; Race *et al.*, 2014). Similarly, due to high pressures involved, the energy requirement for compressors and pumps installed in pipeline network is much greater when the working fluid is CO_2 mixture rather than pure CO_2. In other words, operating expenditure (OPEX) of compressors and pumps are greater when the working fluid is CO_2 mixture rather than pure CO_2 (Oosterkamp and Ramsen, 2008; Lazic *et al.*, 2014; Lemontzoglou *et al.*, 2017; Okezue and Kuvshinov, 2018).

2.3.2.2 Effect of Impurities on Density of CO_2

As explained in section 2.3.1.2, density has a non-linear relationship with pressure and temperature. Sharp discontinuities in the density are encountered near the vapour-liquid equilibrium (VLE) region of CO_2 phase envelope. To avoid the formation of two-phase fluid and disruptive flow rate fluctuations, the transport pipeline must be operated at pressure and temperature conditions far from the vicinity of the VLE region.

As shown in Fig. 2.11, the presence of impurities such as nitrogen, hydrogen, methane and carbon monoxide have the effect of decreasing the overall density of the impure CO_2 stream. This results in greater temperature and pressure drops within the pipeline than would be the case if the working fluid had been pure CO_2 stream (Seevam *et al.*, 2007; Oosterkamp and Ramsen, 2008).

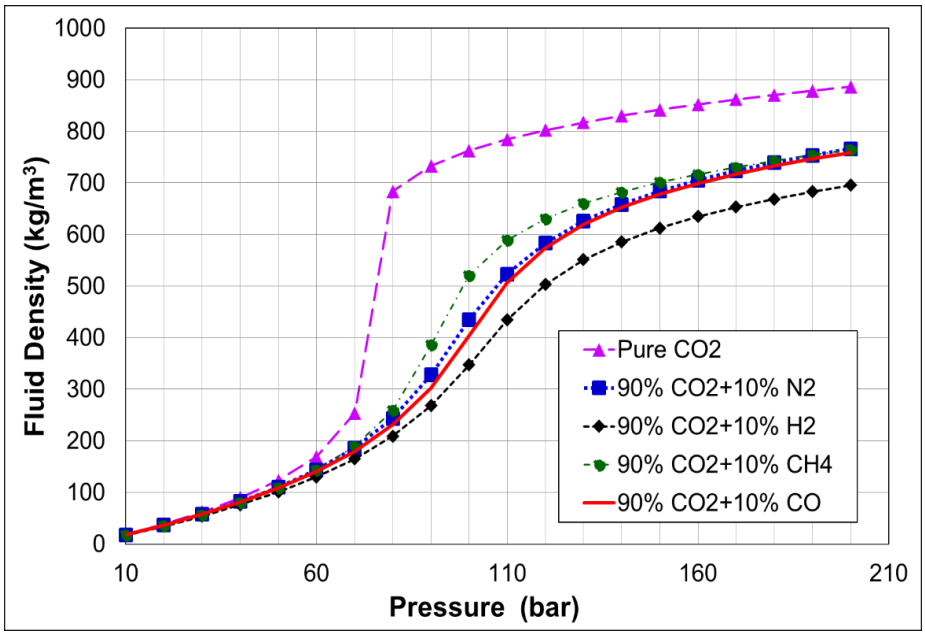

Fig.2.11 Effect of impurities on the density of CO_2 at 304 K

The aforementioned impurities within the CO_2 mixture enlarges the two-phase region and shifts the critical point above that of pure CO_2 as depicted in Fig. 2.10. These realities combined with the greater temperature and pressure drop means that the risk of two-phase fluid formation and disruptive fluctuations in fluid flow rate within the transport pipeline carrying CO_2 mixtures is far greater than in a pipeline carrying pure CO_2. One way of averting these risks is to install more booster pumps at shorter intervals along the length of the pipeline. This will ensure that CO_2 mixture is repeatedly re-pressurized at intervals to ensure that pipeline pressure never falls below the critical point, thereby preventing the supercritical fluid from evolving into a two-phase fluid (Race *et al.*, 2012; Eickhoff *et al.*, 2014). Pipe diameter is inversely proportional to fluid flow rate and pressure drop. Therefore, an increment in the pipe diameter is an alternative to raising the number of booster pumps in the pipeline network. Either way, the costs of the pipeline increases. The first alternative (i.e. higher number of pumps) results in higher operating expenditure (OPEX) while the

second alternative (i.e. increasing pipe diameter) results in greater capital expenditure (CAPEX). Both alternative solutions are discussed in details in section 2.2.2.4.

Separate from its impact on design and operation of the pipeline itself, the density reduction resulting from the addition of impurities to pure CO_2 has a profound effect on the thermodynamic path followed by compressors and booster pumps and consequently, their performance (Eickhoff *et al.*, 2014; Tan *et al.*, 2016; Martynov *et al.*, 2016; Okezue and Wang, 2016). Reduction in density results in a decrease in the discharge pressure; an increase in discharge temperature; greater energy losses; a decline in isentropic efficiency and an increase in overall energy consumption of both machines. Energy consumption and operating costs are further increased, when the speed of both machines are increased to raise and maintain pipeline pressure above the critical point of the CO_2 mixture (Okezue and Wang, 2016; Okezue and Kuvshinov, 2017 and 2018).

2.3.2.3 Effect of Impurities on Specific Enthalpy of CO_2

The addition of impurities to pure CO_2 has a significant effect on change in specific enthalpy of the working fluid within the pipeline network system. Heat transfer, energy consumption, production of heat of compression, isentropic efficiency are functions of change in specific enthalpy (Wright *et al.*, 2010; Tan *et al.*, 2016; Okezue and Kuvshinov, 2018).

Nitrogen, hydrogen, methane and carbon monoxide have lower molar masses than carbon dioxide. Their addition as impurities to CO_2 raise the absolute values of specific enthalpy (h) as shown in Fig. 2.12. More importantly, these impurities increase the change in specific enthalpy (Δh) over the compression process of compressors and booster pumps or expansion process (i.e. fluid flow) in the supercritical CO_2 pipeline. This results in greater heat of compression; higher energy losses; reduction in isentropic efficiency in compressors and booster pumps; and ultimately a large increase in their energy consumption. In other words, the operating costs of running compressors and booster pumps increases significantly when the supercritical working fluid changes from pure CO_2 to impure CO_2 mixtures as a result of increased change in specific enthalpy (Ulfnes *et al.*, 2003; Martynov *et al.*, 2016; Lemontzoglou *et al.*, 2017; Okezue and Wang, 2017).

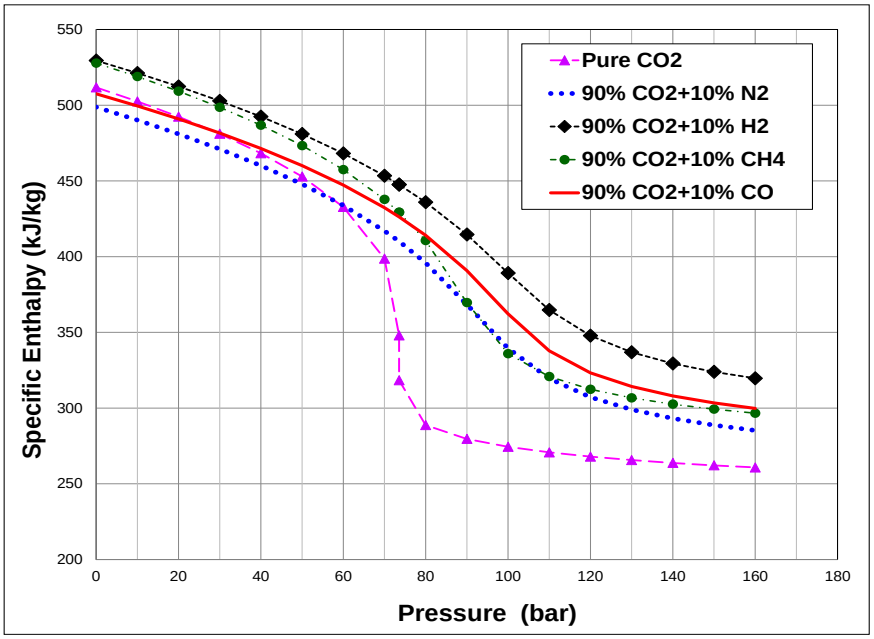

Fig.2.12 Effect of impurities on specific enthalpy of CO_2 at 304 K

Highly accurate mathematical model is necessary for optimal design of bespoke compressors/booster pumps or correct sizing and selection of ready-made compressors/ booster pumps. A prerequisite for the development of such a model is reliable method of calculating the properties of the working fluid, especially at supercritical conditions. However, as explained in section 2.3.1.3, equations of state (EoS) correlations struggle to accurately predict enthalpy of pure CO_2 at the vicinity of the critical point because they are not able to handle large abrupt changes in this particular fluid property which occur in response to minor shifts in pressure and temperature (Imre and Tiselj, 2012; Imre *et al.*, 2015). The presence of impurities in the supercritical CO_2 stream expands the VLE region of the phase envelope, thereby extending the range of pressure and temperature conditions at which abrupt changes in enthalpy occur. This has the overall effect of exacerbating the reliability problems that EoS correlations encounter when applied in enthalpy calculation.

2.3.2.4 Effect of Impurities on Fluid Compressibility of CO_2

As stated in section 2.3.1.4, compressibility is a measure of the sensitivity of a fluid's specific volume to pressure change. Pure CO_2 compressibility varies non-linearly with pressure and temperature. More importantly, for a given temperature, it varies non-monotonically with pressure as demonstrated in Fig. 2.8.

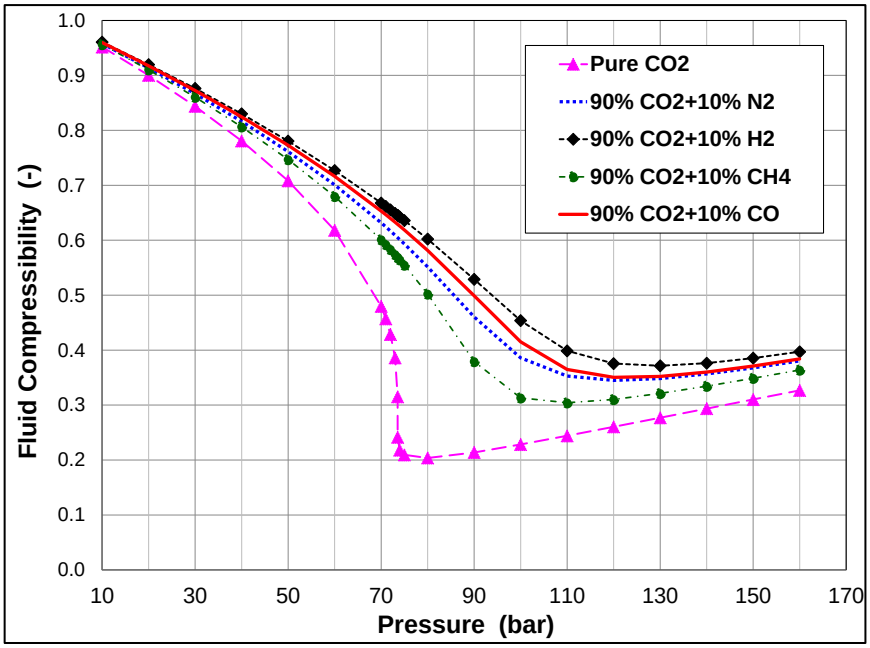

Fig.2.13 Effect of impurities on compressibility of CO_2 at 304K

Compressibility must be taken into account when designing and rightsizing compressor and pumps for a supercritical CO_2 pipeline (Wadas, 2010; Bergamini *et al.*, 2011; Tan *et al.*, 2016; Okezue and Kuvshinov, 2018). This is because of its impact on the efficiency, energy requirement and operating costs of installed compressors and pumps.

CO_2 compressibility is sensitive to the presence of any chemical impurity (Oosterkamp and Ramsen, 2008). As demonstrated in Fig. 2.13, the addition of impurities—nitrogen, hydrogen, methane and carbon monoxide—to pure supercritical CO_2 increases the overall fluid compressibility for a given pressure and temperature. Increment in fluid compressibility translates to reduced isentropic efficiency, greater energy losses and an increase in the overall energy requirement of compressors and booster pumps (Utamura *et al.*, 2012; Kim *et al.*, 2014; Wetenhall *et al.*, 2014; Okezue and Kuvshinov, 2018).

Apart from compressors and pumps, compressibility also affects the hydraulic performance of the transport pipeline itself. This is because of the impact compressibility has on the pipeline delivery capacity (i.e. volumetric flow rate of the working fluid). The steep downward slope of curves in Fig 2.8 demonstrate that at the vicinity of the critical point of pure CO_2, fluid compressibility will change abruptly in response to slight variations in pressure. These abrupt variations in pure CO_2

compressibility are accompanied by density fluctuations, which present flow regulation problems and vibrations within the transport pipeline, representing a general degradation in performance (Imre *et al.*, 2015). Operating the pure CO_2 supercritical pipeline at pressures above 86 bar have been proposed to eliminate this problem (McCoy and Rubin, 2008; Witkowski *et al.*, 2014).

The presence of impurities in the CO_2 stream increases fluid compressibility (Fig. 2.13) and expands the VLE region of the phase envelope (Fig. 2.10), thereby extending the range of pressure and temperature conditions at which abrupt changes in compressibility occur. This means that pipelines carrying impure CO_2 may have to operate at pressures above 100 bar to avoid unstable conditions that cause flow regulation problems and vibration (Imre *et al.*, 2015; Okezue and Kuvshinov, 2018). Maintaining operating pressures as high as 100 bar will require a tougher pipeline to prevent fracture. This can be achieved by using a pipeline with thicker walls or a pipeline made from a stronger material (Cosham, 2012; Race *et al.*, 2012). Either solution will lead to higher capital expenditure (CAPEX). Moreover, the generation and maintenance of high operating pressures leads to greater energy demand and operating expenditures (OPEX) for compressors and booster pumps (Oosterkamp and Ramsen, 2008; Nimtz *et al.*, 2010; Lazic *et al.*, 2014; Okezue and Kuvshinov, 2018).

2.3.2.5 Effect of Impurities on Viscosity of CO_2

As demonstrated in section 2.3.1.5, pure CO_2 fluid viscosity increases non-linearly with increasing pressure and declining temperature. Like other CO_2 properties, near the critical point, viscosity is hypersensitive to minor pressure and temperature change. Even without any further changes in pressure and temperature around the critical point, viscosity will increase or decline abruptly depending on the type of chemical impurities added to pure CO_2 (Oosterkamp and Ramsen, 2008; Wetenhall *et al.*, 2014b). If the impurities added have molar masses greater than that of pure CO_2 then the viscosity will increase. Nitrogen dioxide and sulphur dioxide are examples of such impurities. Conversely, if the impurities added have lower molar masses than that of pure CO_2 (e.g. N_2, H_2, CH_4 and CO), then the viscosity will decline as illustrated in Fig. 2.14.

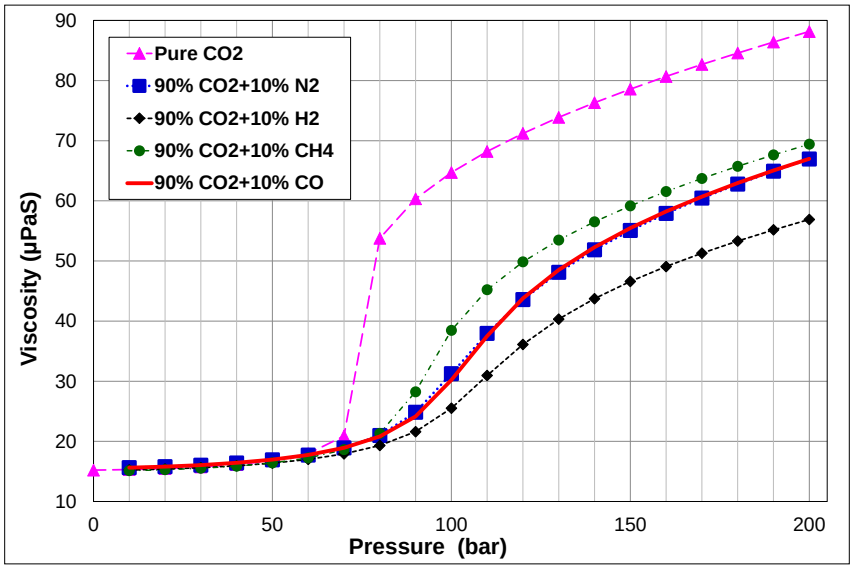

Fig.2.14 Effect of impurities on the viscosity of CO_2 at 304 K

The effect of impurities on CO_2 viscosity have serious consequences for the operation of transport pipeline networks. A CO_2 mixture containing impurities that cause viscosity to increase will generate greater skin friction on the internal pipe wall surface. Skin friction contributes to the overall pipeline pressure drop and is necessary in determining the amount of input energy required by compressors and booster pumps to compensate for pressure losses across the length of the pipeline (Li *et al.*, 2011b; Eickhoff *et al.*, 2014). However, it is important to note that variation of the overall pressure drop in the pipeline is a consequence of the synergetic effects of both viscosity and density. For dense-liquids and supercritical fluids, pressure drop is far more sensitive to variation in fluid density than it is to an equivalent variation in fluid viscosity (Oosterkamp and Ramsen, 2008; Tan *et al.*, 2016). A study performed by Tan *et al.* (2015) showed that a 20% increase in fluid density translates to 16.9% increment in pressure drop while a 20% increase in fluid viscosity results in a mere 2.7% increment in pressure drop. In other words, variation in pipeline pressure drop and the consequent energy requirement for compressors and pump is primarily driven by the impact of impurities on supercritical CO_2 density. For a given pressure and temperature, each of the binary CO_2 mixtures in Fig. 2.14 have lower fluid viscosity than that of pure CO_2. Yet this does not lead to lower pipeline pressure drops nor lower compressor/pump energy consumption for supercritical CO_2 mixtures compared to pure supercritical CO_2. This is because the same set of impurities responsible for decreasing pressure drop by reducing CO_2 viscosity are also responsible for increasing pressure drop by several folds by reducing CO_2

density. Therefore, the adverse effects of density reduction counteract the advantages of viscosity reduction on pipeline pressure drop.

Fluid viscosity variation plays a bigger role in the internal working processes of supercritical CO_2 compressors and booster pumps than it does in the expansion (i.e. flow) of supercritical CO_2 in the pipeline. Flow separation and formation of eddies within the compressor and booster pumps are influenced by fluid viscosity. A fraction of the input energy supplied to supercritical CO_2 compressors and pumps are dissipated as heat due to skin friction contact of the working fluid with the solid surfaces of the rotating impeller and interior walls of the compressor housing (Okezue and Kuvshinov, 2018). Therefore, the input energy requirements of booster pumps and compressors are affected by supercritical CO_2 viscosity (Li *et al.*, 2011b, Wetenhall *et al.*, 2014a). However, these viscosity effects are weak when compared to dominant role of fluid density in determining both heat transfer and overall energy requirement in both machines (Tan *et al.*, 2016; Okezue and Kuvshinov, 2018). In other words, the potential benefits of viscosity reduction due to presence of certain impurities in CO_2 mixtures is neutralized by the fact that density reduction by the same impurities increases kinetic energy directly absorbed by the compression process as well as energy wasted in overcoming friction, leakage and shock losses (Okezue and Kuvshinov, 2018).

2.4 TRACKING PROGRESS IN CO_2 PIPELINE TRANSPORT RESEARCH

Several research studies published on efforts being made to foster greater understanding of the challenges of designing and operating CO_2 transport pipeline systems. Many of these studies are based on the development of complex hydraulic models, which are then used to simulate the behaviour of CO_2 transport pipeline networks at operating conditions within the vicinity of the critical point. A corollary of studies involving the development of hydraulic models is the research on different kinds of existing equations of state (EoS) correlations and the development of new ones. This is because the reliability of any hydraulic pipeline model is strongly dependent on the ability of EoS correlations to accurately calculate the thermophysical properties of pure CO_2 at the vicinity of the critical point and simulate dramatic changes in these properties when impurities are present in the CO_2 stream as described in section 2.3.

In section 2.4.1, published studies on different EoS correlations used for calculating the thermophysical properties of pure and impure CO_2 are reviewed. Section 2.4.2 presents a review of published studies in which different hydraulic models are used in the analysis of those design and operational challenges of CO_2 pipeline transportation first described in section 2.2.

2.4.1 Review of Studies on the Prediction of Properties of CO_2 and its mixtures

Equations of State (EoS) correlations provide the underpinning mathematical relationship between the pressure, volume, temperature and composition of a chemical substance. In the context of CCS, these correlations are necessary for calculating CO_2 thermodynamic properties such as enthalpy, density and viscosity, which are needed as inputs for hydraulic equations used in describing flow of CO_2 stream at supercritical or dense phase conditions. However, near the critical point, a slight change in pressure or temperature can engender in a large change in aforementioned CO_2 properties. This makes accurate property calculation of CO_2 in supercritical or dense phase difficult (Wright *et al.*, 2009, Aritomi *et al.*, 2011; Lazic *et al.*, 2014; Lee *et al.*, 2014). When impurities are present in the CO_2 stream, the difficulty in property calculation is further exacerbated.

Reliable calculation of the CO_2 properties is essential for the cost-effective design and operation of CO_2 transport pipeline network (Li and Yan, 2009a; Li *et al.*, 2011b; Demetriades and Graham, 2016). Accurate prediction of density and pressure drop is necessary for designing compressors and pumps (Wilhelmsen *et al.*, 2012) or facilitating correct sizing and selection of ready-made compressors and pumps (Wadas, 2010).

Given their importance, several types of EoS correlations published in open literature have been analysed by various authors and while no single correlation can perform satisfactorily for all thermodynamic conditions, some correlations will perform better than others under certain conditions (Oosterkamp and Ramsen, 2008; Li *et al.*, 2011a and 2011b; Luo *et al.*, 2014; Demetriades and Graham, 2016). For instance, the highly complex Span and Wagner (SW) correlation produces highly accurate results when the CO_2 stream is pure, but difficult to extend to CO_2 stream containing impurities (Li and Yan, 2009b; Demetriades et al., 2013; Diamantonis *et al.*, 2013a;

Munkejord *et al.,* 2016). Peng-Robinson (PR) and Soave-Redlich-Kwong (SRK) correlations are widely used because of their compelling simplicity, but are generally inaccurate for calculating pure and impure CO_2 at supercritical and dense liquid phase conditions (Li *et al.*, 2011a; Demetriades *et al.*, 2013; Diamantonis *et al.*, 2013a). Benedict-Webb-Rubin (BWR) and Lee-Kessler (LK) generally perform most CO_2 property calculations more accurately than Peng-Robinson (PR). However, there is a remarkable exception— PR performs much better than BWR and LK when applied in the prediction of vapour-liquid phase equilibrium (VLE) boundaries. (Li *et al.*, 2011a).

GERG-2004/2008 and SAFT equations of state (EoS) have shown better potential for highly accurate prediction of properties of impure CO_2 mixtures (Diamantonis *et al.*, 2013a; Ramos *et al.*, 2014). However, despite its high level of accuracy, SAFT-based EoS has not been studied and developed sufficiently for widespread use in modelling CCS transport pipeline at dense or supercritical phase conditions (Luo *et al.*, 2014). On the other hand, GERG-2004 and its improved variant, GERG-2008 are both recognized as the international reference EoS correlations for natural gas (Wilhelmsen *et al.*, 2012; Aursand *et al.*, 2016; Gernert and Span, 2016). Researchers such as Goos et al. (2011), Chaczykowski and Osiadacz (2012), Witkowski and Majkut (2012), Wetenhall *et al.* (2014a) and Okezue and Kuvshinov (2017) have successfully applied GERG-2004/2008 in calculating properties of CO_2 mixtures relevant to CCS.

Despite being the most accurate EoS correlation widely available for impure CO_2 property prediction, GERG-2004 and GERG-2008 both exhibit significant shortcomings when applied in to certain properties and unique mixtures. They do not perform very well when applied in the calculation of thermophysical properties of humid CO_2 mixtures. There are significant calculation errors when used to predict the vapour-liquid phase equilibrium (VLE) boundaries of dry CO_2-rich mixtures. (Li et al., 2011a; Aursand *et al.*, 2013; Løvseth et al., 2014; Gernert and Span, 2016). In response to the aforementioned shortcomings, the EoS-CG correlation was created (Gernert and Span, 2010 and 2016). Span *et al.* (2013), Aursand *et al.* (2016) and Munkejord *et al.* (2016) demonstrated that EoS-CG correlation performs better than GERG-2008 when used to predict VLE boundaries of dry CO_2-rich mixtures and

thermodynamic properties of binary CO_2/H_2O mixtures. However, the application of EoS-CG is still restricted to certain mixtures and remains under development (Aursand *et al.*, 2016; Gernert and Span, 2016; Munkejord *et al.*, 2016; Ke *et al.*, 2017).

The accuracy of EoS correlations are often tied to the degree of their complexity. BWRS EoS, LK EoS, SW EoS, GERG-2004/2008 EoS and EoS-CG are highly complex in structure and generally more accurate than the much simpler PR EoS and SRK EoS. However, complex EoS correlations have the disadvantage of being computationally demanding (Li *et al.*, 2011a; Islam and Carlson, 2012; Diamantonis *et al.*, 2013a and 2013b). In order to tackle this issue, Demetriades *et al.* (2013) proposed a new EoS correlation with a mathematical structure comparable in simplicity to that of PR EoS and yet is capable of predicting the properties of pure CO_2 at dense phase conditions with a level of accuracy similar to that of SW EoS. Demetriades and Graham (2016) extended the new EoS correlation to render it capable of predicting properties of CO_2 in binary mixtures with N_2, O_2 and H_2. While this new equation of state shows promise, it remains under development and yet to be validated extensively.

2.4.2 Review of Modelling and Analysis of CO_2 Pipeline Transportation

Many research studies have been published on CO_2 pipeline transport covering design and operational issues. Feasibility studies conducted by researchers such as Svensson *et al.* (2004), McCoy and Rubin (2008), Demofonti and Spinelli (2011) and Lazic *et al.* (2014) confirmed that conveyance by pipeline is the best of the alternative options available for carbon dioxide transportation in the CCS context. These studies also show that for long distance pipeline transportation, it is best to have the carbon dioxide in supercritical or dense phase. Although, Lazic *et al.* (2014) noted that for short distances and reuse conditions, CO_2 pipeline transport in gaseous phase is more economical than in liquid or supercritical phase. This is because short distance transportation does not justify the energy costs (i.e. additional OPEX) that will be incurred if gaseous CO_2 were to be compressed into supercritical/dense phase.

The economic design and operation of the transport pipeline relies heavily on the accurate modelling of the internal fluid flow and working processes of a typical pipeline network and the impact of CO_2 stream's purity level on them. Likewise,

reliable prediction of pipeline performance under various conditions is dependent on the accuracy of the models used. Bearing that in mind, researchers have developed several pipeline models with varying levels of accuracy.

Seevam *et al.* (2008 and 2010) studied all three main carbon dioxide capture technologies—pre-combustion, post-combustion and oxy-fuel combustion— and categorized the resulting types of impurities in the CO_2 stream channelled into a transport pipeline. The impact of those impurities on key design and operation issues such as pipeline sizing, repressurization distance and energy requirement for compressor and pumps were analysed with the aid of a 1-D steady-state model of a straight horizontal pipeline. Nimtz *et al*. (2010) investigated the temperature, pressure, density and velocity profile along the length of the pipeline carrying pure CO_2 under different operating scenarios using a steady state model of a straight horizontal transport pipeline. They specified the operating conditions under which two-phase fluid flow could occur within the pipeline and how this undesirable flow regime can be avoided. The authors also examined the effects of nitrogen and oxygen impurities on the CO_2 properties– density and phase behaviour, but did not study their effects on the working process of the CO_2 horizontal pipeline. Wetenhall *et al.* (2014b) used a steady-state 1-D model to investigate the effect of various impurities in the CO_2 stream on the diameter and length of the pipeline. They found that impurities such as N_2, O_2, CO, H_2 and CH_4 would require the optimum diameter of a transport pipeline to be increased by 4%–6% compared to the diameter of a pure CO_2 pipeline. This increase in pipeline diameter obviously drives up design costs. Similarly, impurities associated with oxy-fuel combustion capture increase the capital cost per kilometre length of pipeline by up to 16%.

While largely sufficient for studying pipeline design issues, steady-state models are not adequate for predicting transient operational events such as start-up, shut-down, rapid depressurization, valve blockage and variation of fluid flow rate. This is because steady-state models do not capture the dynamics of fluid flow within the pipeline. To tackle this problem several authors have developed unsteady models to simulate the dynamic behaviour of CO_2 transport pipeline networks. Liljemark *et al.* (2011) used a dynamic model to simulate load change, start-up, planned shut-down, normal operation and emergency shut-down scenario in a transport pipeline carrying a mixture of 98% CO_2 and 2% N_2. They found from simulation results that quick shut-

down and load change increased the risk of two-phase fluid flow in the pipeline. Chaczykowski and Osiadacz (2012) developed a far more detailed dynamic 1-D model of a transport pipeline network. From their simulation results, the authors found that mixtures of CO_2 and impurities from different capture technologies showed different dynamic behaviour during pipeline transport. The results also indicated that the operational costs of pipeline transport vary and are dependent on the capture technology involved. Like most steady-state and dynamic models used in CO_2 transport studies, Liljemark *et al.* (2011) and Chaczykowski and Osiadacz (2012) base their work on the assumption that a CO_2 pipeline is completely horizontal and connected to just one source of CO_2 emission. In reality, for economic reasons, it is expected that multiple sources of CO_2 emissions will be connected to a common trunk pipeline, which is likely to have elevations, bends and depressions along its length corresponding to the topographic profile of route taken by that pipeline. These simplifications are likely to have a significant impact on the capacity of the model to make accurate predictions. Luo *et al.* (2014) and Brown *et al.* (2015) are examples of researchers who performed studies with models that allow for a transport pipeline supplied by multiple CO_2 emission sources. Their models accounted for elevations and depressions along the length of the pipeline.

Given the health hazards of CO_2 pipeline rupture, several researchers have conducted theoretical and experimental studies to predict conditions in which corrosion or fracture propagation is likely to occur in order to develop appropriate countermeasures. Race *et al.* (2012) analysed the impact of various impurities on corrosion and fracture propagation. From their numerical analysis, the authors prescribed limits to the level of impurities allowed in a CO_2 stream in order to prevent fracture and corrosion. Cosham (2012) moved in a different direction. He presented a procedure—based on the semi-empirical Battelle Two-Curve Model— for predicting the pipe wall thickness required to prevent fracture propagation regardless of the level of impurities allowed in the CO_2 stream. Mahgerefteh *et al.* (2012a) noted that the semi-empirical Battelle Two-Curve Model does not take into account for the effects of heat transfer and friction between the CO_2 working fluid and the pipe wall on fracture propagation. The authors postulated that not accounting for both effects might result in the underestimation of the pipe toughness (i.e. pipe wall thickness) required to be prevent fracture propagation. They developed an unsteady 1-D

mechanistic model consisting of mass, momentum and energy conservation equations in order to study the effects of heat transfer and friction on a pipeline carrying pure or impure CO_2 gas. The 1-D mechanistic model — validated with test data from shock tube experiments— was used to simulate decompression behaviour of CO_2 gas for different thermodynamic conditions and varying levels of nitrogen, methane and sulphur dioxide impurities. The simulation results revealed that both heat transfer and friction have only marginal effects on fracture propagation of a pipeline carrying pure or impure CO_2 gas. However, for long pipelines carrying supercritical/dense phase CO_2, the authors noted that heat transfer and friction effects might be significant because of the higher levels of fluid viscosity involved. In other words, for gaseous CO_2, those effects can be neglected in pipeline fracture models, but not in the case of dense phase /supercritical carbon dioxide.

Mahgerefteh *et al.* (2012b) used the 1-D model to investigate the relationship between CO_2 capture technologies and pipeline fracture propagation. Pipelines carrying CO_2 stream sourced from post-combustion capture facility were least vulnerable to fracture than other capture technologies because the low level of impurities involved. Pre-combustion capture, which produces CO_2 stream with a higher level of impurities, increases the risk of pipeline fracture. Oxy-fuel combustion capture, which produces the least pure CO_2 stream, exposes the pipeline to the greatest risk of fracture propagation.

Aursand *et al.* (2013) using an unsteady 1-D model extended the work of researchers such as Mahgerefteh *et al.* (2012a) to include the study of fracture propagation for cases where rapid pipeline depressurization results in the formation of gas-liquid two-phase fluid. The authors explained that in order to accurately model fracture propagation, behaviour of the working fluid must be accounted for. In other words, the fracture models must account for mass flow rate of the leaking carbon dioxide and the size of crack from which the fluid is escaping. The model should also account for the transformation of the pure or impure CO_2 stream from dense phase/supercritical fluid to gas-liquid two-phase mixture because of the rapid depressurization of the pipeline. In a follow up paper, Aursand *et al.* (2014), the authors compared semi-empirical fracture models to their unsteady 1-D fracture model for the case of a pipeline carrying pure CO_2. They found that for a given

pipeline material and geometry, the 1-D model predicted that a minimum pipe wall thickness that was more than twice as large as the one predicted by the semi-empirical models. In other words, semi-empirical models grossly underestimate the minimum pipe wall thickness required to stop ductile fracture propagation. The same authors in Aursand *et al.* (2016) using their 1-D model investigated the consequences of using relatively simple cubic equation of state as opposed to highly complex equation of state for CO_2 property calculation in simulating pipeline depressurization and its effects on predicting ductile fractures. They found that the highly complex GERG-2008 EoS predicted pure and impure CO_2 fluid density with a higher level of accuracy than the relative simpler relatively simpler cubic Peng-Robinson EoS. However, in the prediction of ductile fracture, the difference in accuracy between GERG-2008 and Peng-Robinson were minimal. In other words, the choice of equation of state had marginal effect on the predicted fracture behaviour of the pipeline.

Aside from optimal design pipeline and conditioning CO_2 stream to ensure a high level of purity, the long-term economic viability of supercritical carbon dioxide pipeline transport can also be guaranteed if the energy consumption of installed compressors and booster pumps can be minimized. Moore and Nored (2008) was one of the first set of researchers to propose a combined compressor and pumping system for the CO_2 transport pipeline as a means of reducing energy requirement. In this combined system, pure CO_2 gas undergoes a quasi-isothermal compression, which involves cooling CO_2 between centrifugal machine stages until an intermediate pressure of 17.24 bar is reached. Thereafter, a refrigeration unit is used to reduce the temperature of the CO_2 gas to -31.67 deg.C causing it to liquefy. Then, a cryogenic pump is used to raise the pressure of pure CO_2 liquid from 17.24 bar to 151.68 bar. While a prototype of this combined compressor-cryogenic pump unit has been successful tested by the authors as reported in Moore *et al.* (2011) and Kerth *et al.* (2015), it remains a highly complicated system with potential system reliability risks. Liquid CO_2 flowing at subcritical inlet pressures increases the risk of cavitation damage to the cryogenic pump.

In recent years, studies have been published comparing several compression strategies for the CO_2 pipeline network—including conventional multistage centrifugal

compressors, shockwave compressors and combined compressor-refrigeration-pump units— in order to determine the one with the least energy requirement. Witkowski and Majkut (2012) and Witkowski *et al.* (2013) compared different compression strategies for a straight horizontal pipeline bearing only pure CO_2 sourced from a post-combustion capture facility connected to a 900 MW coal-fired power station. They found that the replacement of conventional multistage compressors with either integrally geared centrifugal compressors or combined gas compression-refrigeration-liquid pumping units reduced the overall energy requirement significantly. Luo *et al.* (2014) also performed a comparative study of similar compression strategies, but for a realistic CO_2 transport pipeline consisting of horizontal, vertical and undulating segments carrying impure CO_2 streams sourced from pre-combustion and oxy-fuel capture facilities. This comparative study, which includes detailed techno-economic evaluations of each compression strategy, also found the combined gas compression-refrigeration-liquid pumping option to have the best savings in energy costs.

Whereas Luo *et al.* (2014), Witkowski and Majkut (2012) and Witkowski *et al.* (2013) investigated compression strategies involving pure or nearly pure CO_2 streams, Martynov *et al.* (2016) focussed on CO_2 streams with significant and varying amounts of impurities sourced from pre-combustion and oxy-fuel capture facilities. They found that when the working fluid changed from pure CO_2 to CO_2 mixtures sourced from pre-combustion double flash and oxy-fuel capture facilities, there was no significant effect on the power requirement of all compression strategies considered. This is because the concentration of the impurities in the mixtures were less than 4%. In contrast, the replacement of pure CO_2 with a CO_2 mixture sourced from dehumidified oxy-fuel capture facility increased the power requirement for all compression strategies considered by 12–30% because the impurities were up to 15% of that mixture. The authors also confirmed that for pure CO_2 and CO_2 mixtures with less than 5% impurities, combined gas compressor-refrigeration-liquid pump systems were generally more efficient than conventional multistage centrifugal compressors. Conversely, for the CO_2 mixture with 15% impurities, the authors found that operating the combined compressor-refrigeration-pump unit was not economically viable because of the high refrigeration costs.

2.5 CONCLUDING REMARKS: SCOPE FOR FURTHER IMPROVEMENTS AND NEW DEVELOPMENTS IN SUPERCRITICAL CARBON DIOXIDE PIPELINE TRANSPORTION

A lot of research have been published on CO_2 pipeline transport covering design issues such as pipeline sizing, recompression distance, energy requirement, corrosion and fracture propagation and operational issues such as start-up, shutdown, rapid depressurization, valve blockage and variation of fluid flow rate.

In studies dealing with overall energy requirement of pipeline networks, compressors and pumps are not examined in great depth— the focus being on merely determining the amount of energy that both machines will consume when tasked with raising and maintaining pipeline pressure above the critical point of certain CO_2 mixtures to forestall the formation of two-phase flow. In such studies, the strategy for reducing energy consumption and operating costs are focussed on determining which impurities ought to be reduced in concentration or removed altogether from a given anthropogenic CO_2 mixture in order to maximize its density while simultaneously minimizing its critical point, fluid compressibility and viscosity. The increased purity of the CO_2 mixture decreases pipeline pressure drop, allowing for reduced energy consumption by compressors and booster pumps (Eickhoff *et al.*, 2014; Wetenhall *et al.*, 2014b; Tan *et al.*, 2016; Lemontzoglou *et al.*, 2017). The major limitation of this strategy is that reducing or removing impurities from anthropogenic CO_2 is an energy-intensive process that will drive up the operating costs of capture facilities—hence, attenuating or even offsetting the benefits of reducing the input power requirements for compressors and pumps in the pipeline network (Li *et al.*, 2011a; Cooper, 2012; Cosham 2012). An alternative strategy would be to tolerate various types and amounts of impurities present in the CO_2 mixture and focus on improving the efficiency of compressors and booster pumps. This will eliminate energy and financial waste of increasing the purity of anthropogenic CO_2 mixtures. Besides, this alternative strategy is not restricted to CO_2 mixtures only. Significant savings can also be made in the operating costs of pipelines carrying pure CO_2 by increasing the energy efficiency of compressors and booster pumps (Okezue and Wang, 2016).

Recent years have witnessed the publication of a small number of studies focussed on developing energy-saving fluid compression strategies as a means of reducing the overall operating costs of supercritical CO_2 pipeline networks (see section 2.4.2

for details). While such studies provide useful information on which fluid compression strategy achieves the best savings on operating costs given the working fluid's chemical composition, they are still lacking in practical details.

Before any of the energy-saving compression strategies in open literature can be implemented, the physical equipment involved (e.g. centrifugal machines, intercoolers) must be sized appropriately to ensure their optimal performance when installed in CO_2 pipeline networks. In the field of CCS, no other researcher have published any work containing a systematic method for selection and sizing compressors or booster pumps installed in pipeline networks transporting pure and impure supercritical CO_2. This represents a significant gap in knowledge, which is tackled in chapters 4 to 6. A prerequisite for the development of an algorithmic tool for selection and sizing of centrifugal machines is a detailed evaluation of existing EoS correlations in order to select those most reliable for calculating the properties of the various CO_2 mixtures (See chapter 3).

CHAPTER 3

CO_2 PROPERTY CALCULATION AT THE VICINITY OF THE CRITICAL POINT

A mathematical model may be capable of describing the complex geometry, internal fluid flow and working processes of a compressor or a booster pump with a high degree of precision. However, the accuracy of its simulated results is heavily dependent on the reliable calculation of supercritical working fluid's thermophysical properties (Wilhelmsen *et al.*, 2012; Tan *et al.*, 2016; Okezue and Kuvshinov, 2018).

There are several types of EoS correlations in existence. No single correlation possess the universal ability to perform satisfactorily in all situations. Instead, a particular equation of state may perform better than another equation of state depending the chemical composition of the working fluid, its physical state and range of pressures and temperatures involved (Oosterkamp and Ramsen, 2008; Li and Yan, 2009a). This means that a careful evaluation of different correlations is necessary in order to select EoS appropriate for calculating the working fluid's properties within the compressor model developed in chapter 4.

In the previous chapter, literature review revealed different EoS correlations used in the prediction of the CO_2 thermophysical properties for the purposes of CCS pipeline transport. However, evaluations of correlations performed by various researchers were largely restricted to pipeline operating pressures in the range of 100–200 bar. This is the pressure range usually recommended for supercritical CO_2 pipeline transport (Serpa *et al.*, 2011; Race *et al.*, 2012; Demetriades *et al.*, 2013; Witkowski *et al.*, 2013). However, there are situations where the operating pressure of a supercritical CO_2 transport pipeline is above that recommended pressure range. A good example is offshore CO_2 transport pipelines where the operating pressure can be as high as 300 bar (IEA GHG, 2009). If the storage site of a supercritical CO_2 mixture is a depleted offshore oil and gas field, the discharge pressures of injection pumps at the end of the transport pipeline can reach 310 bar (Soulas *et al.* 2011). For supercritical CO_2 mixtures containing up to 23% hydrocarbon impurities, injection pump discharge pressures of up to 540 bar have been reported (Adams, 2011; Bergamini *et al.*, 2011; Pezzella, 2011).

This chapter presents a detailed comparative study of seven equations of state (EoS) correlations; carried out to select those that produce accurate predictions for varying chemical compositions of CO_2 mixtures over a wider pressure range of 100–1000 bar. The seven correlations studied are Peng-Robinson (PR); Soave-Redlich-Kwong (SRK); Lee-Kessler-Plocker (LKP); Benedict-Weber-Rubin-Starling (BWRS); GERG-2008; Span and Wagner (SW) and EoS-CG.

3.1 CLASSIFICATION OF THE EQUATIONS OF STATE

Equations of state (EoS) can be classified according to its overall structure and the complexity of its constituent equations. The seven EoS correlations featured in this chapter are divided into three categories namely: cubic, virial and Helmholtz free energy models. Compared to other categories of equations of state, cubic models have simplest structure while Helmholtz free energy models have the most complicated structure. Of the three EoS categories, Helmholtz free energy models generally provide predictions closest to experimental data while cubic and virial models exhibit greater deviations from experimental data.

3.1.1 Cubic Equations of State

Cubic EoS correlations are based on van der Waals theory, which is a modification of the classic ideal gas equation to account for the behaviour of real gases and liquids. Cubic EoS is structurally simple and made up of semi-empirical equations that have volume parameters raised to the first, second and third power. These volume parameters can be computed analytically without any need for iterative calculation procedures. Therefore, algorithms based on cubic EoS are computationally fast (Diamantonis *et al.*, 2013a; Wetenhall *et al.*, 2014b; Ke *et al.*, 2017).

Cubic EoS correlations generally give reasonable results for thermodynamic properties including density and vapour-liquid equilibrium, but not in all operating conditions. They are known to have poor accuracy when used for calculating liquid phase density and for predicting heat of evaporation and heat capacities at the vicinity of the critical point (Kunz and Wagner, 2012; Wilhelmsen *et al.*, 2012; Aursand *et al.,* 2016; Munkejord *et al.*, 2016). For this reason, correction factors are usually used to improve the predictive performance of cubic EoS. Despite their shortcomings, the compelling simplicity of cubic EoS makes them popular in engineering applications

(Li *et al.*, 2011a; Demetriades *et al.*, 2013; Diamantonis *et al.*, 2013a). Among the most widely used cubic EoS correlations are Soave-Redlich-Kwong (SRK) developed in 1972 and Peng-Robinson (PR) developed in 1976.

3.1.2 Virial Equations of State

Virial EoS correlations derive from the concept of using a compressibility factor (Z) to account for the deviation of real fluid behaviour from ideal gas theory for a given pressure and temperature. Virial EoS correlations express compressibility factor as an infinite power series expansion of either molar volume, density or pressure. This power series is referred to as a "virial expansion" and the coefficients of terms within the series are called "virial coefficients". These coefficients usually contain parameters, which describe the intermolecular interactions within real fluids based on statistical mechanics.

Compared to cubic EoS, virial equations of state tend to be highly complex in structure and generally more accurate in calculating thermodynamic properties and phase behaviour of chemical compounds (Li *et al.*, 2011a). The complicated structure of virial EoS correlations can be attributed to their numerous parameters fitted to a large experimental database as well as their intricate iterative calculation procedures. Therefore, algorithms based on virial EoS require more computer storage space and time to perform its calculations compared to cubic EoS. (Li *et al.*, 2011a; Diamantonis *et al.*, 2013b).

Benedict-Webb-Rubin-Starling (BWRS) and Lee-Kessler-Plocker (LKP) are examples of widely used virial-type equations of state. Both EoS correlations are descendants of the original Benedict-Webb-Rubin (BWR) equation of state developed in 1940.

3.1.3 Helmholtz Free Energy-based Equations of State

These are semi-empirical multi-parameter equations of state for either pure or mixtures of chemical compounds which are defined in terms of dimensionless Helmholtz energy. This distinguishes Helmholtz energy based EoS from virial EoS, which are expressed in terms of a compressibility factor derived from an infinite power series. Moreover, Helmholtz energy-based EoS correlations are far more complex than virial EoS and contain parameters in far greater numbers. Parameters of Helmholtz energy EoS are usually fitted to a huge database of experimental data

representing the thermophysical properties of various chemical compounds over a wide range of pressures and temperatures. For this reason, this category of EoS correlations tend to be highly accurate and in many cases, can generating relative errors of 1% or even less. Therefore, they perform much better than cubic and virial EoS correlations (Li *et al.*, 2011a; Mazzoccoli *et al.*, 2012; Aimoli *et al.*, 2014; Aursand *et al.*, 2016).

However, the complexity of their structure and vast number of parameters means that algorithms based on them require large amount of computer storage space and consume significant computational time when performing calculations (Wilhelmsen *et al.*, 2012; Islam and Carlson, 2012; Aursand *et al.*, 2016). More importantly, the sheer number of empirical parameters they contain combined with their complex iterative calculation procedures imposes a degree of inflexibility on Helmholtz equations of state (Li and Yan, 2009a; Mazzoccoli *et al.*, 2013).

For example, the Helmholtz energy-based correlation developed by Span and Wagner (1996) is the most accurate EoS in existence for calculating pure CO_2 properties. However, its highly complex structure and 51 empirical parameters makes it impractical for general application to mixtures of carbon dioxide and other chemical compounds. Therefore, its application is restricted to calculations involving pure carbon dioxide (Li and Yan, 2009b; Demetriades *et al.*, 2013; Diamantonis *et al.*, 2013a; Munkejord *et al.*, 2016). Given its high level of accuracy, Span and Wagner (1996) EoS is recognized as the international reference equation of state for pure CO_2 (Ouyang, 2011; Li *et al.*, 2011a; Wilhelmsen *et al.*, 2012; Aursand *et al.*, 2013; Ishmael *et al.*, 2016).

GERG-2004 and its improved variant, GERG-2008 are Helmholtz energy-based equations of state originally developed to predict the thermodynamic behaviour of mixtures of chemical compounds found in natural gas (Kunz *et al.*, 2007; Kunz and Wagner, 2012). Given their high level of accuracy, GERG-2004 and GERG-2008 are both recognized as the international reference equations of state for natural gas (Wilhelmsen *et al.*, 2012; Aursand *et al.*, 2016; Gernert and Span, 2016). Compared to cubic and virial EoS correlations, GERG-2004/2008 have also been found to be far more accurate when used for predicting the thermodynamic properties of CO_2-rich mixtures (Aimoli *et al.*, 2014; Aursand et al. 2016; Gernert and Span, 2016).

Compared to Span and Wagner (1996) correlation, GERG-2004 and GERG-2008 have relatively simpler structures and fewer empirical parameters, which makes them easier to apply in the calculation of thermodynamic properties of mixtures (Kunz and Wagner, 2012; Munkejord *et al.*, 2016). Nevertheless, algorithms based on GERG-2004/2008 are more complex and computationally demanding than cubic and virial correlations (Wilhelmsen *et al.*, 2012; Aursand *et al.*, 2016).

Although GERG-2004 and GERG-2008 remains the most accurate EoS correlations for calculating the thermophysical properties of CO_2-rich mixtures, they exhibits shortcomings especially with regard predicting vapour-liquid equilibrium (VLE) boundaries of the mixtures (Li *et al.*, 2011a; Aursand *et al.*, 2013; Løvseth *et al.*, 2014)

GERG-2004/2008 predictions deviate significantly from reality when applied in the property calculation of humid gas mixtures. These limitations in the performance of GERG-2004/2008 can be attributed to the fact that they were developed for natural mixtures where methane is the majority component (Li *et al.*, 2011a; Gernert and Span, 2016).

EoS-CG correlation is a new Helmholtz free energy-based equation of state focussed on the prediction of thermodynamic properties for CO_2-rich mixtures typically emitted by power plants connected to CCS facilities. It was also developed to better predict the thermodynamic properties of humid exhaust gas mixtures (Span *et al.*, 2013; Gernert and Span, 2010 and 2016; Ke *et al.*, 2017). EoS-CG equation of state is structurally more complex, but as computationally demanding as GERG-2008 (Aursand *et al.*, 2016).

When engaged in the calculation of pure CO_2 properties, EoS-CG predictions are more accurate than those generated with GERG-2004/2008 and identical to those generated by Span and Wagner (1996) the internationally recognized reference EoS for pure CO_2. EoS-CG performs much better than GERG-2008 when used to predict the density and VLE boundaries of CO_2 mixtures including those containing water (Span *et al.*, 2013; Aursand *et al.*, 2016; Gernert and Span, 2016; Munkejord *et al.*, 2016). Despite its high level of accuracy, EoS-CG correlation remains under development and can only be applied to a limited number of mixtures—those

containing CO_2, N_2, O_2, Ar, H_2O, and CO (Aursand *et al.*, 2016; Gernert and Span, 2016; Munkejord *et al.*, 2016; Ke *et al.*, 2017).

In this chapter, the performance of EoS-CG, Span and Wagner (1996) and GERG-2008 are compared to those of virial and cubic EoS correlations.

3.2 COMPARATIVE STUDY OF VARIOUS EQUATIONS OF STATE

In published literature, various EoS correlations have been used to predict the thermodynamic properties of pure CO_2 or CO_2 mixtures with varying levels of accuracy depending on the chemical composition, pressure and temperature of the CO_2 stream flowing in the pipeline. While no single EoS correlation can perform satisfactorily for all thermodynamic conditions, some correlations perform better than others under certain conditions (Oosterkamp and Ramsen, 2008; Li and Yan, 2009a; Li *et al.*, 2011a; Luo *et al.*, 2014). For that reason, it is important to compare different types of EoS correlations against experimental data in order to ascertain which one is best for modelling CO_2 pipeline transport for a specific composition of CO_2 mixture and a given range of operating conditions.

3.2.1 Availability of Experimental Data for CO_2 and Its Mixtures

There is a large amount of published experimental data on thermodynamic and transport properties of CO_2 mixtures. However, there are limitations. It is quite hard to obtain experimental data for certain pressure and temperature conditions as well as for certain CO_2 mixtures, especially those containing impurities such as O_2, Ar and SO_2. For purposes of the comparative study, the author of this PhD thesis was able to obtain experimental data for pure CO_2 and various CO_2 mixtures containing the following chemical impurities: N_2, H_2, CH_4 and CO. The pressure range covered by the carefully selected experimental data are within the 100–1000 bar operating envelope under study in this chapter.

3.2.2 Tools for Evaluating EoS Accuracy for Various CO_2 Properties

For a given chemical composition of a CO_2 stream, the accuracy of predictions performed by each EoS correlation were evaluated using both graphs and the following statistical parameters:

Average Percentage Relative Error (APE):

$$APE = \frac{1}{N_{RUN}} \sum_{RUN=1}^{N_{RUN}} \left[\frac{\text{Prediction} - \text{Experiment}}{\text{Experiment}} \times 100\% \right]_{RUN} \qquad (3.1)$$

Average Absolute Percentage Relative Error (AAPE):

$$APE = \frac{1}{N_{RUN}} \sum_{RUN=1}^{N_{RUN}} \left[\left\| \frac{\text{Prediction} - \text{Experiment}}{\text{Experiment}} \right\| \times 100\% \right]_{RUN} \qquad (3.2)$$

Standard Deviation about the Average Percentage Relative Error (STANDEV):

$$STANDEV = \sqrt{\frac{\sum_{RUN=1}^{N_{RUN}} \left\{ \left(\frac{\text{Prediction} - \text{Experiment}}{\text{Experiment}} \times 100\% \right) - (\text{APE}) \right\}^2}{N_{RUN} - 1}} \qquad (3.3)$$

APE measures the average size of the discrepancy between predictions made with EoS correlations and experimental data. It is also indicates, on average, whether a particular EoS correlation has overestimated or underestimated the CO_2 fluid property under study. Positive APE values indicate overestimation while negative APE values indicate underestimation.

APE is calculated by averaging the percentage relative errors of individual data points. For an APE value to reflect the true performance of an EoS correlation, the percentage relative errors of the individual data points have to be uniformly positive or uniformly negative. When combined in an averaging process, positive and negative values may cancel each other out. Therefore, APE values derived from a heterogeneous dataset of positive and negative percentage relative errors have the disadvantage of not being truly representative of the performance of an EoS correlation. AAPE eliminates this disadvantage because it is obtained by averaging absolute values of individual percentage relative errors. For this reason, AAPE is a reliable measure of the average size of discrepancy between EoS predictions and experimental data. However, it cannot indicate whether an EoS has overestimated or underestimated a CO_2 fluid property on average. STANDEV is a measure of the dispersion (or clustering of) the percentage relative errors of individual data points around their average values.

3.2.3 Evaluation of Equations of State for Density Calculation

In this section, experimental data on fluid density for pure CO_2 and various ternary and binary CO_2 mixtures sourced from Seitz *et al.* (1996a,1996b) were compared to

simulations carried out with the following six EoS correlations: Peng-Robinson (PR); Soave-Redlich-Kwong (SRK); Benedict-Webb-Rubin-Starling (BWRS); Lee-Kessler-Plocker (LKP); Span and Wagner (SW) and GERG-2008. The seventh correlation EoS-CG is only applied in fluid property calculations in sections 3.2.5 and 3.2.6.

3.2.3.1 Analysis of Results for Pure CO_2 Stream

Each of the EoS correlations mentioned in section 3.2.3 was used to predict the density of pure CO_2 for the pressure range of 99.9 bar to 999.3 bar at temperatures of 50 deg.C and 100 deg.C. The simulated density results were compared to experimental data obtained under the same operating conditions.

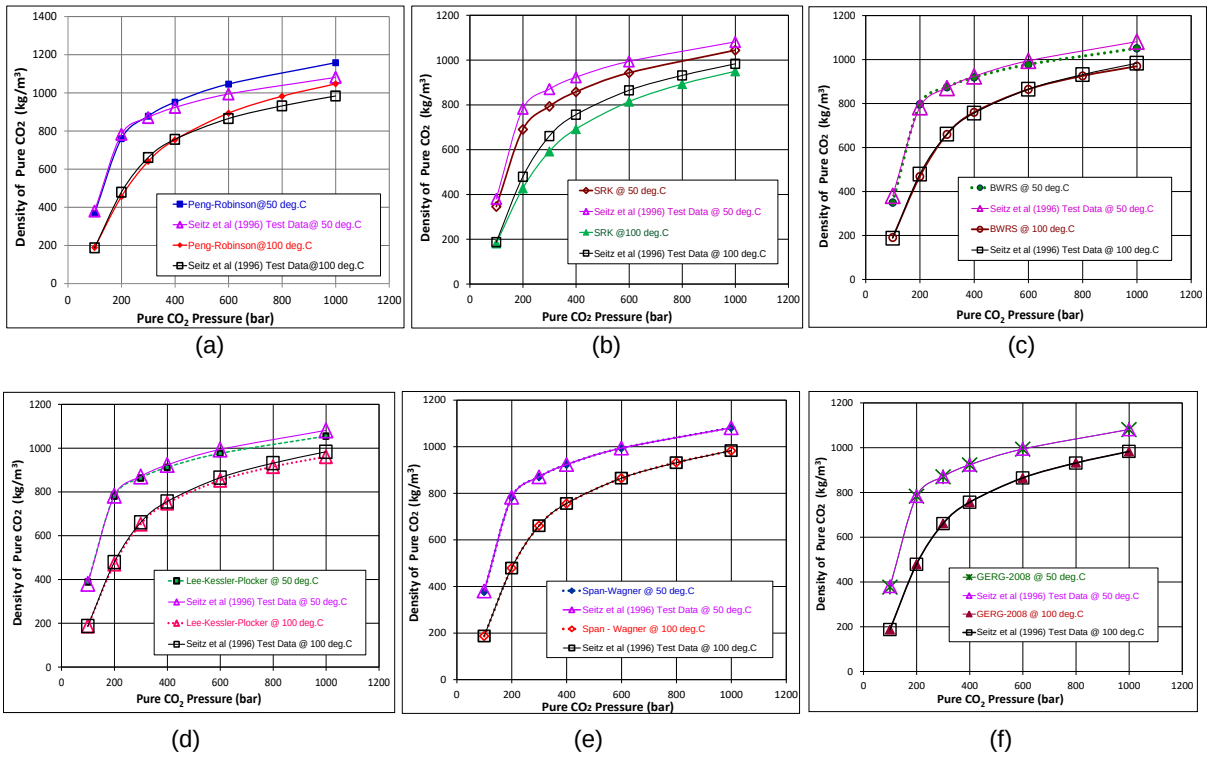

Fig. 3.1 Comparison of experimental and simulated pure CO_2 density at 50 deg.C and 100 deg.C for (a) *Peng-Robinson (PR);* (b)*Soave-Redlich-Kwong (SRK);* (c) *Benedict-Weber-Rubin-Starling (BWRS);* (d) *Lee-Kessler-Plocker (LKP);* (e) *Span-Wagner (SW) and* (f) *Groupe Européen de Recherches Gazières (GERG-2008). All experimental data is culled from Seitz et al. (1996a)*

From Fig. 3.1, it is clear that EoS correlations under study were able to produce predictions of reasonable accuracy. However, predictions of some correlations were closer to the experimental data compared to those of other correlations. For both temperatures, Span and Wagner (SW) and GERG-2008 correlations were the best performing EoS across the entire high-pressure range closely followed by Lee-Kessler-Plocker (LKP) and Benedict-Weber-Rubin-Starling (BWRS). Peng-Robinson (PR) EoS performs much better below 600 bar than above it as demonstrated in Fig

3.1(a). Compared to other correlations, Soave-Redlich-Kwong (SRK) exhibited the poorest performance since its predictions presented the greatest disagreement with experimental data, especially at pressures above 200 bar (Fig. 3.1(b)).

To quantify the divergence of the predicted pure CO_2 density results from the experimental data illustrated in Fig.3.1, all three statistical parameters APE, AAPE and STANDEV were applied. An analysis of the tabulated results for the statistical parameters (Table 3.1) confirms the observations made from Fig 3.1.

Table 3.1: Statistical Evaluation of EoS Correlations for Pure CO_2 Density

EoS CORRELATION	TEMPERATURE	APE	AAPE	STANDARD DEVIATION
	[deg.C]	[%]	[%]	[%]
Peng-Robinson (PR)	50	1.644	3.740	4.268
	100	1.120	3.480	4.239
Soave-Redlich-Kwong (SRK)	50	-7.546	7.550	3.001
	100	-6.581	6.580	3.274
Benedict-Webb-Rubin-Starling (BWRS)	50	-1.788	2.510	3.430
	100	-0.307	1.010	1.366
Lee-Kessler-Plocker (LKP)	50	-0.706	1.460	1.633
	100	-1.349	1.350	0.698
Span and Wagner (SW)	50	-0.128	0.166	0.320
	100	-0.026	0.070	0.090
GERG-2008	50	-0.132	0.155	0.320
	100	-0.016	0.069	0.092

For both temperature values, SW and GERG-2008 are tied as the best performing correlations judging by their extremely low AAPE values followed by LKP and BWRS. SRK was the worst performing EoS since its predictions generated the highest AAPE values. Both Fig.3.1 and Table 3.1 support the assertion made in section 3.1.3 that Helmholtz free energy-based EoS (SW and GERG-2008) have superior accuracy on fluid density predictions compared to virial EoS (BWRS and LKP), which in turn performs calculations with a higher level of accuracy than cubic EoS (PR and SRK).

3.2.3.2 Analysis of Results for Binary CO_2+N_2 Stream

EoS correlations were evaluated for two sets of binary CO_2+N_2 mixtures of differing compositions under the same operating conditions mentioned in section 3.2.3.1.

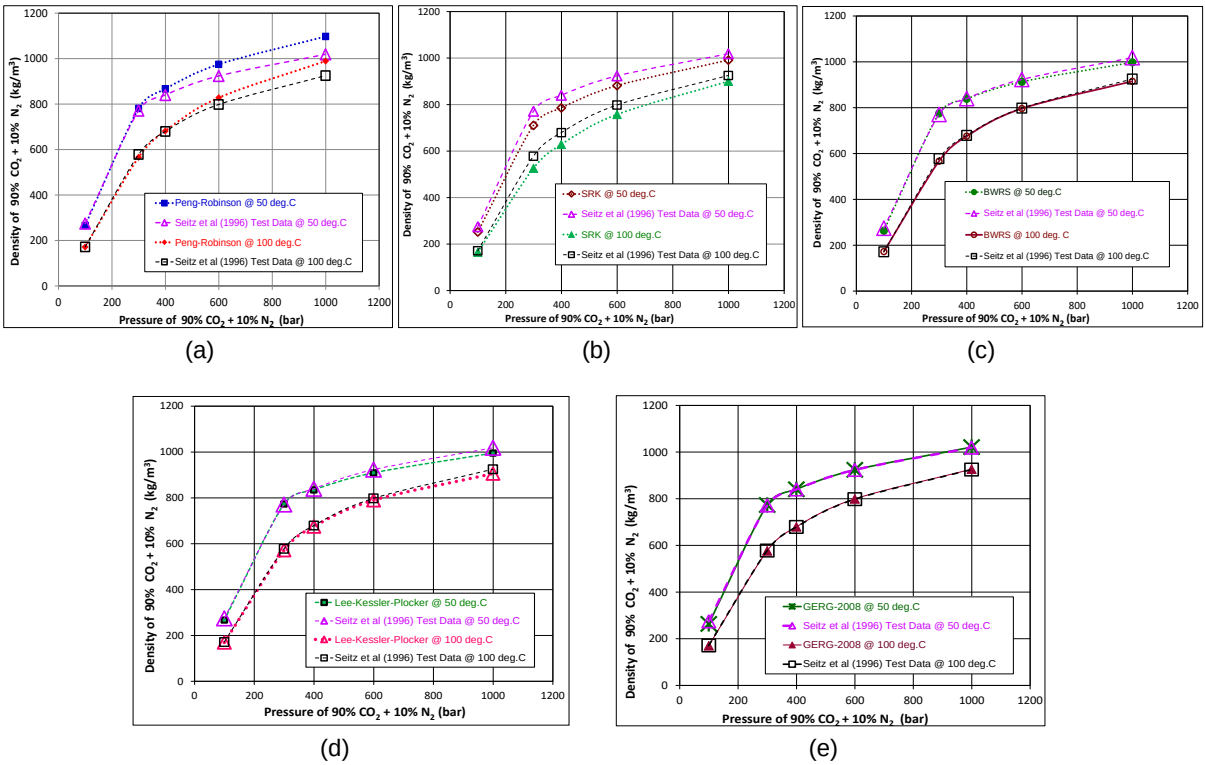

Fig. 3.2 Comparison of experimental and simulated 90% CO_2 + 10% N_2 mixture density at 50 deg.C and 100 deg.C for (a) *Peng-Robinson (PR);* (b) *Soave-Redlich-Kwong (SRK);* (c) *Benedict-Weber-Rubin-Starling (BWRS);* (d) *Lee-Kessler-Plocker (LKP) and* (e) *Groupe Européen de Recherches Gazières (GERG-2008). All experimental data is culled from Seitz et al. (1996a)*

From Fig.3.2, it is clear that the correlations either overestimate or underestimate mixture density of the binary 90% CO_2 + 10% N_2 stream. Table 3.2 contains data on statistical parameters quantifying the discrepancies between experimental and predicted mixture densities.

From Fig. 3.2 and Table 3.2, it is clear that GERG-2008 EoS is the best performing correlation because its predictions are closest in agreement to experimental data. This is followed by LKP and BWRS correlations. SRK EoS gives the poorest performance because its predictions have the greatest divergence from experimental results. (Span and Wagner (SW) EoS was excluded from this analysis because its mathematical structure precludes its application to CO_2 mixtures as explained in section 3.1.3).

Table 3.2: Statistical Evaluation of EoS Correlations for 90% CO_2 + 10% N_2 Density

EoS CORRELATION	TEMPERATURE	APE	AAPE	STANDARD DEVIATION
	[deg.C]	[%]	[%]	[%]
Peng-Robinson (PR)	50	-2.909	4.163	4.166
	100	1.765	2.624	3.561
Soave-Redlich-Kwong (SRK)	50	-5.932	5.932	2.328
	100	-5.590	5.590	2.621
Benedict-Webb-Rubin-Starling (BWRS)	50	-1.385	1.601	1.855
	100	-0.632	0.844	0.918
Lee-Kessler-Plocker (LKP)	50	-1.336	1.461	1.207
	100	-1.221	1.221	0.539
GERG-2008	50	-0.648	0.934	1.851
	100	-0.176	0.310	0.471

For 80% CO_2 + 20% N_2 mixture, GERG-2008 retains its position as the best performing correlation, followed by LKP EoS and BWRS EoS. SRK EoS remains the correlation with the least accurate predictions (See Fig. 3.3 and Table 3.3).

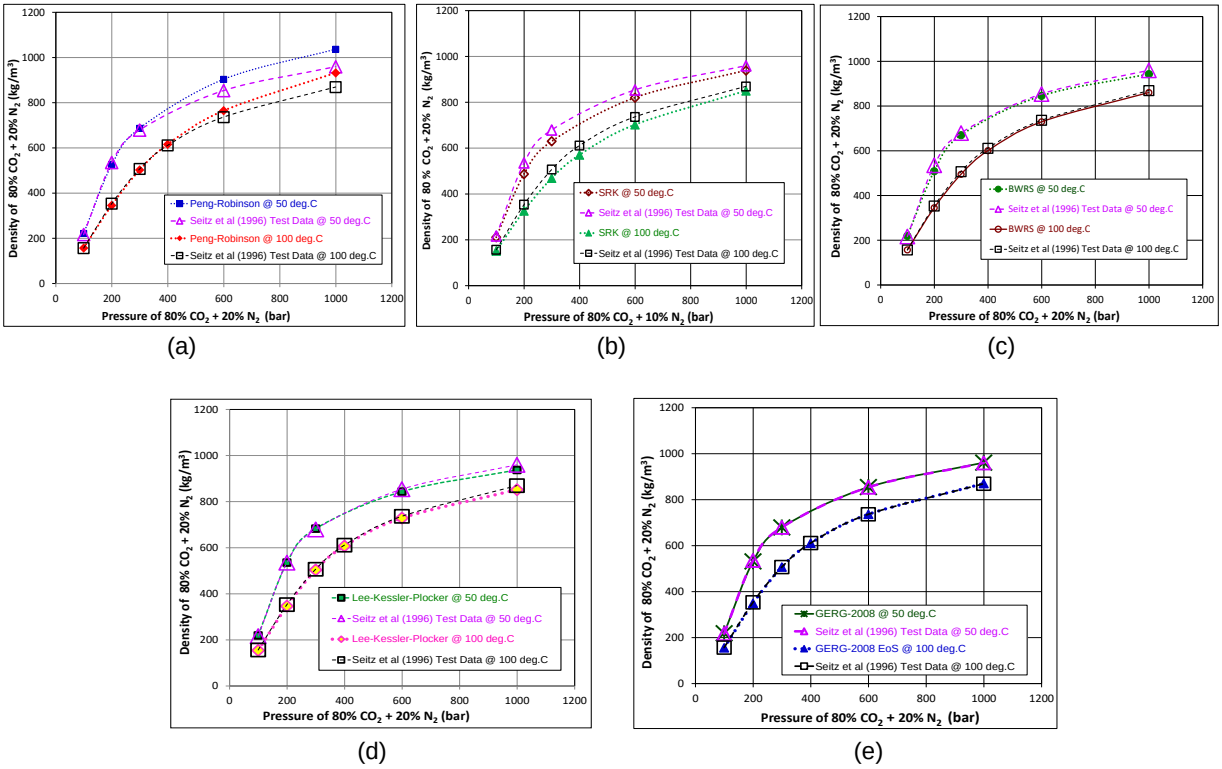

Fig. 3.3 Comparison of experimental and simulated 80% CO_2 + 20% N_2 mixture density at 50 deg.C and 100 deg.C for (a) *Peng-Robinson (PR);* (b) *Soave-Redlich-Kwong (SRK);* (c) *Benedict-Weber-Rubin-Starling (BWRS);* (d) *Lee-Kessler-Plocker (LKP) and* (e) *Groupe Européen de Recherches Gazières (GERG-2008). All experimental data is culled from Seitz et al. (1996a)*

On comparing Figs 3.2 to 3.3 and Tables 3.2 and 3.3, it was observed that increasing the concentration of the nitrogen impurity from 10% to 20% caused the error between predicted and experimental densities to change by less than 1%. Thus implying, that the predictive accuracies of the EoS correlations are not significantly affected by changes in the concentration of nitrogen impurity within the CO_2 mixture.

Table 3.3: Statistical Evaluation of EoS Correlations for 80% CO_2 + 20% N_2 Density

EoS CORRELATION	TEMPERATURE	APE	AAPE	STANDARD DEVIATION
	[deg.C]	[%]	[%]	[%]
Peng-Robinson (PR)	50	3.033	3.845	3.963
	100	1.537	2.542	3.456
Soave-Redlich-Kwong (SRK)	50	-5.004	5.004	3.027
	100	-5.247	5.247	2.286
Benedict-Webb-Rubin-Starling (BWRS)	50	-1.598	2.067	2.242
	100	-1.316	1.443	1.021
Lee-Kessler-Plocker (LKP)	50	-0.355	1.053	1.402
	100	-1.192	1.192	0.587
GERG-2008	50	0.059	0.387	0.600
	100	-0.317	0.349	0.513

3.2.3.3 Analysis of Results for Binary CO_2+CH_4 Stream

Experimental data for 90% CO_2 +10% CH_4 stream at 50 deg.C was unavailable. So the performance of the EoS correlations were evaluated only for 100deg.C temperature condition.

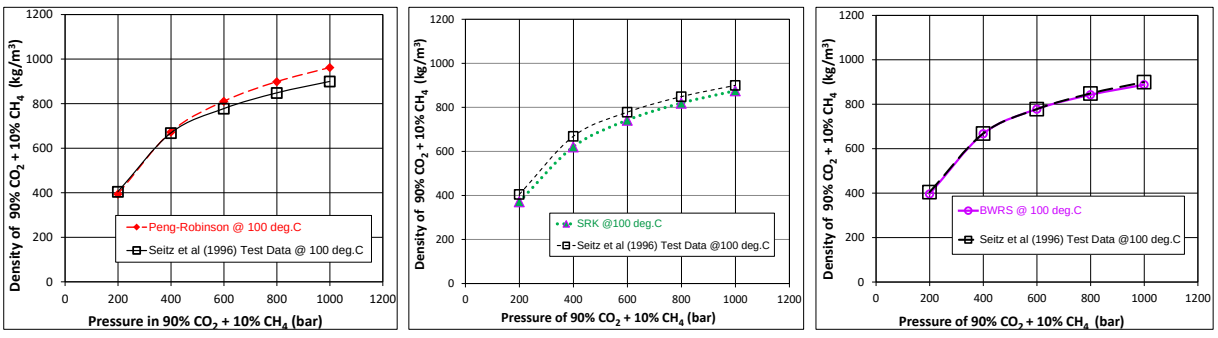

(a) (b) (c)

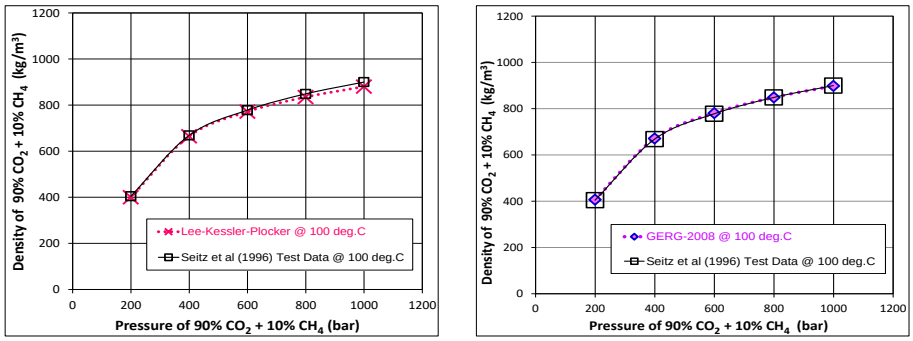

(d) (e)

Fig. 3.4 Comparison of experimental and simulated 90% CO_2 +10% CH_4 mixture density at 50 deg.C and 100 deg.C for (a) *Peng-Robinson (PR);* (b) *Soave-Redlich-Kwong (SRK);* (c) *Benedict-Weber-Rubin-Starling (BWRS);* (d) *Lee-Kessler-Plocker (LKP) and* (e) *Groupe Européen de Recherches Gazières (GERG-2008). All experimental data is culled from Seitz et al. (1996a)*

From Fig. 3.4 and Table 3.4, it is obvious that the Helmholtz free energy correlation GERG-2008 is still the best performing EoS. The virial correlations BWRS and LKP rank second and third after GERG-2008 in terms of predictive accuracy. The two cubic EoS correlations (PR and SRK) are the worst performing correlations.

Table 3.4: Statistical Evaluation of EoS Correlations for 90% CO_2 + 10% CH_4 Density

EoS CORRELATION	TEMPERATURE [deg.C]	APE [%]	AAPE [%]	STANDARD DEVIATION [%]
Peng-Robinson (PR)	100	3.032	4.079	3.958
Soave-Redlich-Kwong (SRK)	100	-5.227	5.227	2.369
Benedict-Webb-Rubin-Starling (BWRS)	100	-0.820	0.844	0.839
Lee-Kessler-Plocker (LKP)	100	-1.244	1.244	0.652
GERG-2008	100	0.245	0.315	0.311

An analysis of Figs. 3.5 and Table 3.5 show that for 80% CO_2 + 20% CH_4 stream, GERG-2008 and LKP are the best performing correlations followed by BWRS. SRK retains its position as the worst performing correlation. A further analysis of the results in Table 3.5 showed that absolute error in the density predictions increase as temperature condition shift from 50 deg.C to 100 deg.C.

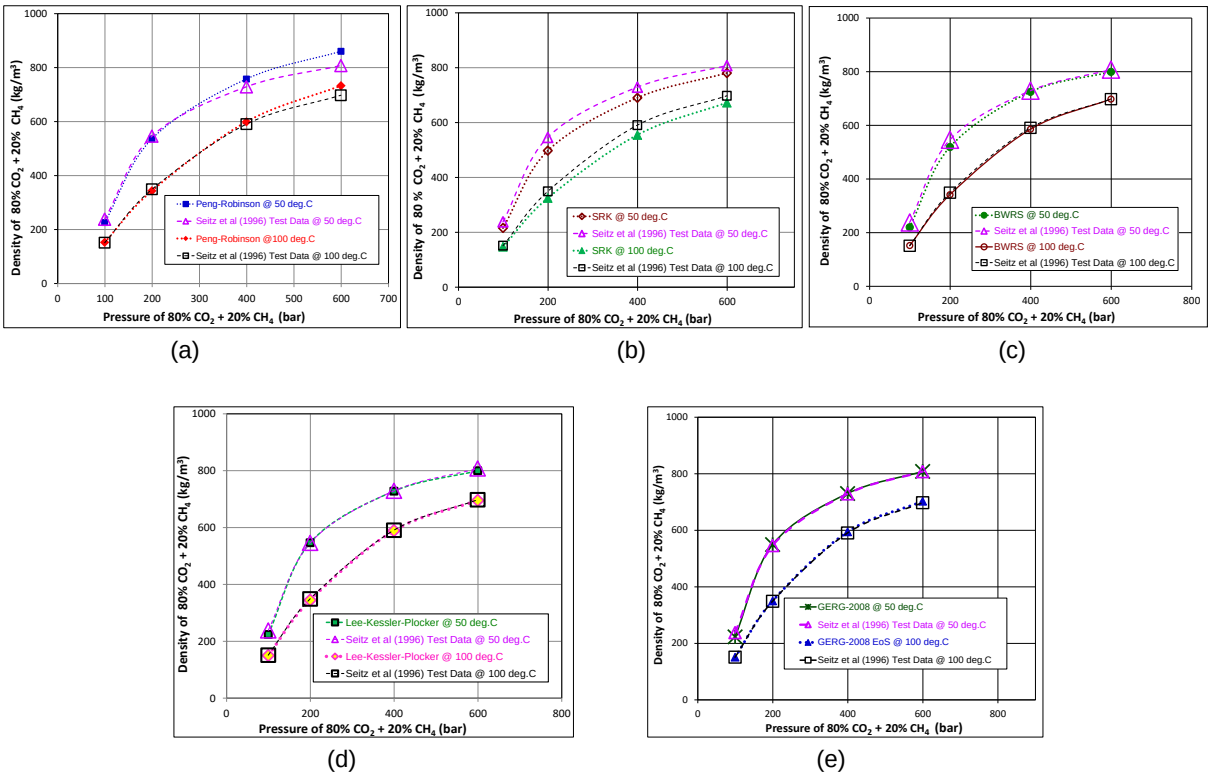

Fig. 3.5 Comparison of experimental and simulated 80% CO_2 +20% CH_4 mixture density at 50 deg.C and 100 deg.C for (a) *Peng-Robinson (PR);* (b) *Soave-Redlich-Kwong (SRK);* (c) *Benedict-Weber-Rubin-Starling (BWRS);* (d) *Lee-Kessler-Plocker (LKP) and* (e) *Groupe Européen de Recherches Gazières (GERG-2008). All experimental data is culled from Seitz et al. (1996a)*

Apart from the fact that GERG-2008 clearly overtakes LKP as the best performing correlation at 100 deg.C, temperature increment did not alter the performance ranking of the EoS correlations. SRK remains at the bottom of the performance ranking as the correlation that produces the least accurate density predictions for both temperature conditions.

Table 3.5: Statistical Evaluation of EoS Correlations for 80% CO_2 + 20% CH_4 Density

EoS CORRELATION	TEMPERATURE [deg.C]	APE [%]	AAPE [%]	STANDARD DEVIATION [%]
Peng-Robinson (PR)	50	0.894	4.358	5.314
	100	3.332	3.873	3.616
Soave-Redlich-Kwong (SRK)	50	-6.739	6.739	2.923
	100	-3.951	3.951	2.058
Benedict-Webb-Rubin-Starling (BWRS)	50	-3.496	3.496	3.290
	100	-0.684	0.899	0.952
Lee-Kessler-Plocker (LKP)	50	-1.713	1.772	2.798
	100	-0.962	0.962	0.629
GERG-2008	50	-1.347	1.779	3.279
	100	0.264	0.329	0.350

On comparing Figs. 3.4 to 3.5 and Tables 3.4, for the same temperature condition of 100 deg.C, it was observed that increasing the methane impurity content of the CO_2 mixture from 10% to 20% caused the absolute errors of PR, BWRS, LKP and GERG to change by less than 0.3%. In the case of SRK, the absolute error rose by 1.3% in response to the increased methane concentration. Therefore, increasing the concentration of the methane impurity within the CO_2 mixture has little effect on the accuracy of density predictions performed with any of the EoS correlations.

3.2.3.4 Analysis of Results for Ternary CO_2+N_2+CH_4 Stream

In previous sections, the ability of different EoS correlations to predict the mixture densities of different binary CO_2+impurity streams was investigated. However, in real-life, industrial process plants and power stations produce anthropogenic CO_2, which tend to contain several chemical impurities.

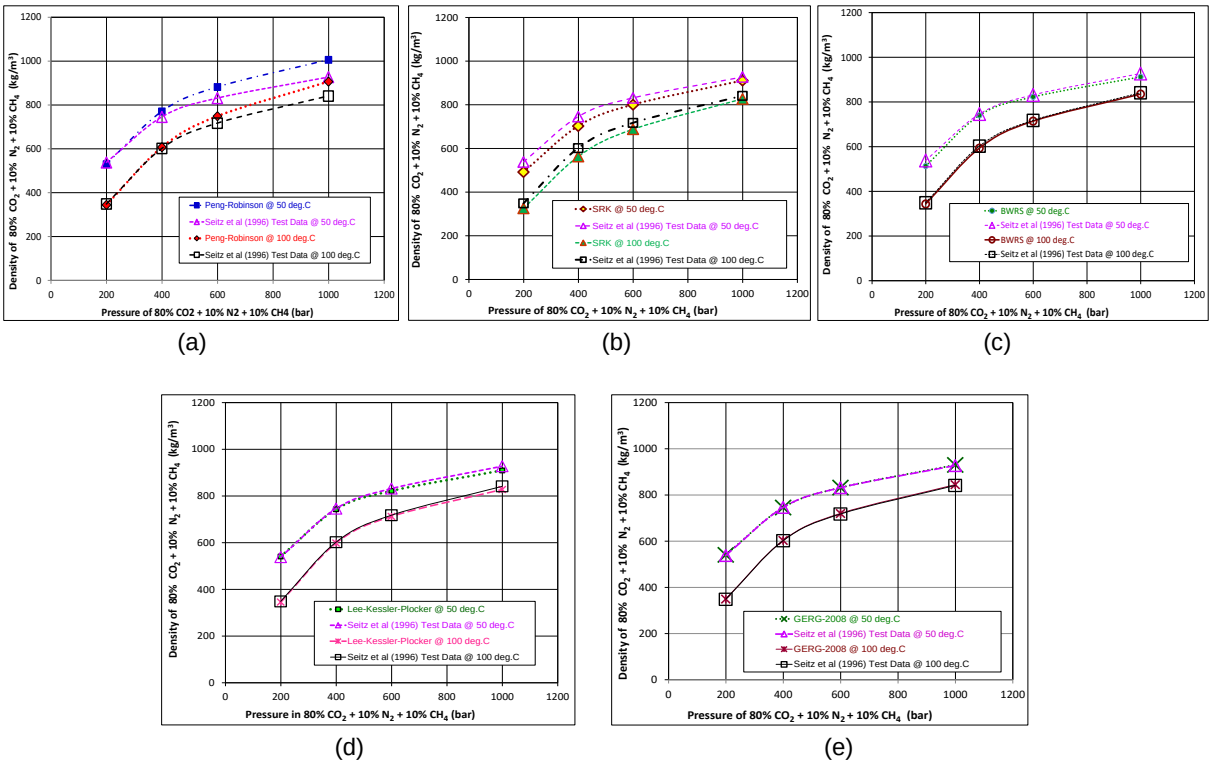

Fig. 3.6 Comparison of experimental and simulated 80% CO_2 + 10% N_2 + 10% CH_4 mixture density at 50 deg.C and 100 deg.C for (a) *Peng-Robinson (PR);* (b) *Soave-Redlich-Kwong (SRK);* (c) *Benedict-Weber-Rubin-Starling (BWRS);* (d) *Lee-Kessler-Plocker (LKP) and* (e) *Groupe Européen de Recherches Gazières 2008 (GERG-2008). All experimental data is culled from Seitz et al. (1996b)*

Since an actual transport pipeline will carry a CO_2 stream with multiple impurities, it is important to evaluate the ability of each EoS correlation to predict thermodynamic properties of ternary CO_2 mixtures with reasonable accuracy. Given the limited

availability of experimental data, the investigation was limited to CO_2 stream containing 10% N_2 and 10% CH_4 as impurities.

As seen in Fig. 3.6 and Table 3.6, GERG-2008 retains its position as the best performing EoS correlation when applied in simulating fluid density for the ternary mixture of 80% CO_2, 10% N_2 and 10% CH_4. SRK remains the worst performing EoS correlation. A comparison of data from Figs. 3.2 to 3.6 and Tables 3.2 to 3.6 indicate that for CO_2 mixtures, GERG-2008 is consistently the best performing correlation. This is because the accuracy of CO_2 mixture density predictions performed with GERG-2008 is superior to those of other EoS correlations.

Table 3.6: Statistical Evaluation of EoS Correlations for 80%CO_2 + 10%N_2 + 10%CH_4

EoS CORRELATION	TEMPERATURE	APE	AAPE	STANDARD DEVIATION
	[deg.C]	[%]	[%]	[%]
Peng-Robinson (PR)	50	4.129	4.853	4.272
	100	2.980	3.589	3.960
Soave-Redlich-Kwong (SRK)	50	-4.934	4.934	2.899
	100	-4.729	4.729	2.329
Benedict-Webb-Rubin-Starling (BWRS)	50	-2.040	2.040	1.771
	100	-1.044	1.044	0.535
Lee-Kessler-Plocker (LKP)	50	-0.741	1.015	1.063
	100	-0.944	0.944	0.451
GERG-2008	50	0.228	0.239	0.266
	100	0.323	0.323	0.093

An analysis of Fig. 3.1 and Table 3.1 shows that when applied in the simulation of pure CO_2 density, GERG-2008 has proven to be equally as good as Span and Wagner (SW), which is internationally recognized as the best correlation for calculating properties of pure CO_2

3.2.4 Evaluation of Equations of State for Viscosity Calculation

Unlike thermophysical properties such as density, compressibility, speed of sound and enthalpy, an Equation of State cannot be applied in the calculation of fluid viscosity. This is because EoS correlations by themselves only perform calculations based on equilibrium thermodynamics. They do not account for fluid dynamics. To overcome this problem, an EoS combined with a specialized correlation, which accounts for fluid flow, is usually applied in the simulation of viscosity (Oosterkamp

and Ramsen, 2008). Examples of such specialized correlations include Vesovic *et al.* (1990), Fenghour *et al.* (1998) and Quiñones-Cisneros *et al.* (2000).

In this section, experimental data on viscosity for pure CO_2 and binary CO_2 mixtures were compared to simulations carried out with the following six EoS correlations: Peng-Robinson (PR); Soave-Redlich-Kwong (SRK); Benedict-Webb-Rubin-Starling (BWRS); Lee-Kessler-Plocker (LKP); Span and Wagner (SW) and GERG-2008. All above-mentioned EoS are capable of predicting viscosity because they function in combination with various specialized correlations that account for fluid flow. The seventh correlation EoS-CG was excluded from this study because it lacks that capability.

3.2.4.1 Analysis of Results for Pure CO_2 Stream

The EoS correlations mentioned in section 3.2.4 were used to predict the viscosity of pure CO_2 over a pressure range of 117 bar to 248 bar at temperatures of 32.2 deg.C and 48.9 deg.C. The simulated viscosity results were compared to experimental data obtained under the same operating conditions by McCollum and Ogden (2006).

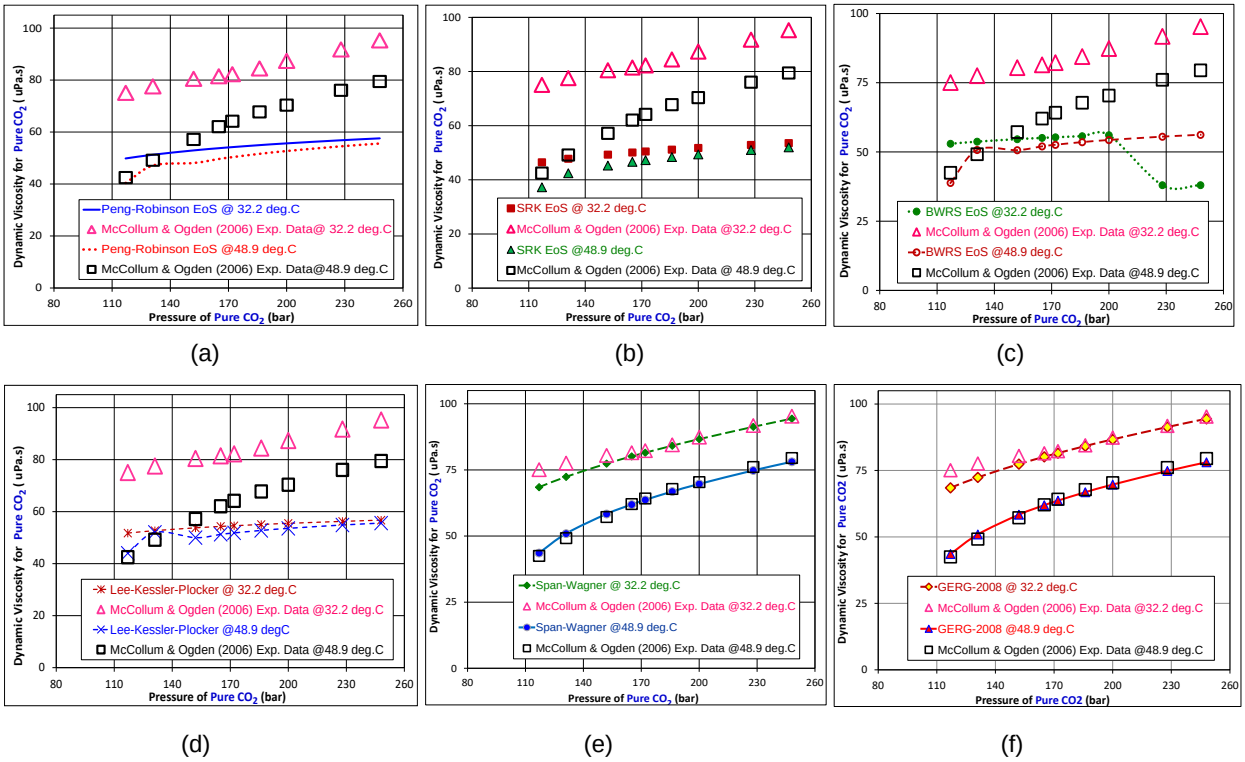

Fig. 3.7 Comparison of experimental and simulated pure CO_2 viscosity at 32.2 deg.C and 48.9 deg.C for (a) *Peng-Robinson (PR);* (b)*Soave-Redlich-Kwong (SRK);* (c) *Benedict-Weber-Rubin-Starling (BWRS);* (d) *Lee-Kessler-Plocker (LKP);* (e) *Span-Wagner (SW) and* (f) *Groupe Européen de Recherches Gazières (GERG-2008). All experimental data is culled from McCollum and Ogden (2006)*

For both temperatures, Span and Wagner (SW) and GERG-2008 correlations were the best performing EoS across the entire high-pressure range. In fact, an examination of the Fig. 3.7 and Table 3.7 reveals that they were the only EoS correlations capable of predicting the viscosity of pure CO_2 with a high degree of accuracy. The remaining EoS correlations perform poorly, producing predictions that diverge greatly from the experimental results.

Table 3.7: Statistical Evaluation of EoS Correlations for Pure CO_2 Viscosity

EoS CORRELATION	TEMPERATURE	APE	AAPE	STANDARD DEVIATION
	[deg.C]	[%]	[%]	[%]
Peng-Robinson (PR)	32.2	-35.445	35.445	2.118
	48.9	-19.350	19.350	9.391
Soave-Redlich-Kwong (SRK)	32.2	-39.838	39.838	2.011
	48.9	-24.879	24.879	7.884
Benedict-Webb-Rubin-Starling (BWRS)	32.2	-38.459	38.459	11.995
	48.9	-16.829	17.527	10.059
Lee-Kessler-Plocker (LKP)	32.2	-34.877	34.877	3.101
	48.9	-15.982	18.067	12.851
Span and Wagner (SW)	32.2	-2.770	2.770	3.065
	48.9	0.100	1.685	2.022
GERG-2008	32.2	-2.742	2.742	3.087
	48.9	0.102	1.686	2.025

A further analysis of the results in Table 3.7 show that error in the viscosity predictions decrease significantly as temperature condition shift from 32.2 deg.C to 48.9 deg.C. In other words, the temperature increase seems to improve the performance of all EoS correlations. However, it has to be pointed out that in spite of the improvement, BWRS, LKP, PR and SRK still predict viscosity with large errors. Considering that their prediction errors increase with rising pressure as illustrated on Fig. 3.7(a)-(d), it is reasonable to conclude that BWRS, LKP, PR and SRK are not suitable for performing viscosity predictions for pure CO_2 at the conditions under study. In contrast to the four poorly performing EoS correlations, the small prediction errors of SW and GERG-2008 diminishes with rising pressure, thus reinforcing the fact that both Helmholtz free energy-based EoS are the most suitable for pure CO_2 viscosity prediction at conditions under study.

3.2.4.2 Analysis of Results for Binary CO_2+H_2 Stream

With one exception, the EoS correlations mentioned in 3.2.4 were used to predict the mixture viscosity of a 95% CO_2 + 5% H_2 stream over two sets of pressure ranges and temperature conditions: 111.3 – 454.10 bar at 35 deg.C and 119.6 – 437.8 bar at 50 deg.C. Subsequently, the viscosity predictions were compared to experimental data collected under the same supercritical operating conditions by al-Sayibi (2013). Span and Wagner is not applicable to CO_2 mixtures as explained in section 3.1.3 and therefore was excluded from the analysis.

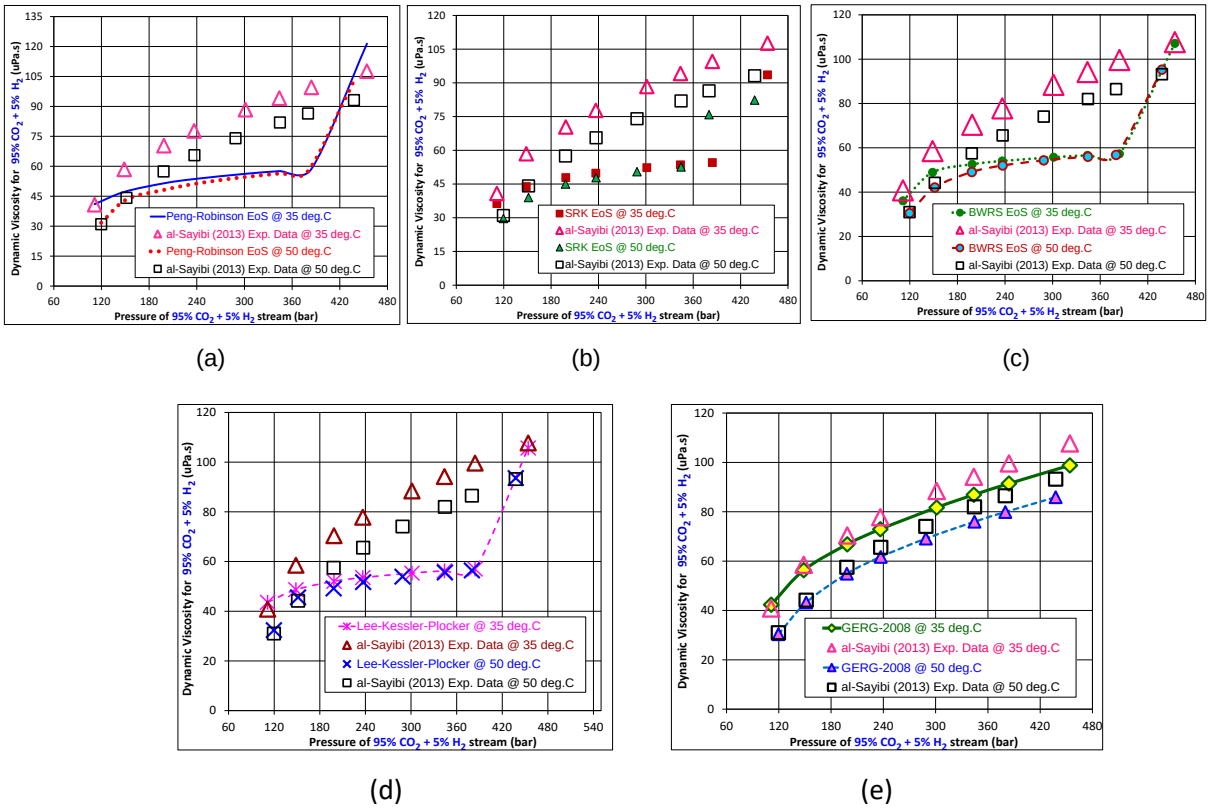

Fig. 3.8 Comparison of experimental and simulated 95% CO_2 + 5% H_2 mixture viscosity at 35 deg.C and 50 deg.C for (a) *Peng-Robinson (PR);* (b) *Soave-Redlich-Kwong (SRK);* (c) *Benedict-Weber-Rubin-Starling (BWRS);* (d) *Lee-Kessler-Plocker (LKP) and* (e) *Groupe Européen de Recherches Gazières (GERG-2008). All experimental data is culled from al-Sayibi (2013)*

An examination of both Fig 3.8 and Table 3.8 reveals that GERG-2008 is the only EoS correlation capable of calculating fluid viscosity with reasonable accuracy for CO_2+H_2 mixtures under the operating conditions set out above. The remaining EoS correlations performed poorly, producing predictions that diverge heavily from the experimental results. Further survey of the data in Table 3.8 reveals that on average, the absolute error in viscosity predictions decline as temperature condition shift from 35 deg.C to 50 deg.C. Nevertheless, these improvements in predictive accuracy are

not significant enough to change the reality that only GERG-2008 is able to predict mixture viscosity with reasonable accuracy. BWRS, LKP, PR and SRK are not suitable for performing viscosity predictions for CO_2+H_2 mixtures at the conditions under study.

Table 3.8: Statistical Evaluation of EoS Correlations for 95% CO_2 + 5% H_2 Viscosity

EoS CORRELATION	TEMPERATURE	APE	AAPE	STANDARD DEVIATION
	[deg.C]	[%]	[%]	[%]
Peng-Robinson (PR)	35	-22.55	25.87	19.57
	50	-14.89	18.07	16.53
Soave-Redlich-Kwong (SRK)	35	-30.76	30.76	13.24
	50	-19.54	19.54	11.24
Benedict-Webb-Rubin-Starling (BWRS)	35	-25.46	25.46	14.90
	50	-16.55	17.10	14.07
Lee-Kessler-Plocker (LKP)	35	-23.70	25.41	18.30
	50	-15.23	17.24	16.12
GERG-2008	35	-5.38	6.33	4.04
	50	-5.52	5.52	2.36

3.2.4.3 Analysis of Results for Binary CO_2+CH_4 Stream

A comparison of predictions performed with EoS correlations against experimental data of for 95% CO_2 + 5% CH_4 mixture confirms GERG-2008 to be the best performing equation of state for all pressures and temperatures considered.

Fig 3.9(c)-(d) shows that at certain pressures and temperatures, BWRS and LKP perform well, generating predictions with errors of less than 5%. However, these must be regarded as outliers. For most pressure and temperatures in this study, both BWRS and LKP generate predictions with huge unacceptable errors. PR and SRK correlations perform poorly at most of the pressures and temperatures considered in this study (Fig. 3.9(a)-(b)).

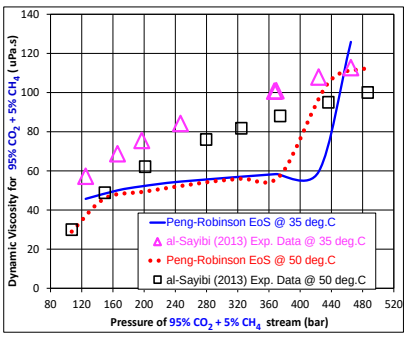

(a)

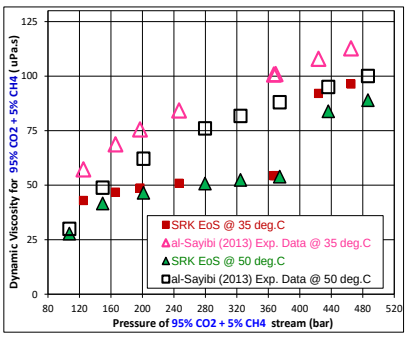

(b)

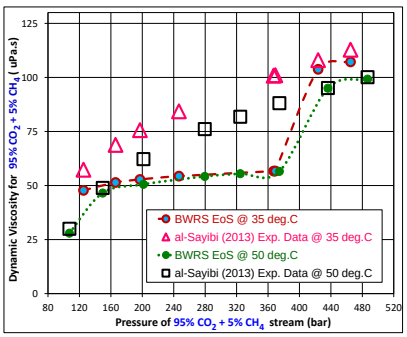

(c)

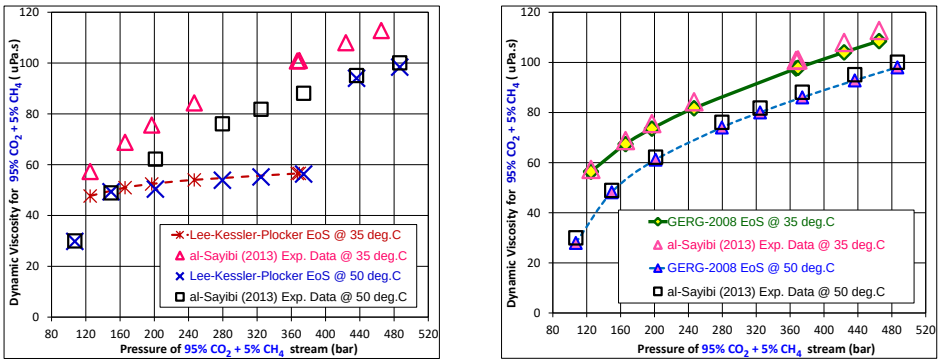

(d) (e)

Fig. 3.9 Comparison of experimental and simulated 95% CO_2 + 5% CH_4 mixture viscosity at 35 deg.C and 50 deg.C for (a) *Peng-Robinson (PR);* (b) *Soave-Redlich-Kwong (SRK);* (c) *Benedict-Weber-Rubin-Starling (BWRS);* (d) *Lee-Kessler-Plocker (LKP) and* (e) *Groupe Européen de Recherches Gazières (GERG-2008). All experimental data is culled from al-Sayibi (2013)*

Table 3.9: Statistical Evaluation of EoS Correlations for 95% CO_2 + 5% CH_4 Viscosity

EoS CORRELATION	TEMPERATURE	APE	AAPE	STANDARD DEVIATION
	[deg.C]	[%]	[%]	[%]
Peng-Robinson (PR)	35	-28.94	31.84	18.41
	50	-12.71	18.48	18.74
Soave-Redlich-Kwong (SRK)	35	-31.67	31.67	12.66
	50	-22.24	22.24	12.54
Benedict-Webb-Rubin-Starling (BWRS)	35	-25.53	25.53	15.85
	50	-16.02	16.02	14.72
Lee-Kessler-Plocker (LKP)	35	-32.89	32.89	10.64
	50	-14.93	15.15	16.03
GERG-2008	35	-2.89	2.89	0.77
	50	-2.68	2.68	1.70

Table 3.9 ranks the average performance of all the equations of state (EoS) considered from best to the worst. From the tabulated data, GERG-2008 is the best performing EoS and the only correlation capable of generating highly accurate predictions consistently for the entire range of conditions under study.

3.2.4.4 Analysis of Results for Binary CO_2+CO Stream

Fig 3.10 shows a comparison of mixture viscosity predictions with experimental data for 95% CO_2 + 5% CO stream under different pressure and temperature conditions. As illustrated in Fig 3.10(e), mixture viscosity predictions of GERG-2008 were found to be in close agreement with the experimental data across all pressure and temperature conditions featured in the study.

Fig.3.10(c)-(d) show that under a few pressure and temperature conditions, BWRS and LKP correlations perform reasonably well with errors of less than 6%. However, these must be regarded as outliers. For most pressure and temperature conditions featured in this study, both correlations generate predictions with large errors.

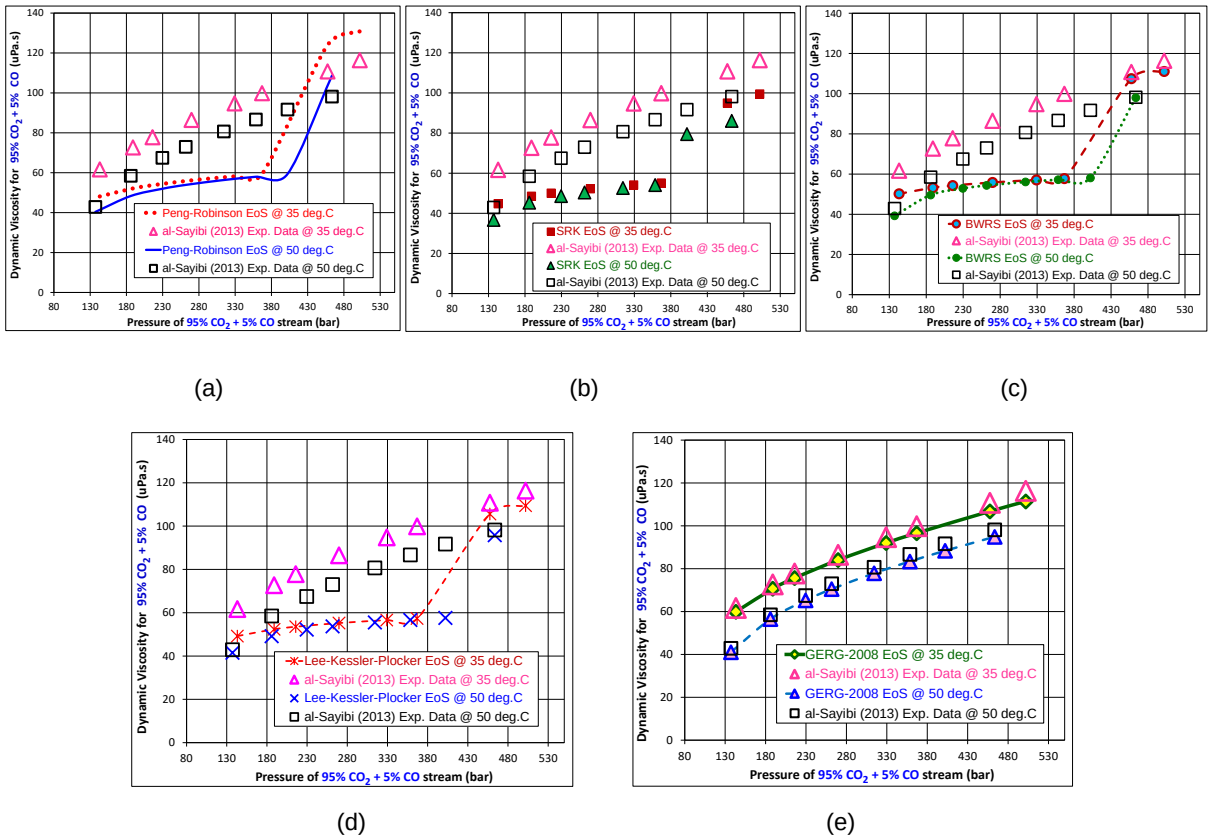

Fig. 3.10 Comparison of experimental and simulated 95% CO_2 + 5% CO mixture viscosity at 35 deg.C and 50 deg.C for (a) *Peng-Robinson (PR);* (b) *Soave-Redlich-Kwong (SRK);* (c) *Benedict-Weber-Rubin-Starling (BWRS);* (d) *Lee-Kessler-Plocker (LKP) and* (e) *Groupe Européen de Recherches Gazières (GERG-2008). All experimental data is culled from al-Sayibi (2013)*

Fig 3.10 (a)-(b) show that PR and SRK consistently produce predictions that diverge significantly from the experimental data. The large errors generated by both correlations makes them unreliable for use in predicting the mixture viscosity of the CO_2+CO stream at pressure and temperature conditions featured in this study.

Table 3.10 ranks the average performance of all the equations of state (EoS) considered from best to the worst. From the tabulated data, GERG-2008 is the best performing EoS and the only correlation capable of generating highly accurate predictions consistently across the entire range of conditions under study. On average, BWRS, LKP, PR and SRK perform poorly.

Table 3.10: Statistical Evaluation of EoS Correlations for 95% CO_2 + 5% CO Viscosity

EoS CORRELATION	TEMPERATURE	APE	AAPE	STANDARD DEVIATION
	[deg.C]	[%]	[%]	[%]
Peng-Robinson (PR)	35	-21.44	27.51	21.55
	50	-20.06	22.72	15.59
Soave-Redlich-Kwong (SRK)	35	-31.58	31.58	11.93
	50	-24.25	24.25	10.07
Benedict-Webb-Rubin-Starling (BWRS)	35	-25.09	25.09	15.09
	50	-21.55	21.55	12.79
Lee-Kessler-Plocker (LKP)	35	-26.14	26.14	14.64
	50	-21.71	21.71	13.45
GERG-2008	35	-3.18	3.18	0.53
	50	-3.62	3.62	0.34

3.2.5 Evaluation of Equations of State for Isothermal Compressibility

Isothermal compressibility is a second-order derivative thermophysical property. It is a quantitative indicator of the sensitivity of a fluid's specific volume to pressure change. It is important to note that isothermal compressibility (K_T) is not the same as the compressibility factor (Z) mentioned in section 2.3.1.4 of this PhD thesis. Absolute values of Z are merely corrective factors that quantifies the deviation of the specific volume of a real fluid from that of an ideal gas for a given pressure and temperature. In contrast, absolute values of K_T measure specific volume change of a fluid in response to pressure. Nevertheless, isothermal compressibility (K_T) is related to the variation of compressibility factor (Z) with respect to pressure as expressed in the equation below:

$$K_T = \frac{1}{P} - \frac{1}{Z}\left(\frac{\partial Z}{\partial P}\right)_T = -\frac{1}{v}\left(\frac{\partial v}{\partial P}\right)_T \qquad (3.4)$$

Generally, experimental data on second-order derivative thermophysical properties such as isothermal compressibility, speed of sound and Joule-Thompson coefficients are scarce for pure and impure CO_2 streams at conditions relevant to CCS. For pure CO_2 and CO_2 mixtures containing even the most common impurities found in CCS facilities, only a limited amount of experimental data are available. For CO_2 mixtures containing certain impurities, no experimental data exist for the range of operational conditions relevant to CO_2 pipeline transportation in the CCS context (Munkejord *et al.*, 2016).

In this section, experimental data on isothermal compressibility was secured for pure CO_2 and CO_2 in binary mixtures with N_2, H_2, CH_4 and CO. Although, the experimental data sourced from al-Sayibi (2013) is limited to certain chemical compositions of CO_2 mixtures, it still meets the 100–1000 bar pressure range required for study conducted in this chapter. The experimental results were compared to predictions performed with the following six correlations: Peng-Robinson (PR); Soave-Redlich-Kwong (SRK); Lee-Kessler-Plocker (LKP); Span and Wagner (SW); Groupe Européen de Recherches Gazières (GERG-2008) and Equation of State for Combustion Gases & Combustion Gas-like Mixtures (EoS-CG). The author of this PhD thesis could not find a BWRS algorithm capable of calculating isothermal compressibility and speed of sound. For that reason, BWRS was not included in the comparative study performed in this section.

3.2.5.1 Analysis of Results for Pure CO_2 Stream

EoS correlations mentioned in section 3.2.5 were used to simulate isothermal compressibility of pure CO_2 over a pressure range of 111.4 bar to 413.8 bar at temperature condition of 28 deg.C. Then the simulation results were compared to experimental data obtained under the same operating conditions by al-Sayibi (2013).

Table 3.11: Statistical Evaluation of EoS Correlation for Pure CO_2 Compressibility

EoS CORRELATION	TEMPERATURE	APE	AAPE	STANDARD DEVIATION
	[deg.C]	[%]	[%]	[%]
Peng-Robinson (PR)	28	36.85	36.85	12.17
Soave-Redlich-Kwong (SRK)	28	36.65	36.65	11.06
Lee-Kessler-Plocker (LKP)	28	-8.22	8.22	4.97
Span and Wagner (SW)	28	-2.45	3.65	4.27
EoS-CG	28	-2.45	3.65	4.27
GERG-2008	28	-2.63	3.91	4.56

Fig. 3.11(a)-(b) show that the cubic correlations PR and SRK predict isothermal compressibility with unacceptably high errors. These errors increase with pressure

and range from 18.7% to 52.2%. As illustrated in Fig.311(c), the performance of LKP across the range of pressure conditions is mixed. The prediction errors of this particular the virial correlation increase from 2.2% to 16.2% as the pressure rises from 111.4 bar to 413.8 bar at temperature condition of 28 deg. C. The Helmholtz free energy correlations—SW, EoS-CG and GERG-2008—generate relatively lower errors in comparison to the others. For most of the pressure conditions under study, the errors produced in all three Helmholtz correlations are less than 4%. For a few pressure conditions, errors of up to 10.3% were observed.

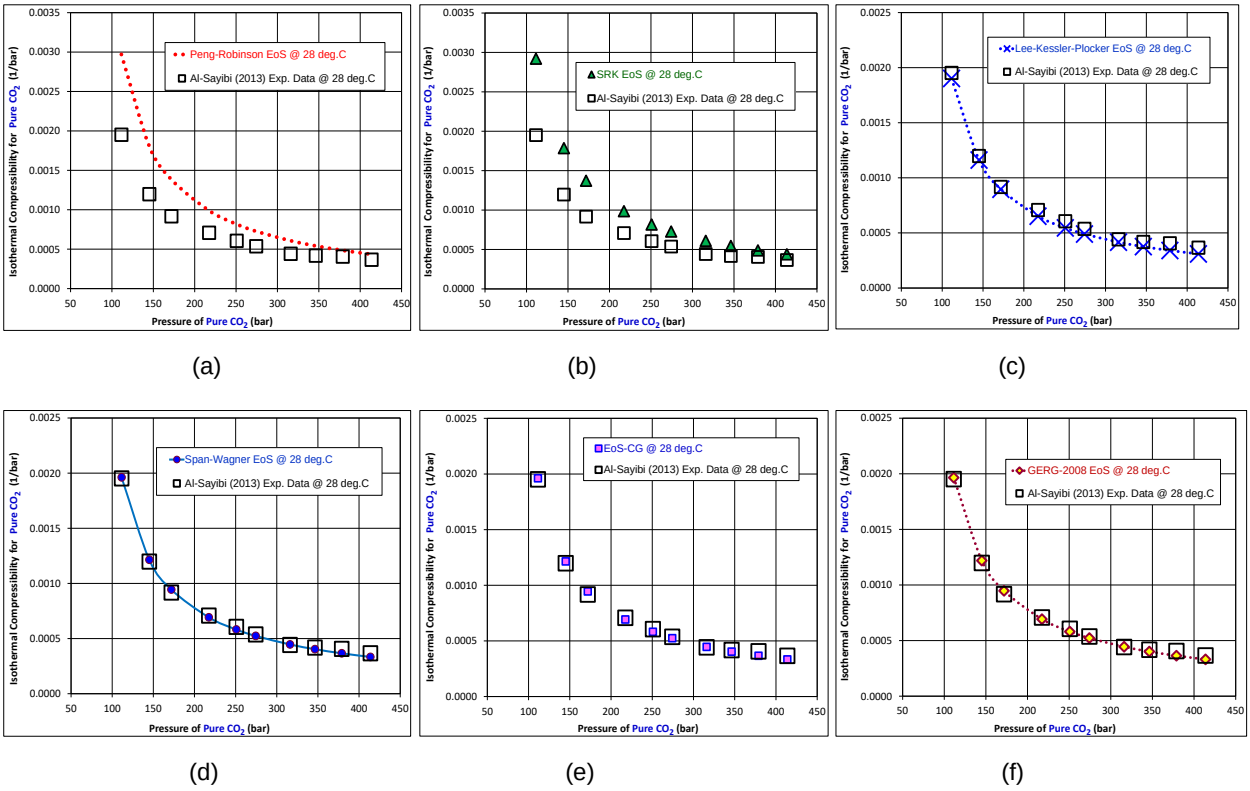

Fig. 3.11 Comparison of experimental and simulated pure CO_2 isothermal compressibility at 28 deg.C for (a) *Peng-Robinson (PR);* (b)*Soave-Redlich-Kwong (SRK);* (c) *Lee-Kessler-Plocker (LKP);* (d) *Span-Wagner (SW); (e) Equation of State for Combustion Gases & Combustion Gas-like Mixtures (EoS-CG) and* (f) *Groupe Européen de Recherches Gazières (GERG-2008). All experimental data is culled from al-Sayibi (2013)*

Table 3.11 ranks the average performance of the equations of state (EoS). SW, EoS-CG and GERG-2008 are tied as the best performing correlations judging by their extremely low AAPE values followed by LKP. PR and SRK were the worst performing EoS since its predictions generated the highest AAPE values.

It is worth noting that the tabulated error data for SW and EoS-CG are identical. This confirms the claim made by Gernert and Span (2010, 2016) the developers of the

EoS-CG that when engaged in the calculation of pure CO_2 properties, this particular correlation dispenses with its mixing rules and applies the same equations as those of Span and Wagner (1996). Because of that particular attribute, EoS-CG predictions are more accurate than those of GERG-2008 when applied in the simulation of pure CO_2 properties.

3.2.5.2 Analysis of Results for Binary CO_2+N_2 Stream

Fig. 3.12 and Table 3.12 compares the isothermal compressibility predictions of various EoS correlations with experimental data for 95.56% CO_2 + 4.44% N_2 stream under different pressure and temperature conditions.

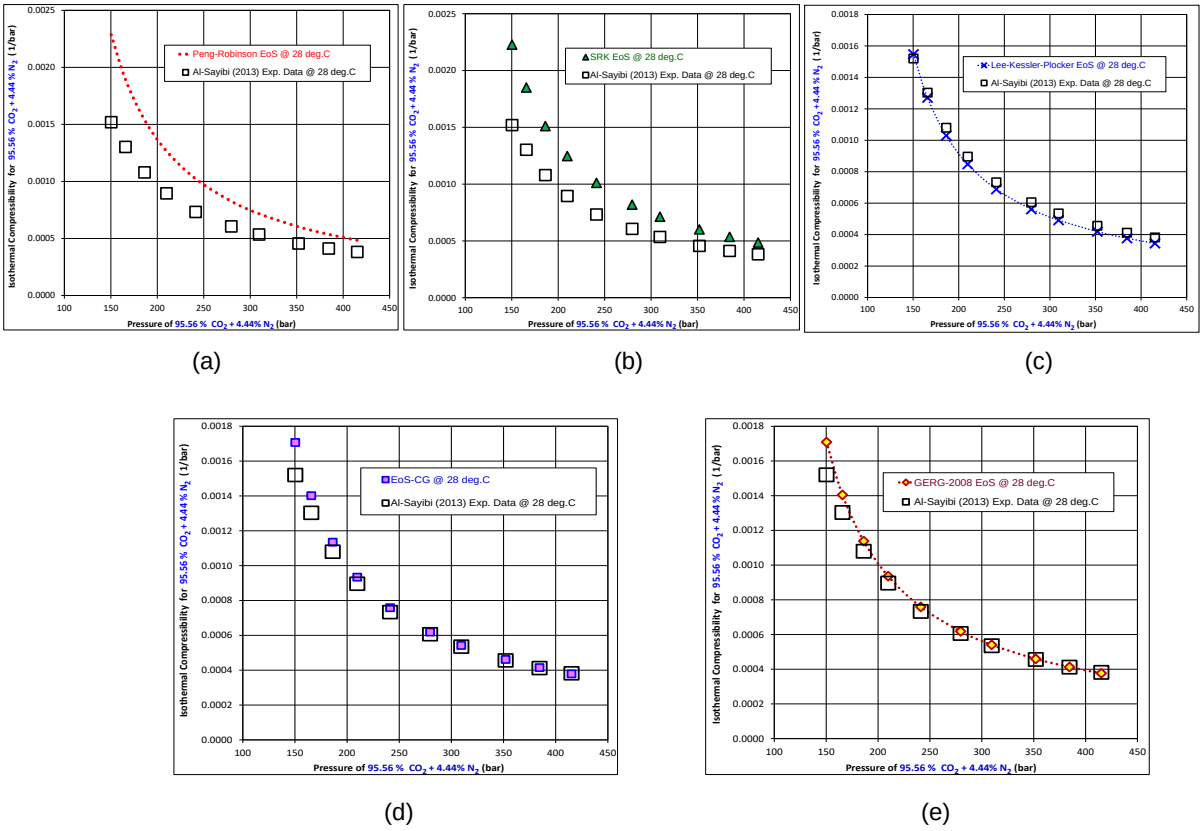

Fig. 3.12 Comparison of experimental and simulated isothermal compressibility of 95.56% CO_2 + 4.44% N_2 mixture at 28 deg.C for (a) *Peng-Robinson (PR);* (b) *Soave-Redlich-Kwong (SRK);* (c) *Lee-Kessler-Plocker (LKP); (d) Equation of State for Combustion Gases & Combustion Gas-like Mixtures (EoS-CG) and* (e) *Groupe Européen de Recherches Gazières (GERG-2008). All experimental data is culled from al-Sayibi (2013)*

Fig 3.12(a) shows that prediction error of PR reduces from 50.5% to 26.9% as pressure increases from 150.3 bar to 415.2 bar. For the same pressure range, errors in SRK predictions drop from 46.6% to 27.1% (Fig. 3.12(b)). These results indicate that both cubic correlations generate large errors, which reduce as pressure

increases. Nevertheless, the lowest errors generated by both correlations is still unacceptably high. Therefore, PR and SRK are unsuitable for performing isothermal compressibility predictions of CO_2+N_2 mixtures at the conditions under study.

As illustrated in Fig.311(c), the performance of LKP across the range of pressure conditions is mixed. The prediction errors of this particular the virial correlation increase from 1.8% to 9.9% as the pressure rises from 150.3 bar to 415.2 bar at temperature condition of 28 deg.C. Fig. 3.12(d) shows that the prediction error of EoS-CG drops from 12.3% to 0.9% as pressure increases from 150.3 bar to 415.2 bar. As shown in Fig 3.12 (e), for the same pressure range, error produced by GERG-2008 reduces from 12.4% to 1.4%. These results demonstrate that the performance of both Helmholtz free energy correlations improve significantly as pressure becomes higher.

Table 3.12: Statistical Evaluation of EoS for 95.56% CO_2 + 4.44% N_2 Compressibility

EoS CORRELATION	TEMPERATURE	APE	AAPE	STANDARD DEVIATION
	[deg.C]	[%]	[%]	[%]
Peng-Robinson (PR)	28	37.89	37.89	7.34
Soave-Redlich-Kwong (SRK)	28	36.35	36.35	5.92
Lee-Kessler-Plocker (LKP)	28	-5.86	6.22	3.45
EoS-CG	28	3.69	3.87	3.89
GERG-2008	28	3.60	3.89	4.14

Table 3.12 indicates that EoS-CG and GERG-2008 are the best performing EoS correlations on average. This is followed by LKP, which performs moderately well on average. As demonstrated by their extremely high AAPE values, PR and SRK are the worst performing EoS correlations on average.

3.2.5.3 Analysis of Results for Binary CO_2+H_2 Stream

Fig. 3.13(a) shows that prediction error of PR reduces from 41.2% to 17.4% as pressure increases from 133.4 bar to 407.5 bar. Fig. 3.13(b) indicates that errors in SRK predictions drop from 37.4% to 17.6% for the same pressure range. These

results indicate that both cubic EoS correlations simulate isothermal compressibility of 95.47% CO_2 + 4.53% H_2 stream with unacceptably large errors. These errors reduce with rising pressure, but not enough to justify the application of both unreliable cubic EoS in the prediction of CO_2+H_2 mixtures for the particular conditions under study.

Fig.3.13(c)-(e) show that across the range of pressure conditions studied, the performance of LKP, EoS-CG and GERG-2008 are mixed.

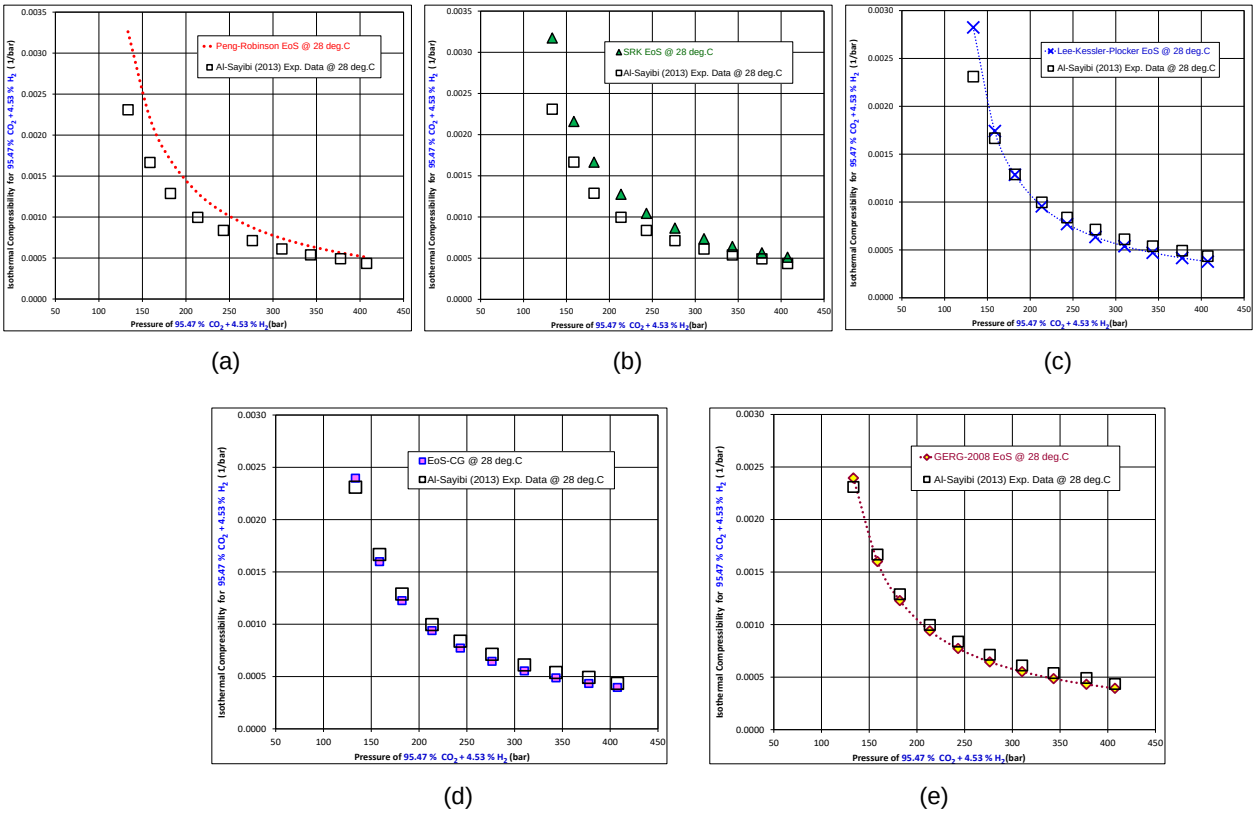

Fig. 3.13 Comparison of experimental and simulated isothermal compressibility of 95.47% CO_2 + 4.53% H_2 mixture at 28 deg.C for (a) *Peng-Robinson (PR);* (b) *Soave-Redlich-Kwong (SRK);* (c) *Lee-Kessler-Plocker (LKP); (d) Equation of State for Combustion Gases & Combustion Gas-like Mixtures (EoS-CG) and* (e) *Groupe Européen de Recherches Gazières (GERG-2008). All experimental data is culled from al-Sayibi (2013)*

At pressures below 214 bar, these correlations perform reasonably well with errors of less than 6%. Above 214 bar, errors generated by LKP can rise up to 15.1%. For EoS-CG and GERG-2008, the errors can reach up to 11.9% and 12.3% respectively.

Table 3.13: Statistical Evaluation of EoS for 95.47% CO_2 + 4.53% H_2 Compressibility

EoS CORRELATION	TEMPERATURE	APE	AAPE	STANDARD DEVIATION
	[deg.C]	[%]	[%]	[%]
Peng-Robinson (PR)	28	25.60	25.60	8.14
Soave-Redlich-Kwong (SRK)	28	24.27	24.27	6.84
Lee-Kessler-Plocker (LKP)	28	-4.99	10.33	11.45
EoS-CG	28	-6.81	7.56	4.41
GERG-2008	28	-6.93	7.66	4.56

Table 3.13 ranks PR and SRK as the worst performing EoS correlations on average based on their APE and AAPE values. Judging by their APE and AAPE, results, LKP, EoS-CG and GERG-2008 correlations perform moderately well on average. A further examination of the tabulated results shows that the standard deviation values of both EoS-CG and GERG-2008 are less than 5% while that of LKP is 11.5%. This means that EoS-CG and GERG-2008 perform better than LKP for a wider range of pressures under study. Therefore, EoS-CG and GERG-2008 are better choices for the predicting isothermal compressibility of the CO_2+H_2 stream compared to LKP.

3.2.5.4 Analysis of Results for Binary CO_2+CH_4 Stream

Fig. 3.14 and Table 3.14 compares the isothermal compressibility predictions of various EoS correlations with experimental data for 95.39% CO_2 + 4.61% CH_4 stream under different pressure and temperature conditions.

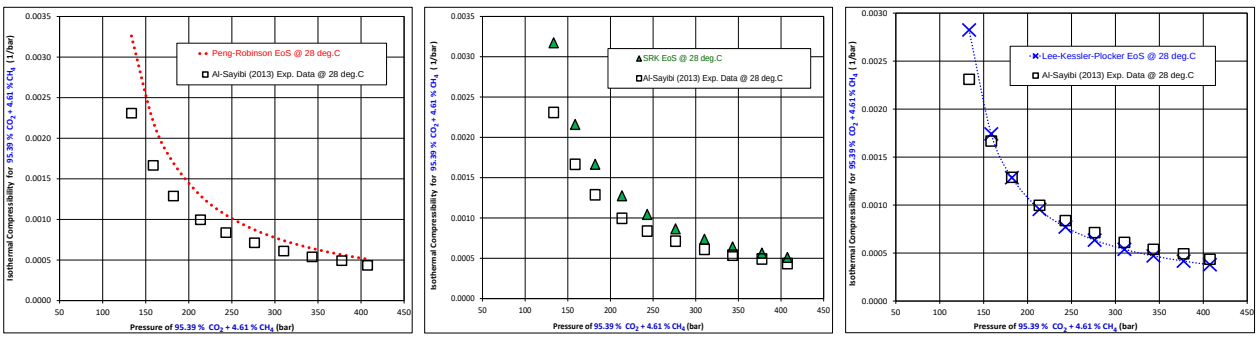

(a) (b) (c)

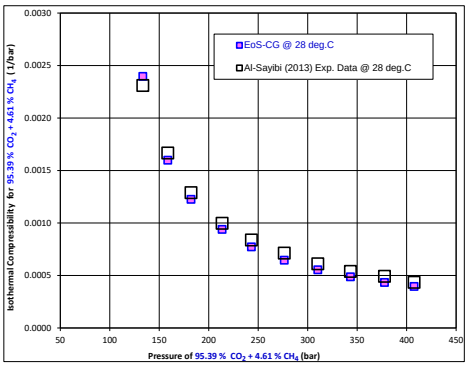

(d)

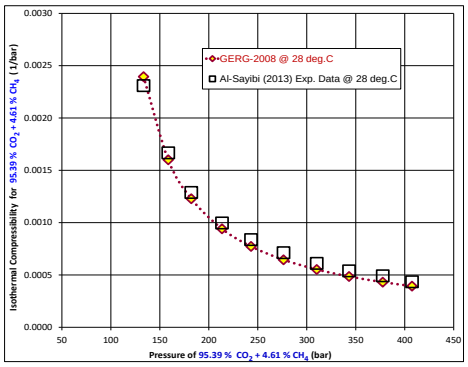

(e)

Fig. 3.14 Comparison of experimental and simulated isothermal compressibility of 95.39% CO_2 + 4.61% CH_4 mixture at 28 deg.C for (a) *Peng-Robinson (PR);* (b) *Soave-Redlich-Kwong (SRK);* (c) *Lee-Kessler-Plocker (LKP); (d) Equation of State for Combustion Gases & Combustion Gas-like Mixtures (EoS-CG) and* (e) *Groupe Européen de Recherches Gazières (GERG-2008). All experimental data culled from al-Sayibi (2013)*

Fig. 3.14(a) shows that prediction error of PR reduces from 52.2% to 16.5% as pressure increases from 103.6 bar to 345.6 bar. Fig. 3.14(b) indicates that errors in SRK predictions drop from 45.3% to 16.3% for the same pressure range. These results indicate that both cubic EoS correlations simulate isothermal compressibility of 95.39% CO_2 + 4.61% CH_4 stream with unacceptably large errors. These errors decline with increasing pressure, but not enough to justify the application of both unreliable cubic EoS in the prediction of CO_2+CH_4 mixtures for the particular conditions under study.

Table 3.14: Statistical Evaluation of EoS for 95.39% CO_2 + 4.61% CH_4 Compressibility

EoS CORRELATION	TEMPERATURE [deg.C]	APE [%]	AAPE [%]	STANDARD DEVIATION [%]
Peng-Robinson (PR)	28	36.46	36.46	9.48
Soave-Redlich-Kwong (SRK)	28	33.75	33.75	7.96
Lee-Kessler-Plocker (LKP)	28	-5.60	8.72	8.57
EoS-CG	28	-1.23	4.10	6.26
GERG-2008	28	-1.25	4.15	6.33

As demonstrated in Fig.3.14(c)-(e), the prediction error of LKP ranges from 4.1% to 18.6%. For EoS-CG, the predictive errors range from 0.29% to 12.3% while errors of

GERG-2008 range from 0.16% to 12.7%. These results combined with data from Table 3.14 indicate that EoS-CG and GERG-2008 are the best performing EoS correlations on average for predicting isothermal compressibility. The average performance of LKP can be ranked “moderate”. In other words, LKP should be used for calculating isothermal compressibility only if EoS-CG and GERG-2008 are unavailable. PR and SRK are the worst performing correlations on average.

3.2.5.5 Analysis of Results for Binary CO_2+CO Stream

Fig. 3.15 and Table 3.15 compares the isothermal compressibility predictions of various EoS correlations with experimental data for 95.61 % CO_2 + 4.39 % CO stream over a pressure range of 103.7 bar to 382 bar at 28 deg.C.

Fig. 3.15(a)-(b) show that at 382 bar, PR and SRK generate predictions with errors of less than 5%. However, these must be regarded as outliers. For all other pressure conditions covered in this study, PR and SRK generate predictions with errors that can reach up to 25.6% and 20.8% respectively.

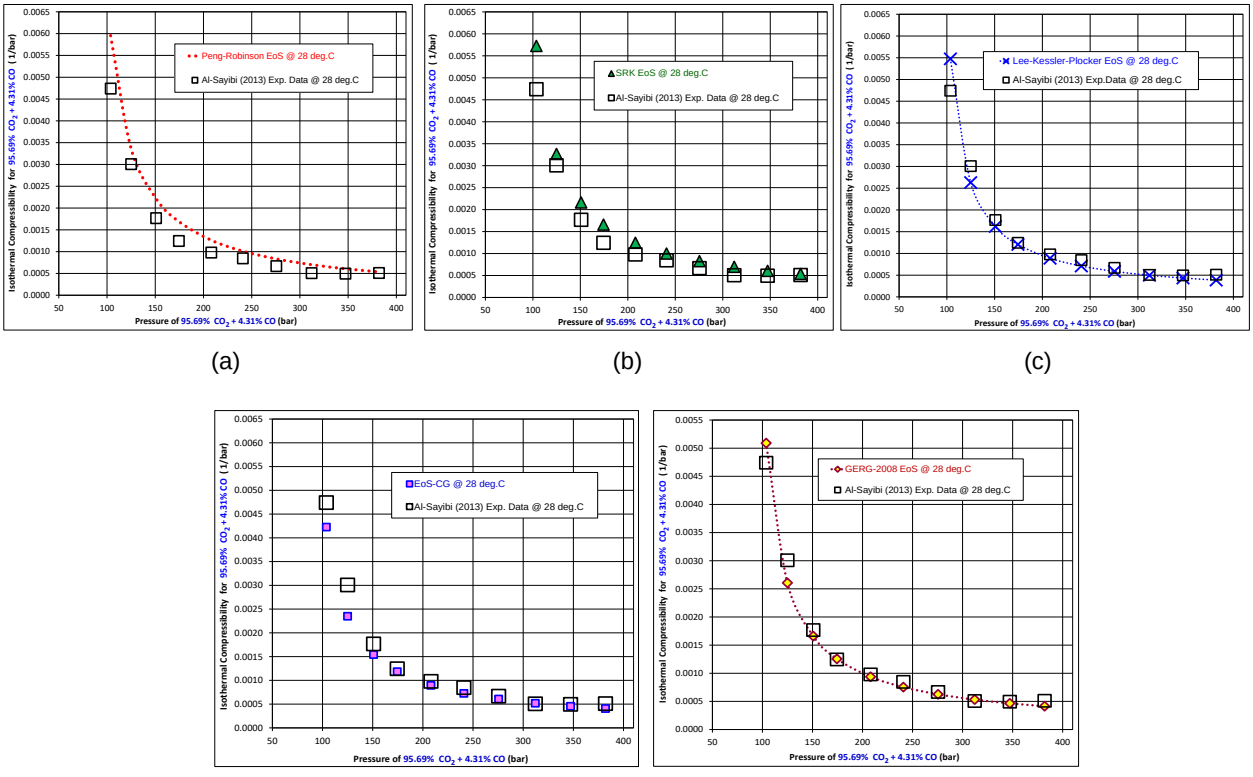

Fig. 3.15 Comparison of experimental and simulated isothermal compressibility of 95.69% CO_2 + 4.31% CO mixture at 28 deg.C for (a) *Peng-Robinson (PR);* (b) *Soave-Redlich-Kwong (SRK);* (c) *Lee-Kessler-Plocker (LKP); (d) Equation of State for Combustion Gases & Combustion Gas-like Mixtures (EoS-CG) and* (e) *Groupe Européen de Recherches Gazières (GERG-2008). All experimental data is culled from al-Sayibi (2013)*

Table 3.15: Statistical Evaluation of EoS for 95. 61% CO_2 + 4. 39% CO Compressibility

EoS CORRELATION	TEMPERATURE	APE	AAPE	STANDARD DEVIATION
	[deg.C]	[%]	[%]	[%]
Peng-Robinson (PR)	28	23.77	23.77	10.06
Soave-Redlich-Kwong (SRK)	28	21.94	21.94	9.97
Lee-Kessler-Plocker (LKP)	28	-8.50	11.59	10.56
EoS-CG	28	-10.80	11.27	7.09
GERG-2008	28	-5.27	7.89	8.07

In other words, both cubic correlations (PR and SRK) are unreliable since they generate unacceptably large errors when applied to CO_2+CO mixtures for nearly all the conditions under study. This is confirmed by data in Table 3.15.

Fig.3.15(c)-(e) show that across the range of pressure conditions studied, the performance of LKP, EoS-CG and GERG-2008 are mixed. However, based on AAPE and standard deviation values in Table 3.15, EoS-CG and GERG-2008 perform much better than LKP on average.

Therefore, the Helmholtz free energy-based correlations (i.e. EoS-CG and GERG-2008) are better choices for the predicting isothermal compressibility of the CO_2+CO stream compared any of the other types of correlations covered in this study.

3.3 CONCLUDING REMARKS: SELECTION OF SUITABLE EQUATIONS OF STATE

In this chapter, seven equation of state (EoS) correlations were evaluated individually and then compared to each other for pure CO_2 and various impure CO_2 mixtures at different supercritical conditions. The seven EoS correlations can be divided into three main categories: cubic, virial and Helmholtz free energy based equations of state.

On average, SRK was consistently the worst performing EoS correlation when applied in prediction of all thermophysical properties covered in the study for both pure CO_2 and impure CO_2 mixtures. Unlike SRK, PR produce predictions of

reasonable accuracy when thermophysical property is density. However, when the predicted thermophysical property is viscosity or isothermal compressibility, both cubic EoS correlations— PR and SRK— tie as the worst performing EoS correlations because of the unacceptably large errors they generate.

Virial EoS correlations (BWRS and LKP) predict density of pure CO_2 and impure CO_2 with low errors for all supercritical conditions studied. Despite the satisfactory performance of virial correlations in estimating fluid density, are no match for Helmholtz free energy-based EoS correlations (SW and GERG-2008) which have a superior accuracy on fluid density predictions. Both virial correlations generate large errors when applied in the simulation of fluid viscosity of pure and impure CO_2. In other words, both virial correlations are unsuitable for calculating fluid viscosity at the supercritical conditions covered in this study. LKP produce predictions of reasonable accuracy when thermophysical property is isothermal compressibility.

On average, the Helmholtz free energy-based correlations (SW, GERG-2008 and EoS-CG) were consistently observed to be the best performing equations of state when applied in prediction of all thermophysical properties covered in the study for both pure CO_2 and impure CO_2 mixtures. The predictions of SW are marginally more accurate compared to those of GERG-2008 when the working fluid is pure CO_2. Unfortunately, the extremely complicated structure of SW precludes its application to impure CO_2 mixtures. The newly developed EoS-CG correlation tackles this problem by applying the same equations as those of SW when applied in the simulation of pure CO_2 properties and employs mixing rules when applied in the simulation of properties of CO_2 mixtures. Because of this, EoS-CG predictions are more accurate than those of GERG-2008 when used in the estimation of pure CO_2 properties. Conversely, when applied in the simulation of properties of CO_2 mixtures, GERG-2008 predictions are more accurate than EoS-CG predictions for the supercritical conditions covered in this study.

From the studies carried out in this chapter, it can be concluded that for pure and impure CO_2 under supercritical conditions, Helmholtz free-energy EoS correlations (SW, GERG-2008 and EoS-CG) are generally superior in accuracy to virial EoS (BWRS and LKP), which in turn performs calculations with a higher level of accuracy than cubic EoS (PR and SRK).

Given their reputation for highly accurate predictions, Helmholtz free energy EoS correlations are obviously the best choice for simulating the thermophysical properties of pure and impure carbon dioxide within a hydraulic model of an entire supercritical CO_2 pipeline network or sub-models of individual compressors and pumps installed on that network.

Therefore as a prerequisite for developing an algorithmic tool for selection and sizing of centrifugal machines (which is the main aim of this PhD project), the highly accurate Span and Wagner (SW) EoS was selected for calculating pure CO_2 properties while GERG-2008 was selected for calculating impure CO_2 properties. Both correlations are an integral part of the quasi-dimensional compressor model in Chapter 4.

CHAPTER 4

MODELLING COMPRESSORS FOR CO_2 TRANSPORT PIPELINE

4.1 INTRODUCTION TO COMPRESSORS

A compressor is a machine that applies energy from an external source to reduce the volume of a fluid in order to increase its pressure. They suited for handling fluids of with high compressibility values such as gases, supercritical fluids and gas-liquid two-phase mixtures with high gas void fractions (Stosic *et al.*, 1992; Fleming *et al.,* 1998; Holloway *et al.*, 2010; Sorokes, 2013).

Pumps are similar to compressors in geometry and design (Okezue and Kuvshinov, 2018). Pumps applies energy from an external source to a fluid in order to increase its pressure and velocity for the purposes of transporting that fluid from one location to another (Douglas *et al.*, 2005; Nourbakhsh *et al.*, 2007).

Unlike compressors, pumps are not designed to compress (i.e. reduce the volume) of a fluid during the process of pressurization and therefore are most suited to handle liquids which are almost incompressible. Nevertheless, pumps can still perform some limited fluid compression when handling supercritical fluids, which are compressible (Okezue and Kuvshinov, 2018).

In the context of Carbon Capture and Storage (CCS), compression requirements of carbon dioxide are vastly different from those of compressors for air or natural gas compression. Some of these differences are attributable to the thermophysical properties of CO_2 and the fact that it has to be converted from gas to supercritical fluid prior to pipeline transportation. The molecular weight of carbon dioxide is much larger compared to those of air and natural gas. Therefore, for a given pressure and temperature, CO_2 is denser than either air or natural gas. The compression process required to convert gaseous CO_2 to a supercritical fluid involves tremendous volume reduction accompanied by generation of high pressures and temperatures (Witkowski and Majkut, 2012). More importantly, at the vicinity of the critical point (73.76 bar; 304.21 K), minor changes in temperature and pressure result in barely controllable, radical and huge changes in pure CO_2 properties. A slight pressure drop in the pipeline risks the single-phase supercritical fluid transforming into gas-liquid two-phase fluid— undesirable as it can lead to slugging and cavitation, which in turn, can damage compressors, pumps and the pipeline itself. Operating the pure CO_2

supercritical pipeline at pressures above 86 bar have been proposed to eliminate this problem (McCoy and Rubin, 2008; Witkowski *et al.*, 2014). When impurities are present in the supercritical CO_2, the range of pressures and temperatures conditions at which abrupt changes in CO_2 properties occur is vastly extended. This means that pipelines carrying impure supercritical CO_2 may have to operate at pressures above 150 bar to avoid unstable conditions that easily led to slugging and cavitation (Knoope *et al.*, 2013; Imre *et al.*, 2015; Okezue and Kuvshinov, 2018).

For compressors to generate extremely high pressures (>100 bar), a huge amount of energy is required (Oosterkamp and Ramsen, 2008; Lazic *et al.*, 2014). To maintain such pressures in a long distance pipeline will require a series of booster pumps placed at suitable intervals along the length of that pipeline (Seevam *et al.*, 2008; Race *et al.*, 2012; Okezue and Kuvshinov, 2018). Compared to a conventional liquid pump, an individual booster pump consumes a greater amount of energy because its working fluid, supercritical CO_2, is compressible (Adams, 2011; Bergamini *et al.*, 2011).

Furthermore, the operation of pipeline transportation infrastructure in the CCS context is on a scale that vastly outsizes operation of pipeline infrastructure for natural gas transportation (Luo *et al.*, 2014; Brown *et al.*, 2015). For a typical CCS project, the transport infrastructure is a vast network containing a large common trunk pipeline connected to several smaller feeder pipelines. Each feeder pipeline connects to the CO_2 capture facility of an individual fossil-fuelled industrial process plant. Through the application of several compressors, these feeder pipelines are able to supply compressed anthropogenic CO_2 in supercritical state to the common trunk pipeline from multiple emission sources. Booster pumps mounted at various intervals along the length of the common trunk pipeline ensures that pipeline pressures remain high enough to keep the CO_2 in supercritical state. A lot of energy is required to keep compressors and scores of booster pumps operating on an industrial scale in a pipeline network charged with transporting several metric megatons of anthropogenic CO_2 per annum to designated places of sequestration (Mertz et al., 2005).

All these make the design and operation of supercritical CO_2 transport pipelines more challenging and costlier than conventional natural gas pipelines where compression

pressures are relatively lower (<85bar) and neither phase change nor radical variations in thermophysical properties are expected (Serpa *et al.*, 2011; Seevam *et al.*, 2008; Luo *et al.*, 2014).

Most of the operating expenditure for the supercritical CO_2 transport pipeline networks goes to the running of installed compressors and pumps. Therefore, the long-term economic feasibility of running such a transport pipeline network is strongly dependent on curbing the high operating costs linked to the energy consumption of both machines (Okezue and Kuvshinov, 2018).

4.1.1 Description of Compressor Technologies and Their Working Principles

As illustrated in figure 4.1, machines for compressing (and pumping) fluids can be broadly divided into two major categories: positive displacement and rotodynamic machine categories.

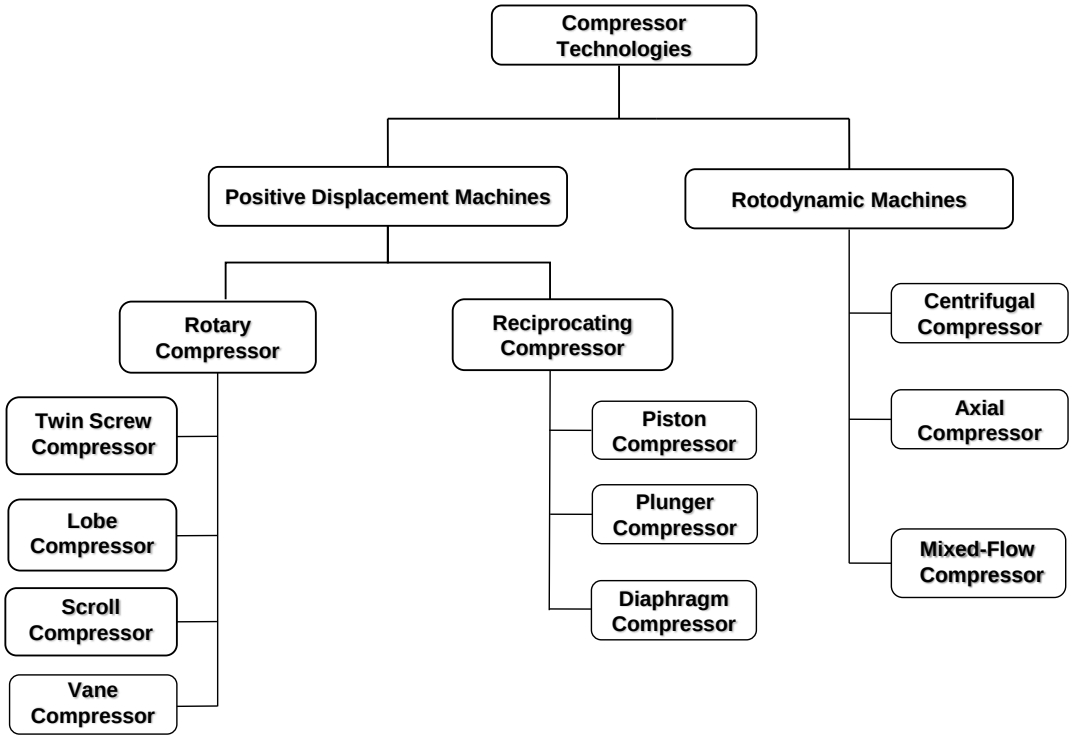

Fig. 4.1 Different types of compressor technologies

Positive displacement compressors operate in a cyclic process, which begins with fluid filling a working chamber at the inlet port and ends when the chamber displaces the fluid out of the compressor through the outlet port. The physical boundaries of the working chamber reduces progressively during the cyclic process causing the

overall volume of the fluid contained within it to be compressed prior to being displaced out of the outlet port at an elevated pressure and temperature. (Douglas *et al.*, 2005; Eastop and McConkey, 1993). Positive displacement machines deliver a fixed amount of fluid per operational cycle. Therefore, volumetric fluid flow rate is a function of the volume of the working chamber and the frequency with which it is filled and emptied of fluid (Douglas *et al.*, 2005; Okezue, 2010). The positive displacement machine category is divided into two subcategories namely: reciprocating compressors and rotary compressors.

Examples of reciprocating machines are piston compressors, diaphragm compressors and plunger compressors. In piston compressors, the working chamber consists of a cylinder fitted with a piston, which move back and forth in a pulsating manner during the course of that machine's operational cycle. The cycle begins with the piston moving away from the top of the cylinder, drawing the working fluid into the cylinder through inlet valves in the suction port. The subsequent movement of piston towards the top of the cylinder decreases the cylinder volume occupied by the confined fluid, compressing the fluid in the process. The cycle is completed when the outlet valves open allowing the compressed fluid to be displaced into the discharge port (Okezue, 2010). Pulsations generated by reciprocating piston compressors are at low frequencies. This limits the delivery capacity (i.e. range of fluid flow rates) of all kinds of reciprocating compressors. However, reciprocating piston compressors are capable of generating extremely high discharge pressures of up to 500 bar or more (Eastop and McConkey, 1993). The operational cycle of plunger and diaphragm compressors are similar to that of piston compressors. Like the piston compressor, plunger and diaphragm machines capable of generating extremely high fluid pressure at low volumetric flow rates. In fact, the main difference among these reciprocating machines is the nature of their moving elements (i.e. pistons, plungers and diaphragms).

Rotary compressors are a category of positive displacement machines that employ single or multiple rotating elements in a housing to achieve fluid compression. In rotary compressors, the working chamber is the volume between the rotating elements and the housing in which they are enclosed. The boundaries of the working chamber decrease progressively as moving elements rotate, causing the fluid

confined within it to be compressed prior to displacement into the discharge port at elevated pressures and temperatures (Okezue, 2010). Unlike, reciprocating machines, rotary compressors tend to have multiple working chambers rotating at high speeds and no valves. These reduce the twin effects of inertia and fluctuations in the discharge of the working fluid from the compressor. The frequencies of pulsations in rotary machines are very high in contrast to low-frequency pulsations of reciprocating machines (Hanlon, 2001). For this reason, the delivery capacities of rotary machines are greater than the capacities of reciprocating machines. Rotary machines are much smaller and lighter than reciprocating machines of equivalent delivery capacity. The range of discharge pressures they are capable of generating are much lower than that of reciprocating machines (Eastop and McConkey, 1993). Examples of rotary machines include twin-screw compressors, lobe compressors, scroll compressors and vane pumps.

In rotodynamic compressors, working fluid freely moves from inlet to outlet without any confinement whatsoever. There are no working chambers in rotodynamic machines. These machines have a rotating element called a runner, impeller or rotor, which spins freely in the fluid. The impeller rotating at high angular speeds impact momentum tangentially to the fluid flowing into the machine through the inlet port. In the passages of the compressor's diffuser, the working fluid flowing at high velocity decelerates in the passages of the compressor's diffuser, causing its specific volume to decrease and the pressure to rise in accordance with Bernoulli's Principle before freely flowing into the discharge duct of the machine. An increase in the angular speed of the impeller results in larger volumetric flow rates and the development of higher pressures at the discharge duct (Eastop and McConkey, 1993; Douglas *et al.*, 2005; Sorokes, 2013; Okezue and Kuvshinov, 2018). There are three types of rotodynamic compressors namely: centrifugal compressors, axial compressors and mixed flow compressors.

It is important to note the difference between rotodynamic compressors and rotary-type positive displacement compressors. Rotary compressors possess rotating working chambers, which cyclically confine fluid, compress it and then displace it to the discharge port. Compression is achieved when the rotating working chambers move their physical boundaries in such a way that the volume of the working fluid

confined to them is reduced significantly (Okezue, 2010). In rotodynamic machines, the working fluid flows freely without any restrictions. As earlier explained, compression is achieved when kinetic energy applied to the free-flowing working fluid by rotating impellers is converted to potential energy in the form of high static pressure (Sorokes, 2013; Okezue and Kuvshinov, 2018).

4.1.1.1 Comparing the Working Principles of Rotodynamic and Positive Displacement Compressors

In rotodynamic machines, the impeller's impact of momentum to the working fluid flowing through the inlet port, the deceleration of that fluid in the diffuser and its exit through the outlet port at an elevated pressure is a *continuous* process. This makes the fluid flow in and out of rotodynamic machines free of fluctuations (Hanlon, 2001).

By contrast, positive displacement machines operates a *pulsating* process in which the working fluid flowing from the inlet port is intermittently confined to and released from a physical space (i.e. working chamber) with boundaries that move to compress and displace the fluid into the outlet port at an elevated pressure. This makes the fluid flow in and out of positive displacement compressors fluctuate at frequencies dependent on the amount of time it takes the machine to complete the cycle of filling, confining, compressing and displacing the fluid. Rotary machines which tend to possess one or more working chamber spinning at high speeds generate high frequency and low amplitude pulsations, which translate to lower levels of fluctuations in fluid flow compared to reciprocating machines where pulsation frequencies are very low and amplitudes very high (Eastop and McConkey, 1993; Douglas *et al.*, 2005; Hanlon, 2001; Okezue, 2010).

4.1.1.2 Evaluating the Performance of Rotodynamic and Positive Displacement Compressors

Positive displacement compressors generally provide greater pressure, but less volumetric delivery than rotodynamic compressors. The relationship between pressure and volume for positive displacement and rotodynamic compressors are different and these affect their performance.

4.1.1.2.1 Compressor response to pipe system characteristic

The delivery capacity (i.e. volumetric flow rate) of a positive displacement compressor is proportional on its shaft speed and independent of the discharge

pressure. The discharge pressure of a positive displacement compressor depends on fluid volume reduction inside the working chambers and whether the outlet port is exposed to the atmosphere or connected to a pipeline (Douglas *et al.*, 2005; Okezue, 2010).

When the outlet port is exposed to the atmosphere, the working fluid will exit the positive displacement machine with the constant discharge pressure developed within its working chambers by volume reduction. Change in shaft speed controls flow rate by increasing or decreasing the frequency with which working chambers deliver a fixed volume of fluid to the discharge port. The magnitude of the discharge pressure is not affected at all by speed change (Douglas *et al.*, 2005; Okezue, 2010).

When the outlet port of a positive displacement compressor is connected to a transport pipeline, the discharge pressure is no longer a function of only internal fluid compression within the working chambers. It is also a function of flow resistance brought on by fluid inertia and frictional losses in the transport pipeline— a system comprising bends, valves, junctions and pipe segments of various orientations. The magnitude of flow resistance will depend on the geometry of these pipe segments and fittings and the roughness of their interior surfaces (Okezue, 2006 and 2010).

Flow resistance in pipeline causes system pressure to build up with the passage of time, altering the behaviour of the positive displacement compressor in the process. In other words, a positive displacement compressor on a fixed speed will switch from delivering a constant flow against a steady discharge pressure when the outlet port is exposed to open air to delivering a slightly reduced near-constant flow against a varying discharge pressure when the outlet port is connected to pipeline. This is because system pressure induces backflow, which increases fluid leakage in the working chambers, reducing the flow rate (Okezue, 2010). The variation of discharge pressure is a consequence of time-dependent build-up of system pressure in the pipeline (Douglas *et al.*, 2005).

In rotodynamic compressors, discharge pressure is a function of volumetric flow rate (i.e. delivery capacity) which in turn is proportional to shaft speed. As stated earlier, an increase in the shaft speed of a positive displacement machine with outlet port exposed to the atmosphere will increase its flow rate without having any effect whatsoever on the discharge pressure. By contrast, an increase in shaft speed will

increase both volumetric flow rate and discharge pressure in a rotodynamic compressor with its outlet port similarly exposed to the atmosphere (Douglas *et al.*, 2005; Okezue, 2010).

When the outlet port of a rotodynamic compressor on fixed shaft speed is connected to the pipeline network, both discharge pressure and flow rate will diminish continuously in response to increasing system pressure. This is in contrast to the case of the positive displacement machine where the flow rate suffers slight reduction, but is otherwise almost constant while discharge pressure rises exponentially as system pressure builds up inside the pipeline (See Fig. 4.2).

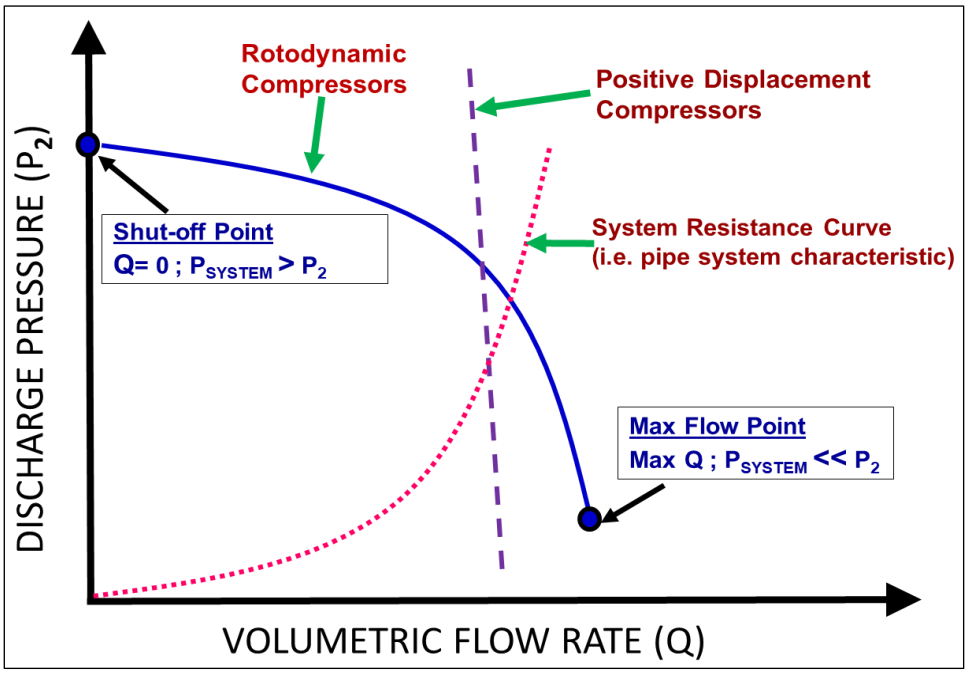

Fig.4.2. Comparing the response of rotodynamic and positive displacement compressors running on a fixed shaft speed to pipe system characteristic

To continue delivering flow against an increasing system pressure, a rotodynamic machine will need to have its shaft speed increased in order to generate enough discharge pressure to overcome flow resistance in the pipeline. When the highest shaft speed is reached, the rotodynamic compressor develops its maximum discharge pressure, beyond which it can no longer produce enough pressure to overcome system resistance. From that moment onwards, flow through the outlet port will cease as the fluid starts swirling round within the circular compressor housing at the maximum velocity, generating heat in the process. If the compressor is kept running, the liquid will eventually evaporate and the compressor could be damaged by overheating (Massey and Ward-Smith, 1998). As shown in Fig 4.2, the

shut-off point is moment when the flow is unable to pass through the outlet port and the corresponding maximum discharge pressure is called *shut-off pressure*.

Positive displacement compressors have no *shut-off pressure*. Under a fixed shaft speed, this compressor type will continue to supply (near-constant) volumetric flow regardless of dangerously mounting system pressure until the pipeline bursts or the machine itself is severely damaged. Hence, pipelines attached to positive displacement compressors are required to have pressure relief valves that can open to release fluid once safe levels of pressure are exceeded (Hanlon, 2001; Okezue, 2010).

4.1.1.2.2 Compressor and pipe system response to the composition of the working fluid

The chemical composition of a working fluid defines its thermophysical properties and by extension, its flow characteristics (Seevam *et al.*, 2008; Jung and Nicot, 2010; Race *et al.*, 2012; Lazic *et al*., 2014). The ability of chemical composition to influence the performance of a machine or system depends on whether the working fluid within them is allowed to flow freely or whether fluid flow is restricted. Transport pipelines and rotodynamic machines allow fluid to flow freely within them. Because of this, they are both sensitive to changes in the chemical composition of the working fluid, especially under supercritical conditions. As illustrated in section 2.3.2 of this PhD thesis, when the working fluid is near or above the critical point, a minor variation in its chemical composition is sufficient to cause abrupt and large changes in thermophysical properties with great consequences for pressure and temperature drop across the length of a pipeline. In the case of rotodynamic machines, radical changes in those fluid properties profoundly affect the magnitude of discharge pressure and volumetric flow rate generated as well as the efficiency and overall energy consumption of both machines (Serpa *et al.*, 2011; Eickhoff *et al.*, 2014; Okezue and Wang, 2016; Okezue and Kuvshinov, 2017).

By contrast, variation in the composition of the working fluid has almost no effect on the performance of positive displacement machines (Gresh, 2001). This is because most of the working fluid is confined to working chambers. Trapped within the working chambers, the fluid is unable to flow on its own kinetic power. Instead, the confined working fluid relies almost entirely on the momentum and shifting

boundaries of the working chambers to deliver volumetric flow and develop discharge pressure. In other words, the fluid inside the working chambers has almost no momentum of its own (Okezue, 2010). Therefore, dramatic changes in thermophysical properties induced by varying the chemical composition of the working fluid have little impact on the volumetric flow rate and discharge pressure generated in positive displacement machines.

It is important to note that while most of the working fluid is confined to the working chambers, a small portion of that fluid is able to flow freely as “backflow” in leakage channels formed from the clearances between the working chambers and compressor housing (Hanlon, 2001; Okezue, 2010). Obviously, the pressure, velocity and kinetic power of this leakage flow is affected by changes in the working fluid’s chemical composition. However, as the leakage flow constitutes a small fraction of the overall working fluid, it has almost no effect on the overall performance of the positive displacement machines. The performance of a positive displacement machine is marginally affected by the fluid’s chemical composition only when it is connected to a transport pipeline network. This is because of the impact of system pressure of the pipeline network upon volumetric flow and discharge pressure of the compressor (Okezue, 2010).

4.1.2 Advantages and Disadvantages of Rotodynamic and Positive Displacement Compressors

Rotodynamic and positive displacement categories of compressors function in different ways and their response to changing operational conditions are dissimilar. These divergent characteristics of compressors confer upon certain advantages and disadvantages on each compressor category (See Table 4.1). For this reason, it is common industrial practice to deploy a particular type of compressor in systems where it is most suitable.

As shown in Fig 4.2, a rotodynamic machine has a higher volumetric delivery capacity than any equivalent sized positive displacement compressor. Therefore, from an efficiency and cost-savings perspective, a compressor in the rotodynamic category is best suited for compressing natural gas for pipeline transportation or compressing pure gases such as carbon dioxide and nitrogen for chemical and petrochemical processes. However, if the petrochemical process involved the use of ethylene gas

in plastic production, then the application of a rotodynamic machine would be inappropriate since large deposits of solid polymer (polyethylene) on its moving parts will ultimately lead to performance degradation and machine damage. By contrast, positive displacement machines (e.g. twin-screw compressor) will be able to operate efficiently with large deposits of solid polymer sticking onto its working chambers and the internal walls of its casing. Rotodynamic machine's advantage of being able to operate efficiently at very high volumetric flow rates may be nullified if applied to a transport pipeline where flow resistance (i.e. system pressure) is severe enough to reduce flow delivery and pressure head substantially. Positive displacement machines are better suited in this case because system resistance barely affects its efficiency and volumetric delivery (Douglas *et al.*, 2005; Okezue, 2010).

Table 4.1: Advantages and Disadvantages of Different Compressor Categories

Compressor Category	Advantages	Disadvantages
Positive displacement machine	Higher discharge pressures than any equivalent-sized rotodynamic machine	Lower volumetric delivery range than any equivalent-sized rotodynamic machine
	Higher compressor efficiency than equivalent-sized rotodynamic machines at low volumetric delivery capacities	Fluctuations in the volumetric flow and pulsations in discharge pressure due to intermittent compression of trapped fluid in the machine
	Fluid properties have little effect on pressure development and compressor efficiency	Large capital costs due to expensive high precision manufacturing required for accurate rotor profiles and close-running clearances needed to minimize leakage flow in rotary machines
	High tolerance for solid contaminants within working fluid in rotary machines	Large reciprocating machines generate loud noise and strong vibrations which can only be absorbed by building machine foundations for them
	Can handle evolution of working fluid from single-phase to two-phase mixture without degradation of machine performance	Higher maintenance costs due to presence of several moving parts, some of which are delicate
	Less prone to cavitation damage compared to rotodynamic machines	Positive displacement machines need overpressure protection unlike rotodynamic machines
Rotodynamic machine	Higher volumetric delivery range than any equivalent-sized positive displacement machine	Lower discharge pressures than any equivalent-sized positive displacement machine
	Smooth continuous production of volumetric flow and discharge pressure due to uninterrupted addition of kinetic energy to fluid flowing freely in the machine	At low volumetric flow rates, compressor may suffer prolonged surging resulting in severe vibrations, overheating and machine damage
	Higher compressor efficiency than equivalent-sized positive displacement machines at high volumetric delivery capacities	Fluid properties have strong effect on pressure development and compressor efficiency
	Lower capital cost due to relatively cheap and simple manufacturing process applied in making impellers and compressor housing	Large amounts of solid contaminants within the working fluid can erode impeller blades and internal surfaces of machine
	Minor vibrations; so compressor operation is quieter and there is no need for a machine foundation to be built	Evolution of working fluid from single phase to two-phase mixture degrades compressor performance
	Lower maintenance costs since machine has few moving parts	More prone to cavitation damage compared to positive displacement machines

Rotodynamic machines are not appropriate for systems where fluctuations in the fluid properties, pressure or changes in operating conditions occur. Change in fluid properties can manifest in several ways, but two examples below should suffice:

- A transition of a working fluid from single-phase (e.g. supercritical CO_2) to two-phase (e.g. mixture of gaseous and liquid CO_2) because of pressure drop in a transport pipeline

- Variation in the chemical composition of a single-phase working fluid as a result of adding chemical impurities (e.g. N_2, H_2, CH_4) to a pure fluid (e.g. supercritical CO_2) or as a result of increasing the concentration of certain impurities in an impure fluid (e.g. supercritical CO_2+N_2 mixture)

In either example, the overall density of the working fluid will decrease abruptly causing discharge pressure and efficiency of the rotodynamic machine to decrease. This deterioration in compressor performance can be counteracted—to keep the discharge pressure constant— by increasing the shaft speed of the rotodynamic machine. However, this comes at the price of higher operating cost for the rotodynamic machine because of the extra input power required to raise rotor shaft speed (Cooper *et al.*, 1996; Okezue, 2010; Okezue and Kuvshinov, 2018).

By contrast, positive displacement machines are perfect for systems where fluctuations in the fluid properties occur since machines in this particular compressor category suffer little or no torque fluctuations due to variations in overall density. This means no deterioration in machine efficiency or discharge pressure head occur in the face of changing fluid properties. Therefore, unlike rotodynamic machines, no extra input power is required to maintain the performance of positive displacement machines (Gresh, 2001; Okezue, 2010).

4.1.2.1 Choice of Compressor Category in the CCS Context

Of several machines used for compressing carbon dioxide for pipeline transportation, two are considered front-runners: reciprocating piston and centrifugal compressors. The former is a positive displacement machine while the latter is a rotodynamic machine. Reciprocating piston compressors have a long history of application in CO_2 transport pipeline for Enhanced Oil Recovery (EOR) and Carbon Capture and Storage (CCS) projects (Seevam *et al.*, 2010).

Compared to centrifugal machines, reciprocating compressors are better in handling periodic variations in flow rate and pressure of anthropogenic CO_2 mixture supplied to the pipeline from power stations undergoing load changes in response to electricity demand. Unlike centrifugal compressors, the performance of reciprocating compressors is unaffected by variations in the chemical composition of the anthropogenic CO_2 mixture, which is common in CCS pipeline network.

However, advantages gained in using reciprocating compressors are nullified by the reality that CCS pipeline networks are designed to operate on an industrial scale, transporting several metric megatons of anthropogenic CO_2 per annum obtained from multiple power stations and other process plants to designated places of sequestration (Mertz *et al.*, 2005). Such a pipeline network will require several compressors and booster pumps with high volumetric capacity. As shown in Table 4.1, reciprocating machines have lower volumetric delivery capacity and higher procurement and maintenance costs compared to centrifugal machines. Therefore, designers of CCS pipeline systems prefer centrifugal machines because of their ability to deliver a higher volumetric flow rate at comparatively lower capital and operating costs. Maintenance costs are lower for centrifugal machines than reciprocating machines (Wacker and Dittmer, 2014; IEA GHG, 2016) since the former is durable because of its few moving parts while the latter contains several moving parts, some of which are quite delicate (Okezue, 2010).

4.1.3 Centrifugal Compressors in CO_2 Transport Pipeline Systems

4.1.3.1 Centrifugal Compressors Compared to Other Rotodynamic Machines

Compressors in the rotodynamic machine category —centrifugal compressors, axial compressors and mixed flow compressors— have the same working principle, which involves the continual addition of kinetic energy to a working fluid with the aid of an impeller rotating at high speed. However, the direction of fluid flow in relation to the plane of the impeller rotation is what distinguishes one type of rotodynamic machine from the other (Douglas *et al.*, 2005; Gorla and Khan, 2003; Ingram, 2009).

An axial compressor is a rotodynamic machine in which the working fluid enters the inlet port in the axial direction, flowing parallel to the axis of the compressor shaft as it passes through a circular array of fixed (stator) blades fixed to the walls of the compressor housing, rotating impeller blades and finally the discharge port (Ingram,

2009). In axial compressors, kinetic energy is impacted to the working fluid by the rotating impeller blades (also called rotor blades) causing its velocity to rise. In the stator blades, the fluid decelerates and experiences a rapid increase in static pressure prior to leaving the compressor axially through the discharge port (Gorla and Khan, 2003; Ingram, 2009).

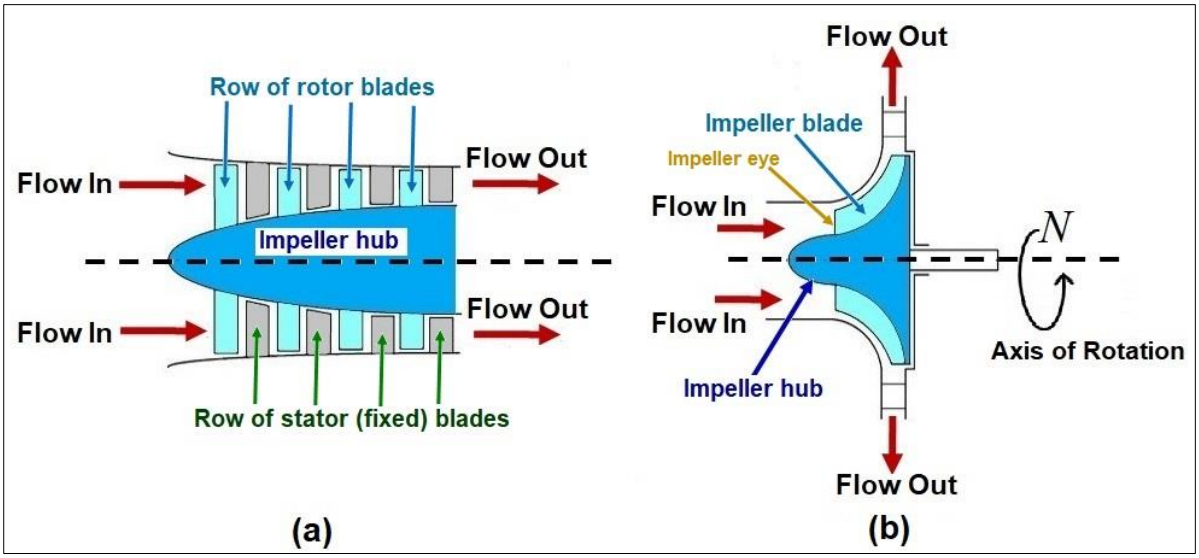

Fig.4.3 Demonstrating differences between (a) axial compressor and (b) centrifugal compressor

In centrifugal machines, the working fluid enters the inlet port axially and flows into the annular shaped eye of the rotating impeller where it turns through an angle to the radial direction while being whirled through that impeller's blade channels. The rotating impeller impacts kinetic energy to the working fluid; thereby increasing its angular momentum. The fluid reaches maximum velocity at the periphery of the impeller before changing direction again, flowing tangentially into the diffuser or volute chamber (shown in Fig. 4.5) where it decelerates, experiencing a rapid increase in static pressure prior to leaving the compressor radially through the discharge port (Douglas *et al.*, 2005; Ingram, 2009; Okezue and Kuvshinov, 2018).

Axial compressors have the greatest volumetric delivery capacity of any compressor of equivalent size in the rotodynamic category (Gresh, 2001; Okezue, 2010). Its energy losses are relatively lower, resulting in higher compressor efficiencies. However, its ability to generate pressure rise is lower than that of any other equivalent-sized rotodynamic machine. It will require several rows (or stages) of delicate rotor and stator blade combinations to achieve a large pressure rise, making

it complex and expensive relative to other rotodynamic machines (Watson and Janota, 1982).

Centrifugal machines are widely used in the process industries because of their smooth operation and high reliability compared to many other types of compressors (Boyce, 2012). Although the volumetric delivery capacity of a centrifugal compressor is large, it is still much lower than that of an axial machine of equivalent size. Centrifugal machines generate higher pressure ratios than any equivalent-sized rotodynamic machine (Gresh, 2001). In fact, a centrifugal machine with a single stage can produce a high pressure ratio that will take several stages of an axial machine to accomplish (Watson and Janota, 1982). Hence, the juxtaposition of a multistage axial machine against a single stage centrifugal machine in Fig. 4.3. A comparison of the geometry of both kinds of rotodynamic machines shows that axial machines have constant cross-sections while centrifugal machines have varying cross-sections with a bend between the inlet and the outlet. The centrifugal machine's varying cross-section allows the rotating impeller to transfer a greater amount of energy to the working fluid compared to axial machines. This explains why centrifugal machines are able to generate much larger pressure ratios than axial machines (Boyce, 2012; Sorokes, 2013). The working fluid's velocity almost triples as it flows from the inlet to the outlet of the centrifugal machine, causing high disk friction and hydraulic losses in contrast to the lower losses in axial machines where fluid velocity is almost constant from inlet to outlet. Furthermore, the shock losses that occur in centrifugal machines when the flow path of the working fluid changes from axial to radial direction is non-existent in axial machines (Okezue and Kuvshinov, 2018). In short, centrifugal machines incur more energy losses during operation than an equivalent-sized axial machine, which explains why the latter machine is more efficient than the former (Boyce, 2012).

Despite having a lower volumetric delivery capacity, lower efficiency and a higher energy requirement, centrifugal machines are preferred to axial machines by designers of CO_2 transport pipeline systems for CCS. The reason for this preference is not just limited to the fact that centrifugal machines can easily generate large pressure ratios of the order required to convert CO_2 from gas to supercritical fluid compared to axial machines. It is also the reality that despite having a lower

volumetric capacity, the operating range for stable mass flow in a centrifugal machine is wider than that of an axial machine for a given shaft speed (See Fig. 4.4). Because of its wider operating range, centrifugal machines can run without surging at much lower mass flow rates than equivalent-sized axial machines. It can also run without experiencing “choking” at much higher flow rates than equivalent sized axial machines (Gorla and Khan, 2003; Boyce, 2012).

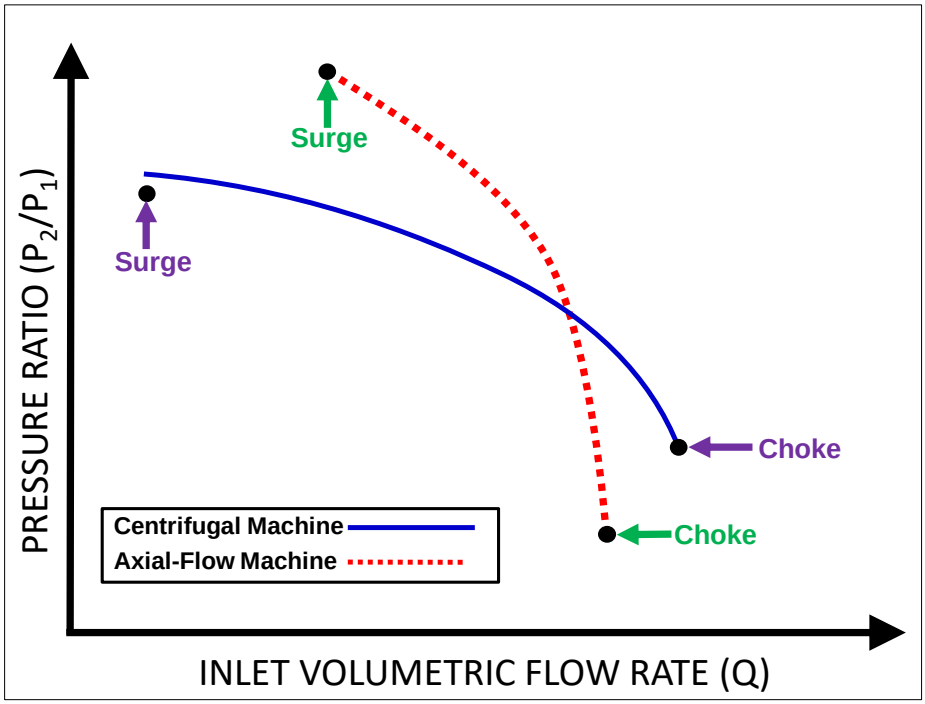

Fig.4.4 For given shaft speed, centrifugal machines can maintain flow stability over a wider operating range compared to axial compressors

The mixed flow compressor combines the mechanical design of a centrifugal and an axial compressor (Douglas *et al.*, 2005). The flow path of the working fluid in mixed flow compressors lies between the axial and radial directions—the fluid travels through the impeller’s blade channels mainly in the diagonal direction. Mixed flow compressors have higher volumetric delivery and generate lower pressure ratios than centrifugal machines (Brown, 1997). Just like axial machines, mixed flow compressors require several stages (i.e. several impellers on a shaft) in order to generate a large pressure ratio. This practically means a bulky mixed flow machine being employed to do what a smaller compact centrifugal machine can do. For this reason, mixed flow machines are rarely found in industrial applications (Brown, 1997; Mobley, 2000). This includes CO_2 transport pipeline systems.

4.1.3.2 Assembly and Configurations of Centrifugal Compressor

At the basic level, a centrifugal compressor consists of a housing and impeller on a shaft supported by a set of bearings (Avallone and Baumeister, 1986; Brown, 1997; Douglas *et al.*, 2005).

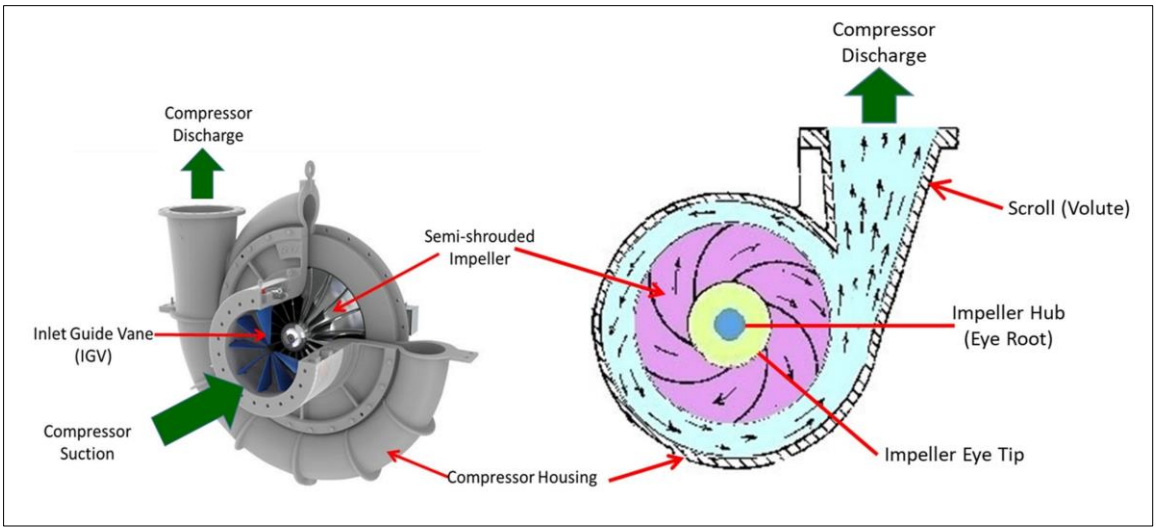

Fig.4.5 The assembly of a single-stage centrifugal compressor with inlet guide vanes (IGVs)

4.1.3.2.1 Compressor housing

The housing is the stationary part of the centrifugal compressor. It contains the suction and discharge ports through which the working fluid freely flows in and out of the machine. Depending on the compressor design, a set of stationary curved blades known as “inlet guide vanes” (IGVs) may be absent or present in the suction duct as shown in Fig. 4.5. When present in a centrifugal machine, IGVs prevents the working fluid from entering the eye of the impeller exclusively in the axial direction as described earlier in section 4.1.3.1. Instead, the IGVs introduces a “pre-whirl” to the working fluid by making it pass through the curved stationary blades. This causes the direction of flow to split into two—part of the fluid enters the eye of the impeller in the axial direction while the remaining part enters the eye tangentially (Saravanamutto *et al.*, 2001; Brown, 1997; Boyce, 2012). This reduces the relative velocity of the working fluid at the eye of the impeller and ensures that it is below the speed of sound. Relative velocities above the speed of sound causes shock losses and “choking” in the compressor. In fact, impeller shaft speeds capable of bring relative velocity close to the speed of sound are regarded as the maximum operating limit of a centrifugal machine beyond which the mass flow rate becomes highly unstable as described in section 4.1.3.1. The presence of IGVs reduces relative velocity and delays the onset

of “choking” until a much higher impeller shaft speed is reached. Therefore, IGVs extend the operating range of the centrifugal machine (Rasmussen and Kurz, 2009). Unfortunately, this is done at the cost of reducing the amount of kinetic energy converted to static pressure in the machine (Avallone and Baumeister, 1986; Saravanamutto *et al.*, 2001). In other words, for a give shaft speed, a centrifugal machine with IGVs will generate smaller pressure ratio compared to an identical centrifugal machine without IGVs.

The spiral shaped part of the housing depicted in Fig. 4.5 is the volute chamber or “scroll”. It receives the working fluid exiting the periphery of the impeller in the radial and tangential direction indirectly through a diffuser (or directly if the diffuser is absent). Where the diffuser is present, the volute chamber plays a complementary role, further slowing down the working fluid, converting more kinetic energy to static pressure before routing the fluid to the discharge duct. In machines that do not have a diffuser, the “scroll” is solely responsible for decelerating the working fluid to allow the conversion of kinetic energy to static pressure prior to routing that fluid to the discharge port (Avallone and Baumeister, 1986; Douglas *et al.*, 2005).

Apart from containing suction and discharge ducts, the compressor housing also contains the stuffing box, which hosts rubber seals, various O-rings and bearings for the compressor shaft (Avallone and Baumeister, 1986). The housing is also designed to absorb the centrifugal forces and axial thrust generated by the rotating impeller (Avallone and Baumeister, 1986; Rasmussen and Kurz, 2009; Sorokes, 2013).

4.1.3.2.2 Drive shaft

Shaft is the cylindrical rod usually made of steel, which connects the impeller to the driver motor. Supported by bearings in fixed to the compressor housing, the shaft transmits rotational power from the motor to the impeller (Okezue, 2010). Shaft are subject to shear stress due to transmission of torque from the motor to the impeller. It also subject to bending moments and axial loads and therefore have to be designed carefully to prevent deflection and damage (Davis, 1972).

4.1.3.2.3 Impeller

The impeller is the most important component of a centrifugal compressor and the only rotating aerodynamic element within that machine. The performance of all

centrifugal machines is dependent on the design of the impeller (Sorokes, 2013). The shape, width, height and direction of the blades on the impeller; the diameters of the root (hub) and tip of the impeller eye and the overall diameter of the impeller determines the volumetric delivery capacity and the magnitude of pressure rise (Lurie *et al.*, 2011). The impeller's blade channels provides 100% of the kinetic energy transferred to the working fluid and a fraction of the static pressure rise generated in the compressor (Sorokes, 2013). The remaining fraction of the static pressure rise generated in the machine occurs within the diffuser and volute chamber of the compressor housing (Saravanamutto *et al.*, 2001). How large the fraction of static pressure rise taking place within the impeller is a function of the shape and direction of its blades (Brown, 1997). For a given shaft speed, the fraction of static pressure produced within an impeller with radially shaped blades is greater than the fraction produced in the diffuser and volute. Conversely, impellers with backward-curved blades are responsible for a small fraction of static pressure while the diffuser and volute are responsible for most of static pressure generated in the compressor (Gorla and Khan, 2003).

It is not possible to achieve a high efficiency in a centrifugal machine if its impeller is poorly designed (Watson and Janota, 1982; Jiang *et al.*, 2006; Sorokes and Kuzdzal, 2010; Sorokes, 2013). This is because the impeller is responsible for most of the energy losses incurred during the operation of centrifugal machines. For instance, badly designed blade channels exacerbates flow separation problems and encourages the formation of eddies and shock losses (Watson and Janota, 1982; Sorokes and Kuzdzal, 2010). Energy losses such as disk friction, leakage and hydraulic/aerodynamic losses are inevitable and generally increase as the size and speed of the impeller increases (Saravanamutto *et al.*, 2001; Okezue and Kuvshinov, 2018). Nevertheless, these losses can be minimized by improving the profile of the impeller eye and the shape of the impeller blades (Watson and Janota, 1982; Sorokes and Kuzdzal, 2010) and then ensuring that the overall impeller is rightsized to ensure the optimal performance of a centrifugal machine in the facility where it is installed (Okezue and Kuvshinov, 2017 and 2018).

Sorokes (2013) makes the case that a well-designed impeller geometry can reduce energy losses to 4% of the total input energy supplied to the centrifugal compressor.

This level of compressor efficiency is certainly achievable when working fluid is conventional (e.g. air and natural gas) with well-understood flow characteristics and thermophysical properties. It is difficult to achieve such a high level of efficiency when an unconventional working fluid (e.g. supercritical CO_2) with anomalous thermophysical properties and flow behaviour that is erratic and poorly understood (Lettieri *et al.*, 2013; Baltadjiev *et al.*, 2015; Okezue and Wang, 2016). As explained in chapter 2 of this PhD thesis, at close proximity to the critical point, large and abrupt changes in the properties of CO_2 occur in response to minor shifts in pressure and temperature. These radical thermophysical property changes, sometimes difficult to control, can induce large density fluctuations that can impose flow stability problems that do not exist in centrifugal compressors handling conventional working fluids (Imre and Tiselj, 2012; Imre *et al.*, 2015; Baltadjiev *et al.*, 2015, Cho *et al.*, 2016). Large specific enthalpies and fluid compressibility values for supercritical CO_2 result in higher aerodynamic/hydraulic losses (Okezue and Kuvshinov, 2018). Due to high density and low viscosity values, Reynolds numbers in supercritical CO_2 compressors are two orders of magnitude larger than in conventional gas compressors (Lettieri *et al.*, 2013; Baltadjiev *et al.*, 2015). These translate to higher disk friction and leakage losses. Overall, energy losses in supercritical CO_2 centrifugal machines are much higher than in gas centrifugal compressors (Lettieri *et al.*, 2013; Okezue and Kuvshinov, 2018).

The performance of a centrifugal compressor is determined by complex interactions between the working fluid; moving surface of the spinning impeller; and interior walls of the stationary machine housing (Lettieri *et al.*, 2013; Baltadjiev *et al.*, 2015; Okezue and Kuvshinov, 2017). Therefore, any successful attempt to minimize energy losses by improving impeller design must include an excellent understanding of the working fluid's flow characteristics under various operating conditions. As pointed out by Lettieri *et al.* (2013) and Okezue and Wang (2016), there are no text books and barely any research publications providing guidelines on how to handle the design optimization of impellers in centrifugal machines handling pure and impure CO_2 at supercritical conditions.

As shown in Fig. 4.6, impellers can be divided into three categories based on mechanical construction and geometry as follows— open (or unshrouded), semi-

open (or semi-shrouded) and closed (or shrouded). Open impeller is the simplest of them. It consists of blades attached round the circumference of a hub, giving it the appearance of a fan propeller. It is also called an “unshrouded” impeller because there are no protective circular sidewall plates (i.e. “shrouds”) attached to the blades. The absence of the shrouds means that the blades of open impellers are exposed and more sensitive to wear and tear than other impeller types. On the plus side, the lack of shrouds renders open impellers lighter, simpler and cheaper to manufacture compared to other types of impellers. More importantly, it can run at higher speeds without incurring high disk friction losses associated with other kinds of impellers. It is capable of generating much higher pressure ratios than other impeller types (Gresh, 2001; Sorokes, 2013). However, the lack of shrouds allows high leakage losses in the clearance between the tip of the blades and the interior wall of the compressor housing, attenuating the efficiency of the open impeller. Despite this drawback, the overall efficiency of compressors with open impellers is still higher compared the efficiencies of machines fitted with other impeller types (Sorokes, 2013).

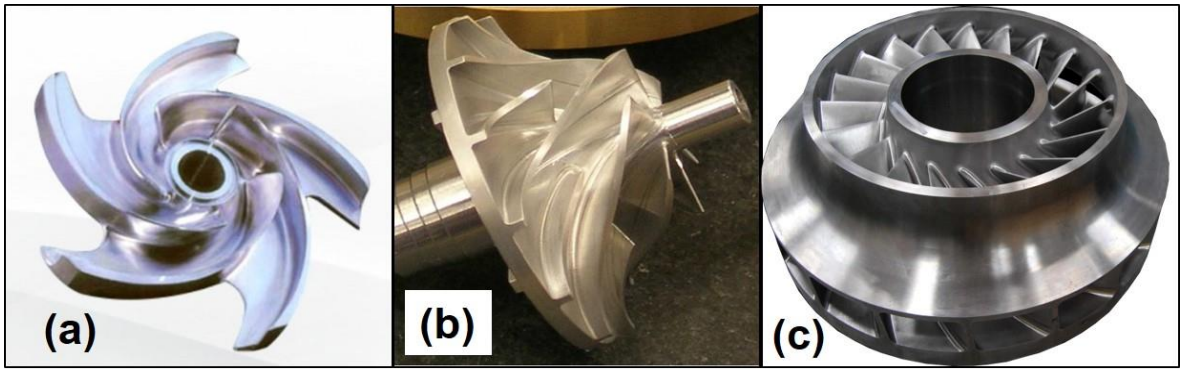

Fig.4.6 Impellers can be categorized as (a) open, (b) semi-open or (c) closed

In closed (or shrouded) impellers, protective circular sidewall plates (“shrouds”) are attached to the front and rear sides of the hub and blade assembly, fully enclosing the blade channels (Brown, 1997; Gresh, 2001; Nourbakhsh *et al.*, 2007). The presence of front and rear shrouds stiffens the blades and protects them from wear and tear. Giving closed impellers the advantage of durability over open impellers. On the other hand, the presence of shrouds mean that closed impellers are heavier, expensive and more complicated to construct than other impeller types. These shrouds reduce the size of the clearance between the periphery of the closed impeller and the interior wall of the compressor housing, thereby decreasing leakage losses

drastically (Sorokes, 2013). However, the efficiency gain for the closed impeller from the reduced leakage is neutralized by the high disk friction losses generated because of large shear stresses formed between the rotating surfaces of both shrouds and the stationary walls of the housing (Gresh, 2001; Okezue and Kuvshinov, 2018). In fact, the overall efficiency of a centrifugal machine equipped with a closed impeller is lower than that of a machine fitted with other impeller types. Since the disk friction losses in closed (shrouded) impeller increases in proportion to the third power of the shaft speed, it is standard practice to restrict the speed of the closed impeller in order to maintain an acceptable level of efficiency (Dixon, 1998; Gresh, 2001). For this reason, the pressure ratio generated by a closed impeller is lower compared to other impeller types. Whereas open impellers —free to rotate at much higher speeds— can produce pressure ratios of 10:1 and greater, closed impellers—rotating at lower speeds— can only muster a pressure ratio of up to 3:1 (Sorokes, 2013).

Semi-open impellers has only a single shroud attached to the rear side of the hub and blade assembly. The front side of the hub and blade assembly has no shroud, leaving the blade channels on that side completely exposed (Brown, 1997). Hence its alternative name “semi-shrouded impeller”. The semi-open impeller category is the compromise between the open and closed impellers. Because it has one shroud instead of two, semi-open impeller is lighter, less expensive and easier to manufacture than closed impeller. For the same reason, a semi-open impeller has a higher efficiency than closed impeller since disk friction losses are much lower. The lone shroud on the rear of the semi-impeller is sufficient to stiffen the blades and minimize wear and tear. This gives the semi-open impellers the advantage of durability over open impellers. Moreover, tip leakage is much lower in semi-open impeller (because of the shroud) compared in open impellers (Dixon, 1998).

4.1.3.3 Multi-staging in Centrifugal Compressors

Generally, compressors of all categories can exist as single-stage or multistage machines. However, there is a notable exception in the rotodynamic machine category—the axial compressor which is manufactured exclusively as a multistage machine (Boyce, 2012). As shown in Fig 4.3, it takes several rows of delicate rotor and stator blade combinations (i.e. multiple stages) to create a practical axial machine capable of generating a significant pressure ratio.

Unlike axial compressors, practical centrifugal compressors can exist either as single-stage or multistage compressors. A centrifugal compressor consisting of just one impeller and one diffuser (i.e. a single-stage machine) is capable of generating large pressure ratios, which explains their widespread use in process industries (Avallone and Baumeister, 1986). However, the range of the pressure ratios a single stage centrifugal compressor can generate without seriously degrading its efficiency is limited (Hanlon, 2001). For most industrial applications, single stage centrifugal machines are artificially restricted to raising the pressure of the working fluid by four folds (i.e. pressure ratio of 4:1). For industrial applications where the required pressure ratio is beyond the 4:1 limit, multistage centrifugal machines are necessary to avoid degradation in performance (Hanlon, 2001; Oakey *et al.*, 2010). Large pressure ratios in are usually accompanied by high temperatures. To avoid thermal damage to single-stage centrifugal machines, discharge temperatures are usually not allowed to exceed the 148.89°C to 176.67°C limit. For applications where discharge temperature is likely to exceed the aforementioned limit, multistage machines should replace single-state machines (PetroWiki, 2012).

In the CCS context, compression of CO_2 mixtures from 1.01 bar to pressures of 100 bar and above is achievable (in theory) with large single-stage centrifugal machines. However, this hundred-fold increase in pressure will result in extremely high temperatures, huge energy consumption and prohibitive operating costs (Oakey *et al.*, 2010). Therefore, for reasons of energy efficiency, it makes more sense to use a series of compressor stages with intercoolers interspersed between them to breakdown the compression process into a succession of steps in which the working fluid is alternately pressurized and cooled until the desired discharge pressure is reached (Moore *et al.*, 2011; Martynov *et al*., 2016). Therefore, the replacement of a single-stage compressor with intercooled multistage compressor in the process of elevating pressure of a CO_2 mixture by a hundred-fold will reduce overall energy consumption and result in lower discharge temperatures which will render the need to construct machine components from special thermal resistant materials unnecessary (PetroWiki, 2012).

Multistage centrifugal compressors can exist in different configurations. However, in the context of CCS pipeline transport, only two multistage centrifugal machine

configurations are relevant— inline and integral gear compressors (Seevam *et al.*, 2010; Mohitpour *et al.*, 2011; Wacker and Dittmer, 2014). As illustrated in Fig. 4.7(a), inline compressors consist of two or more combined impellers/diffuser units (i.e. “compressor stages”) mounted back-to-back in series on a single drive shaft and enclosed within one machine housing (Boyce, 2012). Because of design constraints, the number of external intercoolers available to keep the temperature of the working fluid low after pressurization in compressor stages are limited (Brun and Kurz, 2019). This means that the working fluid is only cooled after pressurization in some compressor stages. Inline centrifugal compressors also suffer from aerodynamic and pressure losses because of the awkward ducting required in routing the flow of the working fluid from the radial outlet port of one compressor stage through a 90-degree bend to the axial inlet port of the next compressor stage aligned on the drive shaft (Sorokes, 2013).

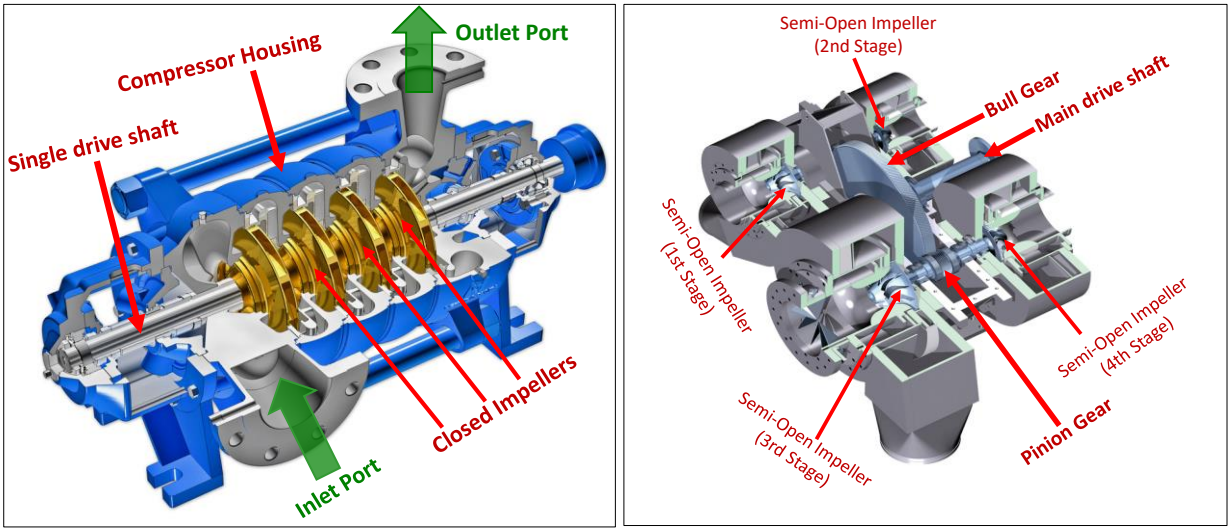

(a) (b)

Fig. 4.7 (a) Inline centrifugal compressor and (b) integrally geared centrifugal compressor

Integrally geared centrifugal machines consist of two or more combined impellers/diffuser units (i.e. “compressor stage”), each with its own machine housing and separate drive shaft. As shown in Fig. 4.7(b), a single giant (bull) gear wheel in the frame of this multistage centrifugal machine is used to rotate several enmeshed pinion gears, each coupled to the individual drive shaft of a compressor stage (Moore *et al*., 2011; Boyce, 2012; Sorokes, 2013; Kerth *et al.*, 2015). This configuration gives the integrally compressor certain advantages over the rival inline compressor. The ducting for integrally geared machines is simpler, has no 90-degree bends and

consequently, aerodynamic and pressure losses are lower (Sorokes, 2013; Brun and Kurz, 2019). Moreover, integrally geared machine configuration allows the application of a larger number of external intercoolers—enough to allow intercooling of the pressurized working fluid after every compressor stage until it exits the machine with the desired discharge pressure. This highly effective intercooling process decreases the working fluid's temperature while increasing its density, thereby producing near isothermal compression, which reduces the overall energy consumed by the compressor and saves on operating costs (Bergamini *et al*., 2011; Mohitpour *et al.*, 2011; Wacker and Dittmer, 2014). In fact, inline centrifugal machines with its relatively fewer numbers of intercoolers requires roughly twice as many compressor stages to achieve the pressure ratio of an integrally geared compressor (Seevam *et al.*, 2010; Mohitpour *et al.*, 2011; Brun and Kurz, 2019). Studies conducted by Wacker and Dittmer (2014) confirmed the assertion by finding that an inline centrifugal machine required 16 compressor stages to raise pressure of pure CO_2 from 1.0 bar to 150 bar in order to convert it from gas to supercritical fluid. By contrast, they found that an integrally geared machine accomplished the same task with only nine compressor stages and consumed 18% less energy than the 16-stage inline centrifugal machine (Almasi, 2011).

Apart from a highly effective intercooling and lower aerodynamic losses, integrally geared machines have other advantages over inline machines. The compressor stages of the integrally geared centrifugal machine all have their own individual pinion drive shafts, which means that they are capable of rotating at different speeds. This flexibility allows each compressor stage to be operated at its own optimal speed, increasing the overall efficiency of the integrally geared centrifugal machine (Sorokes, 2013; Brun and Kurz, 2019). Inline centrifugal machines do not have this flexibility because all compressor stages share the same single drive shaft and therefore must run on the same angular speed, making it impossible to set optimal speeds for each stage that could lead to an improved overall efficiency of the whole machine (Brun and Kurz, 2019). Integrally geared machines not only have the advantage of lower operating expenditure (OPEX), its capital expenditure (CAPEX) are much lower since its 15% to 30% less expensive to manufacture compared to inline machines (Almasi, 2011; Bergamini *et al*., 2011).

Despite all its advantageous characteristics resulting in lower CAPEX and OPEX, integrally geared centrifugal machines are less reliable and require more maintenance compared to inline centrifugal machines (Almasi, 2011; Moore *et al.*, 2011; Kerth *et al.*, 2015). This can be attributed to the fact that integrally geared machines possess a large number of seals and mechanical bearings, some for individual pinion drive shafts of the compressor stages and others for the bull gear. Vibrations related to gear meshing, wobbling impellers and general mechanical instability are examples of problems that occur during the operation of the integrally geared machines. By contrast, inline centrifugal machines have few seals and bearings, allowing them to avoid large dynamic loads that cause damaging vibrations and other forms of mechanical instabilities (Almasi, 2011; Sorokes, 2013; Brun and Kurz, 2019).

The reliability of inline centrifugal machines and their ability to operate for longer periods without need for maintenance is unmatched by integrally geared machines. Nevertheless, the lack of robust intercooling systems means that the overall efficiency of inline machines is still lower than that of integrally geared machines. Moore *et al.* (2011) and Kerth *et al.* (2015) proposed the elimination of the external cooling system that limits intercooling to certain stages of the inline compressor with a novel internal cooling system capable of cooling the working fluid between every stage of the machine. These researchers built prototypes of inline machines circulating liquid coolant within cooling jackets embedded around impellers. The ducting between compression stages within these prototypes are designed to reduce aerodynamic and pressure losses (Moore *et al.*, 2011; Kerth *et al.*, 2015). Successful performance tests on the prototypes—using supercritical CO_2 as working fluids—demonstrated that these novel inline compressors with internal cooling systems could potentially bridge the traditional gap between the overall efficiencies of inline and integrally geared machines. While these prototype inline compressors with their novel internal intercooling systems shows great promise, they remain under development and still require more extensive testing over a wider range of operating conditions.

4.2 DEVELOPMENT OF QUASI-DIMENSIONAL MODEL OF A SUPERCRITICAL CARBON DIOXIDE CENTRIFUGAL MACHINE

4.2.1 Energy Consumption in Supercritical CO_2 Compressors and Booster Pumps

As oft-repeated in Chapter 2, the fluid compression process required to pressurize pure CO_2 from ambient conditions (1.01 bar; 293.15 K) to conditions above its critical point (73.76 bar; 304.21 K) is energy intensive. If the CO_2 stream contain certain impurities (e.g. nitrogen, carbon monoxide, hydrogen), the resultant mixture critical point is even higher than that of pure CO_2 — meaning that compressor discharge pressures as high as 150 bar and above may be required to convert impure CO_2 mixtures from a gas to supercritical fluid. The compressor energy required to facilitate this hundred and fifty-fold increase in pressure will be incredibly high. Equally high would be the combined energy consumed by numerous relatively lower pressure ratio booster pumps installed on the long distance pipeline network to compensate for pressure losses and maintain the CO_2 mixture in a supercritical state. As explained in section 4.1, booster pumps are capable of performing some fluid compression when handling supercritical fluids. For that reason, booster pumps are closer in functionality to compressors than they are to conventional liquid pumps. In fact, it is not unusual for CCS researchers (e.g. Zhang *et al.*, 2006) to refer to these lower pressure ratio booster pumps as "*recompression compressors"*— a misnomer alluding to the fact that these machines are placed at various recompression (i.e. repressurization) points along the length of a pipeline to maintain the supercritical pressure of the CO_2 stream. To put things in perspective, an individual booster pump consume far more energy than a conventional liquid pump of equivalent capacity. Conversely, an individual booster pump (which performs limited compression) consume far less energy than an actual compressor. This is because booster pumps usually have inlet pressures that are already near or above critical pressure of CO_2 and operate at pressure ratios below 4:1 unlike main compressors that have inlet pressure of 1.01 bar and operate at pressure ratios above 100:1.

4.2.2 Need for an Effective Tool for Sizing Compressors and Booster Pumps

Given the high operating expenditure (OPEX) of compressors and booster pumps, the long-term economic feasibility of running such a supercritical CO_2 pipeline network is strongly dependent on curbing energy consumption of both machines. Yet as reported in sections 2.4.2 and 2.5, the vast majority of research on curbing energy

consumption is focussed two measures— optimal sizing of pipelines and purifying anthropogenic CO_2 to eliminate impurities that shifts the critical point high above that of pure CO_2. While both measures have been widely implemented with some success recorded in reducing operating costs, they do not address the actual fluid compression process, which is the largest contributor to the overall OPEX of any supercritical CO_2 pipeline network. Recent years have witnessed the publication of a small number of studies focussed on developing various energy-saving fluid compression strategies described in section 2.4.2 of this PhD thesis. Although these studies provide useful information on which fluid compression strategy achieves the best savings on operating costs given the working fluid's chemical composition, they are still lacking in practical details.

For the promised energy cost saving measures proposed in these studies to become practical reality, the actual centrifugal machines needed to fulfil the fluid compression strategies must be sized appropriately to minimize power losses and guarantee their optimal performance when installed in CO_2 pipeline networks. Existing compressor performance maps, traditionally used for this purpose, are unsuitable in the CCS context, as none account for peculiarities exhibited by CO_2 mixtures at supercritical or dense phase conditions. No other researcher in the field of CCS has developed a systematic method of installed in pipeline networks transporting pure and impure supercritical CO_2.

This represents a significant gap in knowledge, which the author of this PhD thesis proposes to close by developing a new quasi-dimensional model, which can be applied as an effective tool for appropriate selection and sizing of centrifugal compressors and booster pumps installed on a supercritical carbon dioxide transport pipeline.

4.2.3 Modelling Strategies for Centrifugal Machines in the CCS Context

4.2.3.1 Problems Inherent In Traditional Modelling Approaches

4.2.3.1.1 Adiabatic and polytropic process equations

Adiabatic and polytropic equations describes fluid compression in a conceptual way without going into the physical details. These equations does not describe the machine geometry and the complex internal fluid flow processes within a centrifugal compressor.

It is quite traditional to use them in estimating energy consumption of non-descript compressors under the assumption that pressure ratio and isentropic efficiency are fixed (i.e. constant) values known apriori. These assumptions are not always valid, especially in the case of supercritical CO_2 mixtures of varying chemical composition (Okezue and Wang, 2016 and Okezue and Kuvshinov, 2017). Nevertheless, these equations have been widely used by many CCS researchers including Chaczykowski and Osiadacz (2012), Witkowski *et al.* (2013), Luo *et al.* (2014) and Martynov *et al.* (2016).

The neglect of geometry and internal fluid flow processes of a centrifugal machine renders both adiabatic and polytropic equations unsuitable for a comprehensive evaluation of centrifugal compressor performance. For the same reason, both equations cannot be used as an effective tool for centrifugal compressor sizing (Okezue and Kuvshinov, 2017 and 2018).

4.2.3.1.2 Mean-line models

In order to optimally size centrifugal compressors or analyse their performance over a range of operating conditions, a mathematical model that correlates machine geometry, rotor shaft speed and chemical composition of working fluid with the actual input power requirements of the compressor is required (Okezue and Wang, 2016). In the field of turbomachinery design and analysis, mean-line models are the standard tools widely used for that purpose by many researchers (Aungier, 2000; Jiang *et al.*, 2006; Wright *et al.*, 2009).

Mean-line models are based on the assumption that the flow path of the working fluid in the centrifugal machine is one-dimensional and flow characteristics of the working fluid is spatially uniform across the impeller blade channels. Although, it incorporates few theoretical equations describing some features of machine geometry, mean-line models are not highly mechanistic. They usually do not have theoretical equations describing the physics of the complex internal flow processes within a centrifugal compressor, which is crucial for determining the myriad of losses in that machine such as aerodynamic/hydraulic losses, shock losses, leakage loss, disk friction loss, recirculation loss, etc. Instead, mean-line models rely on constituent adiabatic or polytropic equations (based on ideal gas assumptions) to characterize the flow behaviour of the working fluid under compression in the centrifugal machine.

Empirical correlations or coefficients are used in mean-line models to account for internal flow losses (Aungier, 2000; Hashemi and Karimi, 2009; Qui *et al.*, 2010).

In the field of turbomachinery sizing and analysis, mean-line models work remarkably well. This is because most applications of turbomachinery equipment (e.g. centrifugal compressors) deal with conventional working fluids with well-understood flow characteristics and thermophysical properties. Conventional working fluids such as air, natural gas and CO_2 under subcritical conditions behave almost like an ideal gas so the constituent adiabatic process equations within the mean-line models are able to predict key compressor performance parameters such as actual power input and isentropic efficiency. When a particular conventional working fluid (e.g. refrigerant R134a) deviates significantly from ideal gas assumption, its thermophysical properties such as specific enthalpy, specific heat capacity and compressibility are calculated with equation of state (EoS) correlations (Baltadjiev *et al.*, 2015; Okezue and Wang, 2016; Cho *et al.*, 2016). The mean-line model uses the real fluid property data from the EoS correlations to calculate actual work input and isentropic efficiency of the refrigerant compressor with minimal errors.

Application of turbomachinery equipment to unconventional working fluids such as supercritical CO_2 and its mixtures is relatively uncommon. So design, sizing and performance evaluation tools developed specifically for centrifugal machines handling supercritical CO_2 are not yet widely available (Okezue and Wang, 2016). Researchers such as Wright *et al.* (2009) and Modekurti *et al.* (2017) attempted to solve this problem by adapting existing standard design and analytical tools originally developed for conventional working fluids to work for supercritical CO_2 by merely coupling them to EoS correlations capable of predicting CO_2 properties at different operating conditions. Clearly, missing from that attempt is the effort to account for the peculiar behaviour of supercritical CO_2 within the internal flow channels of a centrifugal compressor and its overall effects on the working process of that machine (Okezue and Wang, 2014; Baltadjiev *et al.*, 2015 and Cho *et al.*, 2016).

As already discussed extensively in some sections of Chapter 2, equations of state (EoS) correlations perform excellently for CO_2 under subcritical conditions, but begins to encounter reliability problems when used to predict the anomalous behaviour of CO_2 under supercritical conditions. This is because these correlations cannot

properly simulate the large abrupt changes in CO_2 properties that occur in response to minor variations in pressure and temperature near the critical point. The reliability problems of EoS correlations are worse when applied in the calculation of specific enthalpy because it is derived from isobaric specific heat capacity. Near the critical point, abrupt changes in specific heat capacity of pure and impure CO_2 are both non-linear and non-monotonic (Bergamini *et al.*, 2011; Imre and Tiselj, 2012; Imre *et al.*, 2015; Okezue and Wang, 2016). Calculation errors are worse when EoS correlations are used predict those fluid properties that do not vary monotonically. Because of these reliability issues, attempts to adapt standard design and analytical tools such mean-line models to work for supercritical CO_2 by merely coupling them EoS correlations failed as admitted by Wright *et al.* (2010).

Going into technical details, because of its reliance on enthalpy values obtained directly from EoS correlations, mean-line model generates huge errors in the calculation of isentropic efficiency and actual input power when applied to centrifugal compressors handling supercritical CO_2 (Wright *et al.*, 2009; Aritomi *et al.*, 2011; Utamura *et al.*, 2012; Lee *et al.*, 2014 and 2016).

The alternative method of calculating isentropic efficiency directly from empirical loss correlations or coefficients have been used by researchers such as Aungier (2000), Wright *et al.* (2009) and Modekurti *et al.* (2017). The problem with this method is that these correlations and coefficients are based on curve-fitting experimental data of compressors handling either air or refrigerants under subcritical conditions. For this reason, the accuracy of the empirical loss coefficients and correlations are always in doubt when applied to supercritical CO_2 conditions. In their work, Modekurti *et al.* (2017) admitted as much when they claimed that they had no information on the level of error that will be incurred when these correlations are applied to a working fluid at the vicinity of its critical point.

Given the context laid out above, researchers routinely evaluate the performance of supercritical CO_2 compressors with models assuming a fixed isentropic efficiency value (Witkowski and Majkut, 2012; Luo *et al.*, 2014; Monge *et al.*, 2014; Martynov *et al.*, 2016). The problem with this approach is that isentropic efficiency of a compressor is actually not a single constant value. It varies with respect to both the purity level of the supercritical CO_2 stream and the operating conditions of the

compressor. The variation in efficiency can be large if the concentration of certain impurities (e.g. hydrogen and nitrogen) in supercritical CO_2 mixture is significant (Okezue and Wang, 2016; Okezue and Kuvshinov, 2018).

The deficiencies inherent in existing mean-line models is an indicator that there is scope for the development of a new mathematical model capable of evaluating the performance of supercritical CO_2 compressors with an acceptable level of accuracy

4.2.3.1.3 Three-Dimensional CFD models

Generally, 3D CFD models are capable of producing performance simulations with a level of accuracy closest to reality by accounting for the complexities of geometry and fluid flow in all three polar coordinates of the compressor domain. This ability makes CFD models the best suited for the design optimization of various types of compressors. However, the complexity of CFD models which gives them the advantage of being more accurate than any other kind of model is also the reason why they have the disadvantage of being computationally slower, taking several hours or even weeks to conclude calculations as reported in Kovacevic *et al.* (2007) and Cui and Sauls (2008), respectively. It should be noted that 3-D CFD models developed by both authors are for air compressors and therefore simple ideal gas equations apply. For supercritical CO_2 compressors, a fluid property software package (i.e. EoS correlations) will need to be coupled to the 3-D CFD model. Pecnik and Colonna (2011), Kim *et al.* (2014) and Cho *et al.* (2016) have all reported that the addition of EoS correlations for supercritical CO_2 increases the slowness of 3D-CFD centrifugal compressor model computations and in certain cases can cause solution convergence problems. The one method of ameliorating these solution convergence problems is to couple the CFD models to look-up tables of supercritical CO_2 fluid properties instead of EoS correlations (Pecnik and Colonna, 2011; Lettieri *et al.*, 2013; Baltadjiev *et al.*, 2015; Pham *et al.*, 2016). However, this method has marginal or no effect on the sluggish computational speed of the 3D CFD model. For example, the 3D-CFD model of a supercritical CO_2 centrifugal model developed by Kim *et al.* (2014) still takes 30 hours to complete all computations and generate simulation results despite being coupled to a look-up table.

In conclusion, simulations produced with computationally slow 3-D CFD models are of an order of accuracy closest to reality and have proven to be an excellent tool for

optimal design of air and refrigerant centrifugal compressors. However, given the solution convergence issues associated with the simulation of the erratic behaviour of CO_2 near its critical point, 3D-CFD models for supercritical CO_2 compressors may be more trouble than they are worth.

Luckily, time-consuming generation of realistic 3-D spatially non-uniform distributions of simulated flow data is not necessary for rightsizing compressors or evaluating their performance accurately. These can be achieved with a lumped model capable of generating average fluid flow data along an imagined streamline running from the inlet port through the impeller blade channels to the outlet port of the compressor. For a lumped model to be successfully applied in rightsizing or evaluating the performance of a supercritical CO_2 centrifugal compressor, the average flow data generated should broadly approximate the genuine distributed internal flow field of an actual compressor. A new model fitting that description has been developed as part of this PhD project. Detailed reporting of the new model can be found in the following sections of this chapter.

4.2.3.2 Approach Used To Develop Quasi-Dimensional Model of a Supercritical CO_2 Centrifugal Machine

As explained in previous sections, existing mean-line and 3D CFD models experience problems when applied in the preliminary design, sizing or analysis of centrifugal machines handling pure or impure CO_2 at conditions close to the critical point. To solve this problem, a new computationally fast and yet reasonably accurate mathematical model of a centrifugal machine handling supercritical CO_2 and its mixtures have been developed.

The new mathematical model developed as part of this PhD project describes the geometry, internal fluid flow and working processes of centrifugal machine. This mathematical model can be classified as being ***"quasi-dimensional model"*** since it consists of non-differential steady-state conservation equations applied to a coordinate-free control volume. This is in contrast to conventional 1-D, 2-D and 3-D models, which consists of differential conservative equations acting along one, two and three coordinate directions of a discretised volume, respectively.

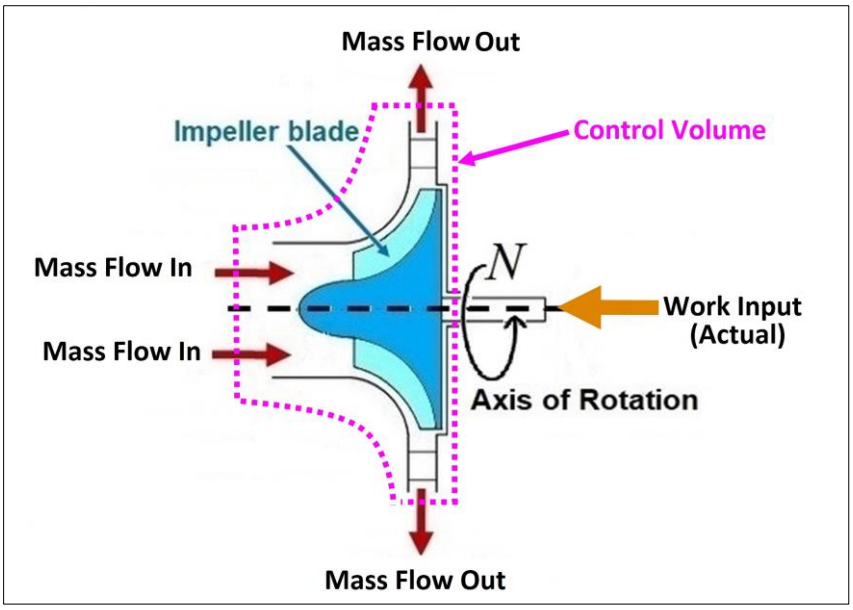

Fig.4.8 Full-section of a single stage compressor modelled as a control volume

As depicted in Fig. 4.8, the steady-state mass and energy conservation equations of the proposed quasi-dimensional model applies to a control volume, which is defined as encompassing the interior working space of a single-stage centrifugal machine. The actual operation of a centrifugal compressor is inherently an unsteady process. Nevertheless, the use of steady-state conservation equations in the proposed model is justified by the fact that the working fluid flows rapidly in and out of the compressor, barely having time to accumulate within the body of the machine due to the action of impeller blades rotating at high speed. The proposed quasi-D model eschews the common practice among many researchers of using empirical coefficients or correlations to account for energy losses within compressor. A mechanistic energy losses sub-model describing the physics of disk friction, leakage and hydraulic losses was developed from "first principles" and incorporated into the larger quasi-dimensional model.

As explained in sections 4.2.3.1.1 and 4.2.3.1.2, other researchers calculate energy requirement of compressors handling impure CO_2 at supercritical conditions with adiabatic or polytropic equations (either on their own or as part of a mean-line model) under the assumption that isentropic efficiency is a fixed value regardless of the working fluid's chemical composition. Okezue and Wang (2016) observed that isentropic efficiency is not a single constant value and can vary significantly if the concentration of certain impurities (e.g. hydrogen) in the CO_2 stream is high.

The new quasi-D model proposed in this PhD thesis does not assume isentropic efficiency is a single constant value known apriori. Therefore, the effect of different impurities in the supercritical CO_2 stream on compressor efficiency can be studied with this new model.

As mentioned previously, the actual operation of a centrifugal compressor is an unsteady process defined by the complex interactions between the working fluid and the rotating and stationary components of that machine. Therefore, no matter how precise a mathematical model is in describing the intricate geometry, internal fluid flow and working processes of a centrifugal machine, the accuracy of its simulated results is heavily dependent on the reliable calculation of thermophysical properties of the working fluid under compression. As already explained in previous sections of this PhD thesis, many equations of state (EoS) correlations suffer reliability problems when compelled to predict CO_2 behaviour at the vicinity of the critical point where large changes in fluid properties occur in an abrupt and non-linear manner when minor shifts in pressure and temperature occur.

To tackle these reliability problems, many researchers have developed new EoS correlations or modified old ones to make them better suited to predict the anomalous and non-linear behaviour of CO_2 at the critical point (see section 2.4.1). The results of their efforts are rather mixed. Today, there are EoS correlations capable of generating minor errors when used to predict CO_2 properties that change abruptly, but monotonically such as fluid density. Unfortunately, even the best available EoS correlations generate significant errors when applied in the prediction of those CO_2 properties that change abruptly and non-monotonically such as adiabatic index and specific heat capacity (See Fig. 4.9). Specific enthalpy varies monotonically with respect to pressure, temperature and chemical composition of CO_2 near the critical point (See Figs. 2.7 and 2.12). Nevertheless, EoS correlations generate significant errors in the calculation of specific enthalpy because of its derivation from isobaric specific heat capacity. For this reason, the classical method of calculating compressor isentropic efficiency and actual power input from specific enthalpy values predicted by EoS correlations is highly unreliable when the working fluid is supercritical CO_2.

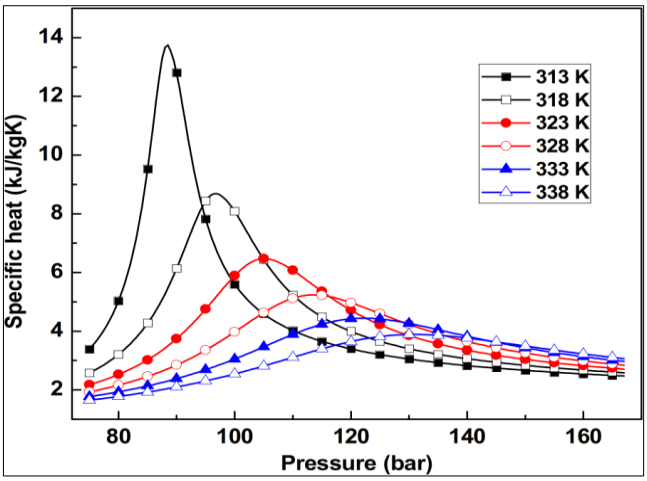

Fig.4.9 Pure CO_2 heat capacity as a function of pressure and temperature (Yadav et al., 2016)

To sidestep these reliability problems, the approach followed in the development of the new quasi-dimensional model involved the minimization of the role of EoS correlations (especially in predicting enthalpy) where possible. Where fluid property calculations are unavoidable (e.g. fluid density predictions), the best EoS correlations available are applied. Based on the comparative analysis of seven different EoS correlations carried out in Chapter 3, the highly accurate Span and Wagner (SW) EoS was selected for calculating pure CO_2 properties while GERG-2008 was selected for calculating impure CO_2 properties. Both high precision EoS correlations were integrated into the computer algorithms of the proposed quasi-dimensional model.

Because of this approach, overall energy consumption of a compressor is calculated in the proposed quasi-dimensional model using information on machine geometry and rotor shaft speed with EoS correlations limited to providing just fluid density and viscosity data. In other words, enthalpy calculations performed with EoS correlations are not required for predicting compressor work input and isentropic efficiency in this PhD study.

4.2.4 Governing Equations of the Quasi-Dimensional Model

As mentioned previously, the proposed quasi-dimensional model is governed by steady-state mass and energy conservation equations. These equations describe the working process of a single-stage centrifugal machine fitted with a semi-shrouded impeller as illustrated in Fig. 4.10.

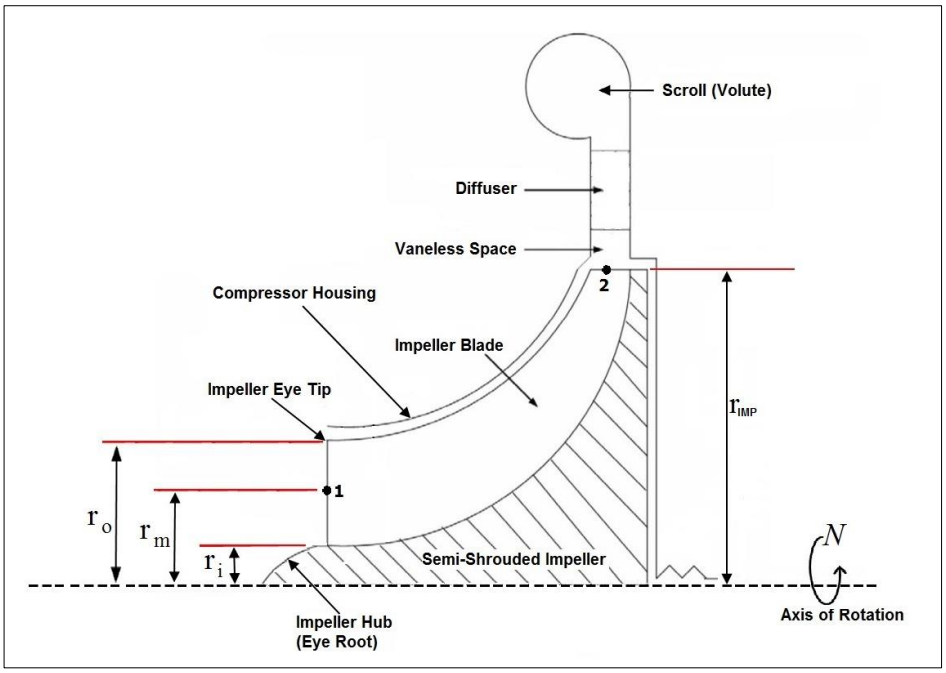

Fig.4.10 Half-sectional (meridional) view of a centrifugal compressor showing diffuser and volute

4.2.4.1 Mass Conservation Law

Mass balance of the working fluid using the entire centrifugal compressor as control volume (Fig. 4.9) gives:

$$\left.\frac{dm}{dt}\right|_{cv} = \dot{m}_2 - \dot{m}_1 = 0 \qquad (4.1)$$

For the inlet (i.e. suction) side of the compressor:

$$V_1 = \frac{\dot{m}}{\rho_1 A_1} \qquad (4.2)$$

$$\rho_1 = \Psi(P_1, T_1) \qquad (4.3)$$

$$A_1 = \frac{\pi\left(d_o^2 - d_i^2\right)}{4} \qquad (4.4)$$

$$b_1 = \frac{\left(d_o - d_i\right)}{2} \qquad (4.5)$$

Ψ = function symbol

where, $\dot{m}$, V_1, A_1, b_1, and ρ_1 represent the actual fluid mass flow rate, axial component of the inlet fluid velocity, inlet flow area, width of impeller at the leading

edge and inlet fluid density, respectively. The inlet fluid density is calculated with an EoS correlation using inlet pressure (P_1) and inlet temperature (T_1). The inlet flow area is an annulus formed by the concentric gap between the diameters of the eye tip (d_o) and eye root (d_i) of the impeller rotor (See Fig 4.5).

$$U_1 = \frac{\pi N\left(d_o + d_i\right)}{120} \tag{4.6}$$

As soon as the compressor shaft starts spinning at a particular rotational speed (N), tip speeds are developed at the leading and trailing edges of the impeller blades. The tip speed at the impeller's leading edge (U_1) is the average of the peripheral speeds at the tip and root of the impeller eye. The rotating blades impacts angular momentum to the working fluid flowing in from the inlet. However, the tangential component of the inlet fluid velocity (V_{t1}) is less than blade tip speed (U_1) owing to flow separation and formation of eddies.

$$V_{t1} = U_1 \times S_F \tag{4.7}$$

The slip factor (S_F) defines "slip" or the deviation of V_{t1} from U_1. Slip factor (S_F) is expressed mathematically using the equation developed by Stodola (1927):

$$S_F = 1 - \left(\frac{\pi \sin\beta}{n_B \cdot \left(1 - \left(\frac{V_{rad2}}{U_2}\right) \cdot \cot\beta\right)} \right) \tag{4.8}$$

It is important to note that V_{t1} only exists if there are internal guide vanes (IGV) at the compressor inlet (as depicted in Fig. 4.5) to channel the axial inflow of the working fluid around the circumference of the blades. For compressors that have no IGV, the value of V_{t1} is simply zero.

$$V_{rel1} = \sqrt{V_1^2 + \left(U_1 - V_{t1}\right)^2} \tag{4.9}$$

The inlet relative velocity (V_{rel1}) at which the working fluid enters the impeller eye can be solved using Pythagoras's theorem since it is one side of a right-angled inlet velocity triangle while U_1, V_1 and V_{t1} form the remaining sides. As illustrated in Fig. 4.11, the inlet velocity triangle is right-angled because there is no "pre-whirl" due to the absence of IGV (See section 4.1.3.2.1 for more information on "pre-whirl").

On the outlet (i.e. discharge) side of the compressor:

$$\rho_2 = \frac{\dot{m}}{V_{rad\,2} A_2} \tag{4.10}$$

$$A_2 = \pi D_{IMP} b_2 \tag{4.11}$$

$$U_2 = \frac{\pi D_{IMP} N}{60} \tag{4.12}$$

$$V_{t2} = U_2 \times S_F \tag{4.13}$$

$$V_2 = \sqrt{V_{rad2}^2 + V_{t2}^2} \tag{4.14}$$

$$V_{rel2} = \sqrt{V_{rad2}^2 + \left(U_2 - V_{t2}\right)^2} \tag{4.15}$$

where ρ_2, A_2, D_{IMP}, b_2, U_2, V_{t2}, and V_{rad2} represent the outlet fluid density; outlet flow area; impeller blade diameter; width of impeller at the trailing edge; tip speed at the impeller's trailing edge; tangential component and the radial component of the exit fluid velocity, respectively. Following in the tradition of turbomachinery design, V_{rad2} is assumed to be approximately equal to V_1. As illustrated in the outlet velocity triangle (Fig. 4.11), the vector sum of the radial velocity component (V_{rad2}) and tangential velocity component (V_{t2}) is the absolute exit velocity (V_2). On the other hand, V_{rel2} is the relative exit velocity.

4.2.4.2 Energy Conservation Law

Performing a specific energy balance of the working fluid using the entire centrifugal compressor as the control volume (Fig. 4.9), yields equation (4.16) which can then be used to obtain the actual exit enthalpy of the fluid at the discharge of the compressor:

$$h_{2a} = \left(h_1 + \frac{V_1^2}{2} + W_{INPUT} \right) - \frac{V_2^2}{2} \qquad (4.16)$$

$$T_2 = \Psi(P_2, h_{2a}) \qquad (4.17)$$

As mentioned earlier, the modelling strategy adopted in this PhD study seeks to minimize the role of EoS correlations where possible. Nevertheless, there are cases where the major use of EoS is unavoidable. Inlet enthalpy (h_1) for equation (4.16) is calculated with the EoS correlations using inlet pressure (P_1) and inlet temperature (T_1) while the actual outlet temperature (T_2) of the working fluid is calculated with the EoS using outlet pressure (P_2) and the actual outlet enthalpy (h_{2a}) as shown in equation (4.17).

In keeping with the strategy of eliminating the use of EoS-predicted enthalpy values in the calculation of the actual work input and isentropic efficiency of the compressor, Euler's turbomachinery equation (4.18) as expressed in Saravanamutto *et al.* (2001) and Douglas *et al.* (2005) was incorporated into the proposed quasi-D model.

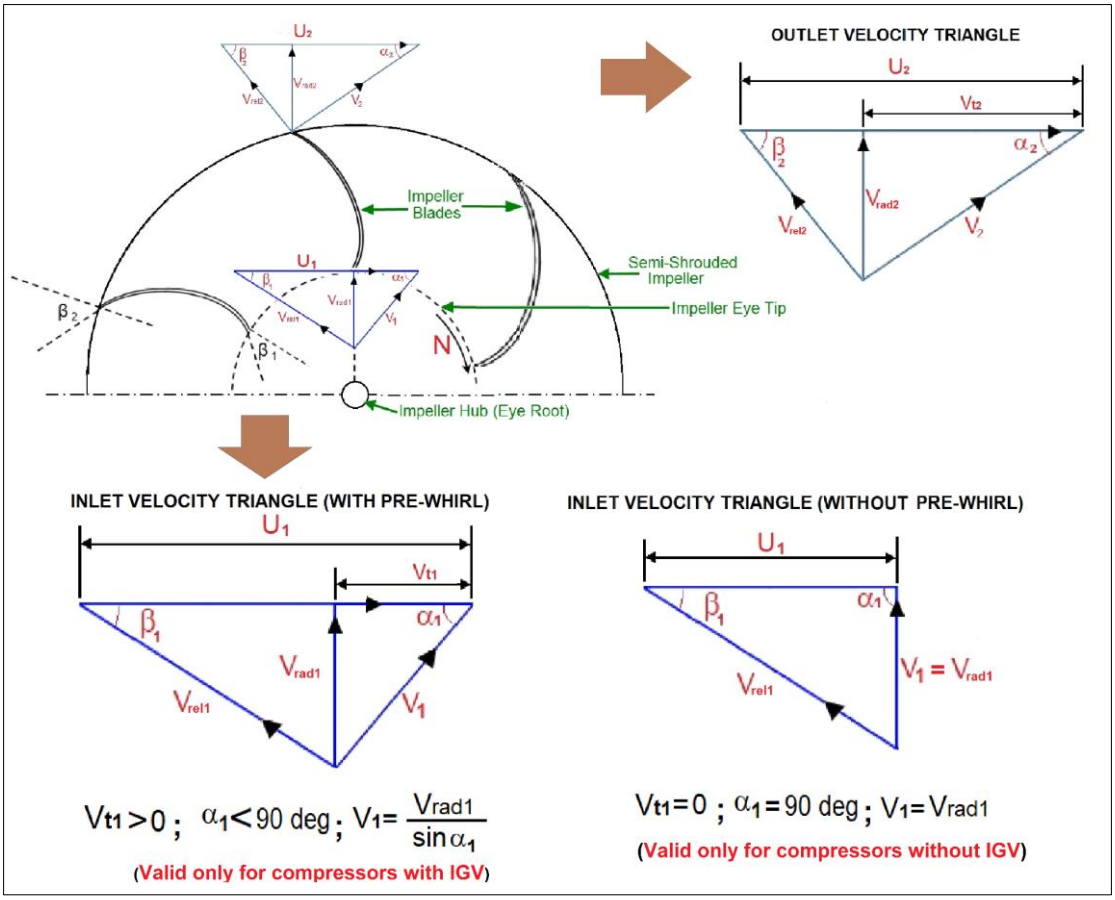

Fig.4.11 Velocity triangles represent momentum transfer from impeller blades to the working fluid

However, Euler's equation (4.18) inaccurately describes the transfer of kinetic energy from impeller blades to the working fluid because it excludes all energy losses (frictional or otherwise) that occur in a real-life compressor. By itself, equation (4.18) only describes the ideal energy (W_{euler}) that will be impacted to the working fluid if it is assumed that compressor operation is frictionless (i.e. compression is an isentropic process). In other words, the equation does not describe the actual energy (W_{INPUT}) supplied to compressor's rotating impeller blades.

$$W_{euler} = \frac{1}{2}\left[\left(V_2^2 - V_1^2\right) + \left(U_2^2 - U_1^2\right) + \left(V_{rel2}^2 - V_{rel1}^2\right)\right] \qquad (4.18)$$

It is common practice to calculate the actual work input (W_{INPUT}) by dividing ideal energy (W_{euler}) with an assumed isentropic efficiency (η_{ISEN}) as demonstrated in most Fluid Mechanics textbooks including Dixon (1998) and Douglas *et al.* (2005). The problem with this methodology is that the same isentropic efficiency value is used regardless of the composition of the CO_2 mixture flowing inside the compressor. Yet it is known that variation in efficiency can be significant if the concentration of certain impurities in the supercritical CO_2 mixture is high (Okezue and Wang, 2016). A commonly used alternative method of calculating actual work input (W_{INPUT}) is to multiply the ideal energy (W_{euler}) with empirical coefficients that account for energy losses as demonstrated in some turbomachinery textbooks such as Saravanamutto *et al.* (2001) and research papers such as Jiang *et al.* (2006) and Wright *et al.* (2009). As explained in section 4.2.3.1.2, these empirical coefficients are based on experimental data of compressors handling either air or refrigerants under subcritical conditions. Therefore, the coefficients cannot be applied in the context of supercritical CO_2 conditions.

$$W_{INPUT} = W_{euler} + \sum W_{losses} \qquad (4.19)$$

$$\eta_{ISEN} = \frac{W_{euler}}{W_{INPUT}} \times 100\% \qquad (4.20)$$

Fundamentally, actual work input (W_{INPUT}) is the sum of the ideal work input (W_{euler}) and energy losses (both internal and external) as shown in equation (4.19). Therefore, quasi-D model calculates W_{INPUT} by combining a modified version of Euler's turbomachinery equation with a highly mechanistic energy loss sub-model

developed from “first principles”. The losses ($\sum W_{losses}$), modelled in section 4.2.4.3, include disk frictional losses, hydraulic losses and leakage losses. Isentropic efficiency (η_{ISEN}) is calculated from equation (4.20).

$$\int dh = \int Tds + \int \frac{dP}{\rho} \tag{4.21}$$

$$\Delta h_{ISEN} \approx \frac{\Delta P}{\rho_{ave}} \approx W_{euler} \tag{4.22}$$

$$P_2 \approx P_1 + \frac{\rho_{ave}}{2}\left[\left(V_2^2 - V_1^2\right) + \left(U_2^2 - U_1^2\right) + \left(V_{rel2}^2 - V_{rel1}^2\right)\right] \tag{4.23}$$

Equations (4.21) to (4.23) describes how the discharge pressure of the compressor (P_2) is calculated by combining the first law of thermodynamics for an isentropic process (Tds = 0) and the equation for energy requirement of an ideal (i.e. frictionless) compressor. Δh_{ISEN} is a close approximation of the isentropic enthalpy change while ΔP and ρ_{ave} are the differential pressure and the average of the inlet and outlet fluid densities, respectively.

4.2.4.3 Modelling Energy Losses

As shown in equation (4.19), the actual compressor work input consists of two parts– ideal work done on the fluid by impeller blades (W_{euler}) and the energy losses. There are several sources of energy losses in a centrifugal machine.

They can be broadly split into two categories namely, internal and external losses. Energy losses in the flow path of the working fluid inside the compressor is categorized as “internal losses”. Examples of internal losses are disk friction loss (W_{disk}), leakage loss (W_{leak}) and hydraulic loss (W_{HYD}). Energy dissipation due to skin contact between exterior components of the compressor are called “external losses”. Examples of external losses are mechanical losses in bearings and seals of the compressor shaft.

The external losses are far much smaller than internal losses. Considering that many modern centrifugal machines today have rotor shafts supported by low friction magnetic or gas bearings, it is reasonable to ignore external losses in the

compressor models. In this study, the energy losses in the compressor is restricted to internal losses alone as shown in equation (4.24):

$$\sum W_{losses} \approx W_{disk} + W_{leak} + W_{HYD} \quad (4.24)$$

4.2.4.3.1 Disk friction loss

The rotation of the semi-shrouded impeller in the working fluid generates shear stresses between its moving surfaces and the stationary interior walls of the compressor housing. Some of the energy supplied to the compressor is lost in overcoming friction associated with these shear stresses which is heavily dependent on the fluid density, shaft speed and impeller size. In the context of CCS transport, this source of energy loss can be quite significant considering the high compressor speeds and large fluid densities of supercritical CO_2-based working fluids involved.

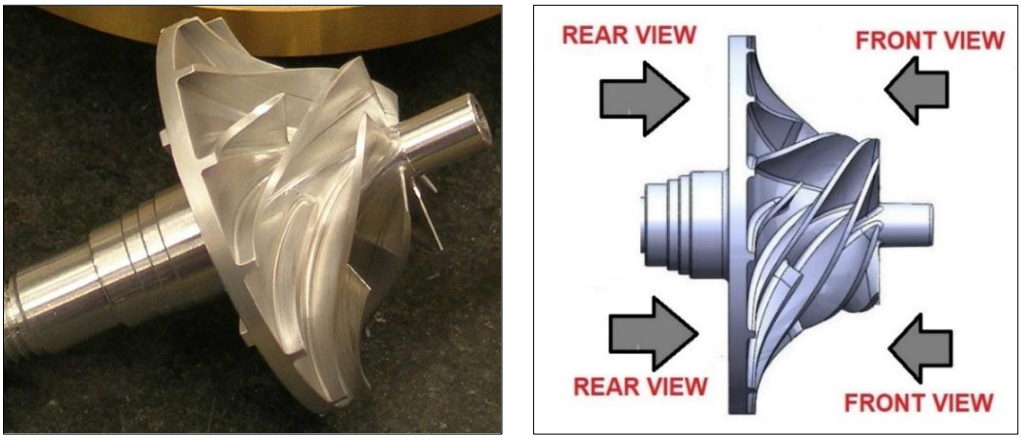

(a) (b)

Fig. 4.12 Semi-shrouded impeller as: (a) it appears in real life and (b) a profile drawing showing its front and rear view

The profile of shear stresses generated on the exterior surface of the rotating impeller runs frontally from the hub to the circumference and then the rear shroud. In order to develop a simplified mathematical expression for the disk friction loss, the complex shape of the semi-shrouded impeller shown in Fig. 4.12(a) is simplified by assuming that its shape is a combination of an annular disc plate and a frustum. This is justified by the fact that from its front view, the impeller resembles a conical frustum (i.e. a cone with its top half removed) while from the rear view, it resembles the annulus of a flat disk as seen in Fig. 4.12(b). In effect, the disk friction loss is modelled as the sum of energy loss on annular disc rotating in the working fluid

(W'_{disk}) and energy loss on the curved surface of a conical frustum (W''_{disk}) as shown in equation (4.25):

$$W_{disk} = W'_{disk} + W''_{disk} \tag{4.25}$$

Energy loss on the annular disc plate (W'_{disk}) is approximate to the actual energy dissipated as a result of the working fluid being in frictional contact with the rotating surface of the rear shroud of the impeller and the stationary walls of the compressor housing. As shown in equation (4.26), W'_{disk} is a function of the angular speed (ω) of the impeller and the torque of the rotor shaft. The torque is a product of the impeller radius (r) and the change in force along the profile of the rear shroud (dF). The shear stress of the working fluid (τ) arises from the force vector acting parallel to the surface of the rear shroud and the interior walls of the compressor housing. The actual mass flow rate of fluid flowing out of compressor discharge port is represented by ($\dot{m}$).

$$W'_{disk} = \frac{1}{\dot{m}} \int \omega r dF = \frac{1}{\dot{m}} \int \omega r \left(\tau dA\right) = \frac{1}{\dot{m}} \int \pi \rho f_{disk} \omega^3 r^4 dr \tag{4.26}$$

The local friction factor corresponding to the shear stresses on the smooth surface of the annular disc plate is calculated using a modified version of the Blasius correlation for smooth turbulent flows as shown in equation (4.27) below:

$$f_{disk} = 0.046 \left(\mathrm{Re}\right)_{disk}^{-0.20} \tag{4.27}$$

The approximate Reynolds Number (Re_{disk}) for a fluid in contact with the annular disc plate is presented in equation (4.28):

$$\mathrm{Re}_{disk} \approx \frac{\rho_2 U_2 \left(D_{IMP} - d_i\right)}{\mu_1} \tag{4.28}$$

Energy loss in the disc plate is modelled as dissipation generated as a result of the working fluid being in frictional contact with the annular-shaped surface of the rear shroud. The surface area of this annulus in the rear shroud is determined by integrating between the radius of the impeller hub (r_i) and the radius (r_{IMP}) of the impeller tip as shown in equation (4.29):

$$W'_{disk} = \frac{1}{\dot{m}} \pi \rho f_{disk} \omega^3 \int_{ri}^{r_{IMP}} r^4 dr = \frac{1}{\dot{m}} \left\{ \frac{\pi \rho f_{disk} \omega^3 \left(r_{IMP}^5 - r_i^5 \right)}{5} \right\} \quad (4.29)$$

Energy loss of a fluid rotating on a curved surface of a frustum ($\dot{W}''_{disk}$) shown in equation (4.30) is approximate to the actual energy drag generated as the curved surface of a conical frustum ($\dot{W}''_{disk}$) rotates in the surrounding working fluid.

$$W''_{disk} = \frac{1}{\dot{m}} \omega r_{ave} \left(\tau A_{curv} \right) = \frac{1}{\dot{m}} \left\{ \frac{\rho f_{curv} \omega^3 r_{ave}^3 A_{curv}}{2} \right\} \quad (4.30)$$

$$r_{ave} = \frac{r_{IMP} + r_i}{2} \quad (4.31)$$

The curved surface area of the conical frustum (A_{curv}) is a function of its height (H_{IMP}) and the radii— r_i and r_{IMP} —as shown in equation (4.32) below:

$$A_{curv} = \pi \left(r_{IMP} + r_i \right) \cdot \sqrt{\left(r_{IMP} - r_i \right)^2 + H_{IMP}^2} \quad (4.32)$$

The local friction factor corresponding to shear stresses on the smooth curved surface is:

$$f_{curv} = 0.046 \left(\mathrm{Re} \right)_{curv}^{-0.20} \quad (4.33)$$

The approximate Reynolds Number (Re_{curv}) for the working fluid surrounding the curved surface of the frustum and filling in the clearance between the impeller tip and interior wall of the compressor housing is:

$$\mathrm{Re}_{curv} \approx \frac{\rho_2 U_2 \left\{ D_{IMP} - d_i + \left(2 \cdot Gap \right) \right\}}{\mu_1} \quad (4.34)$$

4.2.4.3.2 Leakage loss

The difference between the inlet and outlet pressures generated in the compressor causes a portion of the working fluid flowing in the direction of the discharge port to return to the inlet port through the clearance between the impeller's surface and the walls of compressor housing (See Fig. 4.13). The backflow of some of the fluid means that the centrifugal machine's actual delivery capacity is usually lower than

its theoretical capacity. Leakage is a contributor to the overall energy losses in centrifugal machines.

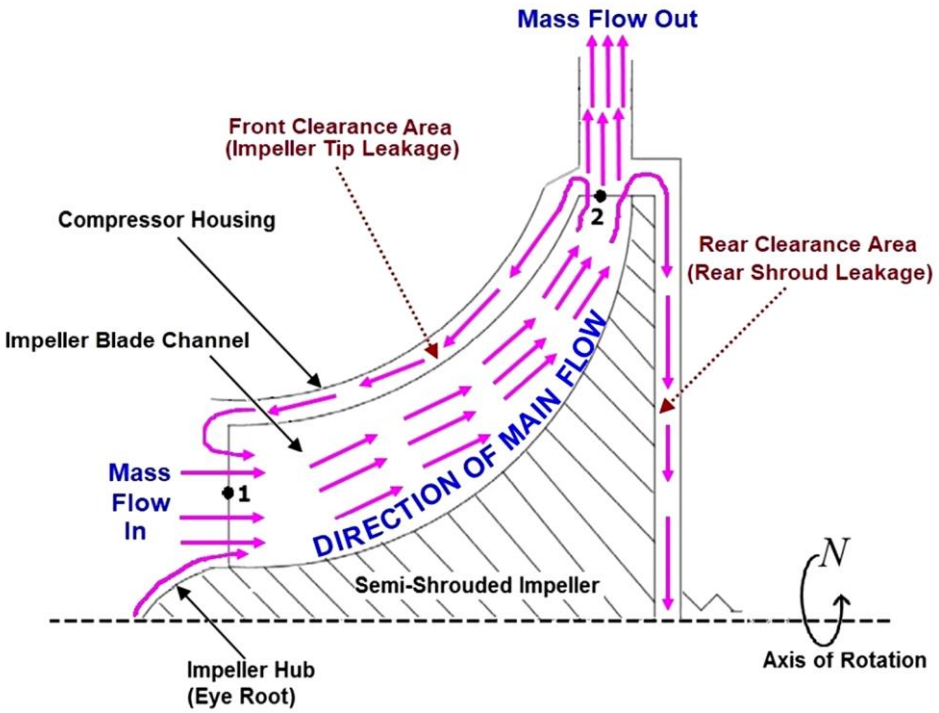

Fig.4.13 Half-sectional (meridional) view of a centrifugal compressor showing leakage flow paths

$$W_{leak} = \frac{1}{\dot{m}} \left\{ \frac{2\dot{m}_{gap} \Delta P_{gap}}{\rho_2} \right\} \tag{4.35}$$

$$\Delta P_{gap} = \frac{\dot{m}\left(r_{IMP} \cdot V_{t2} - r_m \cdot V_{t1}\right)}{n_B \cdot \left(\frac{r_{IMP} + r_m}{2}\right) \cdot \left(\frac{b_1 + b_2}{2}\right) \cdot L_{IMP}} \tag{4.36}$$

As shown in equation (4.35), energy loss due to leakage (W_{leak}) is strongly influenced by leakage mass flow rate ($\dot{m}_{gap}$) and the differential pressure across the clearance (ΔP_{gap}). The actual mass flow rate of fluid flowing out of the compressor discharge port is represented by ($\dot{m}$).

$$\dot{m}_{gap} = \rho_2 \cdot n_B \cdot L_{IMP} \cdot Gap \cdot V_{gap} \tag{4.37}$$

The leakage mass flow rate is a function of the fluid density, leakage velocity (V_{gap}), number of impeller blades (n_B) and flow area of the clearance. The clearance is

assumed to have a rectangular shape. Therefore, its flow area is the product of the width of the clearance (*Gap*) and the length of the impeller blades (L_{IMP}).

$$V_{gap} = \frac{1}{1 - K_{loss}} \cdot \sqrt{\frac{\Delta P_{gap}}{\rho_2}} \tag{4.38}$$

$$K_{loss} = \frac{1}{2}\left(\frac{\text{Gap}}{\text{b}_1 + \text{Gap}} + \frac{\text{Gap}}{\text{b}_2 + \text{Gap}} \right) \tag{4.39}$$

The loss coefficient (K_{loss}) describes the fraction of the working fluid back-flowing through pathways created by the clearance area between the compressor housing and the impeller's leading and trailing edges.

4.2.4.3.3 Hydraulic loss

Hydraulic losses are energy losses associated with the flow of the working fluid through blade channels running from the impeller's eye to the tip of its trailing edge. Energy losses in the diffuser and volute are also included. Hydraulic losses are quite distinct from leakage losses. The former refers to losses incurred as the working fluid flows from inlet to outlet of the compressor while the latter refers to losses incurred when a portion of the working fluid flowing towards the outlet turns around and returns to the inlet via the clearances. Hydraulic losses are generated in four ways:

- skin friction generated as the working fluid flows through blade channels of the impeller
- shock losses due to change in the flow direction of the working fluid from axial to radial direction within the curved impeller blade channels (Fig. 4.14)
- losses due to gradual contraction of the flow area from the inlet to the outlet (Fig 4.14)
- sudden deceleration of the working fluid in the diffuser of the compressor

For the purposes of this study, only the first three sources of hydraulic losses in the centrifugal compressor are modelled:

$$W_{HYD} = 2f_{HYD}\mathrm{V}_{\mathrm{rel,\ ave}}^2\left(\frac{L_{IMP}}{D_{HYD}}\right) + \frac{K_{sum}\mathrm{V}_{\mathrm{rel1}}^2}{2} \quad (4.40)$$

The first term in equation (4.40) describes energy loss due to skin friction between the working fluid and the surface of the impeller blade channels in which it is flowing. The second term describes losses due to change in the flow direction and losses due to the gradual contraction of the flow area of the blade channels from the leading to trailing edge of the impeller. The shear stress developed on the surface of the blade channels carrying the working fluid is dependent on the local friction factor (f_{HYD}); mean relative velocity ($\mathrm{V}_{\mathrm{rel,\ ave}}$); the arc length ($L_{IMP}$) and hydraulic diameter (D_{HYD}) of the blade channels. The mentioned parameters are presented in equations (4.41) to (4.46).

$$f_{HYD} = 0.046\left(\mathrm{Re}\right)_{HYD}^{-0.20} \quad (4.41)$$

$$\mathrm{Re}_{HYD} \approx \frac{\rho_2 \cdot \mathrm{V}_{\mathrm{rel,\ ave}} \cdot D_{HYD}}{\mu_1} \quad (4.42)$$

$$\mathrm{V}_{\mathrm{rel,\ ave}} = \sqrt{\frac{\mathrm{V}_{\mathrm{rel1}}^2 + \mathrm{V}_{\mathrm{rel2}}^2}{2}} \quad (4.43)$$

The hydraulic diameter proposed by Boyce (1972) for the blade channels was used:

$$D_{HYD} = \frac{2\left(A_1 \cos\beta\right)}{\left\{\pi \cdot \left(d_o + d_i\right) \cdot \cos\beta\right\} + \left\{2 \cdot n_B \cdot \left(d_o - d_i\right)\right\}} + \frac{\left(A_2 \cos\beta\right)}{\left\{\pi \cdot D_{IMP} \cdot \cos\beta\right\} + \left\{n_B \cdot b_2\right\}} \quad (4.44)$$

The arc length of the blade channels (L_{IMP}) is a function of the impeller's blade angle (β), wrap angle (θ) and meridional length (L_m):

$$L_{IMP} = \frac{L_m}{\sin\beta} \quad (4.45)$$

where,

$$L_m = \tan\beta \cdot \left(\frac{r_{IMP} + r_m}{2}\right) \cdot \theta = \tan\beta \cdot \left(\frac{r_{IMP} + r_m}{2}\right) \cdot \left(\frac{2\pi}{n_B}\right) \quad (4.46)$$

From Fig. 4.14, it is clear that the profile of impeller blade channel resembles a combination of a pipe bend and a contracting pipe cross-section. Therefore, the second term in equation (4.40) was modelled using the sum of loss coefficients for a pipe elbow (K_{curv}) and gradual contraction of a pipe (K_{con}) as shown below:

$$K_{sum} = K_{curv} + K_{con} \tag{4.47}$$

The loss coefficient for gradual contraction (K_{con}) is based on the Crane (1982) correlation for a pipe with a gradually contracting cross-section:

$$K_{con} = \begin{cases} 0.8\left(1-\frac{A_2}{A_1}\right)\cdot\sin\left(\frac{\phi}{2}\right) & \text{for } \phi \le 45\,\text{deg} \\ 0.5\left(1-\frac{A_2}{A_1}\right)\cdot\sqrt{\sin\left(\frac{\phi}{2}\right)} & \text{for } 45\ \text{deg} \le \phi \le 180\ \text{deg} \end{cases} \tag{4.48}$$

where, A_1, A_2 and ϕ represent the inlet flow area, outlet flow area and the angle of contraction, respectively.

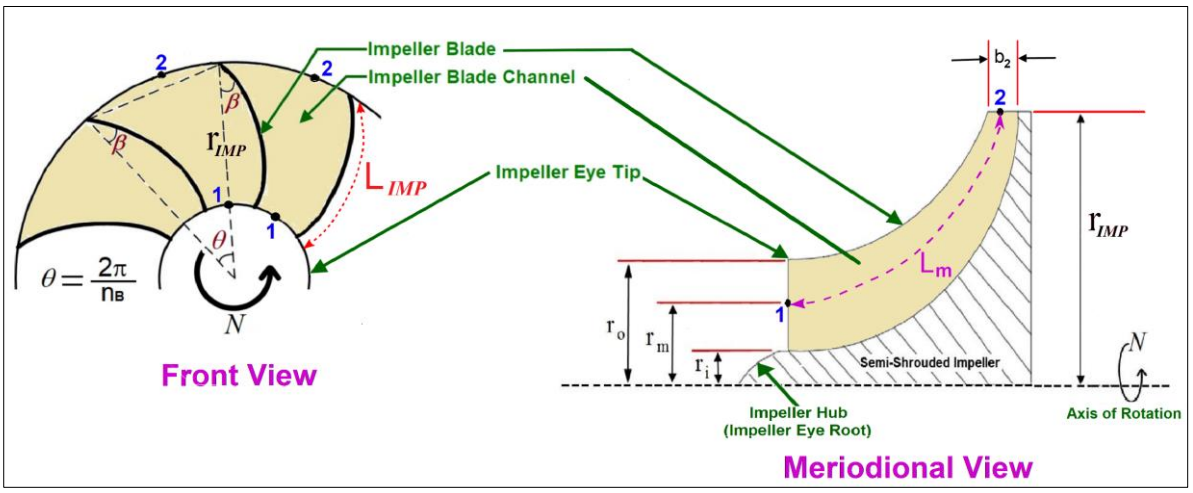

Fig.4.14 Front and meridional views of a semi-open impeller showing geometric parameters that influence hydraulic loss such as the wrap angle, blade angle, arc length of an impeller blade channel and meridional length of an imagined 1-D streamline

4.2.5 Description of a Computer Programme for the Quasi-Dimensional Model

Structurally, the computer programme for the quasi-dimensional model consists of input data files, governing equations based on the laws of conservation, equation of state (EoS) correlations and output data files. The governing equations describes the

geometry, internal fluid flow and working processes of a single-stage centrifugal compressor while the EoS correlations calculate the thermophysical properties of the working fluid based on its chemical composition. Two EoS correlations integrated into the computer programme. Span and Wagner EoS applies only when the working fluid is pure CO_2 stream while GERG-2008 EoS applies when the working fluid is an impure CO_2 mixture. The entire computer programme for the quasi-dimensional model was implemented in MATLAB®.

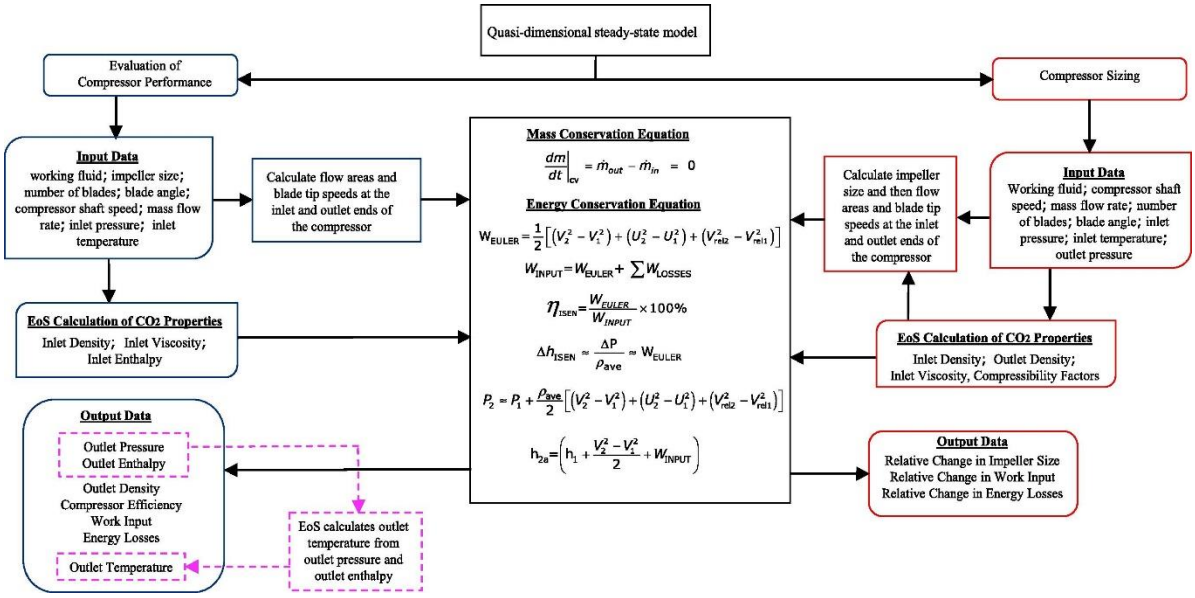

Fig. 4.15 Diagram showing the functionality of the computer programme for the quasi-D model

The computer programme of the mathematical model is set up to be bi-functional. In other words, it is designed to perform two tasks, namely:

1. Evaluate the performance of a particular centrifugal compressor of known size using machine geometry, composition of the working fluid and a wide range of inlet operating conditions as inputs

2. Calculate an optimal size for a centrifugal machine that will deliver the desired compressor performance using composition of the working fluid and a specific set of inlet and outlet operating conditions as inputs

As illustrated Fig.4.15, the computer programme contains two separate algorithms. One algorithm performs the first task listed above while the other algorithm tackles the second task. Both algorithms share the same governing equations and EoS

correlations, but apply them in a very different manner. The algorithms maintain separate sets of input and output data files.

4.2.5.1 First Algorithm: Evaluation of Compressor Performance

The first algorithm calculates output parameters for evaluating the performance of a particular centrifugal compressor using input data file information on machine geometry, chemical composition of the working fluid and a range of rotor shaft speeds (N), mass flow rates ($\dot{m}$), inlet pressures (P_1) and inlet temperatures (T_1).

The algorithm applies the governing mass and energy conservation equations in the calculation of the following output parameters— outlet pressure (P_2), actual outlet enthalpy (h_{2a}), outlet density (ρ_2), compressor efficiency (η_{ISEN}), actual work input (W_{INPUT}) and energy losses ($\sum W_{losses}$). As explained in section 4.2.3.2, compressor efficiency, work input and energy losses are calculated using information on machine geometry and rotor shaft speed with the equation of state (EoS) limited to providing only data on inlet fluid density (ρ_1) and inlet viscosity (μ_1). The equation of state (EoS) unavoidably plays a role in the calculation of the actual outlet temperature (T_2). The computer programme stores the calculated parameters in output data files as depicted in Fig. 4.15.

4.2.5.2 Second Algorithm: Compressor Sizing

The second algorithm functions by generating an appropriately sized centrifugal machine that can yield an optimal compressor performance for a given set of specific inlet and outlet operating conditions. Inputs for this algorithm include mass flow rate ($\dot{m}$), rotor shaft speed (N), inlet pressure (P_1), inlet temperatures (T_1), composition of the working fluid, output pressure (P_2), blade angle (β) and number of impeller blades (n_B). The last two input parameters are the only geometric data which the algorithm requires to determine the optimal machine size capable of delivering the desired compressor performance (i.e. a compression process in which W_{INPUT} is kept as low as possible, considering the given inlet and outlet operating conditions).

Overall, the algorithm uses a two-stage calculation process to produce its output data. At the first stage, the algorithm generates intermediate parameters namely, optimal centrifugal machine size, ideal work input and energy losses. The sum of the last two parameters being the actual work input of the optimally sized machine.

At the second stage, the algorithm compares intermediate parameters calculated for the reference working fluid (i.e. pure CO_2) against those calculated for other working fluids (i.e. various CO_2 mixtures) and then generates relative changes in impeller size, work input and energy losses as its final output data (See Fig. 4.15). These relative parameters are discussed extensively in Chapter 6.

4.2.6 Compressor Design and Operational Set-Up for Model Validation

As is the case with many CCS research work, only a limited amount of experimental or real plant data are available in the public domain. The author of this PhD thesis have not seen any published experimental performance data for anthropogenic centrifugal compressors or booster pumps operating in the context of CO_2 transport under supercritical conditions. For this reason, he was compelled to turn to published studies in the field of nuclear power such as Wright *et al.* (2010), Aritomi *et al.* (2011), Utamura *et al.*(2012) and Lee *et al.* (2014 and 2016) which report on centrifugal compressors used in experimental rigs running on the supercritical CO_2 Brayton cycle. Compressors used in supercritical CO_2 Brayton cycle are much smaller in size and have delivery capacities that are only a fraction of what obtains in CO_2 transport pipelines used in CCS schemes. However, these small compressors operate at very high pressures and temperatures comparable with what obtains in CO_2 pipeline transportation.

For purposes of model validation, the performance of a small centrifugal machine is simulated and compared to experimental data of an identically sized real-life centrifugal compressor running on the supercritical CO_2 Brayton cycle. In order to perform an analysis of compressors and booster pumps relevant to a supercritical CO_2 pipeline network, the validated quasi-dimensional model is applied to a larger (realistically sized) centrifugal machine. Details of the small and large machines can be found in sections 4.2.6.1 and 5.1.1, respectively.

4.2.6.1 Small-scale Compressor

The single-stage centrifugal machine used in this section of the study is unrealistically small for an actual CO_2 transport pipeline. Its maximum delivery capacity is only a small percentage (2%–20%) of typical flow rates observed in supercritical CO_2 pipeline transport. The decision to use this small centrifugal compressor in the study was made because experimental data for a real-life

machine of the same type and size was conveniently available for model validation. The input design and operational parameters of the small-scale compressor are displayed in Tables 4.2 and 4.3, respectively.

Table 4.2 Design Parameters of a Small-scale Compressor Used for Model Validation

Compressor Geometry	Dimensions
Impeller diameter	76.00 mm
Impeller blade height	20.40 mm
Number of impeller blades	16
Inlet diameter at the root of impeller eye	19.94 mm
Inlet diameter at the tip of impeller eye	40.00 mm
Outflow depth (i.e. impeller width at trail edge)	3.42 mm
Impeller blade angle	70.00 deg.
Clearance between impeller and compressor housing	0.254 mm

Table 4.3 Input Conditions of a Small-scale Compressor Used for Model Validation

Operating Condition	Range
Mass flow rate ($\dot{m}$)	2.242 – 4.008 kg/s
Rotor speed (N)	8298 – 14310 rpm
Inlet pressure (P_1)	75.88 – 82.71 bar
Inlet temperature (T_1)	308.30 – 310.60 K

The tabulated design parameters and input operational conditions were culled from the experimental work conducted by Aritomi *et al.* (2011).

4.2.6.2 Validation of Quasi-Dimensional Model

All supercritical CO_2 Brayton cycle test rigs circulate pure CO_2 as the working fluid. Therefore, the proposed model was validated only for the case of the small-scale compressor handling pure CO_2 stream with experimental data from (Aritomi *et al.*, 2011).

As presented on Table 4.4, the proposed model is quite robust with a maximum relative error of just 1.0%. The model could not be validated for the condition of a compressor handling impure CO_2 due to the lack of experimental performance data.

Table 4.4 Validation of Proposed Model Using Experimental Compressor Data for Pure CO_2 condition

N	M	P_1	T_1	Outlet Pressure (bar)			Outlet Temperature (K)		
rpm	kg/s	bar	K	Experiment	Prediction	Error (%)	Experiment	Prediction	Error (%)
8298	2.24	76.08	308.50	78.10	78.37	0.34	310.10	310.44	0.11
10104	2.73	77.43	309.90	80.39	80.81	0.53	312.30	312.75	0.14
10704	2.89	77.63	310.10	80.94	81.43	0.60	312.70	313.27	0.18
11298	3.06	77.98	310.40	81.68	82.23	0.68	313.30	313.90	0.19
11904	3.22	77.91	310.40	82.01	82.61	0.74	313.70	314.26	0.18
12000	4.01	82.71	308.50	91.34	91.76	0.46	311.50	312.39	0.29
12498	3.39	77.74	310.20	82.25	82.93	0.82	313.90	314.46	0.18
13103	3.74	76.21	308.30	81.41	82.02	0.75	312.30	313.04	0.24
13111	3.55	77.86	310.40	82.81	83.55	0.89	314.40	315.05	0.21
13704	3.92	77.06	309.20	82.76	83.39	0.76	313.50	314.36	0.27
13710	3.72	77.97	310.60	83.38	84.17	0.94	314.90	315.64	0.24
14310	3.88	75.88	308.60	81.75	82.57	1.00	313.30	314.15	0.27

Although validated with test data from a small compressor, the quasi-dimensional model can be applied to larger centrifugal machines, without seriously compromising the accuracy of its simulation results. This is because the model inherently scales compressor performance just like the affinity laws of turbomachinery. However, unlike the affinity laws, the model takes into account the non-linear real fluid effects of supercritical CO_2 and its mixtures.

4.3 CONCLUDING REMARKS

In this chapter, different types of compressors and their working principles were presented and their performance compared to each other. Compressors that fall under the rotodynamic machine category are preferred in Carbon Capture and Storage (CCS) projects because their large volumetric delivery capacities allows industrial scale transportation of several metric megatons of anthropogenic CO_2 per annum obtained from power stations and other process plants to designated places of sequestration via pipelines.

Centrifugal compressors generate higher pressure ratios than any other type of rotodynamic machine. They have few component parts, which make them easy to manufacture, operate and maintain, compared to other rotodynamic machines. For this reason, they are widely used in supercritical CO_2 transport pipeline networks.

However, the operating costs of pressurizing CO_2 above the critical point can be prohibitive, even more so if the supercritical CO_2 contain impurities. The long-term economic viability of operating a supercritical carbon dioxide transport pipeline system will only be secure if the energy consumption of compressors and booster pumps can be reduced, thereby lowering operating costs.

Significant savings in operating costs can be made by sizing compressors and booster pumps optimally in order to minimize power losses. Compressor performance maps, traditionally been used for this purpose, are unsuitable in the CCS context, as none have been developed for impure CO_2 streams at supercritical or dense phase conditions.

In this chapter, a new mathematical model was presented as effective tools for performance evaluation and optimal sizing of compressors and booster pumps in a supercritical CO_2 transport pipeline. The model was successfully validated with experimental data currently available in open literature.

CHAPTER 5

ANALYSIS OF COMPRESSOR PERFORMANCE WITH QUASI-DIMENSIONAL MODEL

This chapter presents the application of the quasi-dimensional model in analysing the performance of a supercritical CO_2 centrifugal machine under different operating conditions. Key parameters that characterize compressor performance such as impeller size, shaft speed and composition of the working fluid are identified and their varied effects on both the work input and energy losses of centrifugal machines installed in supercritical CO_2 pipeline transportation are thoroughly investigated. Unlike previous studies by other researchers, isentropic compressor efficiency is not assumed to be a known single constant value that remains fixed regardless of the changing composition of working fluid. Therefore, the impact of different chemical impurities in the supercritical CO_2 stream on isentropic compressor efficiency to be evaluated with the quasi-D model described in Chapter 4.

5.1 SET-UP FOR THE STUDY OF COMPRESSOR PERFORMANCE

5.1.1 Full-scale Compressor

With the completion of model validation with available experimental data in Chapter 4, the small-scale compressor is replaced with a larger machine capable of generating pressure ratios and flow rates relevant to supercritical CO_2 pipeline transportation in the CCS context. The larger machine is referred to as the “full scale compressor” in this chapter. It is twice the size of the small-scale compressor and generates flow rates within the typical operating range found in CO_2 transport pipeline networks. Table 5.1 presents the input design parameters of the full-scale compressor used in this study:

Table 5.1 Design Parameters of the Full-Scale Compressor Simulated With Model

Compressor Geometry	Dimensions
Impeller diameter	152.00 mm
Impeller blade height	45.00 mm
Number of impeller blades	16
Inlet diameter at the root of impeller eye	39.88 mm
Inlet diameter at the tip of impeller eye	80.00 mm
Outflow depth (i.e. impeller width at trail edge)	6.84 mm
Impeller blade angle	70.00 deg.
Clearance between impeller and compressor housing	0.254 mm

5.1.2 Composition of CO_2-based Working Fluids for Full-scale Compressor

For the purposes of this study, pure CO_2 and CO_2 in binary mixtures with N_2, H_2, CO and CH_4 were selected as working fluids for the full-scale compressor. For the impure CO_2 mixtures, two sets of scenarios have been created. In one set, the purity of the CO_2 in the mixture has been fixed at 90% by mole while in the other set, CO_2 purity is fixed at 80% by mole. Obviously, the concentration of impurities in the working fluids used in this study is too high to be reflective of CO_2 streams expected in an actual supercritical CO_2 transport pipeline. They have been selected primarily to study the qualitative effect of each type of impurity on the full-scale compressor performance as well as the impact of impeller sizing and shaft speed on energy requirement of the centrifugal machine.

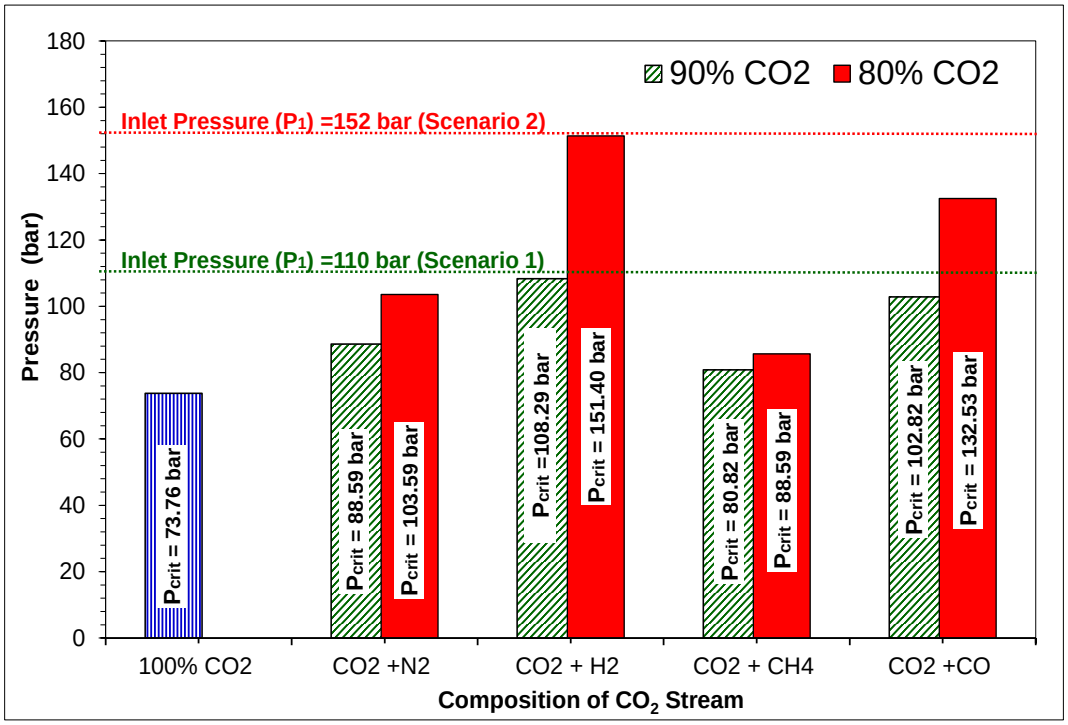

Fig. 5.1 Critical pressures for various working fluids with inlet pressures for scenarios 1 and 2 shown

As illustrated in Fig. 5.1, the shifting nature of the critical pressure (P_{crit}) depending on the type and concentration of the impurity in a CO_2 stream means that the inlet pressure of the full-scale compressor needs to be chosen carefully taking into account the purpose of this study— the evaluation of a centrifugal machine operating exclusively at conditions above the critical point of each working fluid. Table 5.2 shows the operating conditions chosen for the full-scale compressor. Two different scenarios were considered. The first scenario involves binary mixtures of 90% CO_2

purity entering into the full-scale compressor at inlet pressure and temperature of 110 bar and 305 K, respectively. In the second scenario, binary mixtures of 80% CO_2 purity enter the compressor at inlet pressure and temperature of 152 bar and 305 K. In both scenarios, the working fluids are already in supercritical state prior to their entry into the compressor. The same mass flow rates and rotor speeds are used for both study scenarios.

Table 5.2 Input Conditions of the Full-Scale Compressor Simulated With Model

	Operating Condition	Range
Scenario 1 Centrifugal machines compressing pure CO_2 and mixtures with 90% CO_2 purity	Inlet pressure (P_1) Inlet temperature (T_1) Mass flow rate ($\dot{m}$) Rotor speed (N)	110.00 bar 305.00 K 35.00 – 235.00 kg/s 8300 – 16190 rpm
Scenario 2 Centrifugal machines compressing pure CO_2 and mixtures with 80% CO_2 purity	Inlet pressure (P_1) Inlet temperature (T_1) Mass flow rate ($\dot{m}$) Rotor speed (N)	152.00 bar 305.00 K 35.00 – 235.00 kg/s 8300 – 16190 rpm

5.1.3 Real-Life Application of Study Set-Up: "Recompression" Compressors

The full-scale compressor is a single-stage centrifugal machine operating exclusively at supercritical conditions. This makes the simulated compressor performance analysis and compressor sizing work presented in this PhD thesis more practical and directly applicable to centrifugal "recompression" machines (i.e. booster pumps) installed at various repressurization points along the length of a pipeline to ensure that CO_2 stream remains in supercritical phase and at a predetermined target pressure.

In other words, the studies presented Chapters 5 and 6 covers single-stage centrifugal machines with inlet (suction) pressures already near or above critical pressure of CO_2 and operate at pressure ratios below 4:1. The studies do not cover high-pressure ratios of the kind encountered by intercooled multistage centrifugal compressors that have inlet pressure of 1.01 bar and operate at pressure ratios above 100:1.

5.2 ANALYSIS AND DISCUSSION OF SIMULATION RESULTS FOR FULL-SCALE COMPRESSOR

5.2.1 Effect of Impurities on Compressor Performance

Centrifugal compressors function by using impellers spinning at a high speed (N) to impact momentum tangentially to the working fluid flowing into the machine through the inlet port. In the diffuser (near the outlet duct) of the compressor, the fluid flowing at high speed decelerates and converts to pressure in accordance with Bernoulli's Principle.

As shown in Figs. 5.2 and 5.3, the outlet pressure (P_2) is a function of the chemical composition, density and the velocity of the working fluid. For a given working fluid, a simultaneous increase in both shaft speed and mass flow rate will develop a corresponding higher pressure in the compressor's discharge port. Like any other mechanical device, centrifugal machines are not 100% efficient. Some of the energy supplied to the compressor's rotating impeller blades is wasted on overcoming friction, shock losses, leakage, etc.

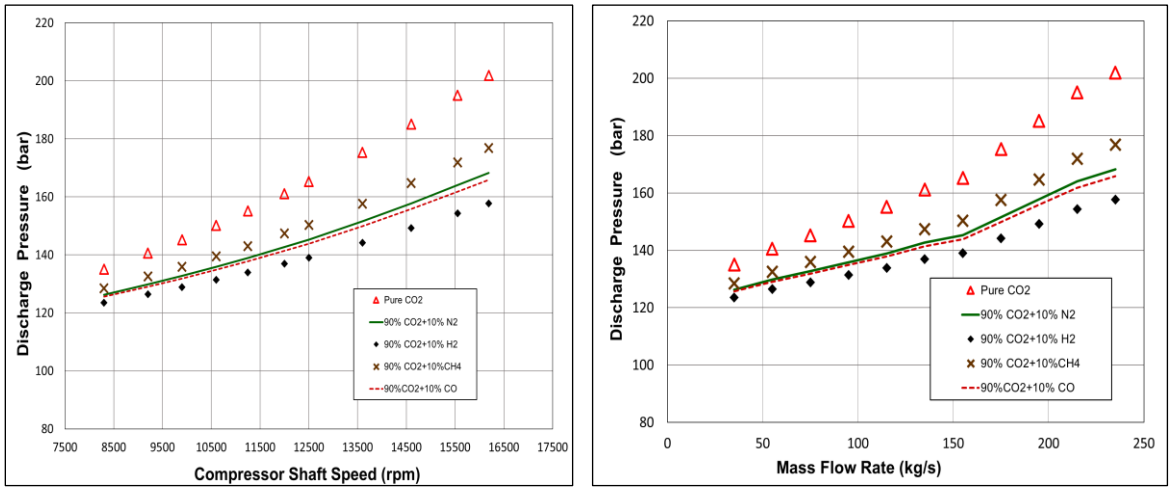

(a) (b)

Fig. 5.2 Discharge pressure as a function of (a) shaft speed and (b) fluid mass flow rate for pure CO_2 and mixtures with 90% CO_2 purity

For any given working fluid, these energy losses increase when both shaft speed and mass flow rate are increased together, resulting in a proportional decline in the isentropic efficiency of the compressor (See Figs. 5.4 and 5.5). The composition of working fluid also plays a role in determining the efficiency of the compressor. The impurities featured in this study namely N_2, H_2, CH_4 and CO all have lower molecular weights than carbon dioxide.

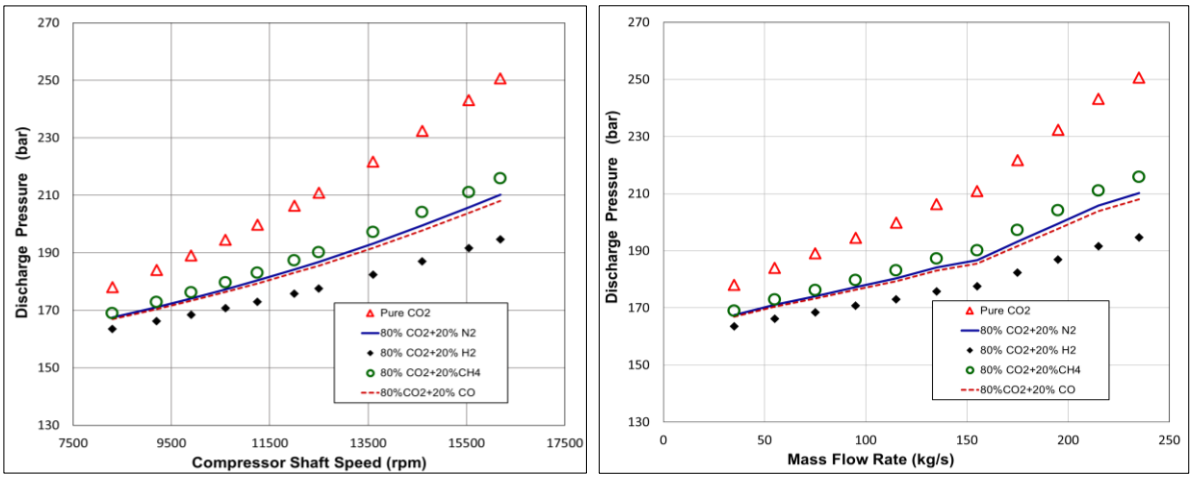

(a) (b)

Fig. 5.3 Discharge pressure as a function of (a) shaft speed and (b) fluid mass flow rate for pure CO_2 and mixtures with 80% CO_2 purity

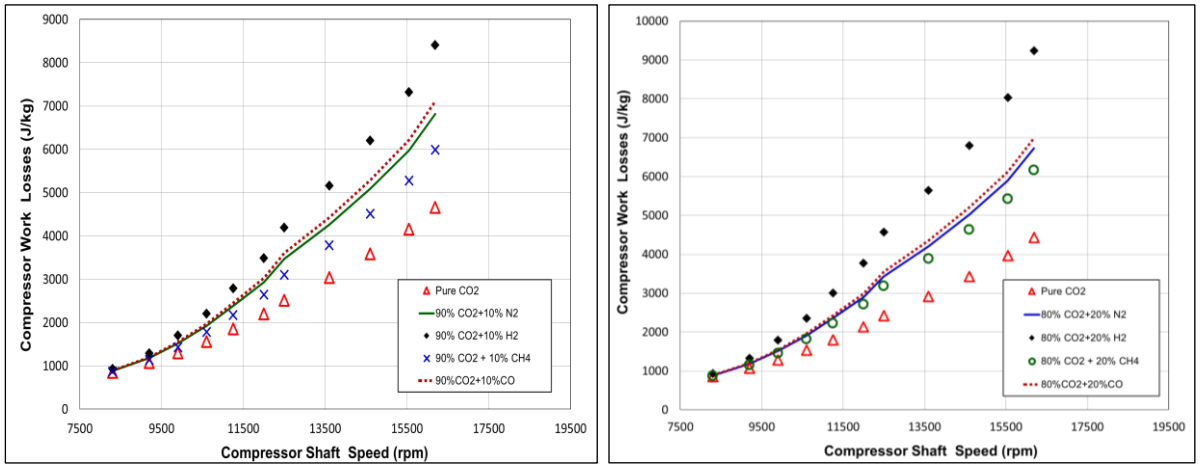

(a) (b)

Fig. 5.4 Energy loss as a function of compressor shaft speed for (a) pure CO_2 and mixtures with 90% CO_2 purity (b) pure CO_2 and mixtures with 80% CO_2 purity

As shown in Fig. 2.10, the introduction of these chemical impurities into the pure carbon dioxide stream will have the effect of reducing the overall density, which in turn, will immediately result in the decline of the fluid angular momentum developed from the torque of the compressor rotor shaft. Reduction in fluid angular momentum will lead to degradation of the discharge pressure head as shown in Figs. 5.2 and 5.3. These impurities also increase energy losses resulting in the reduction in the isentropic efficiency (See Figs. 5.4 and 5.5). In other words, for the same shaft speed and mass flow rate, the full-scale compressor will consume a greater amount of energy (W_{INPUT}) and generate a lower discharge pressure (P_2) if the working fluid changes from pure CO_2 to any of the other binary CO_2 mixtures.

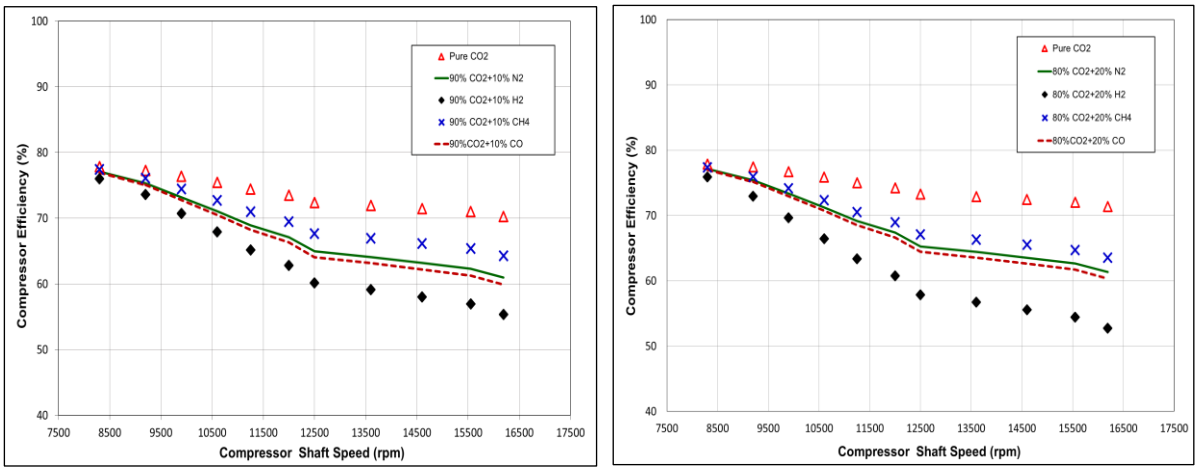

(a) (b)

Fig. 5.5 Isentropic efficiency as a function of compressor shaft speed for (a) pure CO_2 and mixtures with 90% CO_2 purity (b) pure CO_2 and mixtures with 80% CO_2 purity

The severity of the degradation of the compressor performance depends on the type and concentration of the impurity in the CO_2 stream flowing in the machine. From Figs. 5.2 and 5.3, it is clear that for a given shaft speed and mass flow rate, the hydrogen impurity in the CO_2 causes the greatest reduction in the outlet pressure (P_2) built up in the compressor diffuser. At the same time, because of large energy losses, the energy requirement of the compressor is highest while isentropic efficiency is lowest when the hydrogen impurity is present in supercritical CO_2 (See Figs. 5.4 and 5.5). All these can be attributed to the drastic reduction in the overall fluid density because of the sharp contrast between the molar mass of hydrogen (2.016 g/mol.) and that of carbon dioxide (44.01 g/mol.). The other impurities—nitrogen, methane and carbon monoxide— have larger molar masses than hydrogen and therefore their effect on compressor performance are less severe. Comparing Figs. 5.2 to 5.5, it is observed that increasing the concentration of the impurities in the carbon dioxide-based working fluids from 10% to 20%, has the effect of further degradation in compressor performance.

5.2.2 Parametric Effects of Changing Impeller Diameter and Speed on Compressor Performance

Figs. 5.2 to 5.5 demonstrate for a given shaft speed and mass flow rate, compressor discharge pressure and energy losses are dependent on the properties of the working fluid. When the working fluid changes from pure CO_2 to one of the binary CO_2 mixtures, the minimum operating pressure required to maintain that fluid in supercritical phase inside the pipeline will increase. In order to meet the higher

minimum operating pressure in the pipeline, the compressor discharge pressure have to be raised. This can achieved in two ways: (1) the shaft speed (N) can be increased while impeller size remains unchanged or (2) the impeller size can be increased while the shaft speed remains constant.

Either way, an increase in energy losses ($\sum W_{losses}$) is the penalty that must be paid for the discharge pressure to be upwardly adjusted. However, the magnitude of these losses incurred differ depending on the method used to increase the discharge pressure. As a prerequisite for optimizing centrifugal machine performance, the effect of both alternative methods of increasing discharge pressure on compressor energy requirement was analyzed and compared against each other.

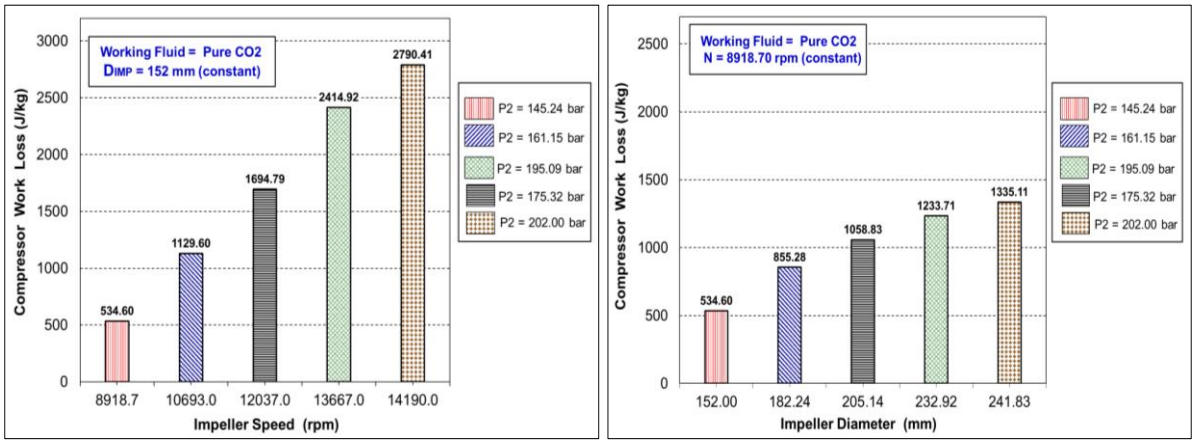

(a) (b)

Fig. 5.6 (a) Effect of impeller speed versus (b) effect of impeller diameter on compressor energy losses for pure CO_2 stream at inlet pressure of 110 bar and inlet temperature of 305 K

Figs. 5.6(a) and 5.6(b) each present five cases of both methods applied in raising the discharge pressure of pure CO_2 and their differing effects on compressor performance. In the initial (reference) case, a compressor with a 152 mm-impeller rotating at 8918.70 rpm increased the pressure of pure CO_2 from 110 bar to 145.24 bar, resulting in an energy loss of 534.60 J/kg. As shown in the second case, to generate the discharge pressure (P_2) of 161.15 bar, the speed (N) of the 152 mm-impeller will have to be raised to 10693 rpm, resulting in a total energy loss of 1129.60 J/kg. Alternatively, if the speed is maintained at 8918.7 rpm and the impeller diameter (D_{IMP}) increased to 182.24 mm, the same discharge pressure (P_2) of 161.5 bar will be generated for a much lower total energy loss of 855.28 J/kg. An analysis of all remaining cases in Figs 5.6(a) and 5.6(b) reveals the same trend—raising P_2 by increasing shaft speed while impeller diameter (D_{IMP}) remains unchanged will incur

higher energy losses ($\sum W_{losses}$) than a proportional increment in rotor diameter while keeping shaft speed constant. In other words, impeller re-sizing while the speed remains constant is a more efficient method of raising discharge pressure because it requires less work input (W_{INPUT}) compared to vice-versa.

5.3 BEHAVIOUR OF PURE AND IMPURE CO_2 IN THE INTERNAL FLOW CHANNELS OF A COMPRESSOR

The performance of a compressor depends on the characteristics of the working fluid as much it depends on its design and operating conditions.

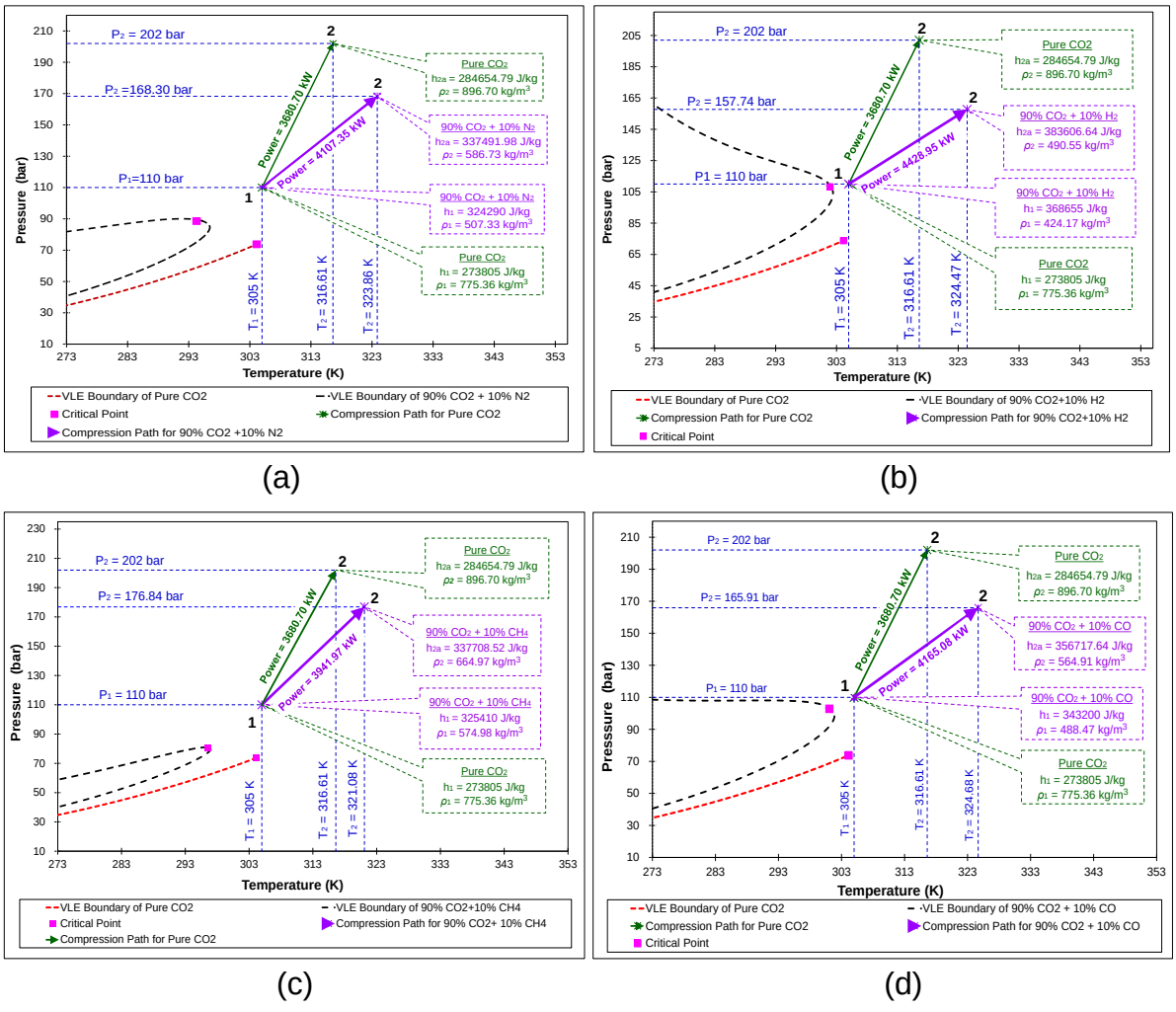

Fig. 5.7 Phase diagrams and thermodynamic paths of a compressor running at 16190 rpm for pure CO_2 compared against the following mixtures: (a) 90%CO_2 +10%N_2 ; (b) 90% CO_2 +10% H_2 ; (c) 90% CO_2 +10% CH_4 and (d) 90% CO_2 + 10% CO

A proper understanding of internal flow behaviour of the supercritical CO_2 stream and its effects on the overall working process of the centrifugal machine is essential for the optimal selection and sizing of compressors and booster pumps for the transport pipeline.

The internal flow behaviour of CO_2 stream is characterized by changes in its thermophysical properties as it travels through channels between stationary and rotating parts of the compressor. Fluid density, specific enthalpy and compressibility are examples of properties that characterize the behaviour of CO_2 stream.

Fig.5.7 presents fluid pressure-temperature phase diagrams showing the vapour-liquid equilibrium (VLE) boundaries for pure CO_2 and various binary mixtures of 90% CO_2 purity. The VLE boundaries of the working fluids are identical to those in Fig. 2.10. Within each phase diagram in Fig. 5.7, the internal flow behaviour of a specific impure CO_2 mixture is compared to that of a pure CO_2 stream under compression in the full-scale compressor operating at inlet pressure of 110 bar, inlet temperature of 305 K, mass flow rate of 235 kg/s and rotor shaft speed of 16190 rpm. Points "1" and "2" on each phase diagrams represent the inlet and outlet of compressor, respectively. They can also be seen as the start and end of the compression process for each of the working fluids.

5.3.1 Fluid Density

Fig 5.7(a) analyzes the internal flow behaviour of CO_2/N_2 stream in reference to pure CO_2 stream. For both working fluids, the compression process starts from the same inlet conditions (110 bar and 305 K) at point "1". Beyond point "1", the pathways of the compression process of the working fluids diverge significantly. During the compression of pure CO_2, fluid density rises from the initial value (ρ_1) of 775.36 kg/m^3 to the final value (ρ_2) of 896.70 kg/m^3. For this 15.7% increment in pure CO_2 density, the full-scale compressor consumes 3680.70 kW. At point "2" where the compression process ends, pure CO_2 exits the centrifugal machine at 202 bar and 316.61 K. When the working fluid changes from pure CO_2 to CO_2/N_2 mixture, inlet density (ρ_1) drops from 775.36 kg/m^3 to 507.33 kg/m^3 and the outlet density (ρ_2) drops from of 896.70 kg/m^3 to 586.73kg/m^3, representing a decline of 34.6%. Meanwhile, compressor input power (i.e. rate of W_{INPUT}) rises from 3680.70 kW to 4107.35 kW, representing an increment of 11.6%. The change in internal flow behaviour due to shift from pure CO_2 to CO_2/N_2 mixture also significantly affect compressor discharge conditions at point "2". The outlet pressure (P_2) declines from 202 bar to 168.3 bar as a result of the reduction of the fluid density while the actual outlet temperature (T_2) increases from 316.61 K to 323.86 K due to greater heat of compression and higher friction losses

within the compressor. An examination of Figs. 5.7(b) to 5.7(d) reveals the same trend as described above for Fig. 5.7(a), thus confirming that fluid density is directly proportional to discharge pressure and inversely proportional to the overall compressor power input requirement. Impurities affect the working process of the compressor by reducing the overall density of the CO_2 mixture which in turn results in reduction in compressor discharge pressure, a corresponding increase in energy losses, a decline in isentropic efficiency and an increase in the overall compressor input power requirement. Compared to other impurities, the hydrogen impurity has the greatest impact on fluid density. As demonstrated in Fig. 5.7(b), the greatest decline in discharge pressure and largest increment in compression power occurs when the full-scale compressor shifts from handling pure CO_2 to handling CO_2/H_2 mixture.

5.3.2 Specific Enthalpy

Specific enthalpy is the sum of internal and flow energies per unit mass of the working fluid: $h=\hat{u} + (P/\rho)$. Internal energy ($\hat{u}$) per unit mass is the thermophysical property which defines the capacity of working fluid to release heat when worked on by the compressor blades. The flow energy per unit mass (P/ρ) is energy spent by the working fluid as it flows through either inlet or outlet port of the compressor. Under supercritical conditions, specific enthalpy is a function both pressure and temperature as well as the chemical composition of the working fluid.

The working process (i.e. performance) of a centrifugal machine is analysed through changes in the specific enthalpy (Δh) of the working fluid as it flows from the inlet to the outlet of the compressor via internal channels between the blades of the rotating impeller and the stationary interior walls of the compressor housing. As shown in Figs. 5.7(a) to 5.7(d), when the full-scale compressor shifts from handling pure CO_2 to a binary CO_2 mixture, the actual change in specific enthalpy (i.e. difference between h_{2a} and h_1) increases significantly, resulting in higher input power requirement. Additionally, higher discharge temperatures are generated due to larger compression heat and heat from power losses in the centrifugal machine.

For instance, when the working fluid under compression shifts from pure CO_2 to CO_2/N_2 mixture, the change in specific enthalpy increases by 21.7%. This translates to an 11.6% increment in compressor input power (Fig. 5.7(a)). When the full-scale compressor shifts from handling pure CO_2 to CO_2/H_2 mixture, change in specific

enthalpy increases by 37.8% while compressor input power rises by 20.3% (Fig. 5.7(d)).

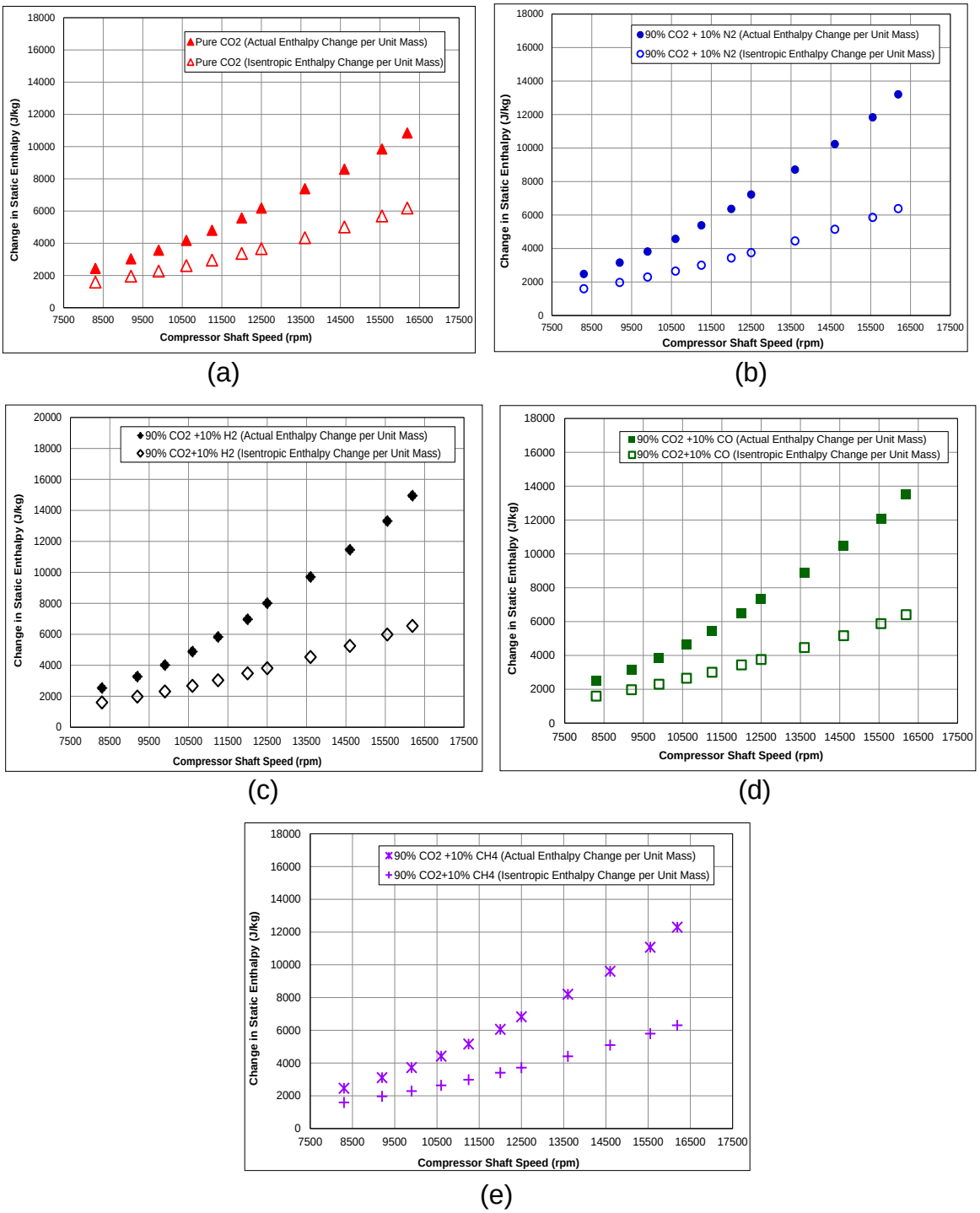

Fig.5.8 Comparing actual and isentropic change in static enthalpy per unit mass (Δh) for (a) pure CO_2; (b) 90% CO_2 +10% N_2 ; (c) 90% CO_2 +10% H_2; (d) 90% CO_2 +10% CO and (e) 90% CO_2 +10% CH_4

In section 5.2.1, a general performance evaluation showed that isentropic efficiency of a compressor is strongly affected by the composition of the working fluid, mass flow rate and shaft speed (Fig. 5.5). However, an in-depth analysis shows that the

variation in isentropic efficiency is a corollary of the internal flow behaviour of pure and impure CO_2 stream. As shown in Fig. 5.8, this internal flow behaviour is characterized in terms of change in static enthalpy per unit mass as a result of an isentropic (i.e. ideal) compression process (Δh_{ISEN}) and change in static enthalpy per unit mass as a result of actual compression (Δh_a). Both Δh_a and Δh_{ISEN} are calculated with modified versions of equations (4.16) and (4.22), respectively. The role of EoS correlations is limited to providing fluid density data for both equations.

From Fig. 5.8, change in actual (Δh_a) and isentropic (Δh_{ISEN}) enthalpies both increase with compressor shaft speed (N). However, Δh_a is larger and more sensitive to speed variation than Δh_{ISEN}. This can be attributed to the difference between the isentropic and actual compression processes. In isentropic compression process, there are no energy losses (frictional or otherwise) in the operation of the centrifugal machine. When compressor speed is raised, isentropic enthalpy change (Δh_{ISEN}) increases only because the impeller blades impact greater kinetic energy to the CO_2 stream, which translates to higher pressure and temperature. In other words, enthalpy change in the working fluid is strictly a consequence of its compression within the internal flow channels of the compressor. In the actual compression process, enthalpy change is a result of both fluid compression and energy losses within the compressor. In other words, Δh_a increases due to the kinetic energy impacted to the working fluid and also as a result of energy losses. These losses ($\sum W_{losses}$) increase in proportion to the third power of compressor speed (N).

The impact of the working fluid's chemical composition on Δh_a and Δh_{ISEN} was also examined in relation to compressor speed (N) by comparing Fig. 5.8(a)–(e). When a compressor running at 9200 rpm shifts from handling pure CO_2 to CO_2/N_2 mixture, Δh_{ISEN} and Δh_a will increase by 0.7 % and 4.1%, respectively. Raising the compressor speed to 16190 rpm translates to a 3.1% increase in Δh_{ISEN} and 21.7% increase in Δh_a. Alternatively, if compressor running at 9200 rpm shifts from handling pure CO_2 to CO_2/H_2 mixture, then Δh_{ISEN} and Δh_a will increase by 1.1% and 7.8%, respectively. At 16190 rpm, Δh_{ISEN} will increase by 5.7% and Δh_a will increase by 37.8%. Similar trend is seen when pure CO_2 (Fig. 5.8(a)) is compared to CO_2/CO stream (Fig. 5.8(d)) and CO_2/CH_4 stream (Fig. 5.8(e)).

Altogether, these observations indicate that chemical impurities in the CO_2 stream generally have a weaker impact on both isentropic and actual enthalpy change at low speeds than they do at higher speeds. However, at very high speeds, these impurities begin to exercise strong influence over the actual compression process. This is because energy losses— already large because of high compressor speeds— are further increased by the impurities. In contrast, the effect of the impurities on the isentropic compression process remains relatively weaker despite the high speeds because of the absence of energy losses. All these reconfirm that compressor (isentropic) efficiency is heavily dependent on energy losses. As demonstrated in Fig. 5.5, shaft speed (N) has a stronger effect on compressor efficiency compared to the composition of the working fluid. This is because energy losses rise exponentially in response to change in the chemical composition of the CO_2 stream. In contrast, energy losses increase in proportion to the third power of the compressor speed (N).

5.3.3 Fluid compressibility

At supercritical conditions, the dividing line between liquid and gaseous phases disappear, meaning that it is not always clear whether a compressor or a pump is best suited for pressurizing the working fluid. In the context of CCS transport, booster pumps rather than compressors are recommended for further pressurization of CO_2 stream already in supercritical phase (Demofonti and Spinelli, 2011; Serpa *et al.*, 2011; Witkowski *et al.*, 2013; Luo *et al.*, 2014). However, pumps are designed to handle incompressible fluids whereas supercritical carbon dioxide (with or without impurities) is a compressible fluid.

Centrifugal compressors and centrifugal pumps are of similar geometry and design. There are few differences between them. The most significant being the difference in the density and compressibility of the working fluids they are designed to handle. In the process of rightsizing centrifugal machines for the purposes of either compression or pumping, the above-mentioned properties of the working fluids play a central role. Hence, centrifugal pumps tend to be smaller than centrifugal compressors of equivalent capacity because they are designed to handle high-density incompressible fluids (i.e. liquids). Centrifugal compressors are necessarily larger because they handle low-density fluids that are highly compressible (i.e. gases). Supercritical fluids have high densities close to those of liquids. However, unlike liquids, supercritical fluids are compressible. In this study, it was observed that under

compression, the density of pure and impure supercritical CO_2 streams could increase by as much as 16%, hence demonstrating their compressibility (see Fig. 5.7). This reality suggests that a centrifugal machine optimally suited for handling supercritical fluids must be somewhere between the design of a gas compressor and the design of a conventional liquid pump.

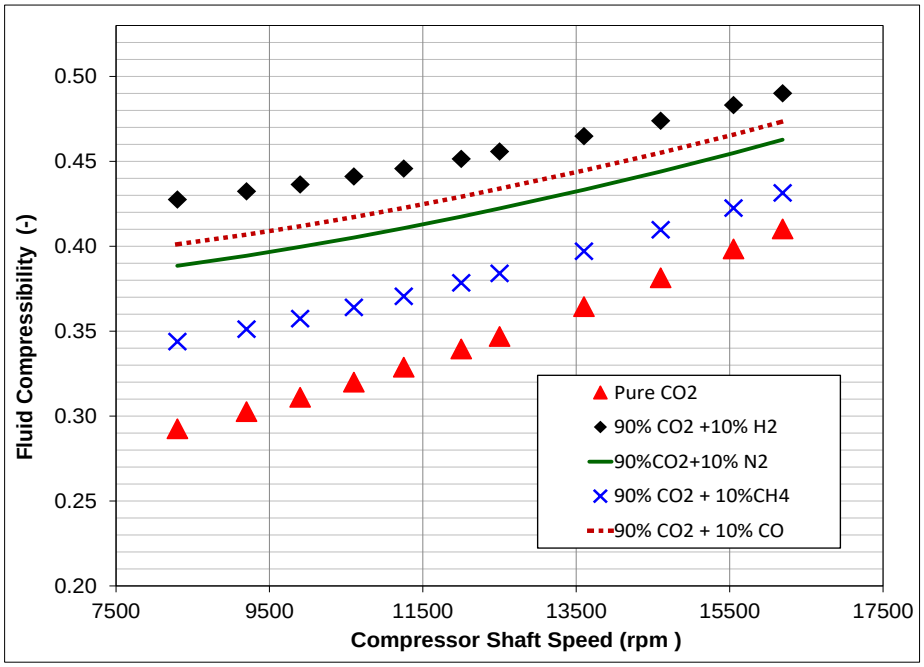

Fig.5.9 Compressibility as a function of shaft speed for pure CO_2 and its binary mixtures

In the context of centrifugal machine selection and sizing, the compressible behaviour of the working fluid is quite important. Compressibility factor (Z) is the property that is commonly employed in this regard. Absolute values of Z are merely corrective factors that quantifies the deviation of the specific volume of a real fluid from that of an ideal gas for a given pressure and temperature. By themselves, these absolute values of Z cannot be used to describe the compressible behaviour of a working fluid. However, the variation of compressibility factor (ΔZ) with respect to pressure or temperature characterizes the compressible behaviour of a working fluid. (ΔZ is related to the fluid property isothermal compressibility described in section 3.2.5).

Fluid compressible behaviour is also characterized by variation of compressibility factor with respect to both mass flow rate and shaft speed because of their strong influence on compressor pressure and temperature. Fig. 5.9 demonstrates the compressible behaviour of pure and impure CO_2 streams. From the graph, it is clear that compressibility progressively increases as the working fluid changes from pure

CO_2 to CO_2/CH_4, CO_2/N_2, CO_2/CO and finally, CO_2/H_2 mixtures. An examination of Figs. 2.11, 5.4 and 5.9 together show that compressibility is inversely proportional to fluid density and directly proportional to both energy losses ($\sum W_{losses}$) and the actual energy input (W_{INPUT}). In other words, working fluids with higher compressibility and lower densities require a greater amount of energy to compress. This explains why a compressor handling the CO_2/H_2 stream — the most compressible and least dense mixture— consumes the largest amount of power (i.e. rate of W_{INPUT}) as demonstrated in Fig. 5.7(b). In contrast, a compressor handling pure CO_2 — the least compressible and densest of the working fluids—consumes the lowest amount power during operation.

Compressibility is directly proportional to specific volume (i.e. the reciprocal of density). Therefore, upward trends in the compressibility data shown in Fig. 5.9 can be reinterpreted as an indication that the net specific volume of the working fluid flowing in and out of the full-scale compressor increases progressively from pure CO_2 to CO_2/H_2 mixture for a given shaft speed (N). The net specific volume is directly proportional to the size of the centrifugal machine. Because of its relationship with net specific volume, fluid compressibility is an important parameter for rightsizing a centrifugal machine for a given working fluid. In addition to other thermophysical properties that characterize the internal flow behaviour of pure and impure CO_2 streams, fluid compressibility data is used by the quasi-dimensional model in determining the optimal size of a centrifugal machine that will deliver desirable compressor performance.

5.4 CONCLUDING REMARKS

In this chapter, the quasi-dimensional model was applied in a comprehensive study of the performance of a single-stage centrifugal machine of realistic size (152 mm) handling pure CO_2 and various CO_2 mixtures in a transport pipeline under different operating conditions.

From this in-depth study, it was observed that the overall performance of centrifugal compressors is a function of the internal flow behaviour of the working fluid characterized by variations in its thermophysical properties with respect to chemical composition, pressure and temperature. One such property is fluid density, which plays a central role in determining the thermodynamic path followed by a compressor.

It is directly proportional to discharge pressure and inversely proportional to overall compressor work input requirement (which includes energy losses). Therefore, any group of impurities (e.g. nitrogen and hydrogen) capable of reducing overall fluid density when added to a pure CO_2 stream will also cause a decline in compressor discharge pressure; a corresponding increase in energy losses; a reduction in isentropic efficiency; and an increase in the overall compressor input power requirement.

Furthermore, the thermophysical properties of supercritical CO_2 are secondary functions of compressor size and speed since both parameters play key roles in determining the pressure and temperature changes within the internal flow channels travelled by the working fluid. In other words, the density, specific enthalpy, viscosity and compressibility of the working fluid inside the compressor are highly sensitive to changes in shaft speed and impeller size.

A parametric analysis conducted in section 5.2.2 of this chapter demonstrates the important role of impeller diameter and speed in determining the input power requirements of a compressor. Therefore, shaft speed and impeller size must be taken into consideration along with the working fluid's properties when evaluating compressor performance.

CHAPTER 6

COMPRESSOR SELECTION AND SIZING

At the design stage of pipeline networks, it is common for engineers to include a margin of safety when selecting compressors and booster pumps to account for future expansions in system capacity. In the context of carbon capture and storage (CCS), this margin of safety is extended to account for changes in the purity of the supercritical carbon dioxide because of its effect on compressor energy requirement. However, when deciding on a margin of safety, it is not always possible to anticipate all the variations that will occur in the chemical composition of the working fluid over a long period of time. Therefore, it may be inevitable that over a long period of time, the energy requirement of compressors and booster pumps will rise beyond what was originally anticipated due to significant changes in the composition of the impure CO_2 stream caused by alteration in capture technology or type of fuel burned in a power plant connected to the transport pipeline.

When the composition of the CO_2 stream changes from pure CO_2 to any of the binary CO_2 mixtures, the minimum operating pressure required to maintain that fluid in supercritical phase inside the pipeline increases. In order to ensure that the compressor discharge pressure remains above the minimum operating pressure, the shaft speed (N) will either have to be increased while compressor size remains unchanged or the compressor can be re-sized while the speed remains constant. In pipeline engineering, it is common practice to adjust shaft speed to maintain the discharge pressure above the minimum operating pressure because it is easier and simpler to implement than re-sizing the compressor's rotor.

However, as demonstrated in section 5.2.2, both compressor resizing and shaft speed increment incur energy losses. However, the latter incurs more energy losses than the former. This makes the former (i.e. compressor re-sizing) the preferable method of raising P_2 because of the long-term savings that can be made in operating costs.

In this section, the quasi-dimensional model is applied as a tool for appropriate sizing and selection of centrifugal machines compressing supercritical CO_2 mixtures of various compositions.

6.1 OPTIMAL RE-SIZING OF "RECOMPRESSION" COMPRESSORS FOR A PIPELINE TRANSPORTING SUPERCRITICAL CO_2 MIXTURES OF VARIOUS COMPOSITIONS

As explained in section 4.2.5.2, the quasi-dimensional model generates an appropriately sized centrifugal machine that can yield optimal compressor performance for a specified set of inlet and outlet operating conditions. Examples of some of these operating conditions include mass flow rate, impeller speed, inlet pressure, inlet temperature, chemical composition of the working fluid and the desired output pressure.

The quasi-dimensional model is tasked with solving three optimization problems, namely cases 1, 2 and 3. In all three cases, a standard discharge pressure (P_2) is chosen for five selected working fluids with CO_2 purity of 90% and 100%. Cases 1 and 2 are optimization problem-solving exercises on compressor re-sizing only. They both involve the application of the model's second algorithm in calculating the optimal impeller size needed by a compressor to generate the stipulated discharge pressure for a given set of operating conditions. In contrast to the two cases mentioned above, case 3 is an optimization problem-solving exercise in which both compressor re-sizing and shaft speed increment as alternative methods of generating P_2 are analysed and compared to each other in order to decide which of the methods is the optimal solution.

6.1.1 Case 1 – Calculating Optimal Compressor Size for Discharge Pressure of 170 bar

For each of the five selected working fluids, the absolute compressor size required to generate 170 bar (while speed remains constant) was calculated. The absolute values for the overall work input and energy losses incurred as a result is also calculated as well. Relative changes in compressor size, work input and energy losses shown in Figs. 6.1 and 6.2, are percentage differences used as a method of evaluating how the increase in optimum diameters at the inlet (d_o) and outlet (D_{IMP}) tips of the impeller affects P_2 and the energy requirement for a compressor handling each of the selected CO_2 mixtures compared to one handling pure CO_2. The quasi-D model calculates the above-mentioned relative changes in compressor parameters by comparing the absolute data for the four CO_2 mixtures against those calculated for the reference working fluid (i.e. pure CO_2) as follows:

$$\delta d_o = \frac{(d_o)_{CO2\_MIX} - (d_o)_{CO2\_PURE}}{(d_o)_{CO2\_PURE}} \cdot 100\% \quad (6.1)$$

$$\delta D_{IMP} = \frac{(D_{IMP})_{CO2\_MIX} - (D_{IMP})_{CO2\_PURE}}{(D_{IMP})_{CO2\_PURE}} \cdot 100\% \quad (6.2)$$

$$\delta W_{INPUT} = \frac{(W_{INPUT})_{CO2\_MIX} - (W_{INPUT})_{CO2\_PURE}}{(W_{INPUT})_{CO2\_PURE}} \cdot 100\% \quad (6.3)$$

$$\delta W_{losses} = \frac{(W_{losses})_{CO2\_MIX} - (W_{losses})_{CO2\_PURE}}{(W_{losses})_{CO2\_PURE}} \cdot 100\% \quad (6.4)$$

where, δW_{INPUT}, δW_{losses}, δd_o and δD_{IMP} represent relative changes in the work input, energy losses, diameters at the inlet and outlet tips of the impeller, respectively.

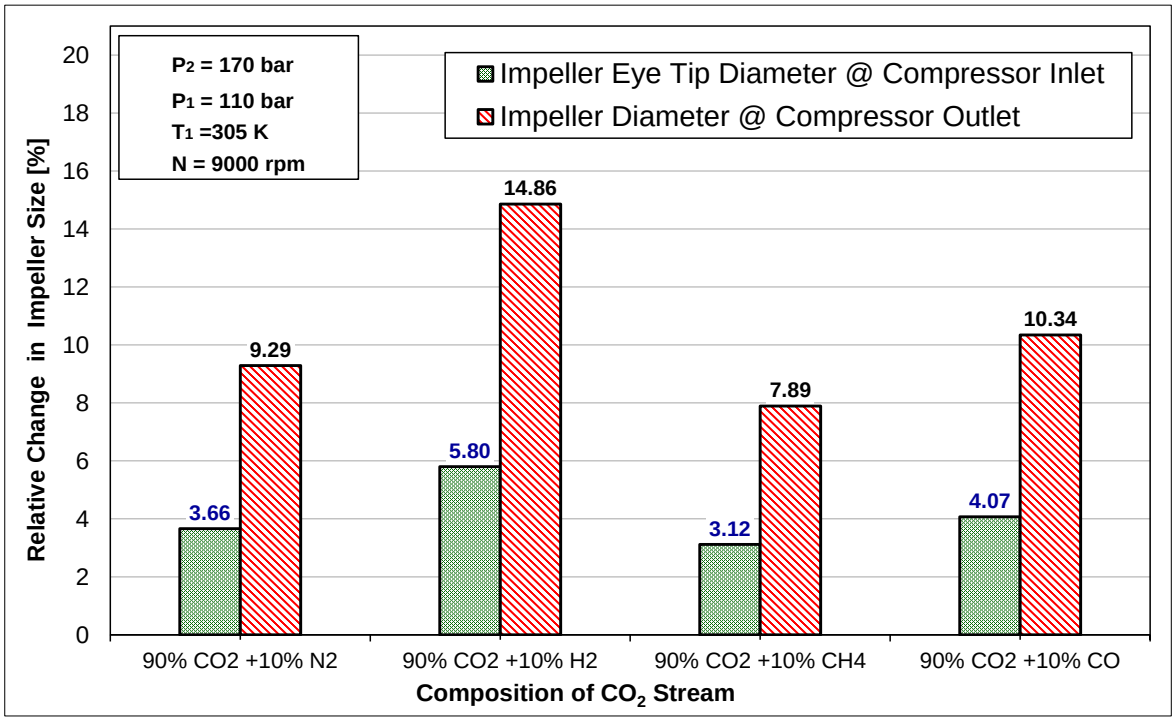

Fig.6.1 Relative change in impeller size for different CO_2 mixtures (P_2 =170 bar)

As explained in sections 5.2.1 and 5.3, the introduction of chemical impurities into pure CO_2 causes the fluid density to decrease while simultaneously increasing fluid compressibility. Therefore, CO_2/H_2 stream as the least dense and most compressible of the 5 selected working fluids will require the highest amount of energy (W_{INPUT}) to

generate the stipulated outlet pressure of 170 bar. For a constant shaft speed of 9000 rpm, this energy requirement will translate to the largest compressor re-sizing effort. In relative terms, optimum diameters at the inlet (d_o) and outlet (D_{IMP}) tips of the impeller will increase by 5.80 % and 14.86%, respectively as shown in Fig.6.1 when the compressor shifts from handling pure CO_2 to CO_2/H_2 mixture. As a result of this impeller resizing effort, the overall work input (W_{INPUT}) will increase by 30.34% and a relative increase in energy loss ($\sum W_{losses}$) of 19.54% is incurred as shown in Fig.6.2.

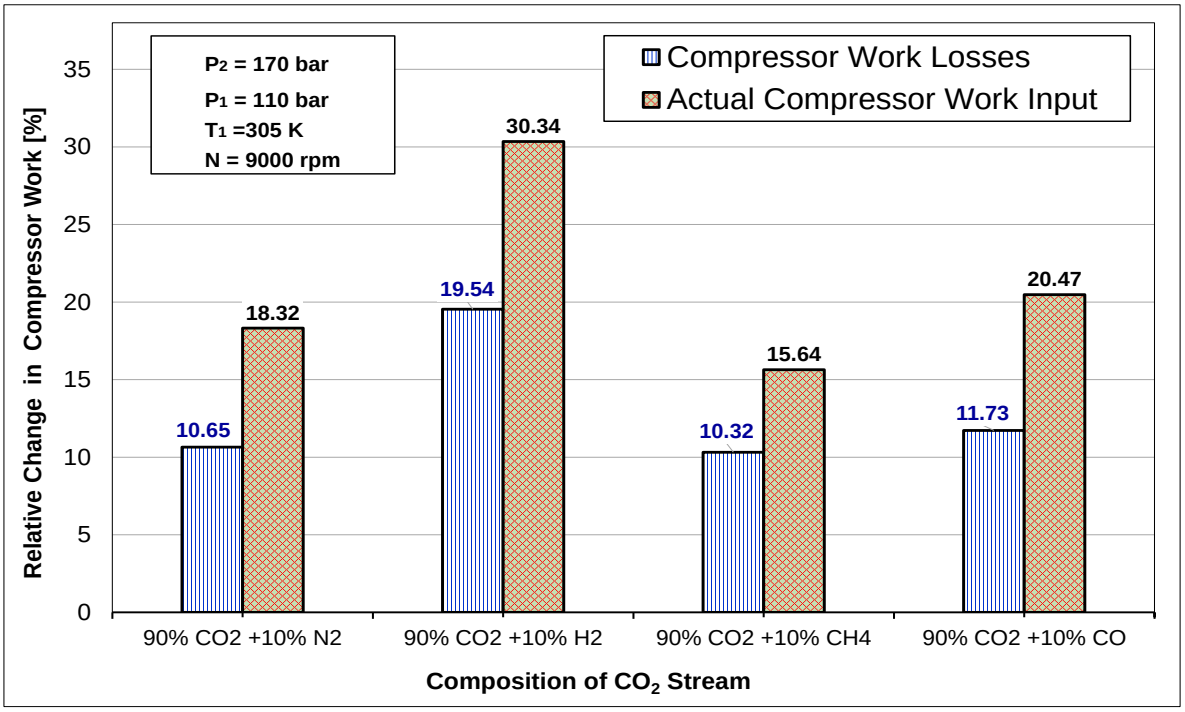

Fig.6.2 Effect of impeller size on work input and work losses for different CO_2 mixtures (P_2 =170 bar)

Compared to the other mixtures, CO_2/CH_4 stream, with the second highest density and second lowest compressibility after those of pure CO_2, requires the least amount of energy and the least compressor re-sizing effort. At the same speed of 9000 rpm, d_o will have to increase by 3.12% and D_{IMP} will increase by 7.89% in order to maintain the stipulated discharge pressure of 170 bar when working fluid changes from pure CO_2 to CO_2/CH_4 mixture. As a consequence of this resizing effort, the work input and energy losses will increase by 15.64% and 10.32%, respectively (see Figs 6.1 and 6.2).

6.1.2 Case 2 – Calculating Optimal Compressor Size for Discharge Pressure of 250 bar

For the second case, 250 bar was chosen as the standard discharge pressure. The group of working fluids and operating conditions (including shaft speed) used in this case is the same as those used in section 6.1.1 above.

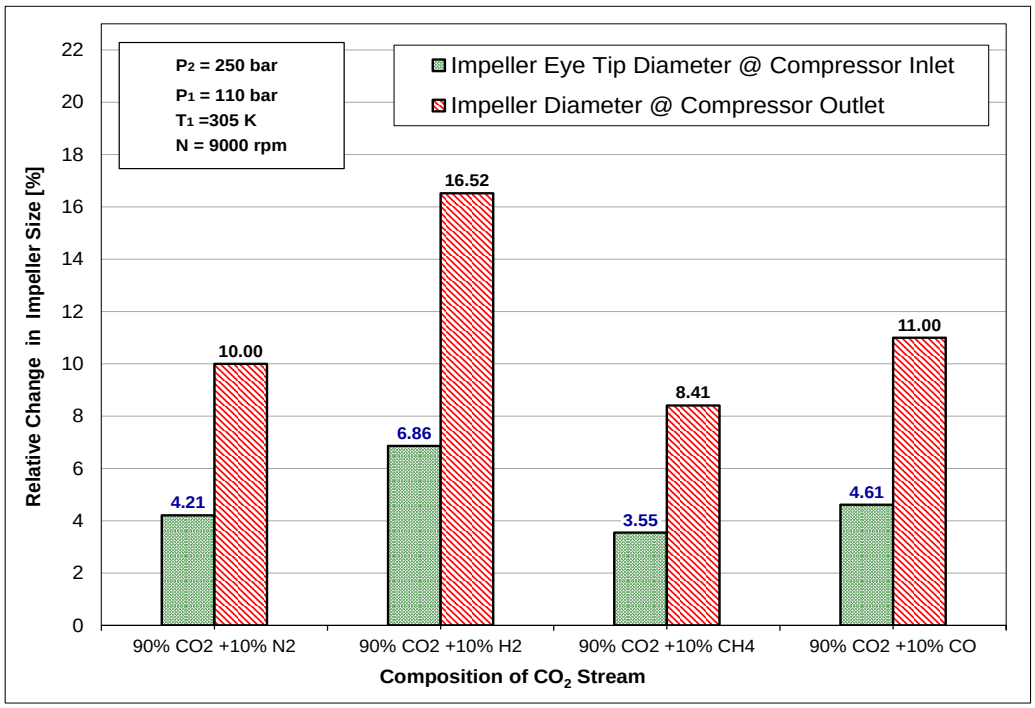

Fig.6.3 Relative change in impeller size for different CO_2 mixtures (P_2 =250 bar)

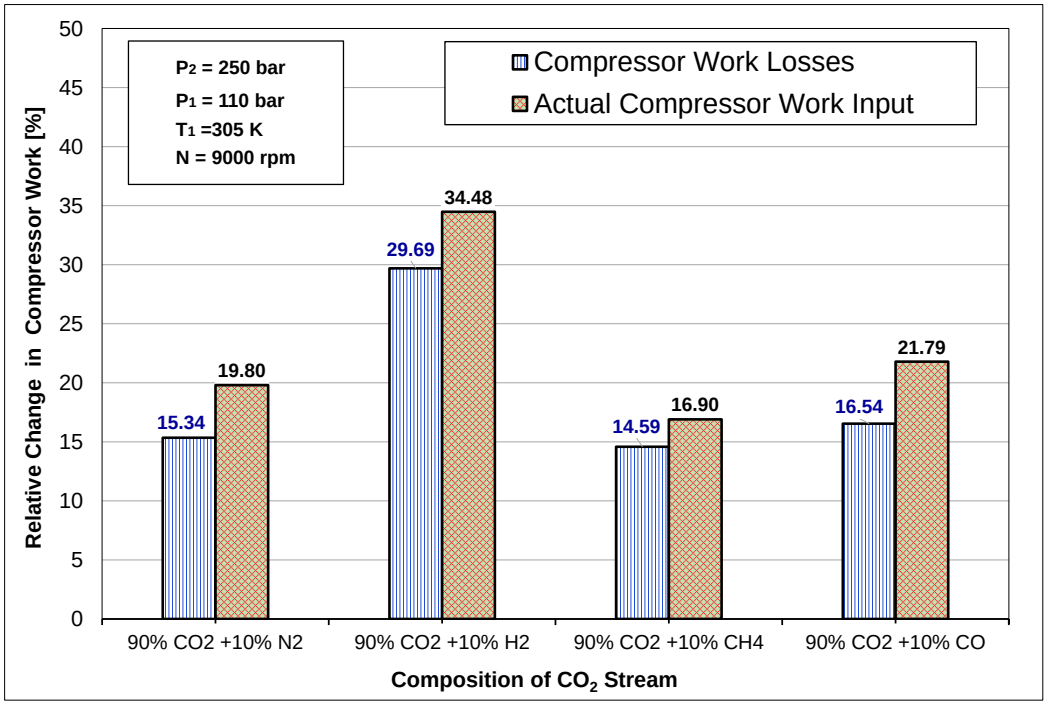

Fig.6.4 Effect of impeller size on work input and work losses for different CO_2 mixtures (P_2 =250 bar)

Just like in case 1, the largest compressor re-sizing effort and highest energy requirement (W_{INPUT}) needed to maintain 250 bar will occur when pure CO_2 is replaced with CO_2/H_2 stream as working fluid. In relative terms, at constant speed of 9000 rpm, the optimum diameter of the tip of the impeller's eye (d_o) will have to be increased by 6.86% while the optimum diameter of the outlet tip of the impeller (D_{IMP}) will increase by 16.52% in order to maintain the stipulated discharge pressure when the compressor shifts from handling pure CO_2 to CO_2/H_2 as shown in Fig.6.3. Consequently, the overall work input (W_{INPUT}) and energy losses ($\sum W_{losses}$) will increase by 34.48 % and 29.69%, respectively (see Fig. 6.4). If the same compressor running at the same speed were to shift from handling pure CO_2 to CO_2/CH_4 mixture, then d_o will have to increase by 3.55% and D_{IMP} will increase by 8.41% in order to maintain the stipulated discharge pressure of 250 bar. This compressor resizing effort translates to a 16.9% increase in the overall work input (W_{INPUT}) and a 14.59% increase in ($\sum W_{losses}$).

On the whole, cases 1 and 2 confirm that for a given shaft speed and discharge pressure, compressor size (in terms of d_o and D_{IMP}) is directly proportional to work input and energy losses. This can be attributed to fluid properties that characterize the internal flow behaviour of the working fluid such as density and compressibility. Fluid density is in an inverse relationship with compressor size, work input and energy losses while fluid compressibility is in a direct relationship with them. At supercritical conditions, all fluid properties are extremely sensitive to changes in the chemical composition of the working fluid. This is clearly demonstrated by the disparities in results obtained for the CO_2/H_2 mixture compared to those obtained for the CO_2/CH_4 mixture (see Figs. 6.1 to 6.4).

6.1.3 Case 3 – Comparing Impeller Resizing and Impeller Speed Increment for Discharge Pressure of 202 bar

The parametric analysis conducted in section 5.2.2 using the model's first algorithm demonstrated the oft-repeated assertion in this paper that compressor consumes less energy (W_{INPUT}) when the discharge pressure (P_2) is raised by enlarging the size of the impeller while shaft speed remains constant compared to the reverse (i.e. increasing shaft speed while impeller size remains unchanged).

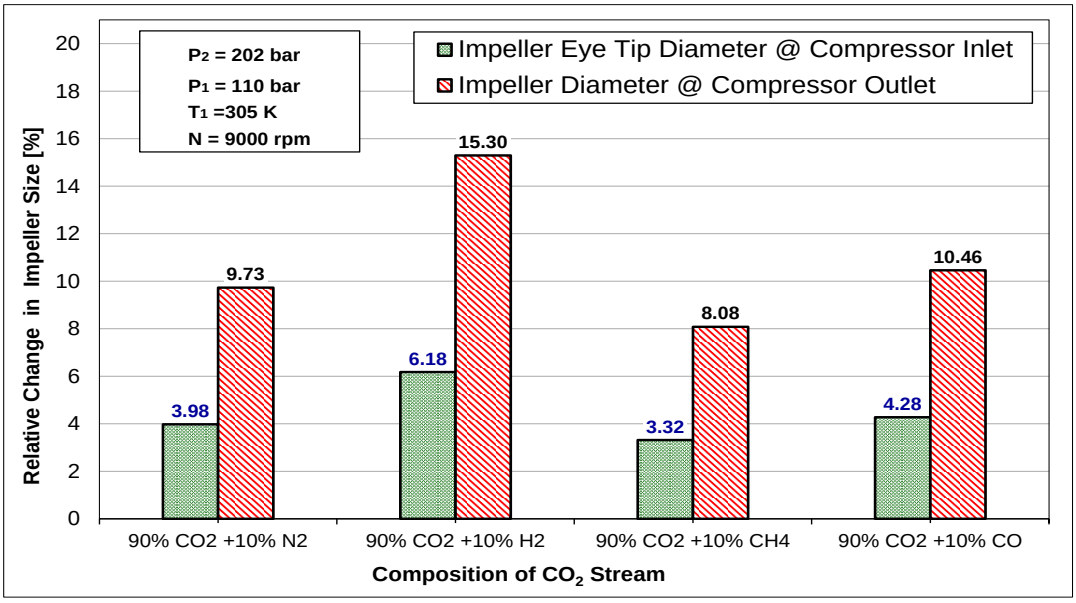

Fig.6.5 Relative change in impeller size for different CO_2 mixtures (P_2 =202 bar)

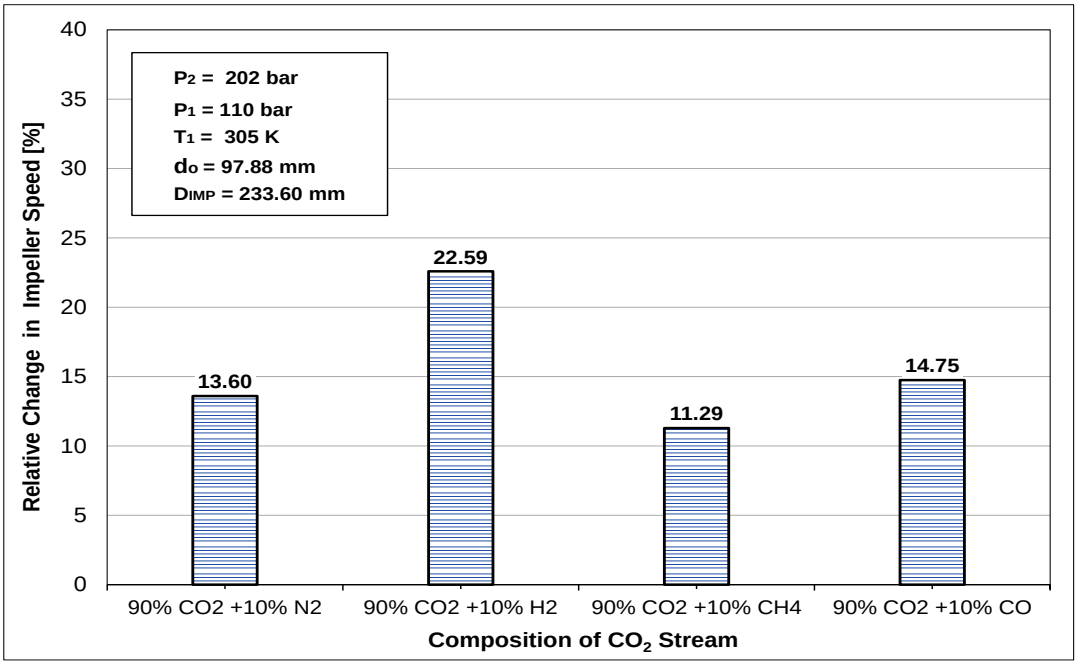

Fig.6.6 Relative change in impeller speed for different CO_2 mixtures (P_2 =202 bar)

In this section, that assertion is reconfirmed through the application of the model's second algorithm to an optimization problem-solving exercise (i.e. case 3) in which both shaft speed increment and impeller re-sizing as alternative methods of raising P_2 are evaluated and compared to each other in order to decide which method is the optimal solution.

For the purposes of fulfilling the aims of Case 3, the quasi-D model calculates an additional parameter— relative change in speed (δN) for a particular impeller size when working fluid shifts from pure CO_2 to an impure CO_2 mixture:

$$\delta N = \frac{(N)_{CO2\_MIX} - (N)_{CO2\_PURE}}{(N)_{CO2\_PURE}} \cdot 100\% \qquad (6.5)$$

As shown in Fig.6.5, in order to generate a standard discharge pressure of 202 bar at a constant speed (N) of 9000 rpm, the optimum diameter of the tip of the impeller's eye (d_o) will have to be increased by 6.18% while the optimum diameter of the outlet tip of the impeller (D_{IMP}) will increase by 15.30% when compressor shifts from handling pure CO_2 to CO_2/H_2 mixture. As shown in Fig. 6.7, this impeller re-sizing effort will result in a 31.47% increase in the overall work input (W_{INPUT}). Alternatively, if the impeller size was left unchanged at d_o = 97.88 mm and D_{IMP} = 233.60 mm as shown in Fig. 6.6, the shaft speed (N) will have to be increased by 22.59% to generate the stipulated discharge pressure of 202 bar when the working fluid shifts from pure CO_2 to CO_2/H_2 mixture. This speed increment will result in a whopping 45.15% increase in the overall work input (W_{INPUT}) as shown in Fig.6.7.

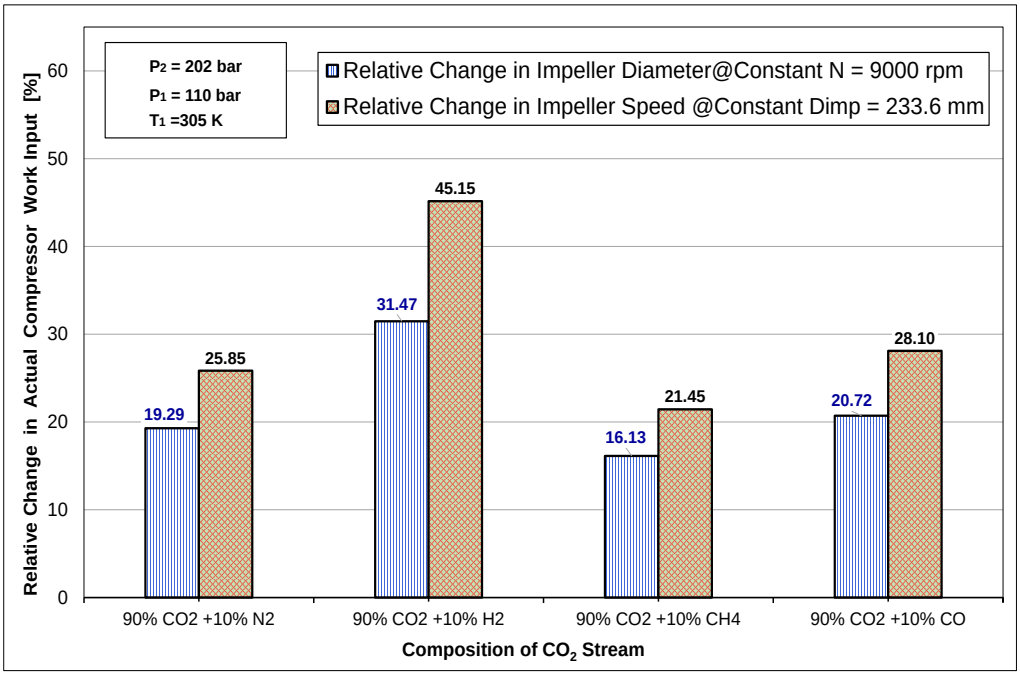

Fig.6.7 Effect of impeller size versus effect of impeller speed on compressor work input for different CO_2 streams (P_2 = 202 bar)

The same trends in relative energy change were observed for the remaining binary CO_2 mixtures, thus reconfirming that impeller re-sizing while shaft speed remains

constant is the optimal method of raising P_2 because it requires less W_{INPUT} compared to the alternative (i.e. increasing shaft speed while impeller size remains unchanged).

6.2 CONCLUDING REMARKS

In this chapter, the quasi-dimensional model was demonstrated as a tool for appropriate sizing of centrifugal machines compressing supercritical CO_2 mixtures of various compositions. The demonstration involved the application of the quasi-D model in solving three optimization problems, namely Cases 1, 2 and 3.

By analysing simulation results from all three cases, it was found that impeller re-sizing is a more efficient method of raising discharge pressure than shaft speed increment because the latter incurs more energy losses than the former. Compressor re-sizing correlates with overall work input requirement, which in turn is directly proportional to fluid compressibility and inversely proportional to fluid density as explained in chapter 5. This means that the type and concentration of the impurity in the supercritical CO_2 stream plays a big role in deciding the optimum size of the compressor which will deliver the best attainable efficiency per power utilized and reduce energy penalty and operating costs of a CO_2 transport pipeline network.

CHAPTER 7
CONCLUSIONS

This PhD thesis presents the development and application of an algorithmic tool for optimal sizing of centrifugal compressors and booster pumps as a direct method of significantly curbing the amount of energy consumed during the operation of pipeline networks transporting pure and impure supercritical CO_2.

Literature survey revealed that the vast majority of researchers approach the issue of curbing the overall energy consumption in pipeline networks by focussing on optimal sizing of pipelines and ensuring that impurities within anthropogenic CO_2 mixtures under transportation are kept very low in order to keep their fluid properties as close as possible to that of pure CO_2.

Both approaches advocated by most researchers in open literature have an ***indirect*** effect on the power requirement of compressors and booster pumps in the pipeline. Optimal pipe sizing reduces the pressure drop incurred across the length of the pipeline, which in turn reduces the amount of input power required by compressors and booster pumps compensating for that pressure drop — a necessary task both machines must perform to forestall the transformation of CO_2 stream from supercritical fluid to a gas-liquid two-phase fluid. Purification of impure CO_2 mixtures increases fluid density while simultaneously reducing critical point, fluid compressibility and viscosity, which in turn reduces the amount of energy consumed by compressors and booster pumps.

These ***indirect methods*** of reducing energy consumption in compressors and booster pumps have almost no effect on the actual fluid compression process. They do not address the subject of improving the performance of compressors and pumps themselves, the largest contributors to the overall OPEX of any supercritical CO_2 pipeline system. Moreover, these ***indirect*** **methods** have disadvantages, which limit their effectiveness as means of reducing either capital or operating costs associated with a supercritical CO_2 transport pipeline.

Optimal sizing of pipelines may reduce OPEX, but it comes at the price of CAPEX. If that optimal sizing involves an increase in pipe diameter then the pipe walls will have to be made thicker to withstand the increased mechanical strain of the pressurized

working fluid and prevent pipeline fracture. CAPEX rises linearly with pipe diameter and pipe wall thickness. In some cases, there might be a need to use expensive superior materials in pipe construction to forestall fracture, further raising CAPEX.

Transporting pure CO_2 instead of anthropogenic CO_2 mixtures— sourced directly from power stations and other process industries— will indeed reduce the input power requirement for compressors and booster pumps in the pipeline network, but it will come at a hefty cost. Purification of anthropogenic CO_2 mixtures in capture facilities is an energy-intensive process that will drive up the operating costs of running those facilities—hence, attenuating or even offsetting the benefits of reducing the input power requirements for both machines by swapping impure CO_2 with pure CO_2 in the pipeline network.

A more effective method of curbing overall energy consumption in transport pipeline networks is to tolerate various types and amounts of impurities present in the anthropogenic CO_2 mixture and focus on enhancing the energy efficiency of compressors and booster pumps by ***direct*** improvement of their performance. This will eliminate energy and financial waste associated with increasing the purity of anthropogenic CO_2 mixtures. As noted in Chapters 2 and 4, a small, but growing number of CCS researchers have begun to study this ***direct method*** because greater savings in energy costs can be made in the pipeline transportation of pure and impure CO_2 compared to the two ***indirect methods*** widely advocated by most CCS researchers.

The small number of published research studies focussed on applying this ***direct method*** provide information on various fluid compression systems capable of achieving the best savings on energy and operating costs for a given composition of anthropogenic CO_2 mixture being pressurized beyond its critical point. The information, while useful, is general and lacking in practical details.

Before any of the energy-saving compression strategies proposed by other researchers to become practical reality, the actual physical equipment (e.g. centrifugal machines; intercoolers; tubing) involved must be sized appropriately to minimize power losses and guarantee their optimal performance when installed in CO_2 pipeline networks. No other researcher in CCS field have published work on a

systematic method for the selection and sizing of either centrifugal compressors or booster pumps installed in pipeline networks transporting pure and impure supercritical CO_2. Existing compressor performance maps, traditionally used for sizing centrifugal machines, are unsuitable in the CCS context, as none account for the peculiar internal flow behaviour exhibited by CO_2 mixtures at supercritical conditions. This represents a significant gap in knowledge, which is tackled in this PhD thesis through the development of an effective algorithmic tool for the performance evaluation and optimal sizing of centrifugal compressor and booster pumps handling supercritical CO_2 streams of varying purity.

In Chapter 4, a highly mechanistic quasi-dimensional mathematical model combining the complex geometry, internal fluid flow and working processes of a single-stage centrifugal machine was developed from “first principles”. The proposed quasi-D model eschews the common practice among many researchers of using empirical coefficients or correlations to account for energy losses within compressor. An original mechanistic sub-model describing various types of energy losses (i.e. disk friction, leakage and hydraulic losses) was developed separately and then merged into the larger quasi-dimensional model. Apart from accounting for various energy losses, the mechanistic sub-model also captures some of the 3-D internal fluid flow effects neglected in the larger quasi-dimensional model. The sub-model accomplishes this through the inclusion of equations describing the overall shape of semi-shrouded impeller, the curved and convergent geometry of impeller blade channels and the clearance between the periphery of the rotating impeller and the interior walls of the stationary compressor housing. Interactions between the supercritical working fluid, the rotating surface of the impeller and the stationary interior walls of the compressor housing are also captured in that sub-model.

Prior to the development of the quasi-D model, a comprehensive study of seven equations of state was carried out in Chapter 3 in order to select those most reliable for calculating the anomalous thermophysical properties of the various supercritical CO_2 mixtures. Two highly accurate equations of state—Span and Wagner (SW) and GERG-2008—were selected and integrated into the computer algorithms of the proposed quasi-dimensional model. Although these equations of state play a limited role in calculations performed with the quasi-D model, they are necessary to ensure

that the peculiar non-linear real fluid effects of supercritical CO_2 and its mixtures are accounted for.

The newly developed quasi-D model was successfully validated with experimental data available in open literature and then applied as effective tools for:

- Evaluating the performance of a centrifugal machine of a given size handling pure CO_2 and various CO_2 mixtures above the critical point under different operating conditions
- Demonstrating that optimal sizing of centrifugal machines minimizes energy losses, thereby reducing the actual work input required to operate them. The vital role played by different supercritical CO_2 mixtures in determining the appropriate compressor size was also examined

The application of quasi-dimensional model in the performance evaluation of a supercritical CO_2 centrifugal machine in Chapter 5 yielded the following findings:

- Overall performance of centrifugal machines quantified in terms of actual power requirement, isentropic efficiency and pressure ratio is strongly dependent on impeller size, shaft speed, mass flow rate and chemical composition of the supercritical CO_2 stream. However, this finding is based on a general “broad picture” analysis of the simulation results from the model. An in-depth analysis of those simulation results show that:
    - Compressor performance is a corollary of the internal flow behaviour of the pure and impure supercritical CO_2 stream which is characterized by changes in its thermophysical properties with respect to chemical composition, pressure and temperature
    - Changes in the thermophysical properties of a given supercritical CO_2 stream (pure or impure) occur as it travels through the flow channels located between stationary and rotating parts of the centrifugal machine. These changes in thermophysical properties are dependent on local pressure and temperature changes within the internal flow channels, which in turn are dependent on

impeller size and speed. So in effect, the thermophysical properties of a given supercritical CO_2 stream are secondary functions of compressor size and speed. In other words, density, specific enthalpy, viscosity and compressibility are not only highly sensitive the chemical composition of the working fluid. They are also highly sensitive to changes in shaft speed and impeller size. This reaffirms the broad assertion that overall compressor performance is dependent on shaft speed, impeller size and composition of the working fluid.

- The parametric analysis in section 5.2.2 showed that for a given supercritical CO_2 stream, a compressor consume less energy (W_{INPUT}) when the discharge pressure (P_2) is raised by enlarging the size of the impeller while shaft speed remains constant compared to the reverse (i.e. increasing shaft speed while impeller size remains unchanged). This particular phenomenon can be directly attributed to the sensitivity of the internal flow behaviour of CO_2 to changes in impeller size and shaft speed since these parameters respectively determine the total flow area of the compressor's internal flow channels and the local velocity of the supercritical CO_2 stream travelling within each channel.

The above-mentioned parametric analysis established that the best procedure for raising discharge pressure (or pressure ratio) while simultaneously keeping energy losses in a compressor as low as possible is altering impeller size while keeping shaft speed unchanged. As demonstrated in Chapter 6, the quasi-dimensional model successfully applies that particular procedure in the optimal sizing of centrifugal machines handling supercritical CO_2 mixtures of various compositions.

CHAPTER 8

RECOMMENDATIONS FOR FUTURE WORK

As mentioned previously, the scope of this PhD project is limited to studying the existing design and operation of generic centrifugal machines and then developing an algorithmic tool for specific application to compressors and booster pumps handling highly unconventional working fluids such as supercritical CO_2 and its mixtures.

This algorithmic tool has two purposes:

1. An in-depth performance evaluation of centrifugal compressors to gain knowledge not available in previous research studies on supercritical CO_2 pipeline transport in the CCS context

2. A systematic procedure for sizing and selection of commercially available ready-to-use centrifugal compressors to ensure that only machines with the best attainable efficiency per power utilized are installed in pipeline networks transporting a particular supercritical CO_2 mixture

Outside the limited scope of this PhD project is the application of this algorithmic tool in the design of a new set of bespoke centrifugal machines compatible with the peculiar flow behaviour of supercritical CO_2 in pure and impure forms. Also outside the scope of the PhD project is the performance analysis and rightsizing of multistage centrifugal compressors handling different supercritical CO_2 mixtures.

Having identified what was not covered in the limited scope of this PhD project, two recommendations for future work were made.

8.1 PERFORMANCE ANALYSIS AND OPTIMAL SIZING OF SUPERCRITICAL CARBON DIOXIDE MULTISTAGE CENTRIFUGAL COMPRESSORS

In accordance with the scope of the PhD project, the quasi-dimensional model developed is applicable to single-stage centrifugal compressors with inlet (suction) pressures already near or above critical pressure of CO_2 and operate at pressure ratios of up to 4:1 limit. This makes the simulated compressor performance analysis and compressor sizing work presented in this thesis more practical and directly applicable only to centrifugal “recompression” compressors (i.e. single-stage booster

pumps) installed at various repressurization points along the length of a pipeline to ensure that pure or impure CO_2 stream remains in supercritical phase and at a predetermined target pressure.

Besides single-stage booster pumps, every supercritical CO_2 pipeline network contain multistage compressors, which is necessary for converting pure or impure CO_2 from its normal gaseous state to supercritical state prior to transportation by pipeline. The conversion of gaseous CO_2 to a supercritical fluid involves compression from an initial pressure of 1.01 bar to final pressures of 80–100 bar. If high concentrations of certain impurities (e.g. H_2 and CO) are present in the CO_2 stream, final pressures of 150 bar and above may be required to convert impure CO_2 from a gaseous mixture to supercritical fluid. The input energy required by multistage compressors to facilitate this hundred and fifty-fold increase in pressure will be incredibly high and usually dwarfs energy consumed by individual single-stage booster pumps.

Given their overwhelming contribution to the overall energy costs of supercritical CO_2 pipeline networks, it is highly recommended that the compressor performance analysis and compressor sizing methodology presented in this thesis be applied to intercooled multistage centrifugal compressors. This is important considering that currently, there are no systematic method in existence for rightsizing multistage centrifugal compressors handling supercritical CO_2 mixtures. Similarly, there are no comprehensive studies focused on investigating the individual and combined effects of rotor shaft speed; impeller size; number of compression stages and chemical composition of different CO_2 mixtures upon the overall performance of a multistage compressor operating at supercritical conditions. These significant gaps in knowledge create opportunities for future research work.

A prerequisite for the fulfilment of this recommended future research work would be the extension of the quasi-dimensional model to incorporate the complex geometry, internal fluid flow and non-linear ***transcritical*** working processes of an intercooled multistage centrifugal compressor. The newly extended model should also be capable of accurately simulating heat transfer within each intercooler and energy losses occurring across all compression stages of the centrifugal machine.

8.2 DESIGN STRATEGY FOR BESPOKE CENTRIFUGAL MACHINES IN SUPERCRITICAL CARBON DIOXIDE TRANSPORT PIPELINES

Existing designs of centrifugal machines are best suited for handling conventional working fluids such as air, natural gas, refrigerants and CO_2 under subcritical conditions. As mentioned in section 4.1.3.2.3, when applied to unconventional working fluids such as supercritical CO_2 and its binary mixtures, the performance of these centrifugal machines are adversely affected by:

- Erratic internal flow behaviour, which may include large density fluctuations resulting in flow stability problems that do not exist in centrifugal compressors handling conventional working fluids

- Large specific enthalpies and fluid compressibility values resulting in aerodynamic/hydraulic losses that is higher than is usually expected in compressors handling conventional working fluids

- High density and low viscosity values result in Reynold Numbers that are two orders of magnitude larger than in conventional centrifugal compressor applications. Larger Reynolds Numbers translates to higher disk friction and leakage losses

The degradation in performance encountered by conventionally designed centrifugal compressors handling supercritical CO_2 can be mitigated through compressor sizing methodology proposed in this PhD thesis.

Generally, compressor sizing is the application of selection criteria to a family of identically designed, but differentially sized ready-made centrifugal compressors. The proposed compressor sizing methodology executed with the quasi-D model narrowly guides an engineer in choosing from within an existing design, a centrifugal machine size capable of running with the lowest power losses possible considering the composition of the working fluid and operating conditions as selection criteria.

In other words, compressor sizing guarantees that the best performance attainable can be extracted from an existing centrifugal machine design. The procedures of compressor sizing does not facilitate the alteration of existing centrifugal machine designs for the purposes of obtaining extra improvements in performance.

Maximum possible improvements in the compressor performance is achievable only through the design of new bespoke centrifugal machines compatible with the peculiar flow behaviour of supercritical CO_2 in pure and impure forms. The development of a comprehensive design strategy is recommended as future research work.

The first algorithm of the computer programme for the quasi-dimensional model can be used an effective tool in the preliminary phase of the comprehensive design strategy. Guided by input data on the anomalous fluid properties of a given pure or impure supercritical CO_2 stream, the first algorithm is capable of exploring different ways in which the shape and dimensions of impeller and diffuser can be altered to maximize isentropic efficiency and minimize of power losses; vastly improving the centrifugal compressor performance.

For the final phase of the comprehensive design strategy, a 3D model of a centrifugal compressor handling supercritical CO_2 will be needed. Therefore, it is recommended that further research be conducted into the possibility of developing new 3D CFD models of a supercritical CO_2 compressor that does not suffer from the solution convergence problems discussed in Chapter 4 of this thesis.

REFERENCE LIST

Adams, R., 2011. "CO_2 capture and pumping". Proceedings of the Twenty-Seventh International Pump User Symposium, Houston, Texas, USA.

Aimoli, C.G., Maginn, E.J. and Abreu, C.R., 2014. "Thermodynamic properties of supercritical mixtures of carbon dioxide and methane: a molecular simulation study". Journal of Chemical & Engineering Data, Vol.59, No.10, pp.3041-3054.

Almasi, A., 2011. "Top tips for choosing a centrifugal compressor". Plant Services. Available at: https://www.plantservices.com/articles/2011/06-top-tips-for-choosing-a-centrifugal-compressor/

Al-Siyabi, I., 2013. "Effect of impurities on CO_2 stream properties". ROS Repository, Heriot-Watt University, Scotland, UK, pp.1-182.

Aritomi, M., Ishizuka T., Muto, Y and Tsuzuki, N., 2011. "Performance test results of a supercritical CO_2 compressor used in a new gas turbine generating system". Journal of Power and Energy Systems, Vol.5, No.1, pp. 45-59

Aungier, R.H., 2000. Centrifugal Compressors: A strategy for aerodynamic design and analyses. The American Society of Mechanical Engineers (ASME) Press, New York, USA. ISBN 0-7918-0093-8; 2000.

Aursand, P., Hammer, M., Munkejord, Wilhelmsen, Ø., 2013. "Pipeline transport of CO_2 mixtures: models for transient simulation". International Journal of Greenhouse Gas Control, Vol. 15, pp. 174-185

Aursand, E., Dørum, C., Hammer, M., Morin, A., Munkejord, S.T. and Nordhagen, H.O., 2014. "CO_2 pipeline integrity: comparison of a coupled fluid-structure model and uncoupled two-curve methods". Energy Procedia, Vol. 51, pp.382-391

Aursand, E., Aursand, P., Hammer, M. and Lund, H., 2016. "The influence of CO_2 mixture composition and equations of state on simulations of transient pipeline decompression". International Journal of Greenhouse Gas Control, Vol. 54, pp.599-609.

Avallone, E.A. and Baumeister, T., 1986. Marks' Standard Handbook for Mechanical Engineers. McGraw-Hill Company., New York, USA

Baltadjiev, N.D., Lettieri, C. and Spakovszky, Z.S., 2015. "An investigation of real gas effects in supercritical CO_2 centrifugal compressors". Journal of Turbomachinery, Vol. 137, Issue No. 9. DOI: 10.1115/1.4029616

Bergamini, L., del Vescovo, C., Milone,F., 2011. "Centrifugal pumps for CO_2 applications". Proceedings of the Twenty-Seventh International Pump User Symposium, Houston, Texas.

Boyce, M.P., 1972. "New developments in compressor aerodynamics". Proceedings of the First Turbomachinery Symposium, Texas, USA, pp.79-89

Boyce, M.P., 2012. Gas Turbine Engineering Handbook (4th Edition). Butterworth-Heinemann, UK. ISBN 978-0-12-383842-1. DOI: 10.1016/C2009-0-64242-2

Brown, R.N., 1997. Compressors: Selection and Sizing (2nd Edition). Gulf Professional Publishing, Butterworth-Heinemann, UK. ISBN 0-88415-164-6

Brown, S., Mahgerefteh, H., Martynov, S., Sundara, V. and MacDowell, N., 2015. "A multi-source flow model for CCS pipeline transport networks". International Journal of Greenhouse Gas Control, Vol.43, pp.108-114

Brun, K., and Kurz, R., 2019. Compression Machinery for Oil and Gas. Gulf Professional Publishing, UK. ISBN 978-0-12-814683-5

Brunsting, S., de Best-Waldhober, M., Feenstra, C.Y. and Mikunda, T., 2011. "Stakeholder participation practices and onshore CCS: lessons from the Dutch CCS Case Barendrecht". Energy Procedia, Vol. 4, pp.6376–6383

Cui, M. and Sauls, J., 2008: "Investigation of suction process of a large R134a scroll compressor". IMechE Journal of Power and Energy, Vol. 222, Part A. DOI: 10.1243/09576509JPE455

Chaczykowski, M. and Osiadacz, A. J., 2012. “Dynamic simulation of pipelines containing dense phase/supercritical CO_2-rich mixtures for carbon capture and storage”. International Journal of Greenhouse Gas Control, Vol. 9, pp. 446-456.

Cho, J., Choi, M., Baik, Y.J., Lee, G., Ra, H.S., Kim, B. and Kim, M., 2016. “Development of the turbomachinery for the supercritical carbon dioxide power cycle”. International Journal of Energy Research, Vol. 40, No.5, pp.587-599. DOI: 10.1002/er.3453

Collie, G.J., Nazeri, M., Jahanbakhsh, A., Lin, C.W. and Maroto-Valer, M.M., 2017. “Review of flowmeters for carbon dioxide transport in CCS applications”. Greenhouse Gases: Science and Technology, Vol.7, No.1, pp.10–28.

Cooper, P., Schiavello B., de Marolles C., de Salis, J., Prang, A.J. and Broussard D.H., 1996: “Tutorial on gas-liquid pumping”. 13th international pump users’ symposium, Texas A&M University, pp.159-173

Cosham, A., 2012. “The saturation pressure and design of dense-phase CO_2 Pipelines”. Journal of Pipeline Engineering, Vol.11, No. 3, 2012, pp. 213-228

Cooper, R., 2012. “National Grid's COOLTRANS research programme”. Journal of Pipeline Engineering, Vol.11, No. 3, pp.155-172

Crane Company, 1982. “Flow of Fluids through Valves, Fittings, and Pipe”. Technical Paper No. 410 M.

Davis, H.M., 1972. “Centrifugal compressor operation and maintenance”. Proceedings of the 1st Turbomachinery Symposium, Texas A&M University, USA. DOI: 10.21423/R1468M

Demetriades, T.A., Drage, T.C. and Graham, R.C., 2013. “Developing a new equation of state for carbon capture and storage pipeline transport”. Journal of Process Mechanical Engineering, Volume 227, Issue No 2, pp 117-124

Demetriades,T.A. and Graham, R.S., 2016. “A new equation of state for CCS pipeline transport: calibration of mixing rules for binary mixtures of CO_2 with N_2, O_2 and H_2”. Journal of Chemical Thermodynamics, Vol. 93, pp. 294-304

Demofonti, G. and Spinelli, C.M., 2011. “Technical challenges facing the transport of anthropogenic CO_2 by pipeline for carbon capture and storage purposes”. 6th Pipeline Technology Conference

Diamantonis, N.I., Boulougouris, G.C., Mansoor, E., Tsangaris, D.M. and Economou, I.G., 2013a. “Evaluation of cubic, SAFT, and PC-SAFT equations of state for the vapour–liquid equilibrium modelling of CO_2 mixtures with other gases”. Industrial & Engineering Chemistry Research, Vol. 52, Issue No.10, pp.3933-3942

Diamantonis, N.I., Boulougouris, G.C., Tsangaris, D.M., El Kadi, M.J., Saadawi, H., Negahban, S. and Economou, I.G., 2013b. “Thermodynamic and transport property models for carbon capture and sequestration (CCS) processes with emphasis on CO_2 transport”. Chemical Engineering Research and Design, Vol. 91, No.10, pp.1793-1806.

Dillon, D.J., Panesar, R.S., Wall, R.A., Allam, R.J., White, V., Gibbins, J. and Haines, M.R., 2004. “Oxy-combustion processes for CO_2 capture from advanced supercritical PF and NGCC power plant”. Proceedings of the 7th International Conference on Greenhouse Gas Technologies, Vancouver, Canada

Dixon, S.L., 1998. Fluid Mechanics, Thermodynamics of Turbomachinery (4th Edition). Butterworth-Heinemann.

Douglas, J.F., Gasiorek, J.M., Swaffield, J.A. and Jack, L.B., 2005. Fluid Mechanics (5th Edition). Pearson Education Limited, UK

Eastop, T. D., and McConkey, A., 1993. Applied Thermodynamics for Engineering Technologists (5th Edition). Longman Group, London, UK

Eickhoff, C., Neele, F., Hammer, M., DiBiagio, M., Hofstee, C., Koenen, M., Fischer, S., Isaenko, A., Brown, A. and Kovacs, T., 2014. “IMPACTS: economic trade-offs for CO_2 impurity specification”. Energy Procedia, Vol. 63, pp. 7379 – 7388

Fenghour, A., Wakeham, W. A. and Vesovic, V., 1998. “The viscosity of carbon dioxide”. Journal of Physical and Chemical Reference Data, Vol. 27, No.1, pp.31-44.

Fleming J.S, Tang Y and Cook G, 1998: “The twin helical screw compressor. Part II- a mathematical model of the working process”. IMechE Journal of Process Mechanical Engineering, Vol. 212, Part C.

Gernert, J., and Span, R., 2010. “EOS-CG: An accurate property model for application in CCS processes”. Proceedings of Asian Thermophysical. Properties Conference, Beijing, China.

Gernert, J. and Span, R., 2016. “EOS–CG: A Helmholtz energy mixture model for humid gases and CCS mixtures”. Journal of Chemical Thermodynamics, Vol.93, pp.274-293.

Goos, E., Riedel, U., Zhao, L. and Blum, L., 2011. “Phase diagrams of CO_2 and CO_2-N_2 gas mixtures and their application in compression processes”. Energy Procedia, Vol.4, pp. 3778-3785

Gorla, R.S. and Khan, A.A., 2003. Turbomachinery: Design and Theory (1st Edition). Marcel Dekker Incorporated, New York, USA

Gresh, T.M., 2001. Compressor Performance: Aerodynamics for the User (2nd Edition). Butterworth-Heinemann, USA. ISBN 0-75-067342-7

Hashemi, E. and Karimi, M., 2009. “Improvement of centrifugal compressor performance prediction with the modified one dimensional analysis”. International Conference on Compressors and their Systems, London, United Kingdom

Hanlon, P.C., 2001: Compressor Handbook. McGraw Hill Co, USA. ISBN 0-07-026005-2

Holloway, S., Horton, W.T., Groll, E.A., Sherman, D. and Albertin, M., 2010. “Experimental performance of a prototype carbon dioxide compressor”. International Compressor Engineering Conference, Purdue, USA.

IEA GHG, 2005. “Weyburn CO_2 monitoring and storage project”. IEA Greenhouse Gas Research and Development Programme Report. Available at: http://www.ieaghg.org/docs/general_publications/weyburn.pdf

IEA GHG, 2006. "CO_2 capture as a factor in power station investment decisions". IEA Greenhouse Gas Research and Development Programme Report. Available at: http://www.ieaghg.org/docs/overviews/2006-8.pdf

IEA GHG, 2009. "CO_2 storage in depleted gas fields". Report Number 2009/01. IEA Greenhouse Gas Research and Development Programme. Available at: http://hub.globalccsinstitute.com/sites/default/files/publications/95786/co2-storage-depleted-gas-fields.pdf

IEA, 2013. "Technological Roadmap -Carbon Capture and Storage", Paris, France

IEA GHG, 2016. "Impact of CO_2 impurity on CO_2 compression, liquefaction and transportation". Report Number 2016/01. IEA Greenhouse Gas Research and Development Programme. Available at: https://ieaghg.org/docs/General_Docs/Reports/2016-01.pdf

Imre, A.R. and Tiselj, I., 2012. "Reduction of fluid property errors of various thermohydraulic codes for supercritical water systems". Kerntechnik, Vol. 77, No.1, pp.18-24.

Imre, A.R., Ramboz, C., Deiters, U.K. and Kraska, T., 2015. "Anomalous fluid properties of carbon dioxide in the supercritical region: application to geological CO2 storage and related hazards". Environmental Earth Sciences, Vol. 73, No.8, pp. 4373-4384.

Ingram, G., 2009. Basic Concepts in Turbomachinery (1st Edition). Ventus Publishing ApS. ISBN: 978-87-7681-435-9

Ishmael, M.P., Lukawski, M.Z. and Tester, J.W., 2016. "Isobaric heat capacity (C_p) measurements of supercritical fluids using flow calorimetry: equipment design and experimental validation with carbon dioxide, methanol, and carbon dioxide-methanol mixtures". The Journal of Supercritical Fluids, Vol.117, pp.72-79.

Islam, A.W. and Carlson, E.S., 2012. "Application of SAFT equation for CO_2+ H_2O phase equilibrium calculations over a wide temperature and pressure range". Fluid Phase Equilibria, Vol. 321, pp.17-24.

Jiang, W., Khan, J. and Dougal, R.A., 2006. “Dynamic centrifugal compressor model for system simulation”. Journal of Power Sources, Vol. 158, Issue No.2, pp.1333-1343

Jung, W. and Nicot, J.P, 2010. “Impurities in CO_2-rich mixtures impact CO_2 pipeline design: implications for calculating CO_2 transport capacity”. SPE International Conference on CO_2 Capture, Storage and Utilization, New Orleans, Louisiana, USA

Ke, J., Suleiman, N., Sanchez-Vicente, Y., Murphy, T.S., Rodriguez, J., Ramos, A., Poliakoff, M. and George, M.W., 2017. “The phase equilibrium and density studies of the ternary mixtures of CO_2+Ar+N2 and CO_2+Ar+H2, systems relevance to CCS technology”. International Journal of Greenhouse Gas Control, Vol. 56, pp.55-66.

Kerth, J., Pacheco, J., Moore, J., Allison, T. and Evans, N., 2015. “Development and testing of multi-stage internally cooled centrifugal compressor”. Proceedings of the 44th Turbomachinery Symposium, Houston, Texas, USA.

Kim, S.G., Lee, J., Ahn, Y., Lee, J.I., Addad, Y. and Ko, B., 2014. “CFD investigation of a centrifugal compressor derived from pump technology for supercritical carbon dioxide as a working fluid”. The Journal of Supercritical Fluids, Vol. 86, pp.160-171.

Knoope, M.M.J., Ramírez, A. and Faaij, A.P.C., 2013. “A state-of-the-art review of techno-economic models predicting the costs of CO_2 pipeline transport”. International Journal of Greenhouse Gas Control, Vol.16, pp.241-270.

Kovacevic, A., Mujic, E., Stosic, N. and Smith I. K., 2007: “An integrated model for the performance calculation of screw machines”. International Conference on Compressors and Their Systems, London, UK. pp. 203-212

Kuijper, I.M., 2011. “Public acceptance challenges for onshore CO_2 storage in Barendrecht”. Energy Procedia, Vol. 4, pp.6226-6233

Kunz, O., Klimeck, R., Wagner, W., Jaeschke, M., 2007. “The GERG-2004 wide-range equation of state for natural gases and other mixtures”. GERG TM15, 2007; Fortschr.-Ber. VDI, Reihe 6, Nr. 557, VDI Verlag: Düsseldorf, Germany.

Kunz, O. and Wagner, W., 2012. “The GERG-2008 wide-range equation of state for natural gases and other mixtures: an expansion of GERG-2004”. Journal of chemical & engineering data, Vol.57, No.11, pp.3032-3091.

Lazic, T., Oko, E. and Wang, M., 2014. “Case study on CO_2 transport pipeline network design for Humber region in the UK”. Proceedings of IMechE Part E: Journal of Process Mechanical Engineering, Vol.228, Issue No.3, pp.210–225

Lemontzoglou, A., Pantoleontos, G., Asimakopoulou, A.G., Tsongidis, N.I. and Konstandopoulos, A.G., 2017. “Analysis of CO_2 transport including impurities for the optimization of point-to-point pipeline networks for integration into future solar fuel plants”. International Journal of Greenhouse Gas Control, Vol. 66, pp.10-24.

Lee, J., Kim, S.G., Cha, J.E., Lee, J.I., 2014. “Uncertainty on Performance Measurement of Supercritical CO_2 Compressor Operating Near Critical Point”. 4th International Symposium - Supercritical CO_2 Power Cycles, Pittsburgh, Pennsylvania

Lee, J., Baik, S., Cho, S.K., Cha, J.E., Lee, J.I., 2016. “Issues in performance measurement of CO_2 compressor near the critical point”. Applied Thermal Engineering, Vol.94, pp. 111-121

Li, H. and Yan, J., 2009a. “Impacts of equations of state (EoS) and impurities on the volume calculation of CO_2 mixtures in the applications of CO_2 capture and storage (CCS) processes”. Applied Energy, Vol. 86, pp. 2760–70

Li, H. and Yan, J., 2009b. “Evaluating cubic equations of state for calculation of vapour–liquid equilibrium of CO_2 and CO_2-mixtures for CO_2 capture and storage processes”. Applied Energy, Vol.86, No.6, pp.826-836.

Li, H., Jakobsen, J.P., Wilhelmsen, Ø. and Yan, J., 2011a. “PVTxy properties of CO_2 mixtures relevant for CO_2 capture, transport and storage: Review of available experimental data and theoretical models”. Applied Energy, Vol. 88, Issue No.11, pp.3567-3579.

Li, H., Wilhelmsen,Ø., Lv, Y., Yan, J., 2011b. “Viscosities, thermal conductivities and diffusion coefficients of CO_2 mixtures: review of experimental data and theoretical models”. International Journal of Greenhouse Gas Control, Vol.5, pp.1119 -1139

Liljemark, S., Arvidsson, K., McCann, M.T.P., Tummescheit, H. and Velut, S., 2011. “Dynamic simulation of a carbon dioxide transfer pipeline for analysis of normal operation and failure modes”. Energy Procedia, Vol. 4, pp. 3040-3047.

Lindeberg, E., Vuillaume, J.F. and Ghaderi, A., 2009. “Determination of the CO_2 storage capacity of the Utsira formation”. Energy Procedia, Vol.1, pp.2777-2784.

Luo, X., Wang, M., Oko, E. and Okezue, C., 2014. “Simulation-based techno-economic evaluation for optimal design of CO_2 transport pipeline network”. Applied Energy, Vol. 132, pp. 610–620.

Lurie, E.A., Van Slooten, P.R., Medic, G., Mulugeta, J.M., Holley, B.M., Feng, J., Sharma, O. and Ni, R., 2011. “Design of a high efficiency compact centrifugal compressor for rotorcraft applications”. American Helicopter Society 67th Annual Forum, Virginia Beach, Virginia, USA

Mahgerefteh, H., Brown, S. and Martynov, S., 2012a. “A study of the effects of friction, heat transfer, and stream impurities on the decompression behaviour in CO_2 pipelines”. Greenhouse Gases: Science and Technology, Vol. 2, No.5, pp.369-379

Mahgerefteh, H., Brown, S. and Denton, G., 2012b. “Modelling the impact of stream impurities on ductile fractures in CO_2 pipelines”. Chemical engineering science, Vol.74, pp. 200-210

Martynov, S.B., Daud, N.K., Mahgerefteh, H., Brown, S. and Porter, R.T.J., 2016. “Impact of stream impurities on compressor power requirements for CO_2 pipeline transportation”. International Journal of Greenhouse Gas Control, Vol.54, pp.652-661.

Martynov, S.B., Talemi, R.H., Brown, S. and Mahgerefteh, H., 2017. “Assessment of Fracture Propagation in Pipelines Transporting Impure CO_2 Streams”. Energy Procedia, Vol.114, pp. 6685-6697

Massey B.S. and Ward-Smith, J., 1998: Mechanics of Fluid (6th edition). Van Nostrand Reinhold International Co. Ltd

Mazzotti, M., Pini, R. and Storti, G., 2009. “Enhanced coalbed methane recovery”. The Journal of Supercritical Fluids, Vol. 47, Issue No.3, pp.619-627.

Mazzoccoli, M., Bosio, B. and Arato, E., 2012. “Analysis and comparison of equations-of-state with p-ρ-T experimental data for CO_2 and CO_2-mixture pipeline transport”. Energy Procedia, Vol. 23, pp.274-283.

Mazzoccoli, M., De Guido, G., Bosio, B., Arato, E. and Pellegrini, L. A., 2013. “CO_2-mixture properties for pipeline transportation in the CCS process”. Chemical Engineering Transactions, Vol. 32, pp. 1861-1866.

McCollum, D. L. and Ogden, J. M., 2006. “Techno-economic models for carbon dioxide compression, transport, and storage and correlations for estimating carbon dioxide density and viscosity”. Institute of Transportation Studies, University of California, Davis (UCD). Report No. UCD-ITS-RR-06-14. Available at: https://escholarship.org/uc/item/1zg00532

McCoy, S. and Rubin, E.S., 2008. “An engineering-economic model of pipeline transport of CO_2 with application to carbon capture and storage”. International Journal of Greenhouse Gas Control, Vol. 2, Issue No.2, pp. 219-229

Metz, B., O. Davidson, H. C. de Coninck, M. Loos and L. A. Meyer (eds.), 2005. “IPCC, 2005: IPCC Special Report on Carbon Dioxide Capture and Storage”. Prepared by Working Group III of the Intergovernmental Panel on Climate Change". Cambridge University Press, UK

Mobley, K.R., 2000. Fluid Power Dynamics. Butterworth-Heinemann. ISBN 0-1239-9628-7

Modekurti, S., Eslick, J., Omell, B., Bhattacharyya, D., Miller, D.C. and Zitney, S.E., 2017. Design, dynamic modelling, and control of a multistage CO_2 compression system. International Journal of Greenhouse Gas Control, Vol. 62, pp.31-45.

Mohitpour, M., Seevam, P., Botros, K.K., Rothwell, B and Ennis, C., 2011. “Pipeline transportation of carbon dioxide containing impurities”. ASME, New York, USA

Moore, J.J and Nored, M.G., 2008. “Novel concepts for the compression of large volumes of carbon dioxide”. ASME Turbo Expo 2008: Power for Land, Sea, and Air, Vol.7: Education; Industrial and Cogeneration; Marine; Oil and Gas Applications, pp.645-653. DOI: 10.1115/GT2008-50924.

Moore, J.J., Lerche, A., Delgado, H., Allison, T. and Pacheco, J., 2011. “Development of advanced centrifugal compressors and pumps for carbon capture and sequestration applications”. Proceedings of the 40th Turbomachinery Symposium, Houston, Texas, USA.

Monaghan, R. and Brennan, G., 2006. “Carbon dioxide capture and storage in Ireland: costs and benefits and future potential”. Sustainable Energy Ireland.

Monge B., Savill, M., Sánchez, D., Sánchez, T., 2014. “Exploring the design space of the sCO2 power cycle compressor”. The 4th International Symposium–Supercritical CO2 Power Cycles, Pittsburgh, Pennsylvania, USA

Munkejord, S.T., Hammer, M. and Løvseth, S.W., 2016. “CO_2 transport: data and models–a review”. Applied Energy, Vol.169, pp.499-523.

Nimtz, M., Klatt, M., Bernd, W., Kuhn, M. and Krautz, H.J., 2010. “Modelling of the CO_2 process and transport chain in CCS systems—Examination of transport and storage processes”. Chemie der Erde, Vol. 70, Supplement 3, pp. 185-192

Nourbakhsh, A., Jaumotte, A., Hirsch, C. and Parizi, H.B., 2007. Turbo-pumps and pumping systems. Springer Science & Business Media, Berlin, Germany. ISBN: 978-3-540-25129-3

Okezue, C., 2006. “The description and analysis of methodology used in measuring the performance of an oil-injected screw compressor in a test rig”. BEng Dissertation, City University, London, United Kingdom

Okezue, C., 2010. “Mathematical modelling of multiphase flows in twin screw pumps”. MPhil Thesis, City University, London, United Kingdom

Okezue, C. and Wang, M., 2014. “A study of the effect of chemical impurities on the performance of a supercritical CO_2 pump for CCS transport pipelines”. 10th European Conference on Coal Research and Its Applications, Hull City, United Kingdom.

Okezue, C. and Wang, M., 2016. “Performance Evaluation of a Pump Used For CO_2 Transport”. 11th European Conference on Coal Research and Its Applications, Sheffield City, United Kingdom.

Okezue, C. and Kuvshinov, D., 2017. “Effect of chemical impurities on centrifugal machine performance: implications for compressor sizing in a CO_2 transport pipeline”. Energy Procedia, Vol. 142, pp. 3675–3682.

Okezue, C. and Kuvshinov, D., 2018. “A comprehensive study of the effect of chemical impurities on selection and sizing of centrifugal machines for supercritical carbon dioxide transport pipelines”. Applied Energy, Vol. 230, pp.816-835.

Oko, E., Wang, M. and Olaleye, A.K., 2015. “Simplification of detailed rate-based model of post-combustion CO_2 capture for full chain CCS integration studies”. Fuel, Vol. 142, pp.87-93.

Oosterkamp, A. and Ramsen, J., 2008. “State of the art review of co_2 pipeline transport with relevance to offshore pipelines”. Report No. POL-0-2007-138-A, Polytec, Norway.

Ouyang, L.B., 2011. “New correlations for predicting the density and viscosity of supercritical carbon dioxide under conditions expected in carbon capture and sequestration operations”. Open Petroleum Engineering Journal, Vol. 4, No.1, pp.13-21

Patchigolla, K. and Oakey, J.E., 2013. “Design overview of high pressure dense phase co_2 pipeline transport in flow mode”. Energy Procedia, Vol. 37, pp. 3123-3130

Pecnik, R. and Colonna, P., 2011. “Accurate CFD analysis of a radial compressor operating with supercritical CO_2”. Supercritical CO_2 Power Cycle Symposium, Boulder, Colorado, USA.

PetroWiki, 2012. “Number of stages of compression”. Available at: https://petrowiki.org/Compressors#Number_of_stages_of_compression

Pezzella, N., 2011. “High pressure CO_2 re-injection GE oil and gas experience”. PowerPoint Presentation in Rome, Italy. Available at: https://www.slideshare.net/canaleenergia/3-nicola-pezzella-ge-oil-gas-high-pressure-co2-reinjection-compatibility-mode

Pham, H.S., Alpy, N., Ferrasse, J.H., Boutin, O., Tothill, M., Quenaut, J., Gastaldi, O., Cadiou, T. and Saez, M., 2016. “An approach for establishing the performance maps of the sc-CO_2 compressor: development and qualification by means of CFD simulations”. International Journal of Heat and Fluid Flow, Vol. 61, pp.379-394.

Porter, R.T., Fairweather, M., Pourkashanian, M. and Woolley, R.M., 2015. “The range and level of impurities in CO_2 streams from different carbon capture sources”. International Journal of Greenhouse Gas Control, Vol. 36, pp.161-174

Oakey, J. E., Kara, F. and Patchigolla, K., 2010. “The effects of impurities for capture technologies on CO2 compression and transport”. Report B93 prepared for British Coal Utilisation Research Association (BCURA), Cheltenham, Gloucestershire, UK

Qiu, X.W., Anderson, M. and Japikse, D., 2010. “An integrated design system for turbomachinery”. Journal of Hydrodynamics, Vol. 22, Issue No.1, pp.347-354. DOI: 10.1016/S1001-6058(09)60219-5

Quiñones-Cisneros, S.E., Zéberg-Mikkelsen, C.K. and Stenby, E.H., 2000. “The friction theory (f-theory) for viscosity modelling”. Fluid Phase Equilibria, Vol. 169, No.2, pp.249-276.

Race, J., Wetenhall, B., Seevam, P. and Downie, M., 2012. “Towards a CO_2 pipeline specification: defining tolerance limits for impurities”. Journal of Pipeline Engineering, Vol.11, No. 3, pp.173-189

Ramos, A., Calado, M., Dias, E., Lawal, A., Rodriguez, J., Samsatli, N., Sanchis, G., Matzopoulos, M. and Pantelides, C., 2014. “CCS system modelling and simulation”. 4th Korean CCS Conference, Jeju Island, Korea

Rao, A.B, Rubin, E.S., Berkenpas, M.B., 2004. “An integrated modelling framework for carbon management technologies”. Carnegie Mellon University, Pittsburgh, Pennsylvania, USA

Rasmussen, P.C. and Kurz, R., 2009. “Centrifugal compressor applications—upstream and midstream”. Proceedings of the 38th Turbomachinery Symposium, Texas A&M University, USA; pp. 169-186

Saravanamutto, H.I.H, Roger, G.F.C. and Cohen, H., 2001. Gas Turbine Theory (5th Edition). Pearson Education Limited, Essex, UK

Seevam, P.N., Race, J.M. and Downie, M.J., 2007. “Carbon dioxide pipelines for sequestration in the UK: an engineering gap analysis”. Journal of Pipeline Engineering, Vol.6, No. 3, 2012, pp.133-146. ISSN 1753-2116

Seevam, P.N., Race, J.M., Downie, M.J. and Hopkins, P., 2008. “Transporting the next generation of CO_2 for carbon capture and storage: the impact of impurities on supercritical CO_2 pipelines”. Proceedings of 7th International Pipeline Conference, Calgary, Alberta, Canada; pp 39-51

Seevam, P.N., Race, J.M., Downie, M.J., Barnett, J. and Cooper, R., 2010. “Capturing carbon dioxide: the feasibility of re-using existing pipeline infrastructure to transport anthropogenic CO_2”. Proceedings of the 8th International Pipeline Conference, Calgary, Alberta, Canada

Seitz, J., Blencoe, J.G. and Bodnar, R.J., 1996a. “Volumetric properties for {(1-x) CO_2 + xCH_4}, {(1-x) CO_2 +xN_2} and {(1-x) CH_4 +xN_2}, at the pressures (9.94, 19.94, 29.94, 39.94, 59.93, 79.93 and 99.93) MPa and temperatures (323.15, 373.15, 473.15 and 573.15) K”. Journal of Chemical Thermodynamics, Vol. 28, pp 521-538

Seitz, J., Blencoe, J.G. and Bodnar, R.J., 1996b. “Volumetric properties for {x_1CO2 +x_2CH4 + (1-x_1-x_2) N_2} at the pressures (19.94, 39.94, 59.93 and 99.93) MPa and temperatures (323.15, 373.15, 473.15 and 573.15) K”. Journal of Chemical Thermodynamics, Vol. 28, pp 539-550

Serpa, J., Morbee, J. and Tzimas, E., 2011. “Technical and economic characteristics of a co_2 transmission pipeline infrastructure”. Joint Research Council (JRC) Scientific and Technical Reports, European Commission. DOI: 10.2790/30861.

Skaugen, G., Roussanaly, S., Jakobsen, J. and Brunsvold, A., 2016. “Techno-economic evaluation of the effects of impurities on conditioning and transport of CO_2 by pipeline”. International Journal of Greenhouse Gas Control, Vol.54, pp.627-639.

Sorokes, J.M., and Kuzdzal, M.J., 2010. “Centrifugal compressor evolution." Proceedings of the 39th Turbomachinery Symposium. Texas A&M University, USA

Sorokes, J.M., 2013. “Selecting a centrifugal compressor”. Chemical Engineering Progress, Vol. 109, Issue 6, pp.44-51.

Soulas T, Desai AR, Colby G, Griffin T., 2011. “CO_2 compression for capture and injection in today’s environmental world”. Proceedings of the First Middle East Turbomachinery Symposium, Doha, Qatar

Span, R. and Wagner, W., 1996. “A new equation of state for carbon dioxide covering the fluid region from the triple-point temperature to 1100 K at pressures up to 800 MPa”. Journal of Physical and Chemical Reference Data, Vol.25, No.6, pp.1509-1596.

Span, R., Gernert, J. and Jäger, A., 2013. “Accurate thermodynamic-property models for CO_2-rich mixtures”. Energy Procedia, Vol. 37, pp.2914-2922.

Stodola, A., 1927. Steam and gas turbines. Volumes I and II. McGraw-Hill, New York, USA.

Stosic N, Milutinovic Lj, Hanjalic K. and Kovacevic A, 1992. “Investigation of the influence of oil injection upon the screw compressor working process”. International Journal of Refrigeration, Vol. 15, Issue No.4, pp.206-220.

Svensson, R., Odenberger, M., Johnsson,F. and Stromberg, L., 2004. “Transportation systems for CO_2—application to carbon capture and storage”. Energy Conversion and Management, Vol. 45, pp. 2343–2353

Tan, Y., Nookuea W., Li, H., Thorin, E., Zhao L., Yan J., 2015 “Property impacts on performance of CO_2 pipeline transport”. Energy Procedia, Vol. 75, pp.2261–2267.

Tan, Y., Nookuea, W., Li, H., Thorin, E. and Yan, J., 2016. “Property impacts on carbon capture and storage (CCS) processes: A review”. Energy Conversion and Management, Vol. 118, pp.204-222.

Ulfsnes RE, Bolland O, Jordal K., 2003. “Modelling and simulation of transient performance of the semi-closed O_2/CO_2 gas turbine cycle for CO_2-Capture”. ASME Turbo Expo 2003, co-located with the 2003 International Joint Power Generation Conference, pp. 65-74. DOI: 10.1115/GT2003-38068.

Utamura, M., Fukuda, T. and Aritomi, M., 2012. “Aerodynamic characteristics of a centrifugal compressor working in supercritical carbon dioxide”. Energy Procedia, Vol.14, pp.1149-1155.

Vesovic, V., Wakeham, W.A., Olchowy, G.A., Sengers, J.V., Watson, J.T.R. and Millat, J., 1990. “The transport properties of carbon dioxide”. Journal of physical and chemical reference data, Vol. 19, No. 3, pp.763-808.

Wacker, C. and Dittmer, R., 2014. “Integrally geared compressors for Supercritical CO_2”. The 4th International Symposium—Supercritical CO_2 Power Cycles, Pittsburgh, Pennsylvania, USA.

Wadas, B., 2010. “Compression and pumping technologies and experience for EOR/CCS applications”. CO_2 Summit: Technology and Opportunity, Engineering Conferences International, Colorado, USA

Wang, M., Lawal, A., Stephenson, P., Sidders, J., Ramshaw, C., 2011. “Post-combustion CO_2 capture with chemical absorption: a state-of-the-art review”. Chemical Engineering Research and Design, Vol. 89, pp.1609-1624.

Watson, N. and M. S. Janota, 1982. Turbocharging the Internal Combustion Engine (1st edition). Macmillan Press Ltd, UK

Wen, J., Heidari, A., Xu, B. and Jie, H., 2013. “Dispersion of carbon dioxide from vertical vent and horizontal releases— a numerical study”. Proceedings of the Institution of Mechanical Engineers, Part E: Journal of Process Mechanical Engineering, Vol.227, Issue No.2, pp.125-139.

Wetenhall, B., Aghajani, H., Chalmers, H., Benson, S.D., Ferrari, M-C., Li, J., Race, J.M., Singh, P., Davison, J., 2014a. “Impact of CO_2 impurity on CO_2 compression, liquefaction and transportation”. Energy Procedia, Vol.63, pp. 2764-2778

Wetenhall, B., Race, J.M. and Downie, M.J., 2014b. “The effect of CO_2 purity on the development of pipeline networks for carbon capture and storage schemes”. International Journal of Greenhouse Gas Control, Vol. 30, pp.197-211.

Wilhelmsen, Ø., Skaugen, G., Jørstad, O. and Li, H. 2012. “Evaluation of SPUNG and other equations of state for use in carbon capture and storage modelling”. Energy Procedia, Vol. 23, pp. 236-245

Witkowski, A. and Majkut, M., 2012. “The impact of CO_2 compression systems on the compressor power required for a pulverized coal-fired power plant in post-combustion carbon dioxide sequestration”. Archive of Mechanical Engineering, Vol. 59, Issue 3. DOI: 10.2478/v10180-012-0018-x

Witkowski, A., Rusin, A., Majkut, M., Rulik, S. and Stolecka, K., 2013. “Comprehensive analysis of pipeline transportation systems for CO_2 sequestration: Thermodynamics and safety problems”. Energy Conversion and Management, Vol. 76, pp. 665-673.

Witkowski, A., Majkut, M. and Rulik, S., 2014. “Analysis of pipeline transportation systems for carbon dioxide sequestration”. Archives of Thermodynamics, Vol. 35, No.1, pp.117-140. DOI: 10.2478/aoter-2014-0008

Wright, S.A., Pickard, P.S., Vernon, M.E. and Radel, R.F., 2009. “Description and test results from a supercritical CO_2 Brayton cycle development program”. 7th International Energy Conversion Engineering Conference, Denver, Colorado, USA.

Wright, S.A., Radel, R.F., Vernon, M.E., Rochau, G.E. and Pickard, P.S., 2010 “Operation and analysis of a supercritical CO_2 Brayton cycle”. Sandia Report, No. SAND2010-0171

Yadav, A.K., Bhattacharyya, S. and Gopal, M.R., 2016. “Optimum Operating Conditions for Subcritical/Supercritical Fluid-Based Natural Circulation Loops”. ASME Journal of Heat Transfer, Vol. 138, Issue 11. DOI:10.1115/1.4031921

Yan, J., and Li, H., 2006. “Impacts of impurities in CO_2-Fluids on CO_2 transport process”. Proceedings of GT2006 ASME Turbo Expo: Power for Land, Sea and Air, Barcelona, Spain, pp. 367-375. ISBN 0-7918-4239-8

Zargarzadeh, P., Chahardehi, A. and Brennan, F., 2013. “Development of failure assessment diagram based method for engineering criticality assessment of CO_2 transportation pipelines”. Journal of Process Mechanical Engineering, Volume 227, Issue No 2, pp. 140-145

Zhang, Z.X., Wang, G.X., Massaroto, P. and Rudolph, V., 2006. “Optimization of pipeline transport for CO_2 sequestration”. Energy Conversion and Management, Vol.47, pp.702–715.